Fall 2013

# Evaluation of methodologies for continuous discharge monitoring in unsteady open-channel flows

Kyutae Lee
*University of Iowa*

# EVALUATION OF METHODOLOGIES FOR CONTINUOUS DISCHARGE MONITORING IN UNSTEADY OPEN-CHANNEL FLOWS

by

Kyutae Lee

A thesis submitted in partial fulfillment
of the requirements for the Doctor of
Philosophy degree in Civil and Environmental Engineering
in the Graduate College of
The University of Iowa

December 2013

Thesis Supervisors: Adjunct Professor Marian Muste
Professor Larry J. Weber

Graduate College
The University of Iowa
Iowa City, Iowa

CERTIFICATE OF APPROVAL

_____

PH.D. THESIS

_____

This is to certify that the Ph.D. thesis of

Kyutae Lee

has been approved by the Examining Committee
for the thesis requirement for the Doctor of Philosophy
degree in Civil and Environmental Engineering at the December 2013
graduation.

Thesis Committee: _____
Marian Muste, Thesis Supervisor

_____
Larry J. Weber, Thesis Supervisor

_____
Allen Bradley

_____
George Constantinescu

_____
Gabriele Villarini

_____
Venkatesh Merwade

To my family

ACKNOWLEDGMENTS

It is my great pleasure and honor to thank all the people who have supported me in many aspects during my study at IIHR (Hydroscience & Engineering) at the University of Iowa. Without their supports, this precious moment of writing my appreciation to them would not have been possible

I would like to special thanks to my thesis advisors, Adjunct Professor Marian Muste and Professor Larry Weber. Their encouragements and valuable guidance through this long journey make it practically possible pursuing this degree. I sincerely respect their insights and intelligence in dealing with challenging research tasks as well as their enthusiasm and professionalism at work.

I also would like to thank all my committee members, Professor Allen Bradley, Professor George Constantinescu, Professor Gabriele Villarini, and Professor Venkatesh Merwade at Purdue University for their valuable comments and supports through my research activities.

Furthermore, I would like to thank to Professor Witold Krajewski for his continuing financial supports since 2009 when the Iowa Flood Center was established. I have had great chances and valuable experiences in learning many field instruments and flood modeling tools. Also, I really appreciate all the IIHR staff members for helping my research works in a lab and field: special thanks to Jesse Piotrowski, Dan Gilles, Tim Houser, and Greg Wagner.

It was great pleasure to meet Professor Jean-luc Bertrand Krajewski and Dr. Jerome Le Coz who I worked together during my 3 months stay at Insa-Lyon University in France for research collaboration. I really appreciate for their valuable advice and warm cordial hearty welcome.

I also express my appreciation to colleagues: Ferrer, Moreno, and Sánchez with the Confederatión Hydrográfica del Ebro (Zaragoza, Spain) for sharing the data analyzed

in the paper and providing unconditional support in clarifying details about the conducted experiments. Without this dataset the value of the study would have been considerably diminished.

To my friends, thank you for listening, and emotionally supporting me through this entire process. Special thanks to Bongchul Seo, Dongsu Kim, Hao Che Ho, Jin-young Hyun, Hyunse Yoon, Seongmo Yeon, Sanghun Choi, Sunghwan Yoon, Donghwan Kim, and all my tennis club players!

I owe my success to my parents, who always respected my opinion through my life, and supported me emotionally and financially. There is the one last person who I cannot fully express my appreciation. I love you, Hunmin and my two sons, Hojin and Hodoo.

ABSTRACT

Ratings curves are conventional means to continuously provide estimates of discharges in rivers. Irrespective of their approach, the most-often adopted assumptions in building these curves are the steady and uniform flow conditions for the open-channel flow that in turn provide a one-to-one relationships between the variables involved in discharge estimation. The steady flow assumption is not applicable during propagation of storm-generated waves hence the question on the validity of the steady rating curves during unsteady flow is of both scientific and practical interest. Scarce experimental evidence and analytical inferences substantiate that during unsteady flows the relationship between some of the variables is not unique leading to loop rating curves (also labeled hysteresis). Neglecting the unsteadiness of the flow when this is large can significantly affect the accuracy of the discharge estimation. Currently, the literature does not offer criteria for a comprehensive evaluation of the methods for estimation of the departure of the looped rating curves from the steady ones nor for identifying the most appropriate means to dynamically capturing hysteresis for different possible river flow conditions and events.

The overarching goal of this study is to explore the uncertainty in the conventional stage-discharge rating curves (hQRCs) during unsteady flows and to evaluate methodologies for accurate and continuous discharge estimation. The study addresses these issues using experiments, modeling and analytical inference applied to hQRCs, index velocity rating curves (VQRCs), and continuous slope area (CSA) method. Included in the analysis is the implementation of a standardized framework for uncertainty assessment of the direct discharge measurements that are the building blocks of the rating curve construction. The study demonstrates using conceptual and analytical inferences that there are possibilities to develop a uniform end-to-end methodology to enhance the accuracy of the current protocols for continuous stream flow estimation for

both steady and unsteady river conditions. Moreover, the study provides methods to test the significance of hysteresis as a function of the site and storm event characteristics. The measurement techniques and analysis methodologies proposed herein will allow to dynamically track flood wave propagation using new measurement protocols or to assess the uncertainty in the conventional RCs when they are used for estimating the discharge. The study findings have implications for all flow-driven stream processes: sediment and pollutant transport and the health and wealth of the aquatic habitat.

TABLE OF CONTENTS

LIST OF TABLES

Table

LIST OF FIGURES

Figure

# CHAPTER I

# EXECUTIVE SUMMARY

## I.1 Background

Floods are the most damaging and frequently occurring natural disasters in the United States (FEMA 1992). Despite extensive flood management efforts by federal, state, and local agencies, flood damage continues to increase (Galloway, 2008.a). Continued occurrences of destructive flooding in our region (e.g. Grand Forks-1997; Midwest-1993, 2008, and 2010), illustrates that our nation has not learned to effectively respond to floods and that there is a considerable disconnect between advances in science and engineering and societal decision making in this area (Galloway 2008.b). One of the major gaps in preventing and/or reducing losses is to provide reliable and timely information to the public about the risk associated with the flooding (FEMA 2001). To accomplish the prevention or reduction of losses, accurate prediction of the flood inundation area and dissemination of information on the inundation areas to emergency managers, city planners, and the general public are necessary.

Among the key variables used for estimating the inundation area is the streamflow data. These data, currently obtained at more than 7,000 stations across the nation, are based on an empirical one-to-one relationship between stage (directly measured) and discharge estimated from rating curves (RCs) established under the assumption of steady flow. Given that the construction of ratings curves to accommodate the wide range of flows and processes occurring in rivers has been a challenging task from many perspectives, the one-to-one RCs continue to be widely used for steady and unsteady flows. Moreover, the inundation maps are mostly created with steady-state models. Overlooking the effect of unsteady flow on the stage-discharge RCs and in modeling may introduce uncertainties in the estimation of both stage and discharge and, consequently, in

the mapping of flood boundaries and timing. The overarching goal of this study is to explore the uncertainty of the conventional approaches for constructing stage-discharge RCs and to evaluate methodologies for accurate and continuous discharge monitoring in unsteady open channel flows with considerations on discharge measurement uncertainty. Special attention will be given to the uncertainty generated by ignoring effect of the unsteady flow associated with the propagation of the flood wave through channels.

Uncertainties in stage-discharge relationship can be grouped into three sources (Schmidt, 2002). The first source is the *natural uncertainty* associated with the randomness of the natural processes, e.g., changes in cross sections – overbank flow conditions, vegetation growth, ice build-up, variable backwater and hysteresis due to flood wave propagation. The second source is *knowledge (conceptual) uncertainty* which indicates incomplete understanding of the physical processes and/or assumptions made in conjunction with them. Any of the natural uncertainties can become a conceptual uncertainty if active but neglected. For instance, using the one-to-one RC (which is established based on the limited number of synoptic measurements) for high flows (where accurate info is critical) may lead critical errors for the prediction of discharges. Similarly, neglecting the unsteady flow effects in the stage-discharge ratings (a.k.a. hysteresis) will negatively impact the reliability on discharge data estimated from the curves. The third source is *data uncertainty* which includes the errors due to measurement processes. This may include, for example the lack of accuracy of the equipment used for the measurement, errors induced by curve fitting the data, time integration errors during the measurements due to changing discharges, etc.

For high and unsteady flows, such as those occurring during floods, the sources of uncertainties of utmost importance are those associated with: the measurement uncertainty, extrapolation of the rating, and neglecting the hysteresis effect. Estimating these individual sources of uncertainties has been subject to experimental, analytical and numerical investigations for more than a century. However, the experimental studies are

scarce and fragmented (due to the difficulty to acquire the measurements), while the analytical and numerical simulations are using various simplifications, and have not been verified on case studies due to the unavailability of data. In sum, the literature does not offer uniform criteria for a comprehensive evaluation of the methods for development of RCs, nor for identifying the most appropriate ones for different possible river flow conditions. Moreover, the RCs' uncertainty, regardless of the way they were developed (empirical and/or analytical formulations), is largely unknown, especially for unsteady conditions at high flows (such as floods) when some of the uncertainties (e.g., hysteresis) affecting the RCs are considerably increased.

## I.2 Motivation

The present study revolves around the quality of the data provided by direct discharge measurements and those estimated via RCs during steady (time invariant) and unsteady river flow conditions. RCs are used to estimate discharges on a continuous basis being typically built using direct discharge measurements. The common feature of approaches for establishing RCs is that they require a set of direct discharge measurements that are subsequently used to relate discharge with one or more directly measured variables (i.e., depth, velocity, or energy slope). The assumptions and protocols used for building RCs have been largely imposed by the capabilities of the available instruments. More specifically, the acquisition of direct discharges with pre-acoustic velocity instruments (before 1980s) was typically effort-intensive, slow, and even posing harm for instruments and operators during fast varying flows. Consequently, the vast majority of the RCs are based on periodic measurements acquired during normal (steady state) conditions followed by the construction of a one-to-one relationship between stage and discharge. The so obtained RCs are subsequently used for estimation of the discharges irrespective of the flow situations occurring in the rivers.

There is a vast amount of analytical studies demonstrating that the difference between the steady and unsteady flow governing equations leads to a non-unique, loop-like shaped, the relationship between discharge and stage with distinct dependencies on the rising and falling limbs of the storm hydrographs. The deviation is called hysteresis and its shape and thickness are dependent on the site and unsteady flow characteristics. The hysteretic behavior is seen as a source of conceptual uncertainty that is additive to all the other sources of errors active in building the RCS. From this perspective, hysteresis is a relevant synthetic representation of the inaccuracy of the RCs obtained with conventional (steady state) protocols when they are used to estimate discharges in unsteady flows. Unsteady river flows are practically occurring after each storm event in the watershed drained by a river, hence affecting the accuracy of the RC with an error of conceptual nature. Many of the studies have proposed algorithms and additional measurements to correct the conventionally-built RCs for the unsteady flow effects (a.k.a. hysteretic behavior). In the US these methods are sporadically applied to some of the nation's large rivers at sites prone to flooding. These corrective methods are engaging new assumptions and/or simplifications and have not been thoroughly validated because of lack of direct discharge measurements. The advent of the new instrumentation (based on acoustic, electromagnetic wave, and images) has considerably evolved allowing today to acquire measurements fast (in many cases in real time), irrespective of the flow magnitude. The new experimental evidence provided by data acquired with these instruments sheds light into the accuracy of the conventionally-built RCs for unsteady flow conditions, hence enabling to assess their capabilities to accurately estimated discharges for various sites and flow conditions.

The main motivation for this study stems from the fact that there are few studies demonstrating the capabilities of the new generation of instruments to improve our current approaches to continuously and accurately estimate discharges in rivers subjected to unsteady flows. Moreover, some of the RC protocols developed for discharge

estimation have been developed under the impetus of the new instruments (the index-velocity and continuous slope-area method) but they have not been compared with the previous RC building approaches to substantiate their quality during steady and unsteady flows. Of special importance for the present study are unsteady flows associated with floods when accuracy is needed most. The improved RC quality may result not only in better quantitative estimation of the discharges but also in providing details of the flood wave propagation such as the timing of the peaks for discharge, velocity, and stages that are useful in assessing the risk during the flood propagation.

A second motivation for the study stems from the fact that the direct measurements documenting hysteresis have been mostly acquired in few sites located on large rivers (e.g., Mississippi) with the purpose to provide more accurate data for streamflow forecasting models (National Weather Service, personal communication). Currently, there is no systematic effort to evaluate the impact of hysteresis in medium and small stream where floods are increasingly present (e.g., Iowa and Cedar Rivers in the U.S.). The outcomes of this study are potentially relevant for rivers located in geographical areas such as the Midwest where currently extreme storms are increasingly frequent as a result of climate change generating runoff that is faster conveyed to streams due to the altered hydrology produced by intensive agriculture (tiling, tile drains, etc.) (Jones and Schilling, 2010). These rapidly developing high flows routed in flat plane rivers are most likely to develop considerable hysteresis (Takahashi, 1969; Graf and Suszka, 1985; Graf and Qu, 2004; Nezu et al., 1997; Fread, 1975). The acquisition of such experimental evidence can uniquely support the sound evaluation of the effect of hysteresis on current monitoring practices and eventually lead to optimized algorithms for improved quality of the RCs for all river sizes.

The third motivation of the study stems from the availability of long records of data at streamgage stations managed by US Geological Survey (USGS) and the potential of mining these data both for assessing the importance of hysteresis and for quantifying

the associated uncertainty as a function of the site characteristics and event types. This study will develop analytical protocols and criteria for the identification of the sites and events that are prone to hysteresis along with a rigorous methodology to use legacy data at gage sites for the assessment of the hysteresis-related uncertainty for any size event and river.

## I.3 Objectives

The overarching goal of the proposed research is to evaluate the accuracy of the current methodologies for continuous monitoring of discharges in unsteady open channel flows. We will do so by evaluating first the importance of the hysteretic behavior in the RCs using experimental evidence and by implementing improved analytical algorithms for accounting for hysteresis. Subsequently, we will evaluate the impact of hysteresis on new RC alternatives such as index-velocity and continuous slope-area methods. In particular, by taking advantage of the new measurement technologies' capabilities (e.g., acoustic instruments, GPS, Lidar surveys) we will deploy a continuous slope-area gaging station to test its capability to dynamically track the flows. A thorough uncertainty analysis is also conducted to fully document one of the major sources of uncertainty involved in the direct discharge measurement that is the building block of the RCs. Moreover, by data mining the records we will create a benchmark for events of various types and their associated uncertainties when estimated with conventional RCs.

The data from experiments and the assumptions of the conducted analyses are studies under the assumption of simple flow conditions in order to isolate the effect of hysteresis. Specifically, the unsteady flows are assumed to be controlled by gravity and friction (channel control) without additional effects from local changes in the channel section geometry (vertical and horizontal plans), bed roughness or the presence of natural or man-made obstructions (leading to backwater). Furthermore, the hysteresis-related uncertainty is estimated only for in-bank flow situations as the change in cross section

occurring in the floodplain flows generate additional uncertainties which are difficult to separate from the mix.

The specific tasks of study are as follows:

a. Modification of Fread approach (1975) solving 1-D shallow flow equation to be applicable for rivers irrespective of their size.
b. Substantiation of the hysteretic behavior of the stage-discharge RC using direct discharge measurements acquired during unsteady flows in several widely-varied river sizes (case studies will be documented for Clear Creek in Oxford, IA, Chattahoochee River in USA, and Ebro River in Spain).
c. Evaluation of the sensitivity to hysteresis for alternative RC protocols (Index-Velocity Rating Curve method and Continuous Slope-Area method).
d. Identification hysteresis diagnostic formula suitable for rapid and efficient assessment of the hysteresis-prone gaging sites. The sites that will be found least prone to hysteresis by the diagnostic protocol will continue to use steady RCs. In this respect, the characterization and evaluation of the significance of unsteadiness parameters was established using 1D HEC-RAS unsteady model and the modified Fread equation.
e. Assessment of the uncertainty in direct discharge measurements acquired with TRDI StreamPro Acoustic Doppler Current Profiler (ADCP) using standardized uncertainty analysis framework (GUM, 1993) based on customized experiments in lab and field as a guidance to address appropriate uncertainty analysis methodologies in discharge measurements.
f. Establishment of comprehensive protocols to account for hysteresis at new and existing gaging sites.

## I.4 Research contributions to science

The main contribution of this research is the development of a uniform end-to-end methodology for assessing the uncertainty in RCs generated by unsteady flows. The methodology is applicable to any river size and allows conveniently examining the uncertainty magnitude due to unsteady flows as a function of the site and storming event characteristics. The research components utilized in the present investigation are state-of-the-art and their integration in the methodology marks a novel approach that has not been reported in the literature. The measurement techniques and analysis methodologies proposed herein can be used to dynamically track flood wave propagation and its characteristics (cross-section discharge, velocity and depth) and to estimate the uncertainty induced in the conventional RCs during flood wave propagation. The developed methodology can be implemented at existing USGS gaging stations, National Weather Service's River Forecast Centers, and new gaging stations such as at the Iowa's bridges equipped with Iowa Flood Center (IFC) stream gages sensors.

New alternative RC approaches such as Index-velocity method is well known and has been implemented for more than decades at locations where backwater and/or hysteresis effects seem to exist; however, there have been a very few discussions about whether the index velocity rating between index velocity and mean channel velocity shows non-unique relationship due to hysteresis and its consequences on the shape of stage-discharge RCs. Similarly, slope-area method has been recognized for many years, but their applicability for dynamically and continuously tracking unsteady flows has been rarely reported. The continuous slope-are method described in this study is recommended for locations where hysteresis is not very large as the basic assumptions of the method stem in the steady-state flow condition with continuous updates on the free-surface slope.

In the present context of global climatic variability, the capability to accurately predict uncertainty for extreme flows is critically important as the availability of the data for these events is not only scarce (due to high-risk) but also prone to errors when using

the current RC estimation procedure. The optimization of the methodologies to more realistically capture unsteady flows will visibly enhance the quality of decision-making and crisis management during floods by enabling to determine dynamically forecasted inundation mapping in real-time. The methodology is also relevant to monitoring river sites where the flow is rapidly varied due to operational considerations (hydropower dams, flood control, irrigation). Overall, it is expected that the outcomes of the present study will also demonstrate that the tools for estimating uncertainty from various sources can be documented and aggregated using a robust methodology that is capable to making uncertainty analysis as an integral part of the physical science.

## I.5 Dissertation procedure and outline

The research is based on a combination of direct measurements, data analysis, data mining, and numerical simulations. Emphasis will be placed on the use of available direct discharge data (new and existing measurements) to better substantiate the physics of the open-channel processes and their interconnection, to evaluate when and where the unsteady flows are important, and to provide a solid analytical formulation for accurate monitoring of flow in various size of streams and conditions. The dissertation is structured as follows:

*Chapter 1 Executive summary* provides the background, motivation, objectives, and plan of this research project.

*Chapter 2 Literature review* highlights the theoretical background associated with hydrodynamic processes and discharge estimation methods for both steady and unsteady flow conditions.

*Chapter 3 Experimental evidence and conceptualization of unsteady flow effects on hQRC* presents the modified Fread equation and its implementations on both small and mid-size river. Experimental evidence of hysteresis captured by direct discharge measurements, index velocity method, and slope-area method will be also presented in

this chapter. In addition, hysteresis diagnostic protocols and characterization of event hydrograph types and site conditions will be discussed.

*Chapter 4 Uncertainty analysis implementation to hQRC* introduces first an existing UA framework, its application to ADCP direct discharge measurements along with a protocol for assessing the uncertainty produced by hysteresis at a gaging site.

*Chapter 5 Summary, implications, and further work* synthesize the study outcomes, their implications and the tasks to be further tackled to substantiate and refine the methodologies and readiness for implementation.

*Appendix A UA Framework* provides details on the uncertainty analysis framework

*Appendix B UA Implementation* illustrates a worked example of the framework implementation for discharge measurements using current propeller meter

# CHAPTER II

# LITERATURE REVEIW

## II.1 Channel flows during storm events

### II.1.1 Introduction

In most of hydraulic studies these days, the output from flood inundation modeling is a single deterministic prediction of the flood area for the peak flow based on one-to-one stage-discharge relationship. Conventional RC estimates streamflow as a function of stage only, and that is of great practical importance as it not only links the discharge and stage in flood routing models, but also it is frequently used to obtain estimates of water level at extreme flood discharges (where this curve is obtained by extrapolation of the RCs). The conventional investigative approaches (experimental and numerical) using steady RCs have considered flood phenomena as the outcome of a stationary, independent, and identically distributed random process in space and time (Jain & Lall, 2000). However, conceptually neglecting and lumping the physics associated with the unsteady nature of the flow into simple random processes without sound theoretical basis would lead to significant errors when assessing the risk of flood. Recently, there is a trend in the hydrological/hydraulics community towards physics based models (Malone et al., 2007), which allows predicting spatio-temporal evolution of the flood over large scales, and more accurate description of the time evolution of the flood levels at locations of interest (such as large cities).

There are known to be various sources of uncertainties associated with the prediction of flood extent. Many researchers (Matott et al., 2009; Mishra, 2009) have discussed the methodologies to effectively evaluate the uncertainties in general modeling area. Among the key sources of uncertainties are: the input uncertainties (initial and

boundary conditions, model parameters, etc.) and model uncertainties (model structure, model resolution, model algorithm, etc.). The uncertainties associated with the estimation of streamflow data (boundary conditions) is thought to be one of the important factors that need to be accurately addressed. Pappenberger et al. (2006) indicated that use of the RCs for upstream boundary conditions can exceed the importance of model parameter uncertainty in the overall uncertainty budget in some areas. Moreover, the author found the fact that 18 to 25% of uncertainty is expected at the peak discharge due to extrapolation of the RCs for high flows. Yen and Tang (1977) also emphasized that the input hydrograph at upstream boundary conditions is the most important factor affecting the reliability of flood warnings, and therefore the assessment of the uncertainties in stage-discharge ratings are critical.

### II.1.2 Governing Equations

It is well known that flow in channels can be classified as uniform or non-uniform and steady or unsteady flows depending on the variation of the discharge (or velocity) and depth (or cross-sectional area) with space and time along the stream. Depending on the particular situation, channel flows further can be classified as steady uniform flow, steady gradually varied flow, steady rapidly varied flow, unsteady uniform flow, unsteady gradually varied flow, and unsteady rapidly varied flow. Gradually varied flow occurs in situations where the rate of change of flow depth with respect to distance is small, and therefore streamline curvature is negligible (pressure distribution is hydrostatic). When the streamlines have large curvature (such as in the case of the flow over spillway crests or buckets), the pressure is no longer hydrostatic and the flow is classified as rapidly varied flow. Flood wave propagation following storm events might be a combination of gradually varied in space and time. The concept of loop RCs is associated with the variation of the flow in time, while the space and time variations are usually inherently linked (Henderson, 1966). This phenomenon is related to the flow

acceleration and deceleration during flood wave propagation (Cunge et al., 1986; Ponce, 1989, etc).

The conventional approach for analytically describing hysteresis is based on the principles of continuity (conservation of mass) and momentum (Newton's second law of motion) equations applied for the one-dimensional unsteady open channel flows. For most of the practical applications, simplified one-dimensional differential equations are deemed adequate. The simplifications include negligence of the terms associated with lateral flow, wind shear, and eddy losses, and by assuming momentum coefficient, β and energy coefficient, α to be unity. The momentum coefficients, β and energy coefficients α are the coefficients used to adjust the velocity variation in a channel section for one-dimensional flow. That is, the true momentum flux through the cross-section, $\int_A \rho u^2 dA$ is not equal to the momentum flux based on mean flow velocity, $\rho QV$ and similarly the true kinetic-energy flux through the cross-section, $\int_A (\rho u^3/2) dA$ is not equal to the kinetic-energy flux based on mean flow velocity, $\rho QV^2/2$ due to the velocity variation in a channel section. Flood wave equation based on one-dimensional continuity and momentum equations are often referred to as de Saint-Venant equations (Ponce and Simons, 1977; Mishra and Singh, 1999; and other researchers) as subsequently will be described.

As illustrated in Figure II.1, the elemental control volume of length *dx* is considered between two cross-sections. To simplify the derivation, the lateral flow *q* is neglected, and therefore the sum of inflow entering the control volume from the upstream is equal to the sum of outflow exiting the control volume to the downstream. Based on the conservation of mass, the rate of change of mass stored in the control volume can be written as:

$$\frac{\partial(\rho A dx)}{\partial t} = \rho Q - \rho(Q + \frac{\partial Q}{\partial x} dx) \qquad \text{(II.1)}$$

Under the incompressible fluid assumption the density is constant, hence dividing the equation (II.1) by *ρdx* ends up with another from of the continuity equation (II.2).

$$\frac{\partial \mathrm{A}}{\partial t} + \frac{\partial Q}{\partial x} = 0 \qquad \text{(II.2)}$$

The momentum equation based on Newton's second law of motion describes the sum of all external forces acting on the control volume is equal to the multiplication of mass and acceleration of the control volume. In other words, the rate of change of momentum is equal to the net force acting on the control volume. The external forces considered in derivation of equation (II.3) are the gravity force, the friction force, and pressure forces. Since the rate of change of momentum storage in the control volume can be expressed as $\rho\partial Q/\partial t dx$, the simplified one-dimensional differential momentum equation (II.3) becomes

$$\frac{\partial Q}{\partial t} + \frac{\partial}{\partial x}\left(\frac{Q^2}{A}\right) + gA\left(\frac{\partial y}{\partial x} - S_0 + S_f\right) = 0 \qquad \text{(II.3)}$$

*where* $S_o$ is the bed slope and $S_f$ is the friction slope. The first term describes local acceleration, and it indicates that the change in momentum occurs due to the change in velocity with time. The second term is convective acceleration term, and it describes the change in velocity with space along the channel mostly due to contraction and expansion of the channel geometry. The third term in the equation refers to the change of pressure force due to the change in water depth, and the fourth term denotes gravity force due to a bed slope. The last term of the equation represents the friction force term, and it is a force proportional to the energy slope (water surface slope).

The simplified continuity and momentum equations are derived based on the following assumptions: a) one dimensional flow (velocity is constant in a cross-section), b) gradually varied flow (hydrostatic pressure distribution), c) no large curvature along the channel reach, d) small bed slope, and e) immobile bed. Under these assumptions the

flow resistance equations can be described by Manning's and Chezy which are valid for steady flow and incompressible fluid of constant density.

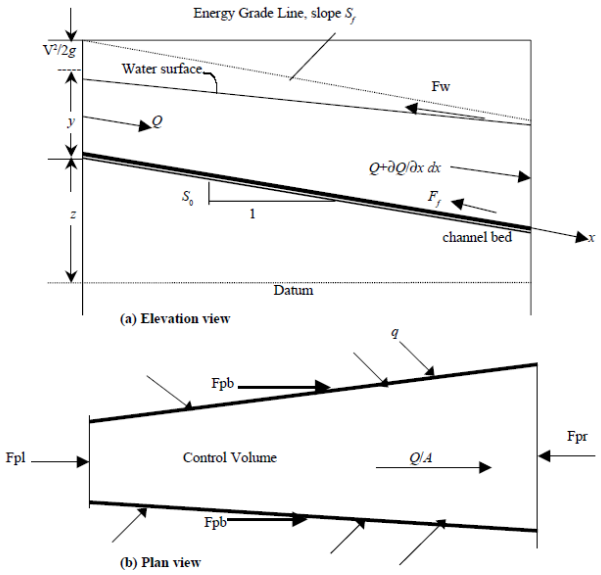


Figure II.1 Definition sketch of the control volume

Source: Mujumdar (2001)

Equations (II.2) and (II.3) are together referred to as de Saint Vernant equations, and they can be solved by numerically from many practical applications. The simplest form of these equations is obtained by neglecting the local acceleration, convective acceleration, and the pressure terms, so the remaining terms in momentum equation describe the steady uniform flow conditions. This simplified equation accounts for the unsteadiness of flows through continuity equation by assuming steady for momentum conservation. However, this is too limited to be applied for flood wave propagation since

backwater effects cannot be reproduced from this assumption. Based on the terms of the momentum equation (II.3), Ponce and Simons (1977) classified the flood waves as kinematic (KW), diffusion (DW), steady-dynamic (SDYW), dynamic (DYW) and gravity (GW) waves. A more popular classification of the same equation is the one provided by Fread (1985) that distinguishes three types of waves: the KW, DW and DYW. KW describes a situation where friction forces and gravity forces are in balance. This situation applies to steep slope channel without backwater. DW occurs when the pressure force becomes important, while DYW includes both inertial and pressure terms in addition to friction and gravity forces. The latter can be applied for conditions where backwater develops in mild slope channel. For easy understanding, equation (II.3) was reorganized in a form of Figure II.2 along with the specification of different types of flood waves. Ponce (1989) demonstrates that the DYW, DW, and KW are developing large loop, mild loop, and no loop, respectively.

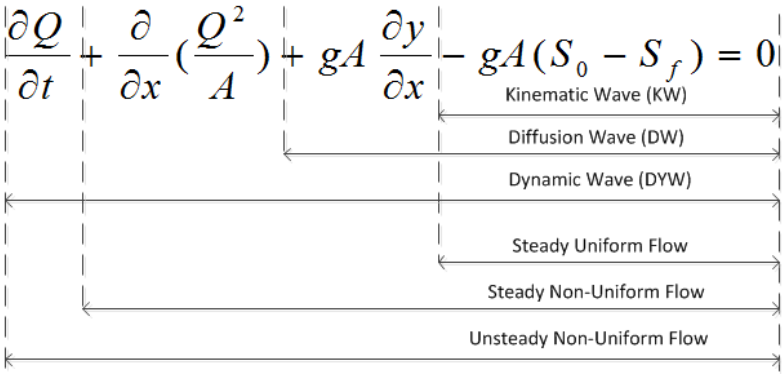


Figure II.2 Types of channel flows and flood waves

From practical perspectives, the solution of the de Saint Vernant equations provides the discharge and depth at a location of interest given the discharge hydrograph

at the upstream boundary, i.e., flood routing. This computation procedure describes the movement of flood wave through the time and space in the channel. Flood routing can be computationally described using physically based distributed hydraulic routing (Kinematic wave routing, Diffusive wave routing, and Dynamic wave routing) and conceptual lumped hydrologic routing (Reservoir routing, Muskingum routing, etc.). The former uses continuity and momentum equations to calculate the flow as a function of time and space, while the latter uses continuity and flow/storage relationship assuming the flow is a function of time without description of the spatial variability.

Widely spread in the investigation of floods is numerical modeling such as Hydrologic Engineering Center (HEC) – U.S. Army Corps of Engineers' software package. The HEC-RAS unsteady module approaches flood wave propagation using a physical based distributed hydraulic routing. The HEC-HMS hydrologic channel routing is applied either as physical or conceptual hydrologic models to estimate the streamflow from the tributaries between upstream and downstream boundary. The next two sections provide more details on the HEC software components. Especially HEC-RAS will be subsequently used in this study.

### II.1.3 Numerical solutions

#### II.1.3.1 HEC-RAS unsteady flow routing

With the advent of computing technology, the solutions for dynamic wave equation are easily obtained using numerical methods. In this section, theoretical basis for one-dimensional flow calculation with HEC-RAS is thoroughly reviewed based on HEC-RAS reference manual (HEC, 2008).

The derivations provided in the reference manual are based on the paper by James A. Liggett from the book "Unsteady Flow in Open Channels" (Mahmmod and Yevjevich, 1975). It is provided that the software follows the one-dimensional continuity and momentum equations as presented in equations (II.2) and (II.3), but it handles the

conveyance of the main channel and floodplain separately. Fread (1976) addressed the conveyance issues for the main channel and floodplain by considering the channel to be formed from two separate channels whereby the continuity and momentum equations are independently applied. Barkau (1982) extended their work by further manipulating the equations. In the current form, the HEC-RAS unsteady module is based on the following equations:

$$\frac{\partial A}{\partial t}+\frac{\partial(\Phi Q)}{\partial x_c}+\frac{\partial[(1-\Phi)Q]}{\partial x_f}=0 \qquad \text{(II.4)}$$

$$\frac{\partial Q}{\partial t}+\frac{\partial(\Phi^2 Q^2/A_C)}{\partial x_c}+\frac{\partial\left((1-\Phi)^2 Q^2/A_f\right)}{\partial x_f}+gA_c\left[\frac{\partial Z}{\partial x_c}+S_{fc}\right]+gA_f\left[\frac{\partial Z}{\partial x_f}+S_{ff}\right]=0 \qquad \text{(II.5)}$$

*where* $\Phi$ is the portion of conveyance in the main channel, and subscripts *c* and *f* represent the main channel and floodplain.

The numerical solution for these equations is approximated using *the four-point implicit finite difference scheme*, and this scheme is the most often used procedure for solving the one-dimensional de Saint-Vernant equation. By directly applying the non-linear equation (II.4) and (II.5) using the *implicit finite difference scheme* may result in a system of non-linear algebraic equations. Instead of using the Newton-Raphson iteration technique which has some convergence problems for discontinuous river geometry, Preissman developed a method to linearize the finite difference scheme (Liggett and Cunge, 1975). The details of the scheme are described in the reference manual (HEC, 2008), chapter 2-38 through 2-41.

II.1.3.2 HEC-HMS hydrologic flow routing

Although the full dynamic wave equation is the most appropriate procedure for solving one-dimensional open channel flow problems, it is often adequate for typical events to use an approximation of the full dynamic wave in the flood routing. For example, it is simple and convenient without needs for putting an extensive effort to draw

the cross-sections along the channel which spreads out in a large scale basin. Approximations are made by combining the continuity equation with a simplified momentum equation which can be either physically or conceptually based.

The flow routing methods available in HEC-HMS model (i.e., Kinematic Wave, Lag, Modified Puls, Muskingum, Muskingum-Cunge, and Straddle Stagger) are listed in Figure II.3. Figure II.3 is provided as an aid to choose appropriate models for different hydrologic conditions. All the methods listed in the table neglect the dynamic wave terms in de Saint Vernant equation, and therefore either assumed kinematic wave or diffusion wave approximation. Irrespective of the approximation methods used, they are solved by the finite difference method by substituting the approximated successive time and space steps into the partial differential equations. Depending on the way to compute those set of algebraic equations, they can be either an explicit or an implicit scheme. Explicit scheme solves the unknown values successively along the stream, and implicit scheme finds those simultaneously for a given time (HEC, 2000).

| If this is true... | ...then this HEC-HMS routing model may be considered. |
|---|---|
| No observed hydrograph data available for calibration | Kinematic wave; Muskingum-Cunge |
| Significant backwater will influence discharge hydrograph | Modified Puls |
| Flood wave will go out of bank, into floodplain | Modified Puls, Muskingum-Cunge with 8-point cross section |
| Channel slope > 0.002 and $\frac{TS_o u_o}{d_o} \geq 171$ | Any |
| Channel slopes from 0.002 to 0.0004 and $\frac{TS_o u_o}{d_o} \geq 171$ | Muskingum-Cunge; modified Puls; Muskingum |
| Channel slope < 0.0004 and $TS_o\left(\frac{g}{d_o}\right)^{1/2} \geq 30$ | Muskingum-Cunge |
| Channel slope < 0.0004 and $TS_o\left(\frac{g}{d_o}\right)^{1/2} < 30$ | None |

Source: HEC (2000)

Figure II.3 Guidelines for selecting routing model

## II.2 Conventional one-to-one rating curve (RC) approaches

### II.2.1 Introduction

The conventional methods used to provide continuous measurement of river discharges are based on the one-dimensional (1-D) view of the river flowing under steady and uniform conditions. These ideal flows are well described by the Manning formula (Henderson, 1966) that relates the cross-sectional area of the stream (*A*) and the mean flow velocity (*U*) – see Figure II.4. For these simple flow cases there are a plethora of guidelines for constructing RCs for the stage-discharge (Rantz et al. 1982; Herchy, 2009), index-velocity (e.g., Morlock et al., 2002; LeCoz et al., 2008; Levesque and Oberg, 2012) and slope-area (e.g., Dalrymple and Benson, 1967) discharge estimation methods.

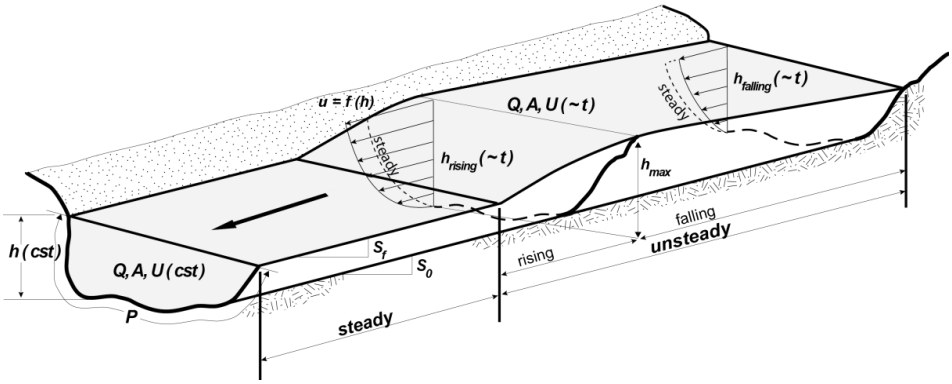


Figure II.4 one-dimensional (1-D) view of the river flow during flood wave propagation

### II.2.2 Stage-discharge rating curve (hQRC) method

The theoretical basis of conventional one-to-one RC curve approach assumes that the discharge is a unique function of stage with a constant water surface slope. This assumption is valid only for steady flow situation. From the continuity equation (II.6) as

it is described below, the term $K\sqrt{S_f}$ which accounts for the resistance and friction slope is assumed constant along the stream, and therefore the discharge uniquely depends on the product term, $A\sqrt{R}$ which is further a unique function of the stage as long as the cross-section does not change with sediment deposition and erosion.

$$Q = AV = AK\sqrt{RS_f} = \left(A\sqrt{R}\right)K\sqrt{S_f} \quad \text{(II.6)}$$

*where A* is the cross-sectional area; *V* is the mean flow velocity at the cross-section; *R* is the hydraulic radius; $S_f$ is the friction slope; and *K* is the resistance coefficient which can be calculated with methods such as Manning's, Chezy and Darch-Weisbach. For steady and uniform flow conditions, the friction slope $S_f$ and the bed slope $S_o$ in the momentum equation are equal.

The conventional steady RCs are based on the unique stage-discharge relationships developed using empirical equations relating stage (directly and continuously measured) to discharge (directly measured through repeated measurements over a range of stages). Depending of the type of flow control, the empirical equation can be either based on:

i) open-channel flow (Herschy, 1999; Kennedy, 1984, Rantz et al., 1982):

$$Q = C\left(a + h_g\right)^{\propto} \quad \text{(II.7)}$$

*where Q* is the discharge; $h_g$ is the stage; *a*, *C* are constants; and $\alpha$ is an exponent, or

ii) flow over weir (Rantz et al., 1982)

$$Q = C_W L_w \left(h_g - a\right)^{\propto} \quad \text{(II.8)}$$

*where* $C_w$ is a weir constant; $L_w$ is the weir length; and $\alpha$ is an exponent. A typical stage-RC is shown in the Figure II.5.

These empirical equations are unique for all type of flows developing in the channel. The methodologies for obtaining these RCs are well established, widely applied, and relatively simple (e.g., Buchanan and Somers, 1969). However, they are critically limited in capabilities because the estimation methodology is based on an empirically

derived hQRCs under the assumption of uniform steady flows which are rare in the natural streams. Shifting, discontinuities, and loops in the steady RCs may result from a number of physical factors such as unsteady flow due to flood wave propagation, backwater, in-channel storage, vegetation, etc. Therefore, there is the need for adjusting RCs whenever deviations from the conventional RCs are observed. For this purpose, USGS recommends eight to ten discharge measurements annually for most gauging stations (Rantz et al., 1982).

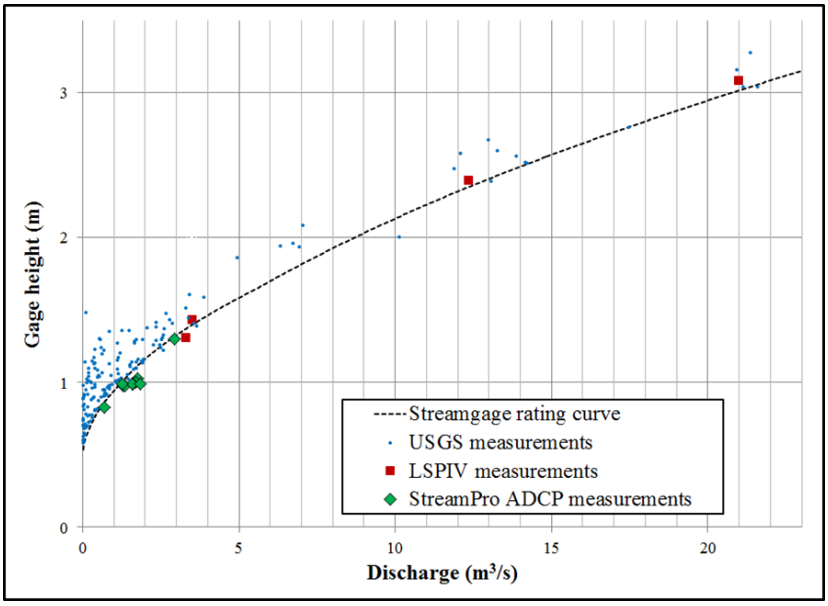


Figure II.5 Example of typical stage-RC at USGS (05454220) stream gage at Clear Creek near Oxford, IA, USA

### II.2.3 Index velocity rating curve (VQRC) method

With the advent of low-cost instruments such as Doppler velocity meters (ADVMs), an application of the VQRC method for computing continuous records of

discharge has become increasingly common. The VQRC method is currently being used for approximately 470 gaging stations managed by USGS in 2011. The USGS deployed fixed hydroacoustic current meters at streamflow-gaging stations to compute streamflow using VQRC method. The water velocity measured by an instrument in a portion of a river can be used as a surrogate to relate it to the mean-channel velocity. This method is different from the conventional hQRC method because it separates velocity and area into two ratings – the index to mean velocity rating and stage-to-area rating. The outputs from the two ratings (*V* and *A*) based on the VQRC method are multiplied together to compute a discharge. Usually, mean velocity (*V*) in a section is only a function of the streamwise component of the index velocity. However, there are the sites where *V* may be a function of index velocity and stage and even of cross-stream index velocity and the velocity head (streamwise index velocity squared), while the area is always a function of stage and channel cross-sectional shape. An index rating referring to the relation between mean-channel velocity and the index velocity is developed using regression technique based on the data obtained from field measurement campaigns. Figure II.6 below describes the example of an index rating.

### II.2.4 Slope area (SA) method

The SA method calculates a discharge using the measured cross-sections, estimates for the channel roughness, and the water-surface slope derived from field evidence. The energy slope in Manning equation is used to calculate a discharge, and it is very important to note that the conventional assumption for this method is steady-flow condition. The method is applied to unsteady flow conditions by ignoring the acceleration head in the energy equation and using the measured slope as a single steady flow rating. Precautions in the selection and conduct of the measurements are needed to accurately capture the free-surface slope on short straight river reaches and low slopes.

Similarly to the RC-based methods, site selection is critical in order to ensure that the governing equations on which the method is based are applicable at the site. For slope-area method it is essential to avoid sites with significant change in the shape of the channel as they will affect the measured energy losses. The site selection criteria for SA method are well described by Darlymple and Benson (1967), ISO 1070 (1992), and Chaskar (undated) as shown in Table II.1 below.

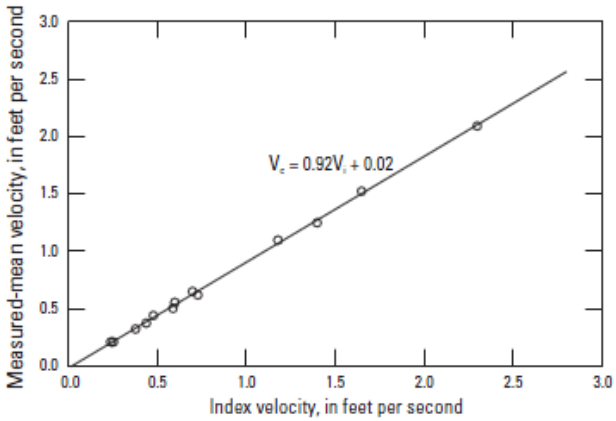


Figure II.6 Example of an index rating

Source: Levesque and Oberg (2012)

Table II.1 Important site selection criterion for implementation of SA method

<table>
<tr>
<td>a. Darlymple and Benson (1967)<ul><li>Reach length > 75x mean depth in the channel</li><li>Reach fall > the velocity head</li><li>> 0.50 ft</li></ul></td>
<td rowspan="2">c. Chaskar (undated report)<ul><li>Straight channel with stable bed and banks</li><li>Uniform cross-section</li><li>Reach length > 300m</li><li>Fall > 15 cm</li><li>No significant disturbances, draw-down or back-water effect</li><li>Flow normal to the prevailing wind</li><li>In-bank flow for all stages</li><li>Avoid windy site</li><li>Accessible at all times</li><li>Converging reach rather than diverging</li></ul></td>
</tr>
<tr>
<td>b. ISO 1070 (1992)<ul><li>No scour and fill</li><li>No abrupt change in the bed slope, uniform cross-section, and free from obstacles</li><li>Consistent bed material</li><li>Reach length: fall > 10x uncertainty in difference / fall > 20x uncertainty in measurement at one gage</li><li>No major tributaries</li><li>No overbank flows if possible</li><li>Consistent flow regime</li><li>Avoid significant curvature</li><li>No time lag in the reach (short distance)</li></ul></td>
</tr>
</table>

## II.3 Hysteresis in RC

### II.3.1 Introduction

The steady and uniform flow assumptions for constructing hQRCs are rarely valid in natural channels whereby the cross-section and slope are typically irregular in the longitudinal direction and the discharge varies in time when inflows occur. While the flow uniformity can be considerably limited by a careful selection of the gaging station site (see WMO, 2011), the effect of unsteadiness on RC is unavoidable as it is created periodically (by tides) or randomly (by surges, flood waves, dam operations or collapse).

Tides are oscillating unsteady events that, depending on the location, can repeat one several times per day. Among the random category, the non-oscillating unsteady flows produced by storm runoff directed to inland rivers are the most frequent. The passage of the storm wave can last minutes, hours, days or even more depending on the location, rainfall intensity and duration. Typically, the rising stage of the flood wave propagation is much shorter than the falling stage hence the associated acceleration rates are different for the two limbs of the hydrograph.

Most of the data and knowledge about hysteresis are associated with hQRCs as VQRCs are relatively new and the continuous slope area method has not been extensively applied. The hysteretic effect in hQRCs is illustrated in Figure II.7. If the flow is assumed steady for all moments of the hydrograph, the maximum cross-section velocity ($U_{max}$), the discharge ($Q_{max}$), and the depth ($h_{max}$) are reaching their peak at the same time as shown in Figure II.7 (a). For the steady assumption, the stage-discharge relationship is unique as prescribed by the dotted line in Figure II.7 (c). For unsteady flow situations, however, the three peaks are separate as illustrated in Figure II.7 (b) with $U_{max}$ are peaking first, followed by $Q_{max}$ and then $h_{max}$ (Graf and Qu, 2004). This differentiation is captured by the loop hQRC shown in Figure II.7 (c) that is distinct for rising and falling limbs of the hydrograph from the one-to-one steady RC. In the present context, the loop RCs are important as they account for the fact that: a) the maximum discharge and water stage do not arrive at the same time; and, b) for the same stage, the discharge is higher during rising limb than during falling limb (i.e., there are two different flows for a single stage). The available experimental data show that the differences between steady and unsteady hQRCs are significant for low gradient channel slopes exposed to large flow unsteadiness (Faye and Cherry, 1980; Fread, 1975; Fenton and Keller, 2001; Di Baldassarre and Montanari, 2009; Dottori et al., 2009) as shown in Figure II.8. The latter condition is quite typical during flood events when the RCs' accuracy matters most.

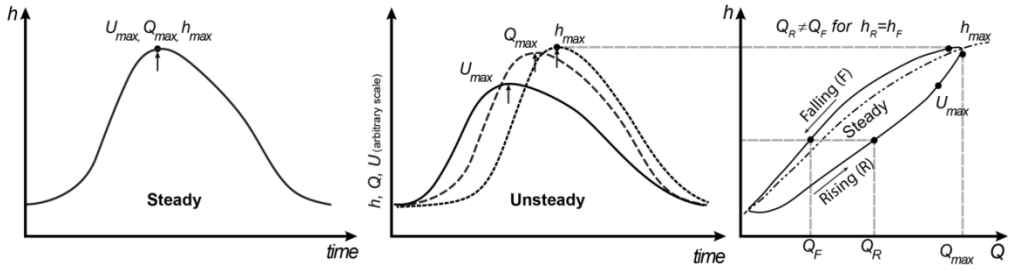


a) b) c)

Source: adapted from Graf & Qu (2004)

Figure II.7 Hysteretic behavior of dynamic flood routing

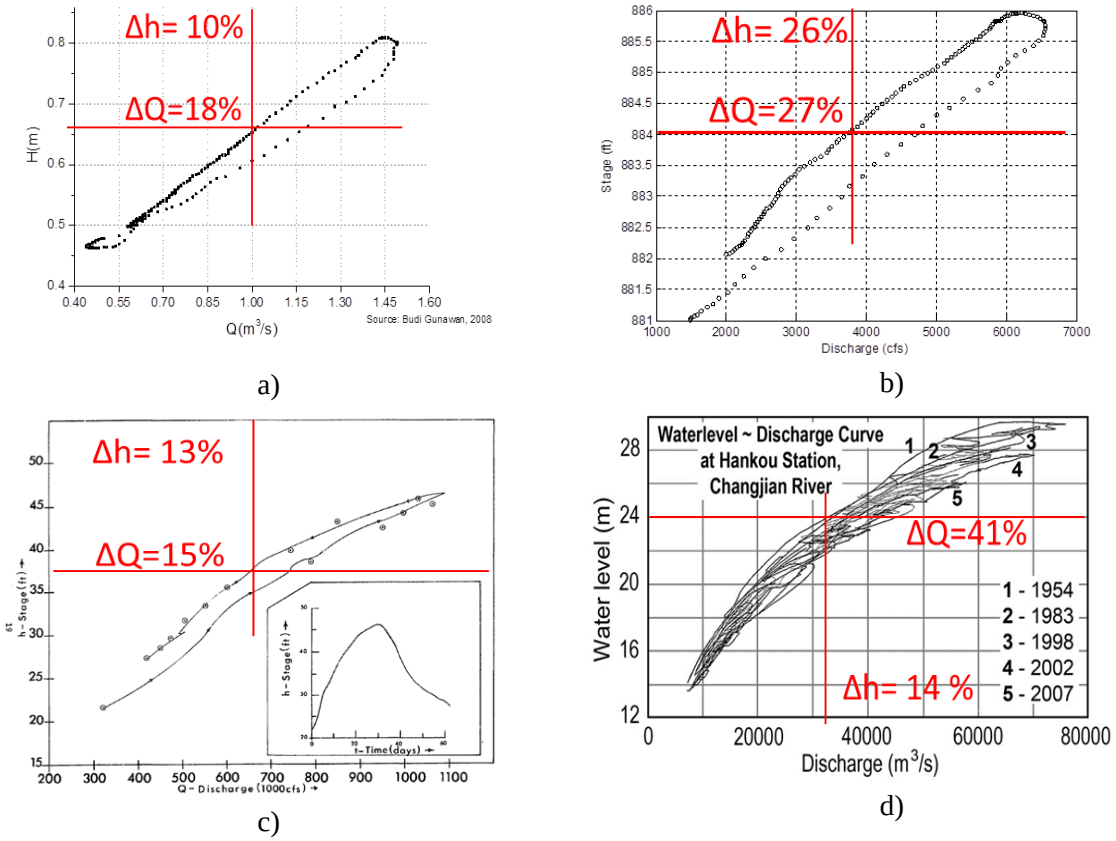


Figure II.8 Hysteresis evidenced by direct discharge measurements: a) Small stream: Blackwater in UK (Gunawan, 2010); b) Medium river: Chattahoochee river in USA (Faye and Cherry, 1980); c) Large river: Mississippi river in USA (Fread, 1973); d) Large river: Yantze river in China (Herschy, 2009)

### II.3.2 Current approaches to correct for the effect of hysteresis in hQRCs

In order to capture the loop or "dynamic" hQRCs, one has to track the event as it develops by measuring continuously both the depth and discharge at a sampling rate commensurate with the time scale of the flood wave propagation. However, currently this procedure is not easy to implement since individuals always has to be physically present at sites on right timing and therefore expensive as well. Alternatively, numerous relationships are available for adjusting the RCs, and most of them are associated with backwater and changing of discharge due to flow unsteadiness (Schmidt, 2002). Typically these relationships link general flow conditions to a "normal" steady condition on the single hQRC. Normal flow often refers to average, or typical flow conditions (Schmidt, 2002). The generic relationships between the discharge Q for any condition and the "normal" discharge $Q_n$ is provided by Knight (2006) as shown in equation II.10:

$$Q = \underbrace{\left(A\sqrt{R}\right)K\sqrt{S_0}}_{Q_n}\sqrt{\underbrace{1}_{a} - \underbrace{\frac{1}{S_0}\frac{\partial h}{\partial x}}_{b} - \underbrace{\frac{V}{gS_0}\frac{\partial V}{\partial x} - \frac{1}{gS_0}\frac{\partial V}{\partial t}}_{c}} \qquad \text{(II.9)}$$

*where A* is the flow cross section area; *V* is the mean flow velocity in the cross section; *R* is the hydraulic radius; *K* is a conveyance coefficient (which can be obtained from Chezy, Darcy-Weissbach, or Manning); $S_0$ is the bed slope; *h* is the flow depth; and *x* is the distance in streamwise direction. Discarding the last three terms of the equation, leaves us with the steady normal flow equation that it is assumed for the construction of the steady RCs.

Consideration of more than the first term in equation (II.9) provides a more realistic description of the flood routing (i.e., non-uniform, unsteady flow) that results in changes of the shape and position or loops in the curves. Specifically, the equation's terms indicate different types of flood routing model: kinematic wave (term *a* only), diffusion wave (terms *a* and *b*), and full dynamic wave (terms *a*, *b*, and *c*) as described

earlier in Figure II.2. The loop in the RCs for a site is commensurate with the type of flood wave. Dynamic wave produces the largest loop and kinematic wave practically does not produce a loop in the RCs.

The approaches developed to correct the steady (fixed) RCs and to approximate the unsteady (dynamic) RCs are semi-empirical, purely empirical (e.g., Davenport, 1943; Rutter et al., 1938; Linsley et al., 1949; Kennedy, 1984; Tawfik et al., 1997, etc.), simulated (e.g., Dottori et al., 2009), or analytical (e.g., Schmidt, 2002). The most often used approaches are the semi-empirical ones as the simulated and analytical approaches are using simplified assumptions that have scarcely been validated by direct measurements and the purely empirical one has no sound theoretical basis to justify the methods. The semi-empirical methods are typically based on the 1-D open-channel-flow equations applied to the empirically obtained curves. These methods are used to correct discharges made during unsteady flow conditions to determine steady RCs or to estimate discharge during periods of changing stage using the steady RCs as basis. Schmidt (2002) extensively reviewed the available methods and distinguished the following semi-empirical methods:

a) *discharge as a function of stage and water water-surface slope* (single-gauge methods mostly to account for discharge changing effects – Jones, 1916; Wiggins, 1925; Boyer, 1937; Lewis, 1939; Henderson, 1963& 1966, etc., multiple-gauge methods mostly to account for backwater effects – Hall et al., 1915; Blanchard, 1932; Perry, 1932; Eisenlohr, 1964; Chow, 1959; Fenton and Keller, 2001; Dottori et al., 2009, etc.)
b) *discharge as a function of stage , water-surface slope, and convective acceleration* (Mitchell, 1954), and
c) *discharge as a function of stage, water-surface slope, and convective and local acceleration* (Chatley, 1919; Boyer, 1939; Posey 1943; Gilcrest, 1950; Henderson, 1963, 1966; Fread, 1975 & 1982, etc.).

Since this study will examine the impact of unsteady flow hydraulics on the steady RCs, the full dynamic wave equation which includes the local acceleration term is the major focus (category *c)* above). In this regard, equation (II.9) shows that the discharge is a function not only of stage but also the water-surface slope, change in the area along the channel, and change of the flow with time (unsteadiness). Measurements or auxiliary relationships are needed to provide information for the additional terms in equation (II.9).

Table II.2 summarizes selected methods for the correction of the steady RC due to hysteresis or for the direct estimation of unsteady flows along with some additional specifications, and it is also important to note that these selected methods are all based on stage measurements at a single section. Considering the fact that most of the stream gage stations operated by USGS in the US are based on a single stage gage, the selected methods in Table II.2 were considered practicable.

The review of the hysteresis correction methods was well covered by the extensive study conducted by Schmidt (2002) and Dottori et al. (2009), and therefore will not be repeated here. In this study, emphasis will be placed only on two methods: Jones formula (the most well-known method; Jones, 1916) and Fread formula (full dynamic equation; Fread, 1975 & 1982). Especially the latter is the method adapted for this study because it captures the full dynamic aspects of the flood routing, and requires stage measurement at just one location given the single-curve stage discharge RC corresponding to normal (steady, uniform) flow.

Table II.2 Semi-empirical methods using stage measurements at a single section

| | Method | Data required | Flood Routing |
|---|---|---|---|
| 1 | Jones (1915) | $Q_o$, $S_o$, $c$, and $(\partial h/\partial t)$ | Kinematic approximation |
| 2 | Henderson (1966) | $Q_o$, $S_o$, $c$, $(\partial h/\partial t)$, and $r$ | Parabolic approximation |
| 3 | Di Silvio (1969) | $Q_p$, $Q_b$, $S_o$, $F_r$, $\varphi$, $T_r$, $T_f$, $A$, $A_p$, $\bar{A}$, $R$, $R_p$, $m$, and $p$ | Triangular approximation |
| 4 | Fread (1975) | $A$, $D$, $n$, $S_o$, $K$, $B$, $(\partial h/\partial t)$, $Q'$, $A'$, $\Delta t$, and $r$ | Parabolic approximation |
| 5 | Marchi (1976) | $Q_s$, $S_o$, $A$, $B$, m, and $(\partial A/\partial t)$ | Kinematic approximation |
| 6 | Faye and Cherry (1980) | $c$, $D$, $n$, $S_o$, $R$, $\alpha$, $(\partial h/\partial t)$, and $(\partial V/\partial t)$ | Kinematic approximation |
| 7 | Lamberti and Pilati (1990) | $Q_s$, $S_o$, $c$, $B$, $T_1$, $T_2$, $a$, $b$, and $\Delta t$ | Kinematic or quasi-kinematic approximation |
| 7 | Fenton (1999) | $Q_s$, $S_o$, $c$, $D_f$, $G$, $(\partial h/\partial t)$, $(\partial^2 h/\partial t^2)$, and $(\partial^3 h/\partial t^3)$ | Long wave approximation (Higher order advection diffusion approximation) |
| 8 | Perumal (2004) | $Q_s$, $S_o$, $c$, $B$, $(\partial h/\partial t)$, and $(\partial^2 h/\partial t^2)$ | Advection diffusion approximation |
| 9 | Boyer(1937) | $Q_o$ , $Q_m$, and $(\partial h/\partial t)$ to graphically determine $1/(cS_o)$ | Kinematic approximation |
| 10 | Lewis (1939) | $Q_o$ , $Q_m$, and $(\partial h/\partial t)$ to graphically determine *constant* $1/(cS_o)$ *(simplification to Boyer method)* | Kinematic approximation |
| 11 | Wiggins (1925) | $Q_o$, $S_e$, $c$, and $(\partial h/\partial t)$ | Kinematic approximation |
| 12 | Peterson-Øverleir (2006) | $n$, $m$, $N$, $\beta$, $S_o$, $h$, $(\partial h/\partial t)$, and nonlinear regression model with BFGS (Broyden-Fletcher-Goldfarb-Shanno) algorithm | Kinematic approximation |

*where*

$A$ – cross-sectional area

$A_p$– cross-sectional area corresponding to peak discharge

$\bar{A}$ – mean cross-sectional area corresponding to base and peak discharge

$A'$ – the cross-sectional area at time t-Δt

$a$ and $b$ – the first and second order incremental ratios (Lamberti and Pilati formula (1990))

$\alpha$ – the energy coefficient

$B$ – the width of the channel at the water surface

$\beta$ – dimensionless scale parameter (Peterson-Øverleir (2006))

$c$ – flood wave velocity

$D$ – the hydraulic depth

$D_f$ – the second order diffusion coefficient (Fenton formula (1999))

$F_r$ – Froude number

$G$ – the third order diffusion coefficient (Fenton formula (1999))

$h$ – the water depth

$K$ – wave celerity coefficient

$m$ – the exponent of the hydraulic radius in the friction law ($m$=1/2 for Chezy equation)

$N$ – dimensionless shape parameter (Peterson-Øverleir (2006))

$n$ – Manning roughness coefficient

$p$ – the exponent of the wetted area in the friction law ($p$=2 for Manning equation)

$Q_o$ – reference discharge at steady uniform flow condition

$Q_p$ – the peak discharge of the flood wave

$Q_b$ – the base discharge of the flood wave

$Q_m$ – the measured discharge

$Q_s$ – the steady flow discharge (given by the steady-flow RC)

$Q'$ – the discharge at time t-Δt

$R$ – hydraulic radius

$R_p$– hydraulic radius corresponding to peak discharge

$r$ – the ratio of the channel bottom slope to the entering wave slope (to account for wave subsidence)

$S_o$ – water surface slope at steady uniform flow condition (=channel bed slope)

$S_e$ – energy slope

$T_r$ – the duration of the rising limb

$T_f$ – the duration of the falling limb

$T_1$ and $T_2$ – the characteristic channel time (Lamberti and Pilati formula (1990))

$\Delta t$ – the computational time step

$(\partial h/\partial t)$ – the rate of change of water depth in time

$(\partial A/\partial t)$ – the rate of change of cross-sectional area in time

$(\partial V/\partial t)$ – the rate of change of mean flow velocity in time

$(\partial^2 h/\partial t^2)$ – a second order time derivate of the water depth

$(\partial^3 h/\partial t^3)$ – a third order time derivate of the water depth

$1/(cS_o)$ – the inverse product of water surface slope and the flood wave velocity

$\varphi$ – a variable for wave celerity (Di Silvio (1969))

II.3.2.1 Jones formula

Jones (1915) developed a method based on geometric analysis which accounts for the effect of discharge variation as a function of the stage and water surface slope. The final form of the equation is as follows:

$$Q = Q_r \left[1 + \frac{1}{S_r V_s}\frac{\partial h}{\partial t}\right]^{1/2} \quad \text{(II.10)}$$

*where* $Q_r$ represent a "reference or normal" discharge for the given stage; $S_r$ is a "reference or normal" water-surface slope; and $V_s$ is the water surface velocity. Jones defined the water surface velocity, $V_s$ as estimated by dividing the cross-sectional mean

velocity with the coefficient (0.9 for large streams and 0.85 for small streams), and the "reference or normal" condition is assumed the discharge and water-surface slope at a steady flow condition. Later, Gilcrest (1950), Henderson (1963, 1966), Posey (1943), Thomas (1937), and Chow (1959) proved that Jones formula can be derived by neglecting convective and local acceleration terms in equation (II.9) and assuming "uniform-progressive wave" which means the flood wave moves downstream with a constant velocity without changing its profile (Schmidt, 2002).

Changes to the standard form of Jones formula were brought by Henderson (1966) by substituting the water surface velocity, $V_s$, with the wave celerity, $v_w$ and assuming the steady and uniform flow condition. Equation (II.11) illustrates this alternative Jones formula:

$$Q = Q_o \left[1 + \frac{1}{S_o v_w}\frac{\partial h}{\partial t}\right]^{1/2} \qquad \text{(II.11)}$$

*where* $Q_o$ represent a "reference or normal" discharge for the given stage; $S_0$ is a "reference or normal" water-surface slope corresponding to steady-uniform flow condition; and $v_w$ is the wave velocity (celerity).

It is important to note that the original form of Jones formula was developed to correct the steady RCs based on stage measurements at a single section, but it still needs a second gage to establish the relationship which accounts for "reference or normal" slope varying with stage. In addition, Thomas (1937) recommended using a second gage to accurately estimate the wave celerity at the successive gage locations.

II.3.2.2 Fread formula

Fread (1975) developed a method based on the full one-dimensional unsteady channel flow equation. It can compute either stage or discharge once the temporal variation (time derivative) of the other variable is given. Stage or discharge can be provided by either observations or estimations. This method is different from many

others because it directly estimates either stage or discharge for a non-uniform unsteady flow conditions instead of correcting the steady state RCs.

Fread (1975) made the following assumptions for deriving his method.

a. Lateral flow is negligible.
b. The width of a channel is constant along the stream.
c. Energy losses due to friction and turbulence are described by Manning's equation.
d. The geometry of cross-section is assumed constant (no sediment deposition or erosion)
e. The bulk flood wave moves downstream as a kinematic wave (water surface slope approximately equals to the bottom slope).
f. The flow at the cross-section is controlled by the channel geometry, friction, bottom slope, and the type of flood waves.

By using the full one-dimensional unsteady channel flow equation, Manning's equation, and the space derivative introduced by Henderson (1966) (equation (II.12)), the final form of Fread method (1975) is shown in equation (II.13).

$$\frac{\partial y}{\partial x} = \frac{-1}{c}\frac{\partial h}{\partial t} - \frac{2S_o}{3r^2} \qquad \text{(II.12)}$$

$$Q - 1.486\frac{AD^{\frac{2}{3}}}{n}\left\{S_o + \left[\frac{A}{KQ} + \left(1 - \frac{1}{K}\right)\frac{BQ}{gA^2}\right]\partial h_s + \frac{\frac{Q'}{A'} - \frac{Q}{A}}{g\Delta t} + \frac{2S_o}{3r^2}\left(1 - \frac{BQ^2}{gA^3}\right)\right\}^{\frac{1}{2}} = 0 \qquad \text{(II.13)}$$

*where* $K = \frac{5}{3} - \frac{2A}{3B^2}\,dB/dh$ ; r is the ratio of the channel bottom slope to the entering wave slope; $r = \frac{56200(Q_P - Q_O)}{(h_P - h_o)\bar{A}\tau S_0}$ ; $\Delta t$ is the computational time step, in sec; $Q'$ is the discharge at time $t$-$\Delta t$, in ft$^3$/sec; $A'$ is the cross-sectional area at time $t$-$\Delta t$, in ft$^2$ ; $\partial h_s$ is the change in water surface elevation during the $\Delta t$ time interval, in ft/sec; $\bar{A}$ is the wetted cross-sectional area associated with average stage (mean stage between the base and peak); and $\tau$ is the time between base and peak flow (rising time), in days.

Equation (II.13) can be solved iteratively to determine either the rate of change of stage or discharge when either of those parameter values is known. However, the latter is typical in practical cases (i.e., discharge is unknown with known stage values). The Fread equation is known to be correct in kinematic or quasi-kinematic flow conditions in wide channels with approximately constant width of a channel (Fread, 1975).

### II.3.3 VQRC method

Most of the operating hQRCs and VQRCs based gaging stations assume that the flow in the channel is steady in the construction and use of RCs. The validity of this assumption was extensively studied for hQRCs leading to a plethora of algorithms for correcting the unsteady flow effect on the steady RCs as it is described in Section II.3.2. While it is expected that VQRCs are also affected by hysteretic behavior, the lack of analyses is mostly due to the fact that VQRCs have been recently implemented (in conjunction with the advent of the acoustic measurement technology - AVMs, ADCPs) leaving no enough time for their evaluation.

A few detailed laboratory studies (Tu and Graf, 1992; Nezu and Nakagawa, 1995; Song and Graf, 1996; Graf and Qu, 2004) and field measurements (Nihei and Sakai, 2006; Ferrer et al., 2013) show that the index- to mean channel velocity relationship is non-unique for unsteady flows. The notable differences between the channel velocities on the falling and rising stage of the unsteady flow hydrograph are: a) the departure of the vertical velocity profiles from the steady flow profile (see Figure II.9 (b)), and b) a loop RC between the channel depth and the corresponding channel velocity (Figure II.9 (c)). The experiments conducted by Song and Graf (1996) showed that during the passage of the hydrograph the velocities on the rising limb are larger than on the falling limb for the same flow depth. The difference was larger in the outer layer of the flow than in the inner layer where they stay close to the profile described by logarithmic law (Tu and Graf, 1992; Nezu and Nakagawa, 1995). These experiments also showed that the difference

increases with flow unsteadiness. The depth-averaged velocities, that intuitively represent the magnitude of the velocity profile over the entire cross section, are also different leading to a non-unique relationship between stage and mean channel velocity, as illustrated in Figure II.9 (c). If we extend these observations to the discharge obtained with VQRCs the result is that the discharges on the rising and falling limbs of the hydrograph are not following a one-to-one relationship similarly to what is substantiated by the loop hQRCs.

For illustration purposes, result of laboratory studies and field measurements are provided in Figure II.10. The figure illustrates that the stage-mean velocity relationship displays a hysteretic behavior (Figure II.10 (a)); the shape of the vertical velocity distribution and the flow depth are a function of the acceleration/deceleration phase during the event propagation (Figure II.10 (b)). There is field data documenting that hysteresis occurs not only in the hQRCs but also in the VQRCs, as illustrated in Figure II.10 (c), where it can be observed that the RCs display distinct curves for the rising and falling phases of the storm propagation compared to the steady RC. It also can be noted from in this figure that the significance of hysteresis is more prominent for large events.

The VQRCs are more suitable for event-based sampling than hQRCs as they simultaneously measure two variables with high frequency (typically one measurement every minute). If however, the protocols for building the VQRCs are not adjusted for capturing unsteady events, the validity of the steady curve for unsteady flows will be affected by uncertainties similar to those propagating in hQRCs. There are well-documented studies that address the hysteresis in VQRCs for tidally affected areas where unsteadiness continuously affects discharge gaging (Ruhl and Simpson, 2005; Sassi et al, 2011). The key element for capturing the oscillatory flow, including its unsteadiness aspects, is to appropriately relate the sampling frequency of the direct calibration measurements with the time scale of the event. For example, Ruhl and Simpson (2005) reports that in order to capture the dynamics of the flow in tidal area the construction of

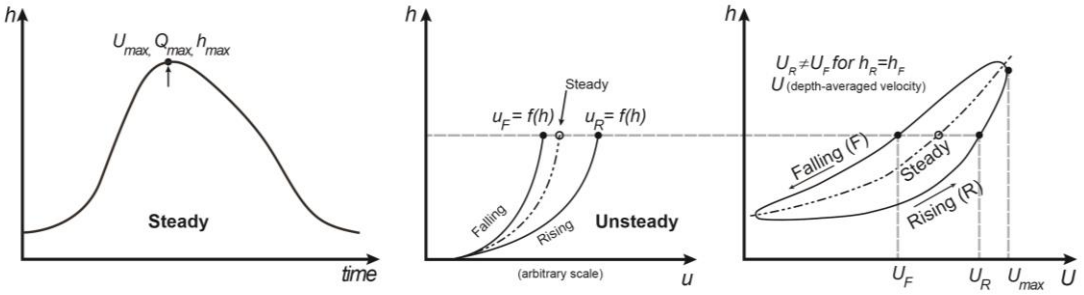


a) b) c)

Figure II.9 Hysteresis in channel velocity

Source: adapted from Graf and Qu (2004)

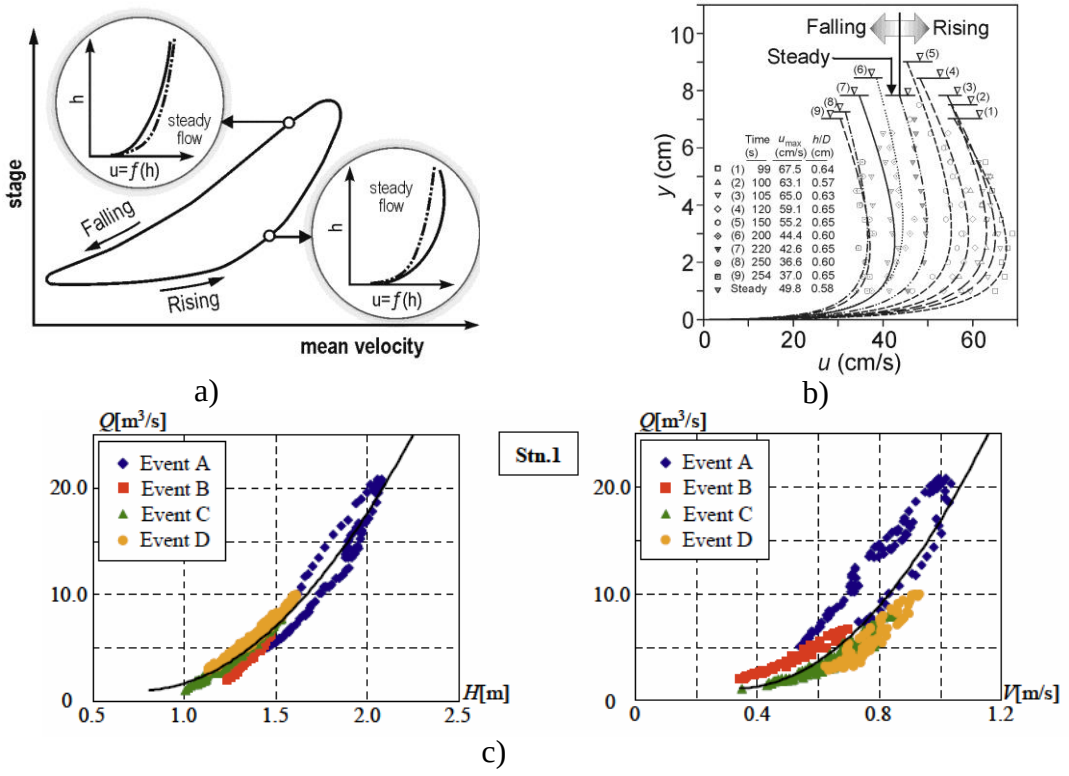


a) b) c)

Figure II.10 Experimental evidence illustrating hysteresis in VQRC: a, b) laboratory studies by Graf & Qu (2004) and Tu et al. (1995), respectively; c) field data by Nihei & Sakai (2006)

the VQRC has to be broken in several categories distinguishing between flood phases (e.g., flood-to-ebb, ebb-to-flood, and the transitions between the two flows). For each of these phases a specific index-velocity versus mean-velocity relationship is established through direct measurements. The authors specified that 50-120 direct discharge measurements were needed over 12- to 13-hour period to accurately capture the tide dynamics. Storm events in inland rivers are practically fractions of the oscillatory unsteadiness experienced by tidal flows, hence they also require appropriate sampling rate for the flow phases to accurately capture the distinct curves characterizing the rising and falling limbs of the hydrograph. Hydroacoustic instruments are well positioned to improve our capabilities to capture the dynamic RCs better than any time before.

### II.3.4 Continuous slope area (CSA) method

The conventional slope-area method is typically used to extend the hQRCs for high flows using surrogate information such as high water marks from large flood events as well described in Section II.2.4. More recently, the method attracts renewed interest with the advent of low-cost recording pressure transducers used to directly measure stages (Smith, et al., 2010). The CSA method was implemented on the Babocomari River in Arizona in 2002 by Smith et al. (2010) using eight pressure transducers deployed at both sides of the bank in four cross-sections. It was shown that CSA method can be used to compute continuous discharge hydrograph and to generate a unique hQRC. Example of monitoring stage and water surface slope along the reach for one of presented events in the report is shown in Figure II.11. More recently, the researchers from University of Arizona and USGS co-published the paper about the implementation of the CSA gaging method at a network of sand-bedded ephemeral stream channels in southeast Arizona (Steward et al., 2012), and concluded that the gaging efforts succeeded in monitoring and estimating discharges by comparing their estimates to the discharges estimated using sharp-crested weir equation at the most upstream location. However, both

implementations were conducted on steep channels where the hysteresis is not a major concern.

As it is described, the CSA method is not originally developed to monitor unsteady flows; rather it is developed to accurately compute a continuous discharge hydrograph based on steady flow assumptions with surveyed cross-sections and estimated channel roughness values. Therefore, while both conventional SA method and "original" CSA method are targeting on minimizing the effect of unsteady flows in developing a rating, there is a possibility that CSA method may adequately be used to address unsteady flow effects by continuously monitoring the change of water surface slope during flood wave propagation. In the following chapter, a case study of CSA method to continuously monitor hysteretic behavior of the unsteady flow will be examined.

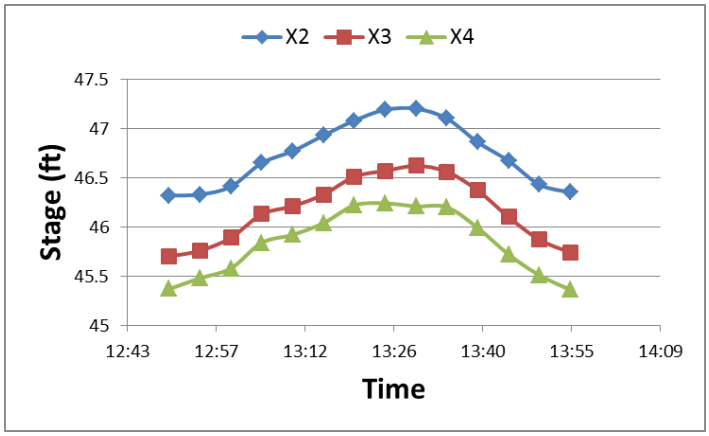


a)

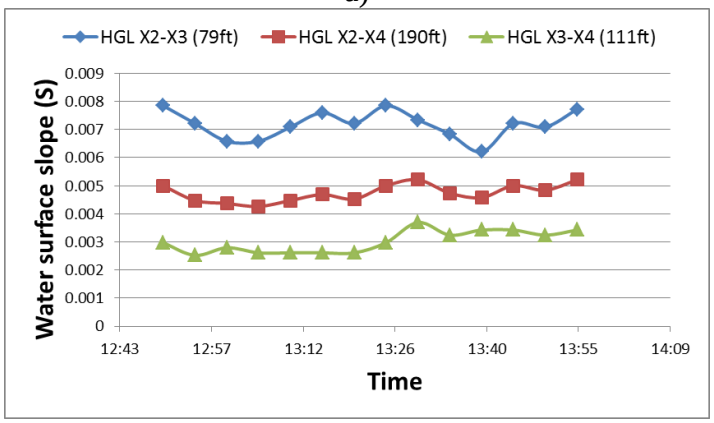


b)

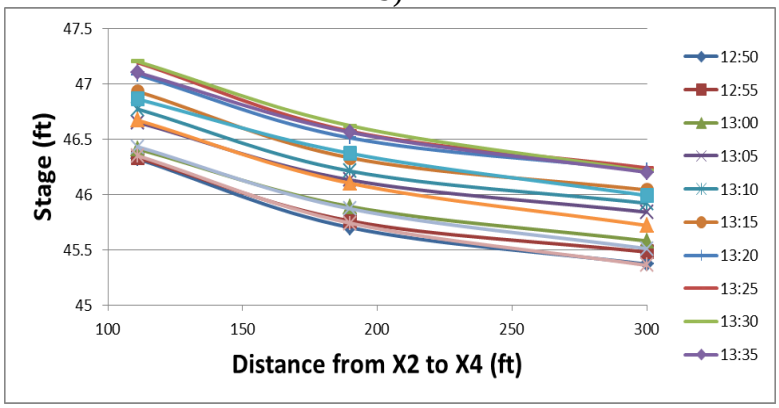


c)

Figure II.11 Stage and water-surface slope changes during an event along the reach: a) Stage time-series at different cross-sections; b) Water surface slope changes in time for various segments of channel reach; c) Water-surface profile changes in time along the reach

# CHAPTER III
# EXPERIMENTAL EVIDENCE AND CONCEPTUALIZATION OF UNSTEADY FLOW EFFECTS ON RC

## III.1 Introduction

The first section of this chapter will introduce the modification of Fread approach (1975) solving 1-D shallow flow equation to make it applicable for any size of the rivers. The method is subsequently implemented to both a small creek (Clear Creek in Iowa) and a mid-size river (Chattahoochee River in Georgia). In the second section, the newly developed method will be tested in conjunction with experimental evidence provided by direct ADCP measurements, virtual Horizontal ADCP (VQRC method), and the CSA method. In the last section of this chapter, hysteresis diagnostic protocols and significance of hysteresis parameters will be investigated using a 1D numerical model (HEC-RAS unsteady) and an analytical method (modified Fread equation).

## III.2 Modified Fread equation

### III.2.1 Methodology

Fread (1975) analytically derived an equation based on combining the Saint-Vernant and Manning's equations. The following assumptions were made by Fread (1975) for deriving the new modified equation:

- Wide rectangular channel, which assumes the hydraulic radius ($R$) is equal to the hydraulic depth ($D$)
- The channel width does not vary in time nor in the longitudinal direction (i.e., $\frac{\partial B}{\partial t} = 0 \;\; \frac{\partial B}{\partial x} = 0$ )

- The wave celerity coefficient (*K*) representing the ratio between the celerity of flood wave and the mean channel velocity is assumed constant (i.e., *K*=1.3). Wave celerity is a function of the shape of the channel.
- The lateral flow is negligible.
- The energy losses caused by channel friction and turbulence can be described by Manning's equation.
- The bulk of the flood wave moves as a kinematic wave, meaning the energy slope (*S*) is approximately equal to the channel bottom slope ($S_0$).
- Channel geometry, friction, the channel bottom slope and the shape of the flood wave are the key parameters controlling the flow at the section.

Among the aforementioned assumptions, the first three assumptions associated with the channel geometry prevent this equation from being used to small to mid-size streams, since accurately accounting for channel geometry is more critical for small streams. Therefore, the author herein suggested modified equation, and the original equation can be referred to Fread (1975).

The one-dimensional (1D) continuity and momentum equations can be written as:

$$\frac{\partial \mathrm{A}}{\partial \mathrm{t}} + \frac{\partial Q}{\partial x} = 0 \qquad \text{(III.1)}$$

$$S = S_0 - \frac{\partial y}{\partial x} - \frac{V}{g}\frac{\partial V}{\partial x} - \frac{1}{g}\frac{\partial V}{\partial t} \qquad \text{(III.2)}$$

*where A* is the channel wetted cross-sectional area; *Q* is the discharge; *y* is the flow depth; *V* is the channel mean velocity; *So* is the channel bottom slope; *S* is the energy slope.

The discharge Q is estimated using Manning's equation as shown below (English units):

$$Q = \frac{1.486}{n} AR^{2/3} S^{1/2} \qquad \text{(III.3)}$$

*where R* is hydraulic radius; *n* is Manning's roughness coefficient.

Equation (III.1) can be rewritten as:

$$\frac{\partial V}{\partial x} = -\frac{V}{A}\frac{\partial A}{\partial x} - \frac{1}{A}\frac{\partial A}{\partial t} \tag{III.4}$$

Equation (III.4) was derived without assuming the channel width does not vary in time and in the longitudinal direction.

Using the assumptions provided by Henderson (1966), Gilcrest (1950), Posey (1943) and Thomas (1937), one can remove the need for explicitly knowing how the water depth varies in the longitudinal direction. The term $\partial y / \partial x$ in equation (III.2) may be expressed as:

$$\frac{\partial y}{\partial x} = -\frac{1}{c}\frac{\partial h}{\partial t} - \frac{2S_0}{3r^2} \tag{III.5}$$

*where c* is the kinematic wave celerity; *r* is the ratio of the channel bottom slope to an average flood wave slope, $r = \frac{S_0}{\partial y / \partial x}$.

The last term in equation (III.5) is considered by Henderson (1966) to account for the effect of wave subsidence. Its expression is derived assuming a wide rectangular channel with a parabolic wave profile. Further investigation may be needed to find out the effect of the diffusion term on small to mid-size streams.

The speed of the kinematic wave, *c* is given by

$$c = \frac{\partial Q}{\partial A} \tag{III.6}$$

and it can also be expressed as

$$c = KV \tag{III.7}$$

*where K* is the wave celerity coefficient, which can be rewritten using equations (III.3) and (III.6) as:

$$K = \frac{5}{3} - \frac{2}{3}\frac{A}{P}\frac{dP}{dA} \tag{III.8}$$

*where P* is the wetted perimeter of the channel cross-section.

Fread (1975) assumed a constant wave celerity coefficient (*K*=1.3). The average flood wave slope (*r*) can be modified to account for variable wave celerity as a function of channel geometry.

$$r = \frac{43200(Q_p + Q_0)}{(h_p - h_0)\bar{A}}\Gamma S_0 K \tag{III.9}$$

*where* $Q_p$ and $Q_o$ represents the peak discharge and the discharge prior to the start of the flood, respectively, $h_p$ and $h_o$ represents the peak stage and the stage prior to the start of the flood, $\bar{A}$ is the average wetted area corresponding to the average stage $(h_p+h_o)/2$ and τ is the elapsed time between $h_o$ and $h_p$ in days.

Upon substituting equations (III.4) and (III.5) into the momentum equation (III.2), the following expression for the variable energy slope is obtained:

$$S = S_0 + \frac{1}{c}\frac{\partial h}{\partial t} + \frac{2S_0}{3r^2} - \frac{V}{g}\left(-\frac{V}{A}\frac{\partial A}{\partial x} - \frac{1}{A}\frac{\partial A}{\partial t}\right) - \frac{1}{g}\frac{\partial V}{\partial t} \tag{III.10}$$

The term $\frac{\partial A}{\partial x}$ in equation (III.10) can be expressed in a similar form to equation (III.5) based on kinematic wave equation as:

$$\frac{\partial A}{\partial x} = -\frac{1}{c}\frac{\partial A}{\partial t} - \frac{2S_0}{3r^2} \tag{III.11}$$

By substituting equation (III.11) into equation (III.10) and combining it with equation (III.3) one obtains the final form of a full dynamic equation which is applicable for streams of any size. This implicit equation can be solved iteratively.

$$Q - 1.486\frac{AR^{2/3}}{n}\left[S_0 + \frac{A}{KQ}\frac{\partial h}{\partial t} + \left(1 - \frac{1}{K}\right)\frac{Q}{gA^2}\frac{\partial A}{\partial t} + \frac{1}{g}\left(\frac{\frac{Q'}{A'} - \frac{Q}{A}}{g\Delta t}\right) + \frac{2S_0}{3r^2}\left(1 - \frac{Q^2}{gA^3}\right)\right]^{1/2} = 0 \tag{III.12}$$

*where* $Q'$ and $A'$ are the discharge and the cross-sectional area at time t-Δt

### III.2.2 Implementations: Clear Creek and Chattahoochee River

The suggested full dynamic equation (III.12) is implemented for a small stream (Clear Creek) and for a medium river (Chattahoochee River). The following analysis will focus more on the small stream.

*Clear Creek*

Clear Creek is situated nearby Oxford in the state of Iowa where an USGS stream gage station (05454220) is located. The storm event on April 14 - 17 in 2012 is selected for analysis because there are no complexities associated with the shape of hydrograph, in which often multi-peaks are present. The cross-sections were surveyed three on September in 2011, July in 2012, and September in 2012 after a significant storm passed using the Trimble R8 RTK instrument. No significant morphological changes have been observed. In the following analysis, the cross-section surveyed on July, 2012 is used, since it has the largest number of measured points. The parameter values associated with area ($A$), hydraulic radius ($R$), wetted perimeter ($P$), wave celerity coefficient ($K$) and the rate of change of area in time ($dA/dt$) are all obtained based on this cross-section geometry. The Manning's roughness coefficient, $n$ is estimated using USGS stage-discharge records and surveyed cross-sections based on equation (III.3). The Manning's roughness coefficient can be subsequently estimated based on area and hydraulic radius obtained for this cross-section, the discharges from USGS steady-based stream gage data, and the bed slope ($S_o$=0.0007) surveyed using the Trimble R8 RTK. The survey used the Iowa RTN Network at the base flow condition. Surveying the bed slope using the GPS device along the river channel is not ideal because measurements are subject to human errors and also the vertical accuracy of the instrument (typically ±2cm) is limited. Despite these shortcomings it was the best available choice at the time of measurements. To obtain more accurate measurements of the bed slope requires at least two gages. The measurement duration at each point was 8 seconds to get averaged values, and 12 points

were sampled over 2,500ft of the channel reach. The surveyed bed slope was also compared to the slope estimated using a LiDAR-based 1m resolution digital elevation model (DEM). The agreement between the values predicted by the two methods was good. Figure III.1 shows three surveyed cross-sections from 2011 to 2012, the measured water surface elevation points displayed on DEM and the estimated channel bed slope based on a linear regression equation. Figure III.2 shows photos taken at the beginning of this study in 2011. Figure III.3 illustrates the various activities made since the beginning of the study in 2011.

Based on this information, three tests have been analyzed as follows:

***In Test 1***, the performance of the formula proposed by Fread (1975) is compared to the suggested dynamic equation. The formula proposed by Fread (1975) was originally intended to be used in large rivers where the assumption that the hydraulic radius is equivalent to flow depth (hydraulic depth) is acceptable. This is not the case for small rivers. The major differences between the predictions given by the two equations are primarily due to this assumption. Figure III.4 shows the event discharge hydrograph for this analysis. Figure III.5 shows that the suggested formula (red) is in very good agreement with the direct discharge measurements (green) collected using a TRDI StreamPro ADCP during the falling limb of the storm event. Several attempts have been made to track the storm event during the time the discharge is increasing, but we were not successful due to practical and technical difficulties. Therefore, the validity of this algorithm is also verified using other discharge data sets measured in a mid-size river in Spain. The details will be presented in Section III.3.1. Figure III.5 also indicates that there are significant differences in the discharge predictions between the original and the modified formula represented by blue and red lines, respectively. The black dotted line in Figure III.5 represents the USGS steady rating curve. Figure III.6 represents how the relative magnitude of the discharge differences vary with time (max ~ 7.5%) with respect to discharges estimated based on the modified formula. Figure III.7 shows the absolute

temporal differences in the estimation of the hydraulic radius and hydraulic depth at this small stream. Figure III.8 visualizes the relative differences (~ max 1%) in estimating the energy slope term with respect to the original equation given by Fread (1975). Results in Figure III.8 may indicate that the modified formula should be considered as a better solution even though the differences are not very important. Figure III.9 describes the temporal variation of the estimated uncertainties due to unsteady flow relative to the steady-state discharges. The original equation proposed by Fread was not able to converge to the steady-state condition even at the end of the event (+3%) indicating that it gives systematic errors. The main reason for these errors is the assumption made about the hydraulic depth.

***In Test 2***, the contributions of each of the energy slope terms (terms *b* through *e* – *see below*) relative to the bed slope (term *a*) were investigated. Before the beginning of the storm event, the energy slope ($S_f$) is equal to the bed slope ($S_o$) due to the steady-state flow assumption (terms *b* through *e* are zero). Subsequently, the energy slope is changing with time depending on the contributions of each term. The left column in Figure II.10 gives these relative contributions in time. The right column demonstrates the number of occurrences (frequency in y-axis) throughout the event. The x-axis in the right column of the graphs represents the normalized values of each term relative to the bed slope. Therefore, the positive (+) or negative (-) values indicate either steeper or milder slopes than the bed slope, respectively. As one can see in Figure II.10, term *b* has the greatest contribution. This indicates that that pressure force caused by the rapid changes in water depth with time has the largest effects. The other terms that show non-zero contributions are term *e*, term *d*, and term *c* in their order of magnitude. Similar to findings reported in other studies, the spatial and temporal velocity changes representing terms *c* and *d* are fairly small (<1%). However, it is also very important to note that this may change depending on the specific event type analyzed and the site conditions.

$$S_f = S_o + \left[\frac{A}{KQ} + \left(1 - \frac{1}{K}\right)\frac{BQ}{gA^2}\right]\frac{\partial h}{\partial t} + \frac{\frac{Q'}{A} - \frac{Q}{A}}{g\Delta t} + \frac{2S_o}{3r^2}\left(1 - \frac{BQ^2}{gA^3}\right)$$

Term *a* | Term *b* | Term *c* | Term *d* | Term *e*

In addition, Figure III.11 (a) and III.11 (b) shows how various moments (labeled as 1 through 6) in discharge hydrograph where the energy slope is abruptly changing affect the shape of the RC. These various moments are indicated on the Figure III.11 (c) illustrating the contribution of each energy slope term in time. Figure III.11 (c) also indicates that the pressure term (blue line) dominates the other terms.

***In Test 3,*** three different methods for estimating the wave celerity coefficient (K) were tested. For convenience, the mathematical expressions are presented below. Equations (III.8), (III.13) are based on the modified Fread and the original Fread (1975) equation. In equation (III.14), the value of *K* is assumed to be constant (Corbett, 1943; Linsley, et al., 1949) which is common assumption in many natural channels.

$$K = \frac{5}{3} - \frac{2}{3}\frac{A}{P}\frac{dP}{dA} \tag{III.8}$$

$$K = \frac{5}{3} - \frac{2}{3}\frac{A}{B^2}\frac{dB}{dh} \tag{III.13}$$

$$K = 1.3 \tag{III.14}$$

Figure III.12 compares the variations of the wave celerity coefficients estimated using the three equations during the event as a function of stage. As one can see, equation (III.8) (red) predicts slightly narrower range of values than equation (III.13) (blue). The value given by equation (III.14) (black) represents approximately the median value within the variation of *K* given by the other two equations.

Figure III.13 describes the relative uncertainty in Q based on the modified Fread equation using different wave celerity coefficients. Overall, there are no great differences observed between the modified and the original Fread equations. However, when a constant *K* is used, the discharge is overestimation by about 2% over the rising limb. Therefore, the uncertainty in estimating the discharge ranges from about -5% (falling limb) to 13% (rising limb) when a constant *K* is used. The uncertainty is slightly smaller, ranging from -4% (falling limb) to 11% (rising limb), when a variable *K* is used.

*Chattahoochee River*

The Chattahoochee River is located in northeast Georgia within the upper Chattahoochee river basin. The basin size is about 3,550 square miles. The total length of the streams within the river basin is close to 250 miles. Chattahoochee River is about 17 miles long. 11 USGS gage stations are present along the river reach. The most upstream gage station is Buford Dam and followed by Georgia Highway 20, Littles Ferry Bridge, Georgina Highway 120 and Georgia Highway 141, as indicated in Figure III.14 (red circles from the top). Except for Buford Dam, the other four stations are the locations where Faye and Cherry (1980) collected the data and they subsequently used to test their 1D hydrodynamic equation.

Faye and Cherry (1980) developed a mathematical model based on the 1D continuity and momentum equations. The final form of their equation is similar to Fread's (1975) model. However, their equation is applicable for highly dynamic flow situations. Faye and Cherry model is different from the model given by Fread (1975) because:

- The lateral distribution of the mean velocity is accounted for via an energy coefficient, α, which accounts for the convective acceleration of the unsteady flow.

- The wave subsidence term proposed by Henderson (the last term in equation (III.5)) is neglected.
- The wave velocity is directly measured based on two gage stations using the peak discharge timing.
- Rather than simulating a natural flood wave, the model is targeted for simulating highly dynamic flows created by hydropower dam operation in mid-size rivers (the channel width: 150-300ft).
- Relatively accurate geometric information is used for the model obtained using sounding or Fathometer. Fread (1975) assumed simple prismatic channel.

However, Faye and Cherry also assume that hydraulic radius is equal to the hydraulic depth, similar to Fread (1975).

Discharge and stage measurements were recorded every 5 min and the channel bed slope and Manning's roughness coefficient values were estimated based on data collected between March 20 and 23 1976. The values of these variables are presented below in Table III.1. Manning's roughness coefficient was measured three times at different flow conditions. It was then linearly interpolated for unknown values. In Table III.1, results at Little Ferry Bridge are not included for comparison with the modified Fread's equation because this location is affected by large-scale dredging and pumping operations which result in significant scour at the channel bottom.

Figures III.15-17 describes the comparison between the modified Fread's formula and Faye and Cherry's simulations. Figure III.15 present results for Georgia Highway 20, very close location of Buford Dam. Results in this figure shows that the modified Fread formula gives significant errors during the falling limb of the hydrograph. It seems that this is because Fread equation was not able to give correct predictions at times when the rise or fall of the stage is too fast. However, the other two cases presented in Figures III.16 and III.17 show that the modified Fread equation is able to successfully compute

the unsteady flow. The solid squares in Figure III.17 (d) and III.17 (e) represent the USGS stage-discharge rating curve.

The cases for Georgina Highway 20 are further analyzed to better understand the sensitivity of the solution to the rate of change in stage. Figure III.18 describes the changes in the shape of the rating curve due to the change in *dt* from 5 minutes (original time interval) to 10 minutes, and 15 minutes successively. The results with 5 minutes and 10 minutes indicate significant errors are present. However, this is not the case in the results obtained with 15 minutes. Figure III.18 (c) which is based on using a *dt* of 15 minutes shows very similar results to those obtained using Faye and Cherry (1980) method. However, this result also implies that the modified Fread equation has limitations with this respect.

Table III.1 Summary of channel parameters

| Station name | Date in 1976 | Time | Discharge ($ft^3/s$) | Hydraulic radius (ft) | Effective channel slope (ft/ft) | Mean flow velocity (ft/s) | Manning's $n$ ($s/ft^{1/3}$) | Maximum flow depth (ft) |
|---|---|---|---|---|---|---|---|---|
| **Georgia Highway 20** | March 22 | 0700 | 577 | 4.26 | 0.00024 | 0.68 | 0.089 | 6.59 |
| | March 22 | 1500 | 4,370 | 8.80 | .00024 | 2.02 | .049 | 12.42 |
| | March 23 | 1135 | 8,660 | 11.60 | .00024 | 2.71 | .044 | 16.63 |
| **Littles Ferry Bridge** | March 20 | 1505 | 774 | 5.13 | .00036 | .96 | .088 | 10.61 |
| | March 22 | 1700 | 4,180 | 9.66 | .00036 | 2.31 | .056 | 16.48 |
| | March 23 | 1240 | 7,450 | 12.20 | .00036 | 3.10 | .048 | 19.59 |
| **Georgia Highway 120** | March 22 | 0920 | 940 | 3.45 | .00036 | 1.65 | .039 | 4.64 |
| | March 22 | 1805 | 4,320 | 8.42 | .00036 | 2.97 | .039 | 10.46 |
| | March 23 | 1330 | 7,000 | 10.10 | .00036 | 3.63 | .036 | 12.49 |
| **Georgia Highway 141** | March 22 | 1055 | 1,080 | 3.92 | .00031 | 1.34 | .049 | 6.92 |
| | March 22 | 1620 | 3,880 | 6.80 | .00031 | 2.62 | .036 | 10.18 |
| | March 23 | 1440 | 6,550 | 8.62 | .00031 | 3.39 | .033 | 12.29 |

Source: Table 2 from Faye and Cherry (1980)

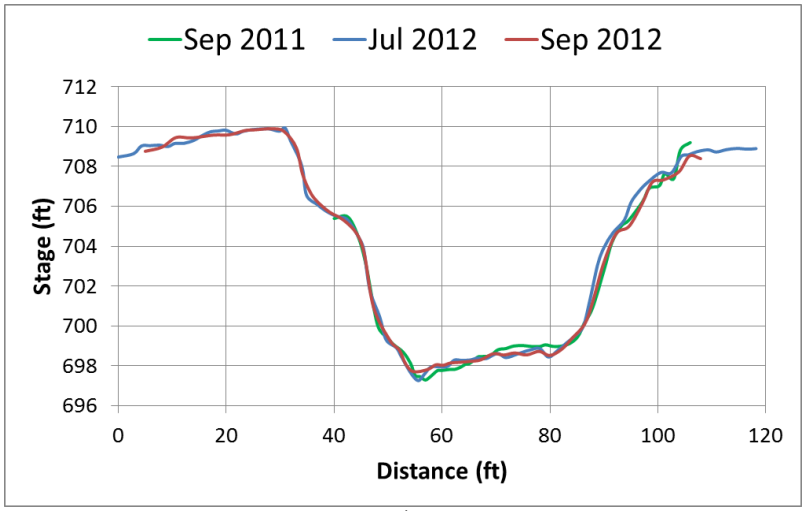


a)

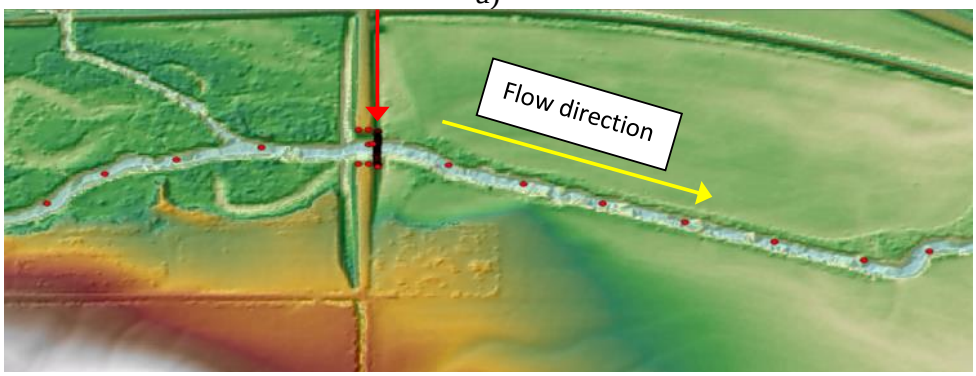


b)

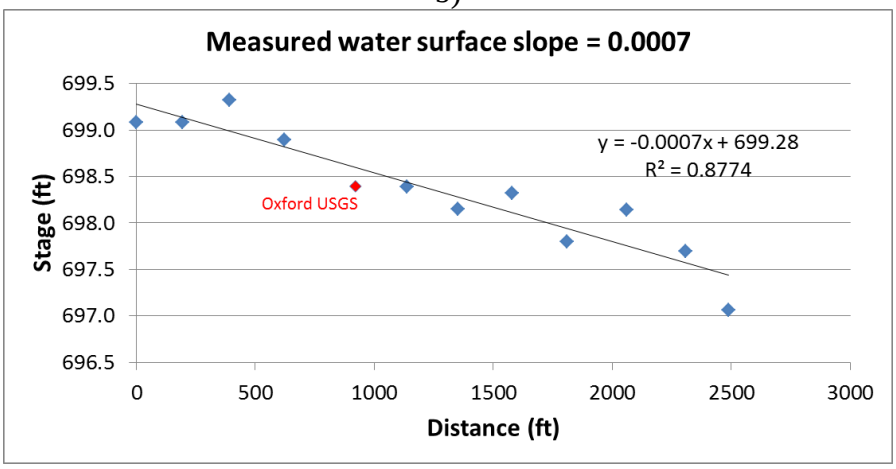


c)

Figure III.1 Measured cross-sections and water surface slope: a) cross-section comparisons; b) measured points on DEM; c) estimated water surface slope based on using a linear regression equation

a)


b)

c)

Figure III.2 Site conditions at Clear Creek on April 4, 2011: a) Upstream view; b) Bridge view c) Downstream view

a) June 17, 2011

b) September 30, 2011

c) April 4, 2012

d) April 15, 2012

e) March 10, 2013

Figure III.3 Site conditions and activities at Clear Creek: a) Velocity measurements using PIV and Flowtracker ADV on monitoring steel bridge; b) discharge measurements at low flow conditions using a FlowTracker ADV; c) discharge measurements using an RDI StreamPro ADCP for uncertainty analysis; d) discharge measurements (~350cfs) conducted during the falling limb of the storm event using an RDI StreamPro ADCP (this was the selected event for the analysis); e) extreme flood (~2300cfs) –downstream view

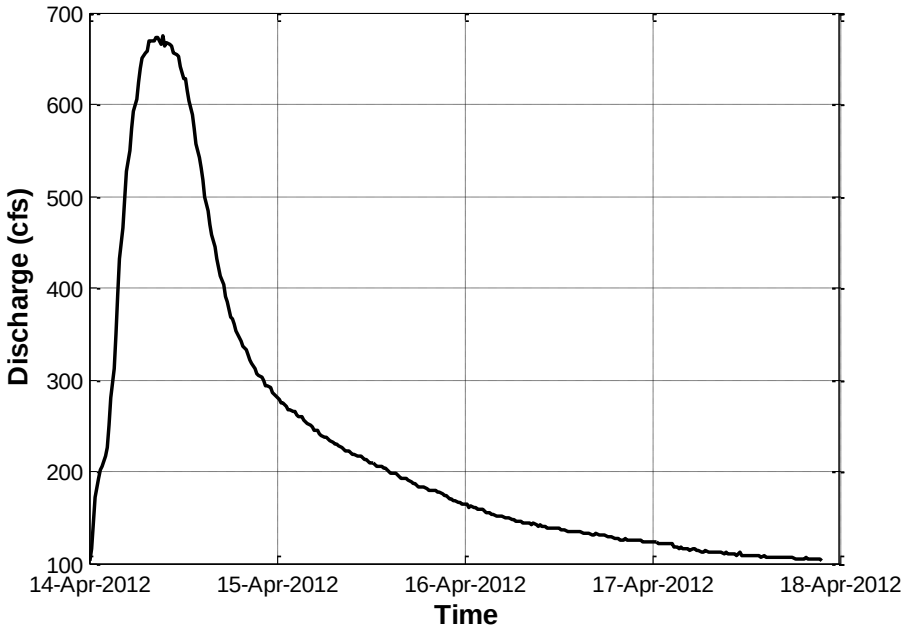


Figure III.4 Event discharge hydrograph based on USGS steady RC

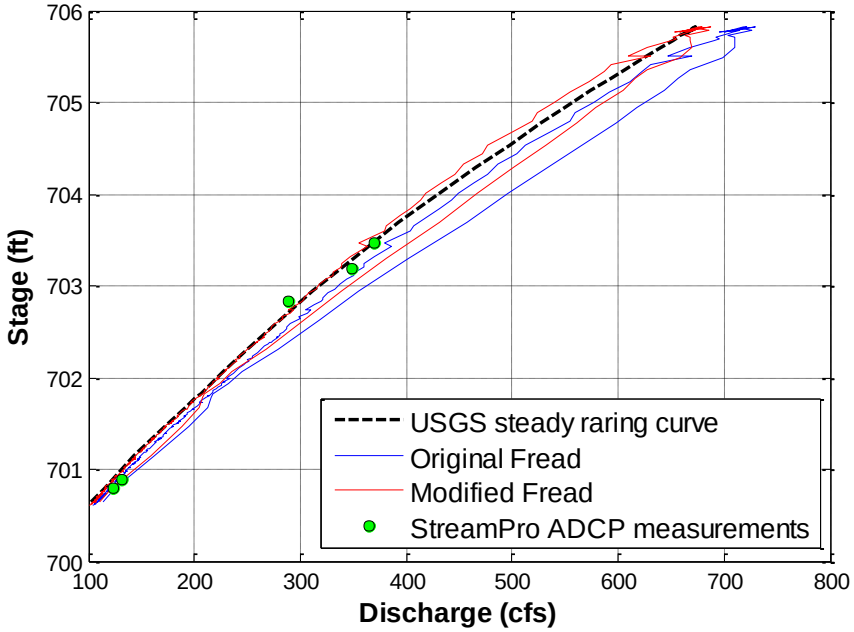


Figure III.5 hQRC comparisons

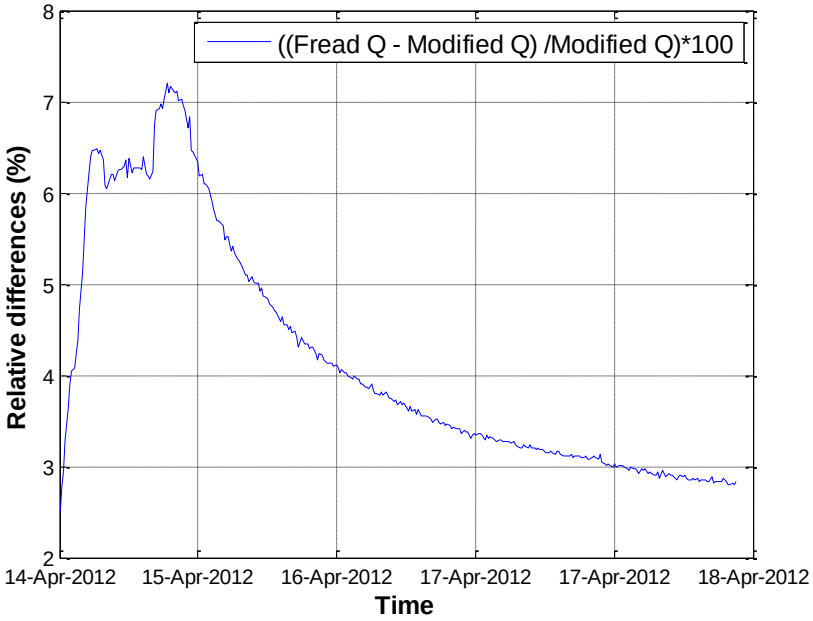


Figure III.6 Relative differences (%) in estimating the discharges

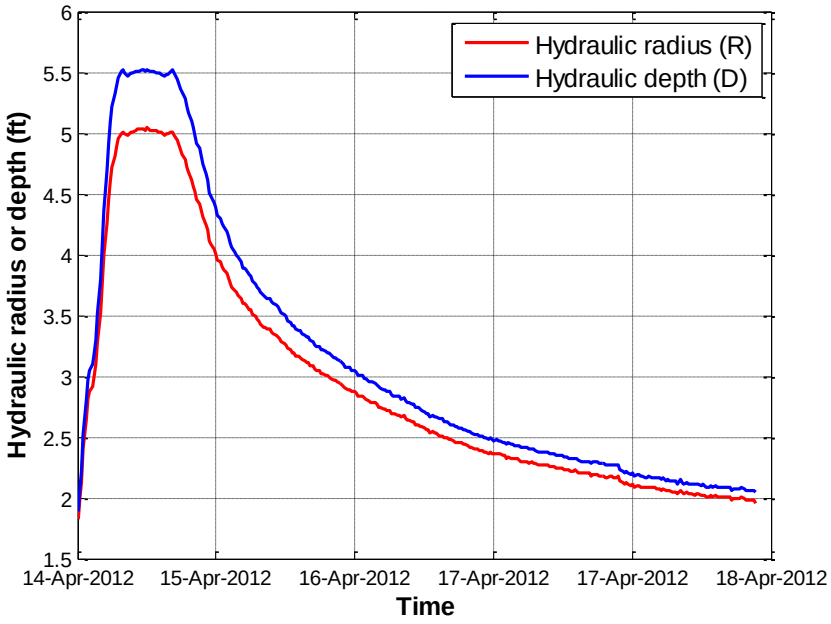


Figure III.7 Temporal variation of the absolute difference between the hydraulic radius and the hydraulic depth

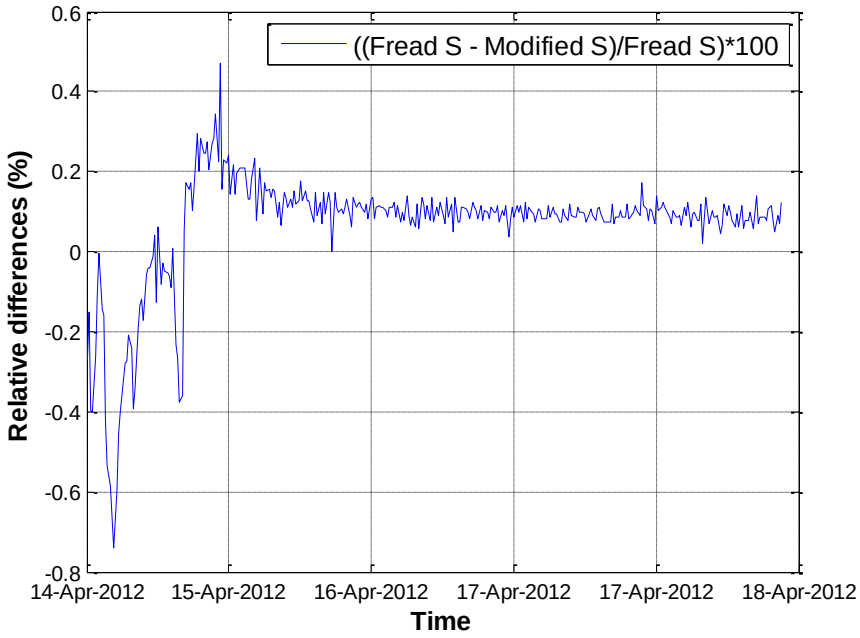


Figure III.8 Relative differences (%) in estimation of energy slope

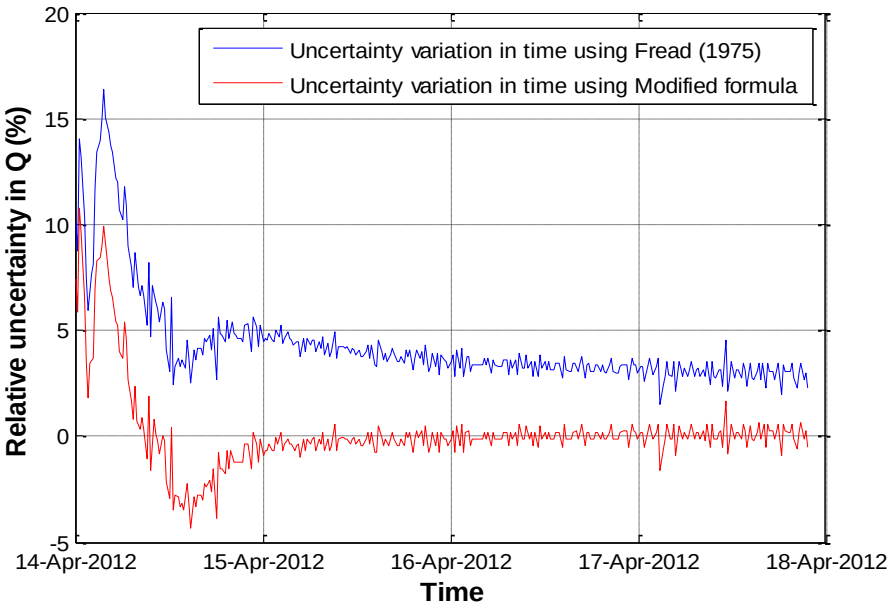


Figure III.9 Comparison of computed uncertainties predicted by original Fread (1975) and the modified equation with respect to steady USGS discharges

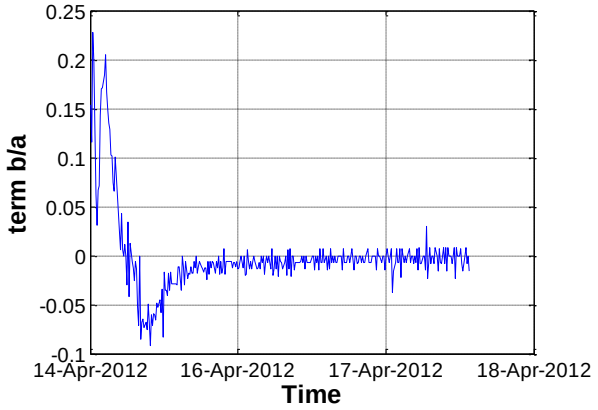


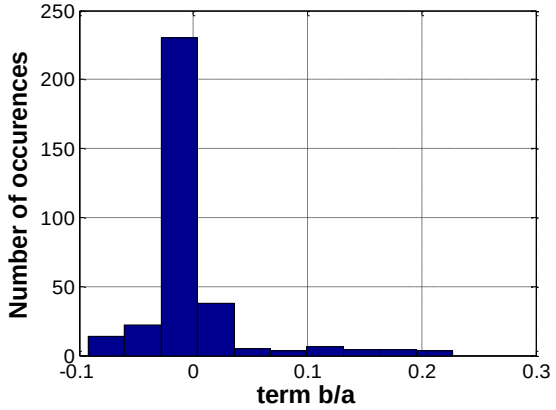


a) Term: *b/a* – contribution of pressure term relative to *the bed slope* (-10% to +25%)

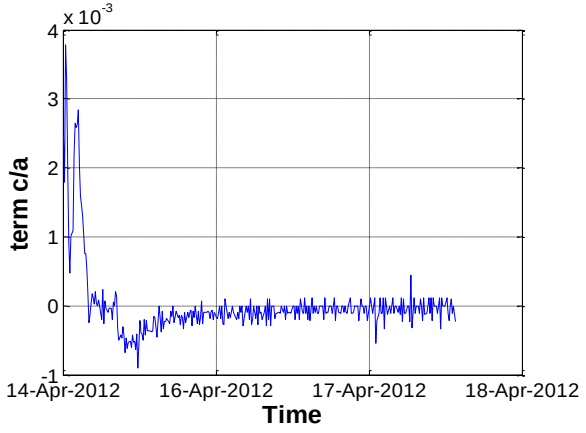


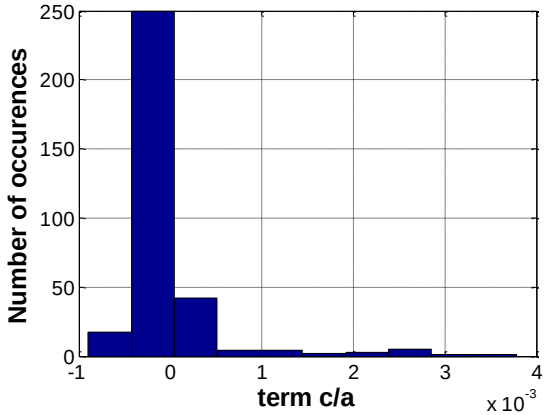


b) Term: *c/a* – contribution of convective acceleration term relative to *the bed slope* (-0.1% to +0.4%)

Figure III.10 Contributions of the terms in the modified Fread equation (Continues on next page)

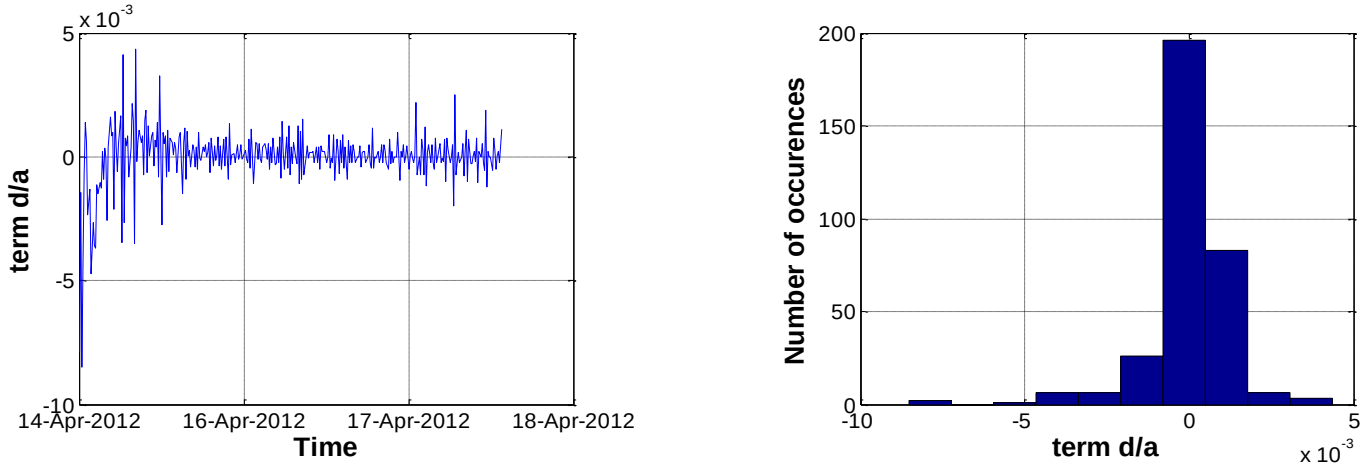


a) Term: *d/a* – contribution of local acceleration term relative to *the bed slope* (less than ±1%)

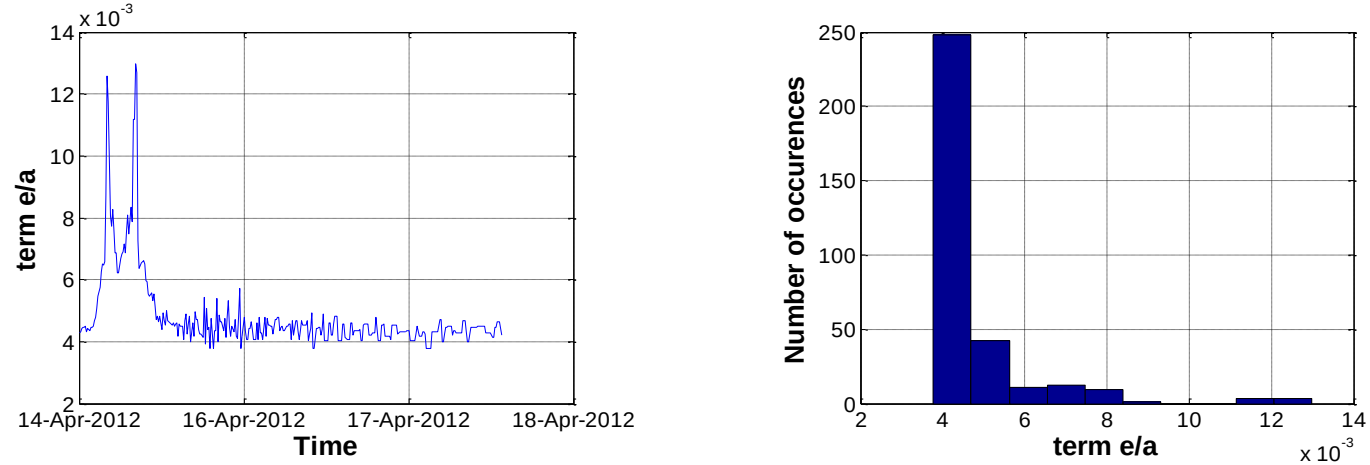


b) Term: *e/a* – contribution of wave subsidence term relative to *the bed slope* (+0.4% to +1.4%)

Figure III.10 Contributions of the terms in the modified Fread equation

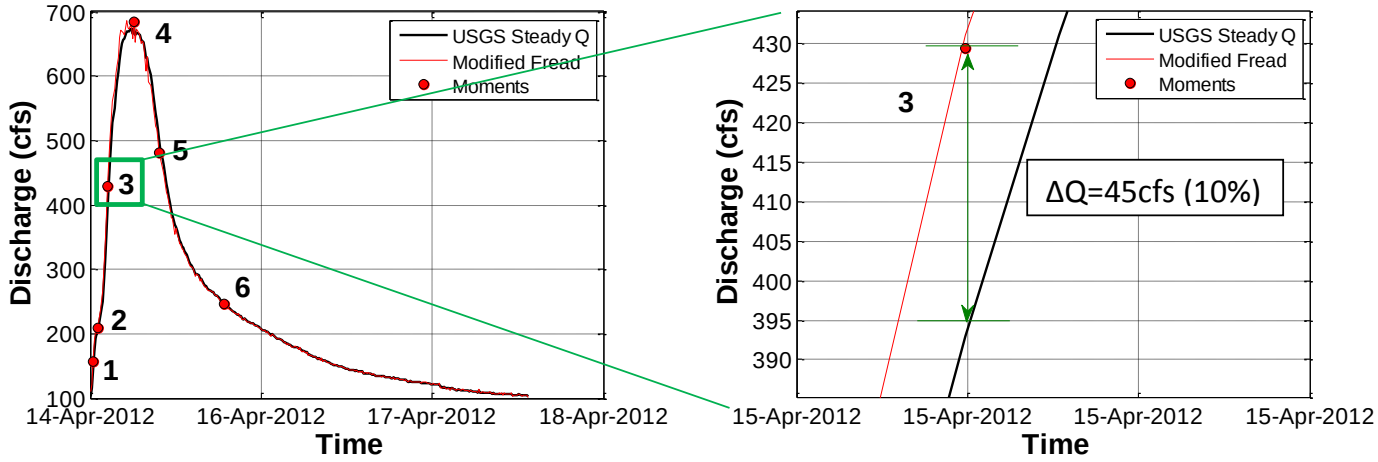


a) Snapshot of representing discharge uncertainty due to unsteady flow at *moment 3*.

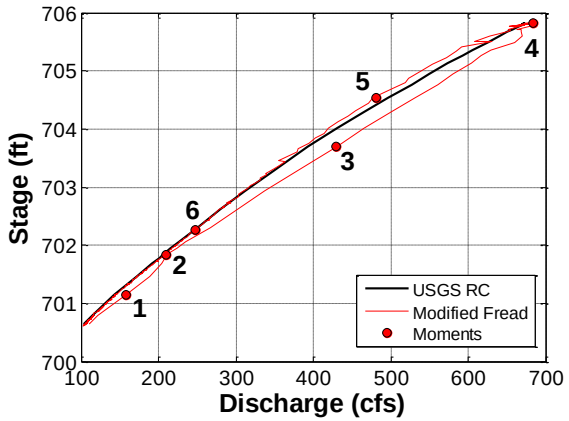


b) Various moments on unsteady rating curve

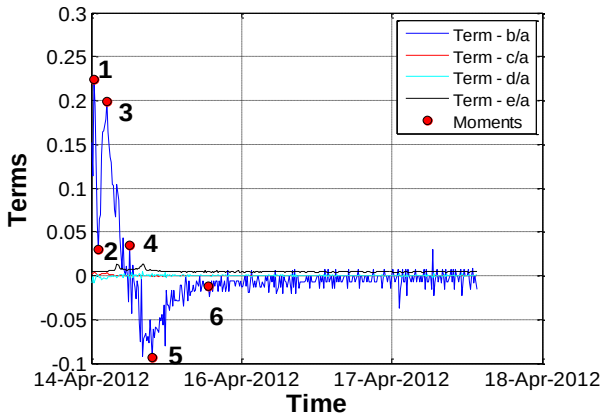


c) Various moments on energy slope terms

Figure III.11 Effects of energy slope changes in time on the shape of the RC

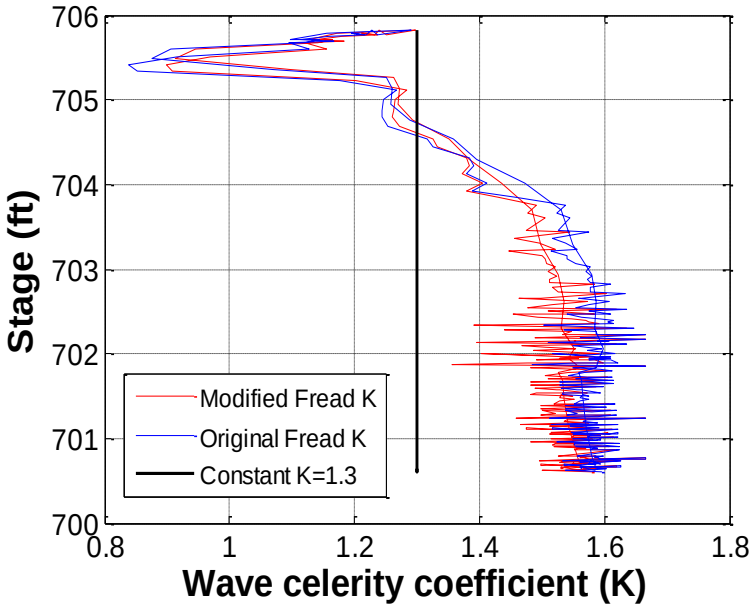


Figure III.12 Relative differences (%) in estimation of the energy slope

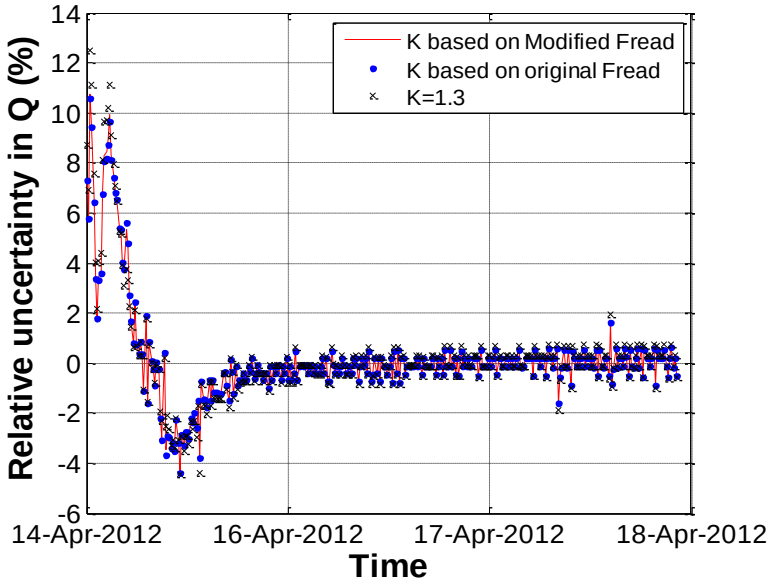


Figure III.13Relative differences (%) in estimation of the energy slope

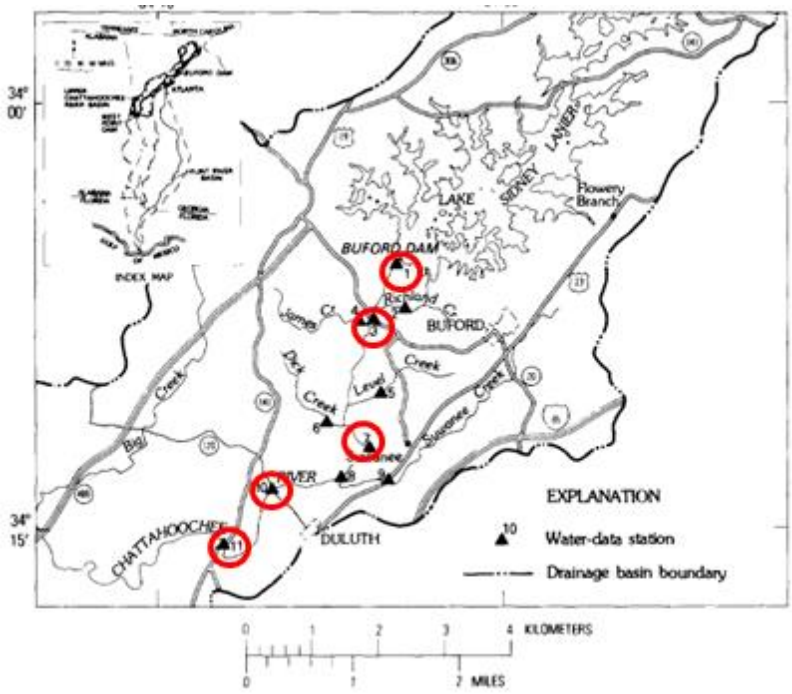


Figure III.14 Chattahoochee River location in Georgia State

Source: Faye and Cherry (1980)

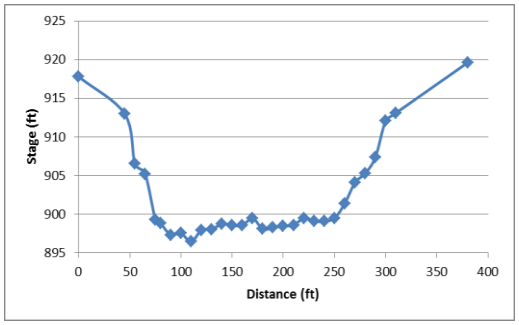


a) Cross-section

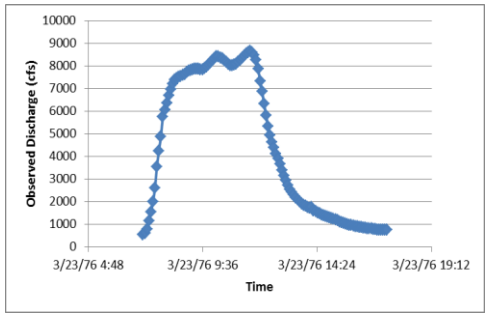


b) Observed discharge hydrograph

- Channel slope: 0.00024
- Manning's roughness: Varies with stages (0.089 at 903.02ft, 0.049 at 908.85ft, and 0.044 at 913.06ft. Linear interpolation between known values)

c) Parameter values

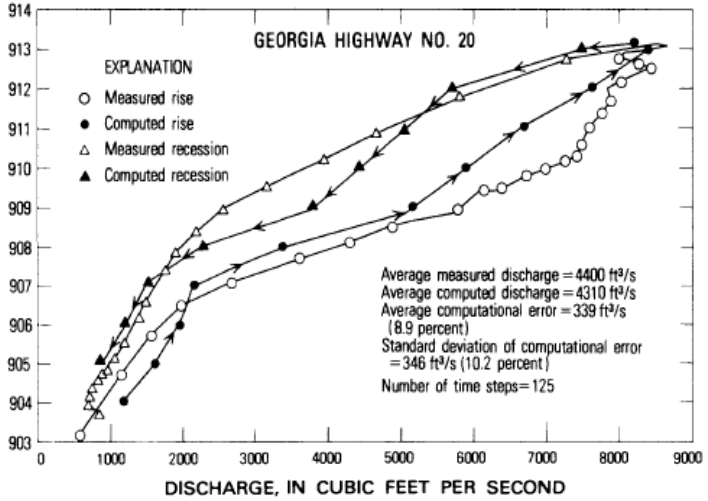


d) Faye and Cherry (1980)

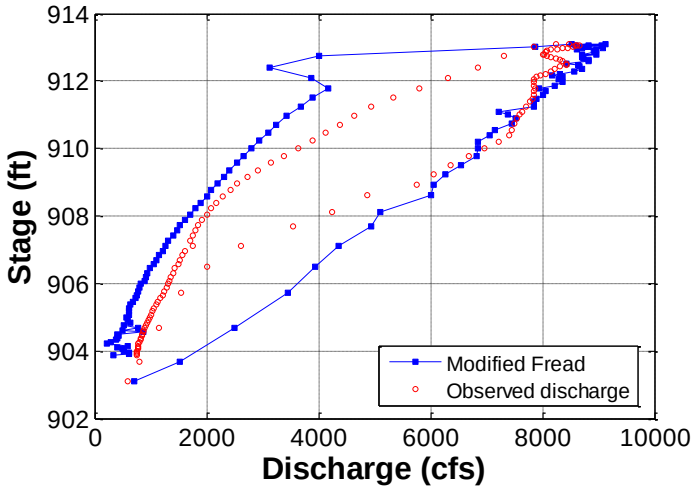


e) Modified Fread

Figure III.15 Simulation comparison between Faye and Cherry (1980) and the modified Fread equation at Georgia Highway No.20

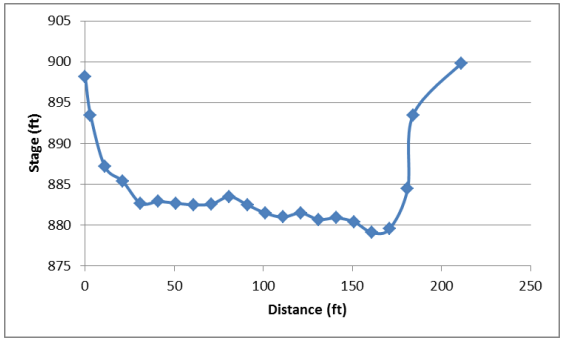


a) Cross-section

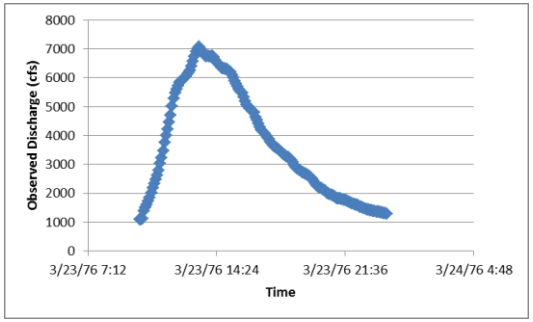


b) Observed discharge hydrograph

- Channel slope: 0.00036
- Manning's roughness: Constant with stages (0.039)

c) Parameter values

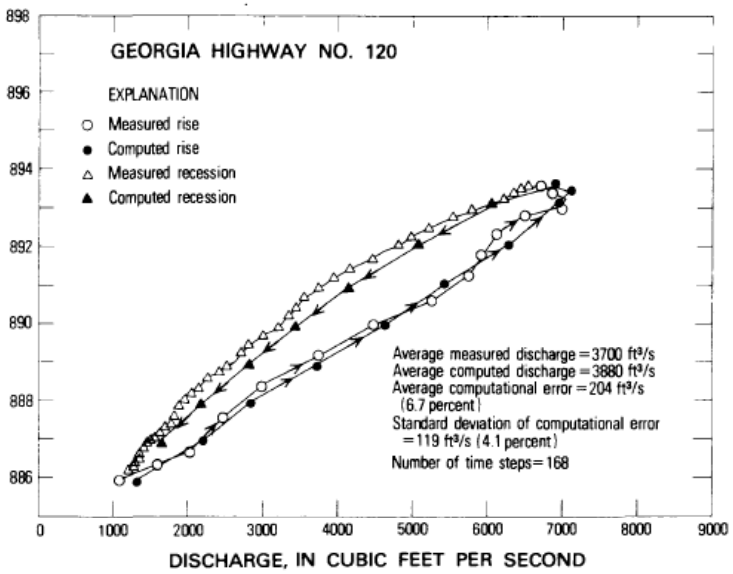


d) Faye and Cherry (1980)

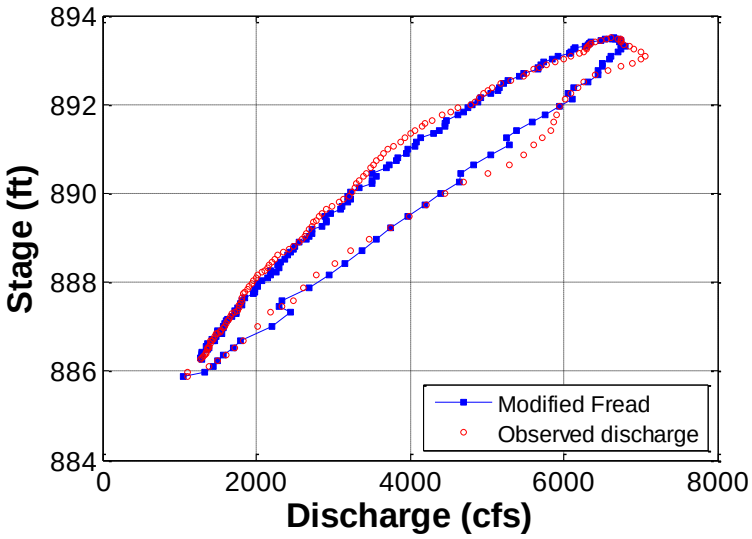


e) Modified Fread

Figure III.16 Simulation comparison between Faye and Cherry (1980) and the modified Fread equation at Georgia Highway No.120

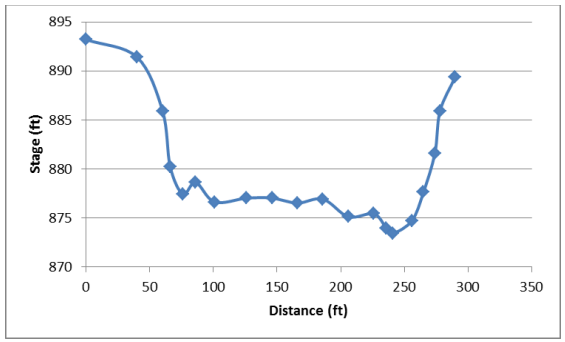


a) Cross-section

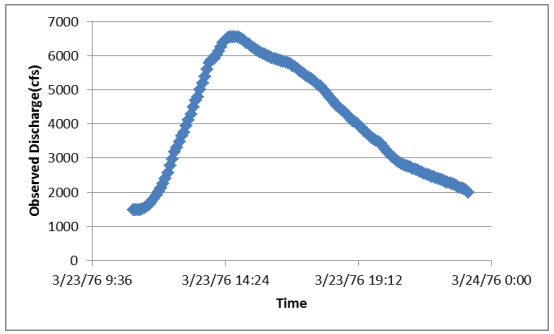


b) Observed discharge hydrograph

- Channel slope: 0.00031
- Manning's roughness: Varies with stages (0.049 at 880.34ft, 0.036 at 883.60ft, and 0.033 at 885.71ft. Linear interpolation between known values)

c) Parameter values

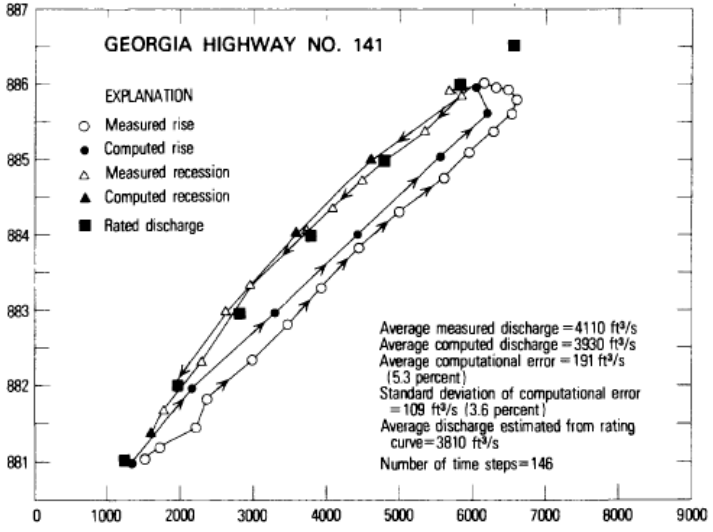


d) Faye and Cherry (1980)

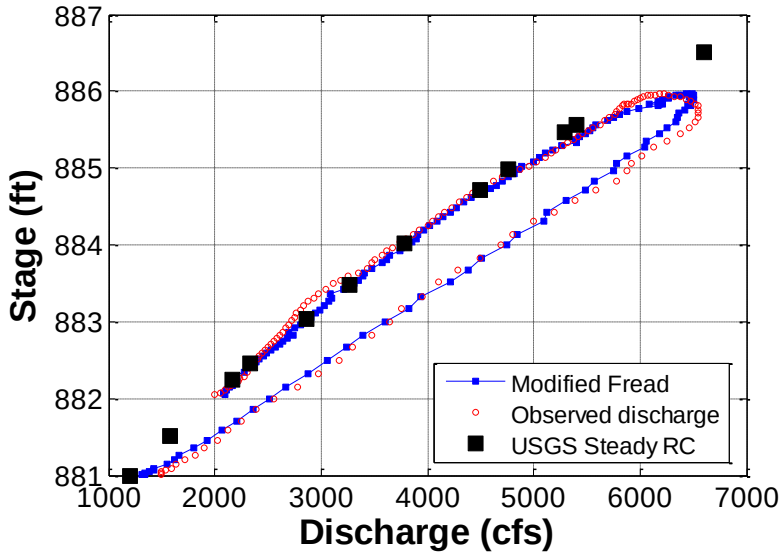


e) Modified Fread

Figure III.17 Simulation comparison between Faye and Cherry (1980) and the modified Fread equation at Georgia Highway No.141

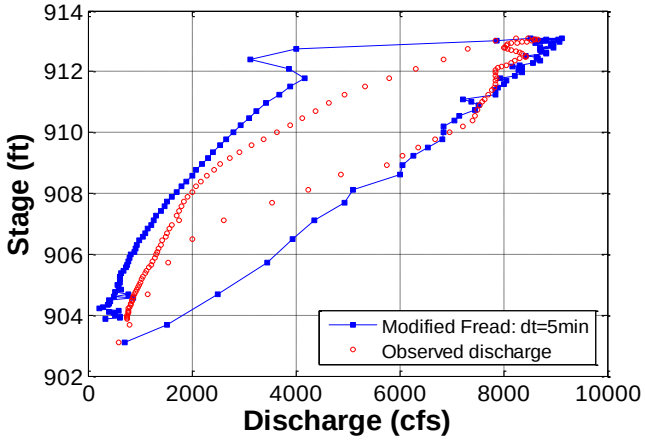


*a) dt = 5 mins*

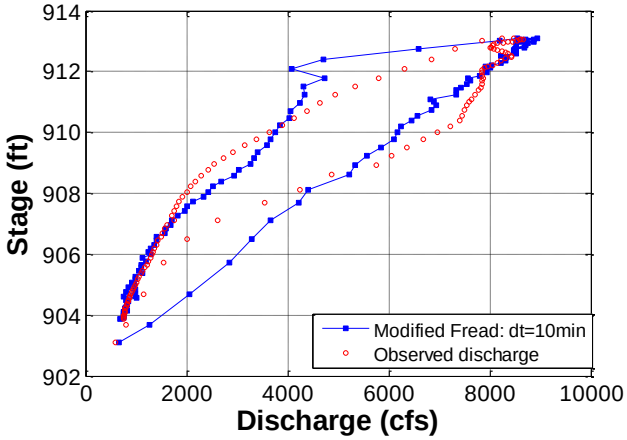


*b) dt = 10 mins*

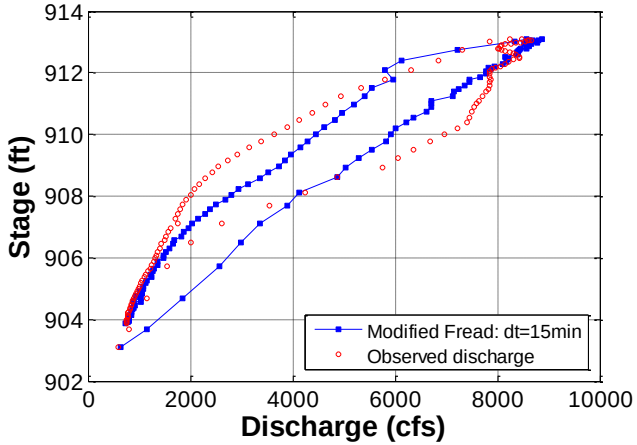


*c) dt = 15 mins*

Figure III.18 The limitation of the modified Fread method for highly dynamic unsteady flows: the changes in the RC shape due to the change in *dt*

## III.3 Experimental Evidence

### III.3.1 hQRC method

The advent of the hydroacoustic instruments, especially ADCPs, has made possible the development of discharge-measurement systems capable of more accurately measuring flows affected by unsteadiness (Muste and Lee, 2013). An ADCP-based discharge-measurement system is dramatically faster than conventional ones and has comparable or better accuracy. ADCP experiments require, however, a significant amount of operator training on the flow and acoustic physics as well as knowledge of ADCP operation, software, and ancillary techniques involved in the measurement process. The need for these special skills added to the fact that storm events are rare and still pose measurement challenge makes it difficult to obtain reliable sample data for understanding and substantiating the importance of unsteady RCs in practical situations.

One of the few sets of such data was collected at a gaging station located on the Ebro River by Ferrer et al. (2013). The station provides continuously discharges using stage measurements acquired by a float-counterweight system that are subsequently fed in the hQRC established for the station. The gaging station is located about 100 km upstream from its sea mouth and downstream from a series of dams for flood control. Given the controls available in the system, unsteady flows can be created through dam operations for various purposes. Two such "artificial" floods were captured using high-density stage-discharge data uniformly spread over the duration of the hydrograph passing (18 data pairs for the first events and 28 for the second). Figure III.19 (a) replicates the hydrograph for the second (approximately half day) event along with the 28 direct stage-discharge measurement pairs taken at about 30 minutes interval. Discharge measurements were acquired by two teams using Sontek M9 ADCPs (http://www.sontek.com/riversurveyor-s5-m9.php). The stream cross section at the gaging location and the range of depth (stage) variation during the flood propagation are

shown in Figure III.19 (b). Figure III.19 (b) also illustrates a selected depth-averaged distribution in the channel indicating that the flow is relatively uniform.

Figure III.20 illustrates the impact of the flood wave propagation through the gaging station on the hQRC. Figure III.20 (a) shows the steady hQRC used at the time of measurements and the loop RC formed by the ADCP directly measured discharges. Also plotted in the Figure Is the loop RC obtained with modified Fread formula applied to the steady RC as discussed in previous sections. As it is indicated, the modified Fread equation was well able to compute the unsteady discharges compared to the ADCP measured ones. It can be noted that the range of relative differences for the discharges at the same depth and for the depths at the same discharge which correspond to the points on the rising and falling limbs of the hydrographs are about 40% and 30%, respectively. These differences are approximately half if we take as reference the steady RC displayed in the figure with black continuous line. The quasi-symmetric location of the steady RC with respect to the loop RC is not typical, as observations of several datasets previously analyzed by the authors indicate that the falling limb of the loop RC is closer to the steady RC then the rising limb. Figure III.20 (b) shows that the maxima for the channel velocity, discharge and stage occur at different times with a time interval between $U_{max}$ and $h_{max}$ of about 30 mins. The experimental data points in the two plots display inherent experimental scattering especially near the hydrograph peak where the measurement environment is more challenging. A larger than normal measurement scattering was anticipated for this dataset as the 28 reported ADCP discharge measurements are obtained from only one ADCP transect. The current ADCP operational guidelines recommend acquisition of multiple transects (at least two) or acquisition over specified minimum time durations for individual transects to produce accurate discharges (e.g., USGS, 2011). However, in the context of the present measurements, operators have to choose the right balance between measurement accuracy and the need to sample fast the rapidly time-varying event.

### III.3.2 VQRC method

Based on the same ADCP data sets provided by Ferrer et al. (2013), Figure III.21 displays several relevant features of the VQRC. The velocity information is provided by the direct measurements acquired with the ADCP deployed on moving boats. In order to illustrate the VQRC method, a "virtual" H-ADCP was created herein by identifying the in-bin ADCP measured velocities along a horizontal line across the channel width. This analysis is practically equivalent to the deployment of a "virtual" H-ADCP (side-looker) that reads an index-velocity across the channel width at a given elevation as illustrated in Figure III.19 (b).

The analysis previously described was successively applied to 13 of the total of 28 ADCP measurements acquired during the flood event to replicate measurements of the index-velocity. Some of the measurements around the hydrograph peak were not considered in the analysis as the particular flood event show some oscillations around the peak, hence making the interpretation of these data more difficult. The width-averaged velocity at a given depth is obtained by spatially averaging the in-bin velocities identified along the line of sight (Kim et al., 2005). Application of this procedure at various depths produces a set of "virtual" H-ADCPs that provide index velocity profiles across the vertical as illustrated in figures III.21 (a), III.21 (b), and III.21 (d).

Selected velocity profiles acquired with the protocol described above are plotted in Figure III.21 (a) and III.21 (b). The consecutive profiles on the rising and falling limbs of the hydrograph show a continuous change of the magnitude of the velocities as well as of the flow depth. Slight differences can be noted in the shape of the velocity profiles as the flood wave propagates through the test section. Figure III.21 (c) visualizes the effect of flow unsteadiness on the relationship between stage and channel mean velocity (obtained from individual ADCP transects). This effect is materialized by the prominent loop in the plot which is similar to the one shown in Figure II.10 (c). Figure III.21 (d) displays the width-averaged velocity profiles for two direct ADCP measurements

(measurement #5 and #27, red circles in Figure III.21 (c) acquired on the rising and falling limbs at practically the same stage (about 4.3m). Despite the slightly higher 3-D nature of Ebro River flow field, the profiles in Figure III.21 (d) show the same trends as those displayed in Figure II.10 (b) by their laboratory counterparts.

The notable aspect in Figure III.21 (d) is that the magnitude of the index-velocity profile is larger on the rising limb compared with the falling limb throughout the depth indicating that a "virtual" H-ADCP would read different index velocities for equal-depth points on the hydrograph limbs. Consequently, the corresponding channel velocities on the rising and falling limbs are also different. For example, the mean channel velocities corresponding to the quasi equal-depth flows identified in Figure III.21 (c) are 1.25 m/s and 0.74 m/s, respectively. Collectively, these combined results will lead to a loop relationship between stage and discharge relationship obtained with VQRC method as illustrated in Figure III.21 (e). Specifically, the discharge used in the latter plot was established with the stage-area RC and the mean velocity was obtained with a one-to-one RC between the index and channel velocity. This unique relationship was obtained by following the standard protocols for VQRC methods (e.g., Rantz et al. 1982; Levesque and Oberg, 2012; Birgand et al., 2005) for inland rivers without considering the hysteretic effects in the derivation of the VQRC. Specifically, all the direct measurement points collected with the ADCP disregard of their event phase (rising or falling) were used to estimate the VQRC for the H-ADCP deployed at a stage of 1.5m (6m from the channel bottom). The agreement between the discharges derived with the unique VQRC relationship and the direct ADCP measurements is good with slight differences that will be discussed next.

The subsequent discussion emphasizes aspects of the impact of the unsteady flows on the VQRC method as there are relatively few data and analyses available on this subject compared to the hQRC alternative. The VQRC method seems to have intrinsic capabilities to capture relatively accurate hysteresis if the measurement protocol is

commensurate with the scale of the passing flood wave. This observation is illustrated by the results potted in Figure III.21 (e) that reveals a good agreement between the stage-discharge relationship obtained via VQRC and the direct ADCP measurements and modified Fread method applied to steady hQRC. Some degree of improvement in capturing aspects of unsteady flow by the VQRC method is expected as it is based on two direct and fast sampled simultaneous measurements. Given that for a fixed bed channel the stream area is related to stage to a one-to-one relationship regardless of the flow is unsteady or non-uniform. Also, the fact that the actual index velocity is captured as the unsteady flow progresses will lead to two different discharges for the same depth on the rising and falling limbs of the hydrograph even if the VQRC is unique. From this perspective it can be stated that the VQRCs are better capturing the unsteady flow events than the hQRCs. The remaining question is if the index-velocity to channel mean velocity used in the VQRC is unique for unsteady flows.

For demonstration purposes, we apply herein the "segmentation approach" to a "virtual" H-ADCP data located at a stage of 1.5m (6m from the channel bottom) and the protocol of obtaining the index-velocity described in the previous section. "Segmentation approach" intends to separately account for the phases of the flow (rising and falling limbs). The results of this analysis are presented in Figure III.22. The VQRC developed with linear regression applied to data points acquired on the rising limb (red triangles) and separately to data points acquired on the falling limb (blue triangles) are plotted in Figure III.22 (a). Also plotted in this Figure is the linear regression applied to all data points on the rising and falling limbs that resulted in a unique VQRC. It is the unique RC that was used to obtain the discharges plotted in Figure III.21 (e) (i.e., the Index Velocity 1 to 1 curve).

The visual inspection of the plots displayed in Figure III.22 (a) indicates a slight separation between the rising and falling regression lines suggesting a non-unique index-to channel mean velocity RC. The difference will also be reflected in the comparison of

the stage-discharge relationship obtained with the unique VQRC and the segmented index-velocity one, as shown in Figure III.22 (b). As expected, the one-to-one VQRC displays slightly smaller difference than the segmented VQRC for points of the same depth on the rising and falling limbs. The difference is a reflection of the different acceleration rates occurring on the two phases of the unsteady event. The different acceleration rates are reflected in the measurement of the actual index-velocities captured with fast sampling rates during the event. This difference is "washed out" when a unique regression line is built using the mixture of data points on rising and falling limbs. The difference between the segmented and unique RC is expected to vary with: a) the magnitude of the unsteadiness with respect to the initial flow, and b) the location of the H-ADCP in the vertical. The first effect is related to the shape and magnitude of the hydrograph and the slope of the gaging site. The second effect is related to the fact that the difference between rising and falling index-velocity profiles is different for the inner and outer region of the flow. Similar inferences were made by Nihei and Sakai (2006) using an up-looking ADCP for measuring the index velocity.

Additional similarities between this analysis and previous work are highlighted below to emphasize other relevant aspects in developing VQRCs for unsteady flows. The one noted by Tu and Graf (1992) and Rantz et al. (1982) is that the relative water depth where the point velocity equals the vertically averaged velocity cannot be assumed as a constant (i.e., typically considered to be 0.6 the depth measured from the free surface) during a hydrograph. The direct implication of this observation is that the relation between index-velocity and channel mean velocity can be expected to vary with stage because the index velocity is a measure of the mean velocity along a line at a fixed elevation in the cross section (see also Figure III.21 (a) and III.21 (b). As the stage rises, the position of this line is moved downward in the cross section relative to the total depth, and resultant changes in the velocity distribution in the vertical column cause a change in the ratio between the two velocities. Based on this observation, Rantz et al. (1982)

conclude that the VQRC need to be correlated with the stage. Furthermore, Qu (2003) observes from his flume experimental study that the shape and magnitude of the index-velocity profiles are different on the rising and falling limb of the hydrograph for the same depth-averaged velocity (see figure 4.18 in Qu, 2003). This difference increases near the bed and with the flow unsteadiness. This experimental finding seems to be related to the non-uniqueness of the VQRCs for the rising and falling limbs in our analysis.

### III.3.3 CSA Method

In this section, a case study using the CSA method applied to Clear Creek (the small stream discussed in Section III.2.2) will be examined. This case study is of interest because the hysteresis behavior of the unsteady flow was monitored continuously. Previous studies with the CSA method (Smith et al., 2010; Stewart et al., 2012) proved that the method can successively be implemented to monitor dynamic water surface slope and conveyance between gages, and therefore the methodology can be used to correctly compute the discharge. However, the application of the CSA method was limited to sites where hysteresis is not likely to occur (i.e. steep sloped channel). The average channel slopes in Smith et al. (2010) and Steward et al. (2012) were approximately 0.009 and 0.012, respectively. These values were estimated using the most upstream and downstream gage locations. Sudheer and Jain (2003) indicated that flood waves show a marked kinematic behavior when the slope of the channel bed is greater than 0.001. In all the other cases the variable energy slope associated with the dynamic inertia and pressure forces should be considered in the analysis. During June 2013, our team identified appropriate site reaches close to the Oxford USGS gage station (05454220) in Clear Creek, Iowa, as described in Figure III.23. The selected reach is accessible, straight and uniform and meets the requirement of 0.5ft minimum fall. Moreover, the other site selection criteria presented in Table II.1 in Section II.2.4 were carefully examined before

the deployment of pressure sensors. Two pressure transducers were deployed and installed at about 200m distance from each other. In Figure III.23, the 2nd IIHR gage corresponds to the upstream pressure transducer installed on the left bank of the reach (looking downstream), and the 3rd IIHR gage corresponds to the downstream pressure transducer installed on the right bank of the reach. Smith et al. (2010) and Stewart et al. (2012) recommended installing two sensors on both sides of the banks and at least at 3 cross-sectional locations to address peculiarities in computing discharges and to provide safety in case of instrument malfunction. However, it is considered that using only two sensors will give us a good indication of the hysteresis behavior based on water surface slope measurements. Moreover, an USGS pressure sensor is present 100m upstream of the 2nd IIHR gage (upstream deployed gage), and is considered as auxiliary one.

Figure III.24 shows the photos taken when the sensors were deployed. Figure III.24 (a) and III.24 (b) show the upstream sensors and Figure III.24 (c) and III.24 (d) show the downstream sensors looking either upstream or downstream to demonstrate the presence of good straight uniform channel conditions. Figure III.24 (e) contains a photo showing the measuring of the channel centerline needed to accurately estimate the distance between gages using the Trimble R8 GPS RTK instrument. Figure III.25 illustrates the steel pipe casing designed for the pressure transducers. The transducers can measure up to 10ft of water column, which corresponds to approximately bank full elevation in Clear Creek.

The pressure transducers were manufactured by Global Water Instrumentation, Inc. The product name is WL15 level logger, as shown in Figure III.26. This level logger is composed of three parts: data-logger, cable and sensor. The data logger is able to record 24,400 readings and is programmable to change the recording interval from one second to one day. The data logger can be connected to a laptop using a COM port for data retrieval, and needs a 9V lithium battery for its power source. With a 5 min recording interval that was used, the battery needs to be changed about every 45 days.

After the deployment, the level sensor elevations were measured based on the USGS reference mark near stream gage station using the Topcon Total Station which has slightly better vertical accuracy than the Trimble R8 RTK. Also, the cross-sections were measured adjacent to the installed sensors using either the Topcon Total Station or the Trimble R8 RTK. Figure III.27 shows the three cross sections surveyed on the day when the sensors were deployed. The upstream PT and downstream PT, representing the deployed two sensor locations, have very similar cross-sectional areas even though there are some local differences. These probe surveys have been repeated to ensure there were no vertical displacement of the sensors as well as no change in the cross-section geometry during each visit. Should the vertical locations of sensors move during the events, this movement may lead to erroneous estimation of water surface slope. Moreover, other site conditions such as the type of bed material and the presence of transition points where the vegetation type is changing were also identified to help interpret the data. It was observed that the channel bed was composed of primarily clay and the banks were covered with thick vegetation. In addition, the channel reach was subject to a slight contraction between the USGS gage and the upstream PT, as can be seen in Figure III.27.

Since the deployment of the sensors, only two sufficiently severe storm events occurred on June 24, 2013 and June 26, 2013, as also shown in Figure III.28. The water level increased by about 6ft from the base to the peak flow during the first storm event and about by about 2.5ft during the second storm event. These storms correspond approximately to medium and small scale storms based on analysis of the average discharge records in Clear Creek. Based on the measured water levels at these three stream gauge locations, the water surface slopes were computed between the USGS gage and the upstream PT and then between the upstream PT and the downstream PT using the distance surveyed by the Trimble R8 GPS RTK along the centerline of the channel.

Figure III.29 shows the magnified stage hydrographs for each event. It is observed that the fall between the USGS gage and the upstream PT was not sufficient to produce

accurate estimations. Moreover, relatively large oscillations in the USGS stage records were observed. In Figure III.29 (a), the USGS gage showed a concave shape of the hydrograph near the peak stage. This seems to be related to the sudden expansion of the cross-sectional area at a stage of about 705.5 ft, as can be observed from Figure III.27. Moreover, in Figure III.29 (b) the water surface drop at the USGS gage is approximately equal to 702.7ft. Thus, the downstream stage (upstream PT) is very close to the upstream USGS water level. Therefore, the data collected at this USGS gage station was discarded.

Figures III.30 (a) and III.30 (c) represent the computed variation of the water surface slopes as a function of time during the events on June 24, 2013 and June 26, 2013, respectively. As expected, the water surface slope is increasing over the rising limb and is decreasing over the falling limb of the hydrograph. Figures III.30 (b) and III.30 (d) visualize the corresponding stage-water surface slope relationships during these events. The results clearly show hysteresis behavior. The water surface slope moved clockwise during the first event and anti-clockwise during the second event. This seems to be due to effects of vegetation. During the first event, the uprooted vegetation during the rising limb produces large resistance to the flow, while it was inclined due to the excessive shear during the rising limb therefore resulting in less friction during the falling limb hence higher water surface elevation. During the second event, it seems that there was not enough time for the vegetation to regain its vertical position. Therefore, the channel roughness was similar during the rising and the falling limb of the hydrograph. These observations lead to the conclusion that the counter-clockwise hysteresis is triggered and governed by unsteady flow factors such as dynamic inertia and pressure forces.

Based on the water surface slope data illustrated in Figure III.30 and the conveyances computed using the surveyed cross-sections and channel roughness estimated using USGS steady based discharges, unsteady discharges and dynamic hQRCs are estimated. The results of this estimation are presented in figures III.31 for the first event and in Figure III.32 for the second event, both at the USGS gage and at the

upstream PT. The results at the downstream PT are excluded because it was found that the simulation underestimates the peak discharge by approximately 15%. This was mainly due to underestimation of the cross-sectional area. The cross-sections were surveyed two times at this location. Both measurements considered relatively inaccurate at the banks due to the difficulties of surveying the highly inclined banks. Moreover, the channel bed elevation in the downstream PT was similar to that in the upstream PT, as shown in Figure III.27. The water surface elevation still drops by about 0.5ft between these locations. This may imply that a mild adverse slope with an "*A2"* water surface profile is present, which results in a smaller conveyance compared to the upstream cross-section. Dalymple and Benson (1967) defined the term "spread" to describe the closeness of the fit in peak discharge estimation between conveyances relative to the conveyances bounding the slope-area reach. Stewart et al. (2012) stressed out that the "spread" needs to be estimated using a minimum of 3 conveyances to be able to assess the uncertainties associated with the discharge estimation based on the CSA method.

The discharges and RCs based on modified Fread equation and USGS steady based records are also plotted in Figures III.31 and III.32 to compare them to those estimated by the CSA method. It is assumed that the Manning's roughness coefficient values estimated from the USGS discharge records at the USGS gage location can be transferred to the upstream PT location if one assumes homogeneous channel roughness (e.g., vegetation) in the streamwise direction. While this is a rough approximation of the channel roughness at the upstream PT location, it still provides a fairly good estimation compared to using a single roughness value estimated by other means. In ungagged streams, a channel roughness should be estimated by direct discharge measurement, using a table (e.g., Chow, 1959), or by comparison with a reference stream shown in Figure III.33. The second assumption was that the water surface slope calculated between the upstream PT and the downstream PT is equal to the water surface slope at the USGS gage

station. This assumption was needed because the USGS stage record showed relatively large scatter which precludes it from being used.

The results showed that the CSA and the modified Fread methods give predictions that are close to the USGS discharges even though the magnitude of the hysteresis is not sufficiently large in both cases (the hysteresis for the second event is slightly larger), hence it is difficult to make inferences. However, Figures III.30 b) and III.30 d) clearly describe the hysteretic behavior as the slope has distinct trajectories on the rising and falling limbs of the hydrograph. This evidence confirms that the CSA method show promising capabilities to dynamically track dynamic flow in streams.

It is important to note that for a successful implementation of the CSA method, the critical evaluation of channel roughness including changes of vegetation shape during events (Jarrett, 1987) and accurate estimation of the water surface slope are the key elements. In addition, field deployment details such as transducer clock drift (especially when the battery is not in good condition), the time synchronization errors between gages, the movement of the sensors and sediment induced errors should be carefully considered when managing the sensors and analyzing the data (Steward et al., 2012).

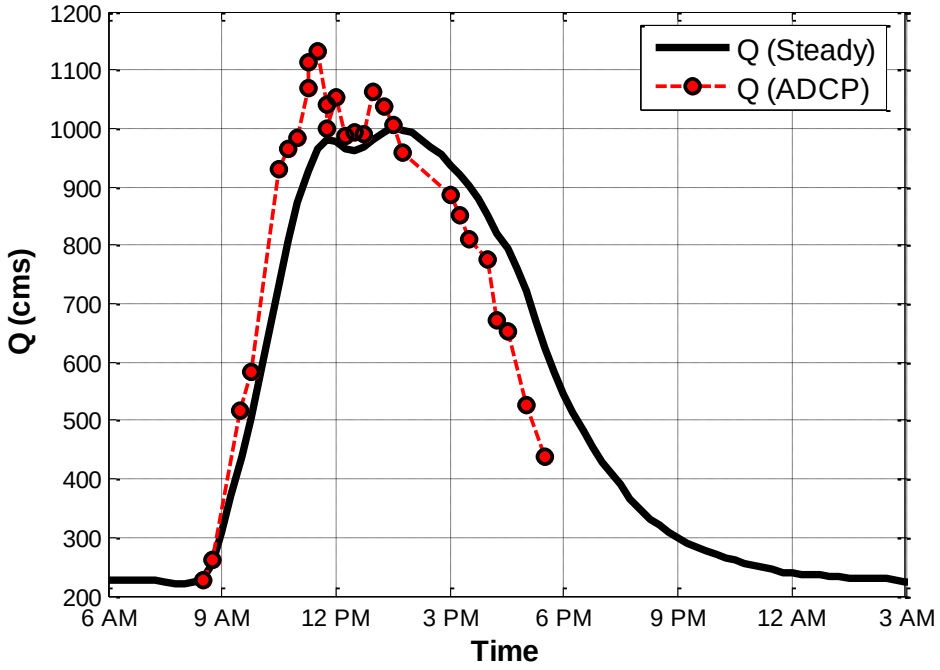


a)

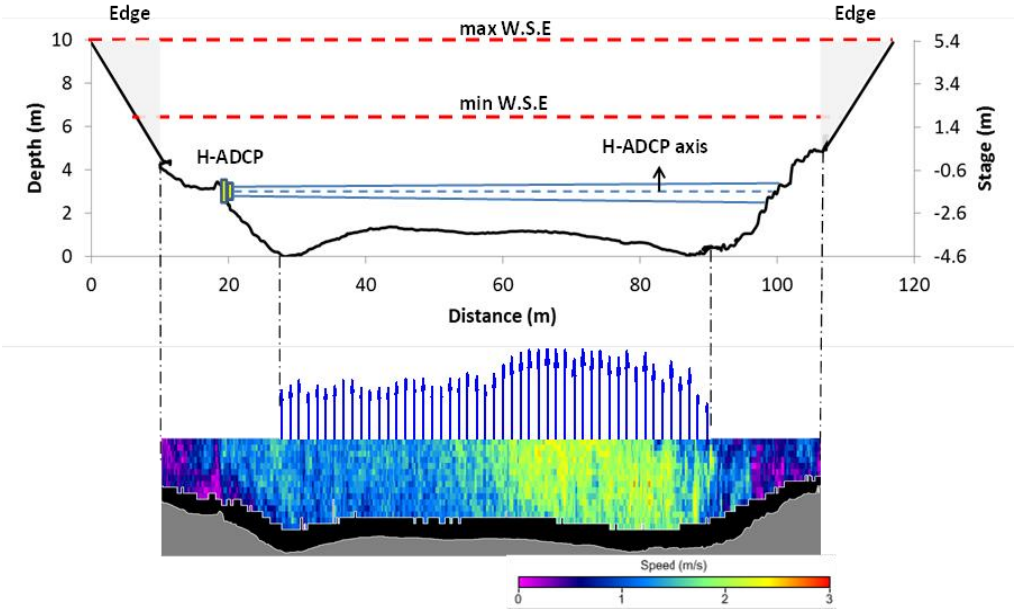


b)

Figure III.19 Flood event in Ebro River: (a) storm hydrograph; (b) cross section at the gaging site and depth-averaged velocity distribution for one of the transect (stage 5.3m)

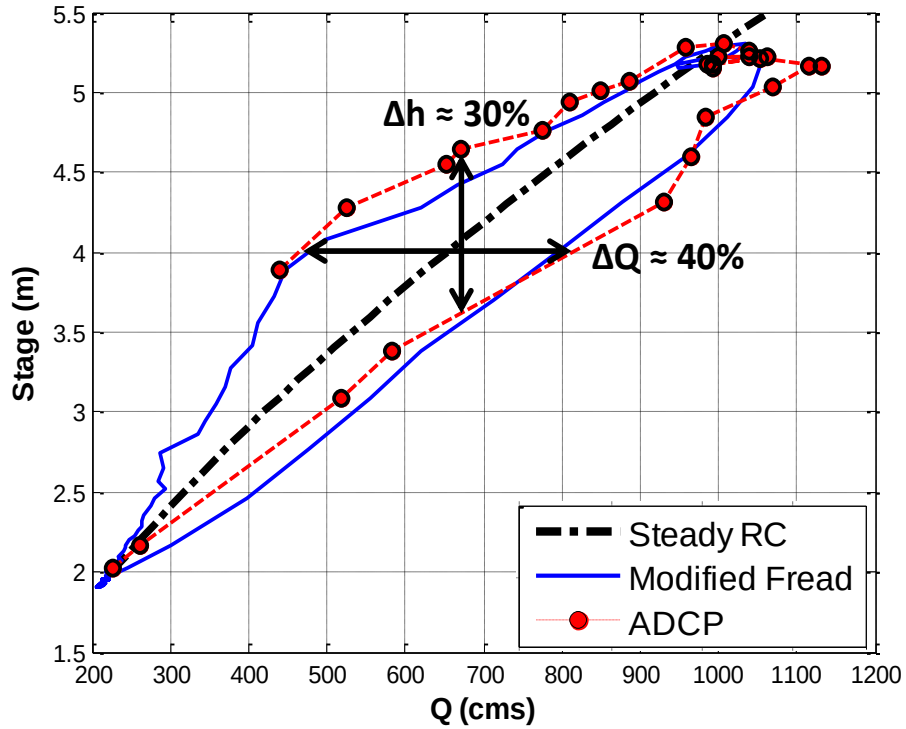


a)

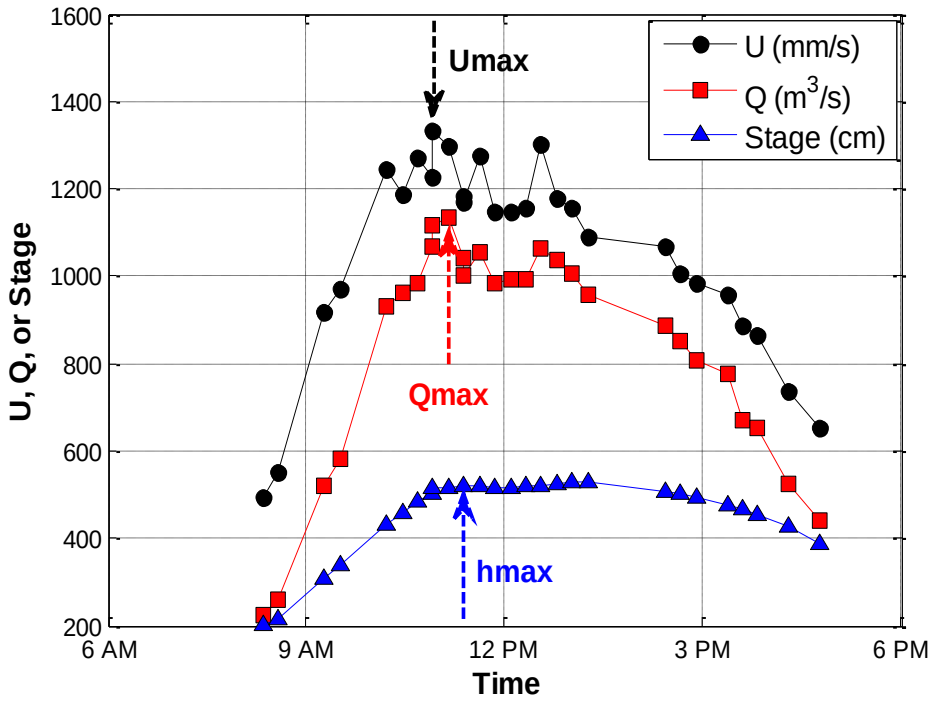


b)

Figure III.20 Unsteady flow effects on: (a) the hQRC; (b) the time sequence of the discharge, mean velocity, and depth variation during the event

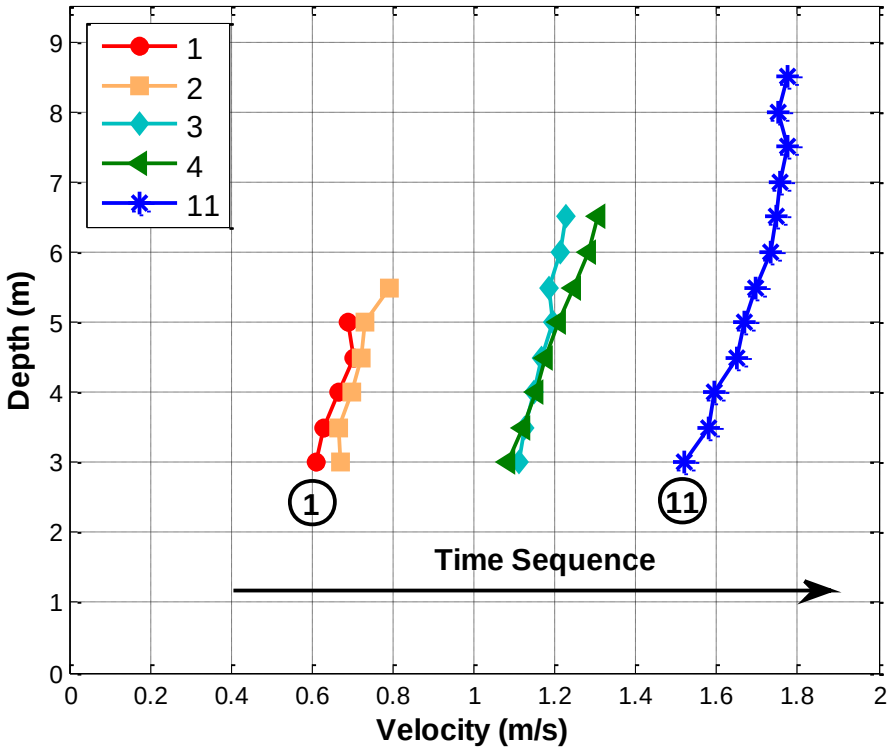


a)

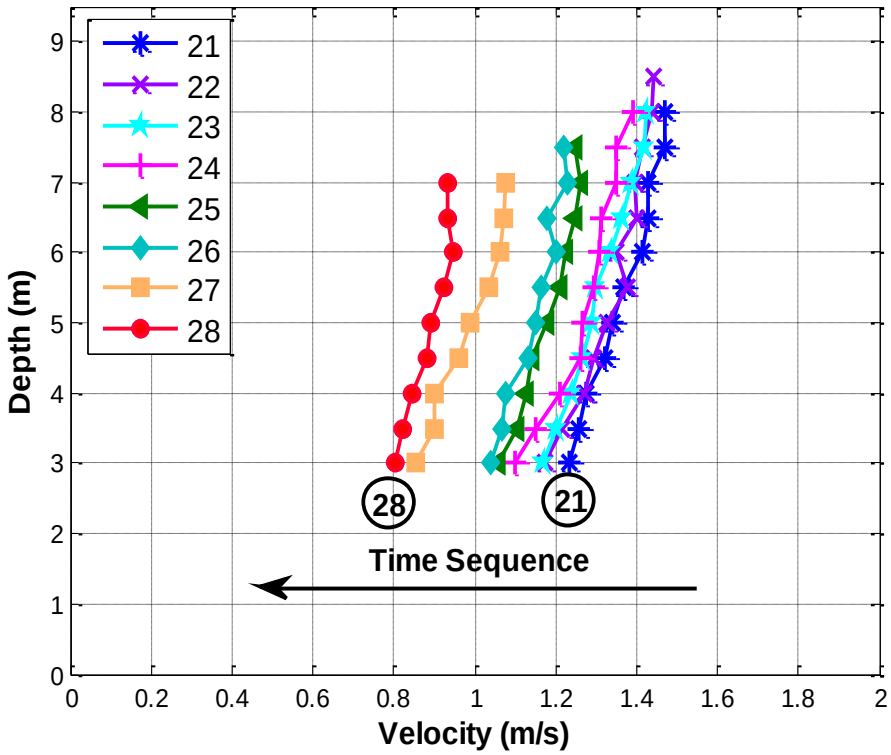


b)

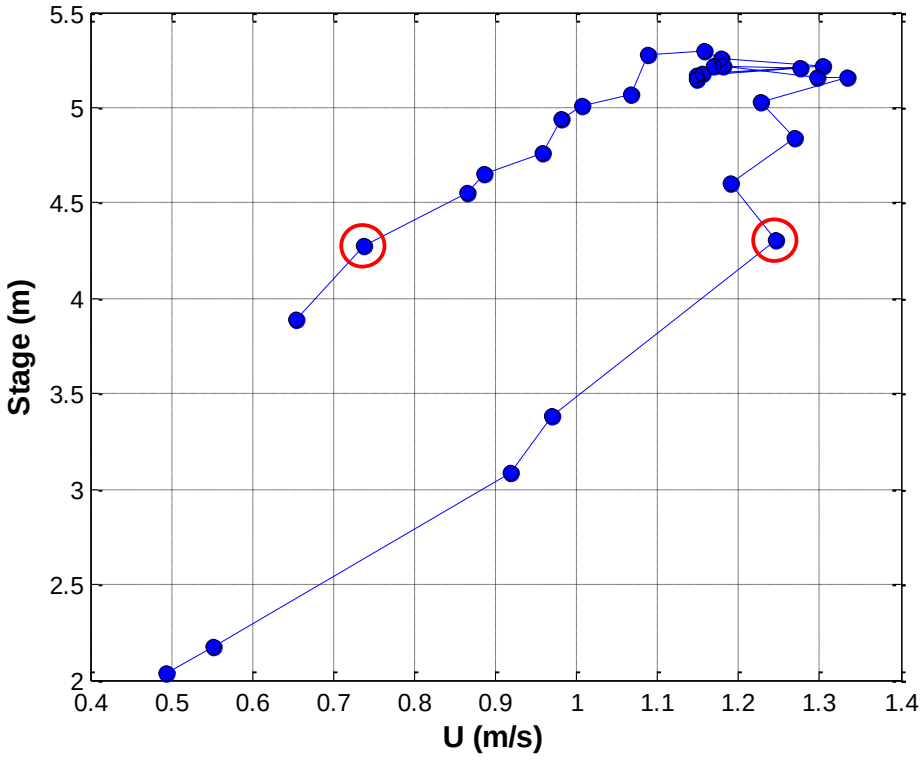


c)

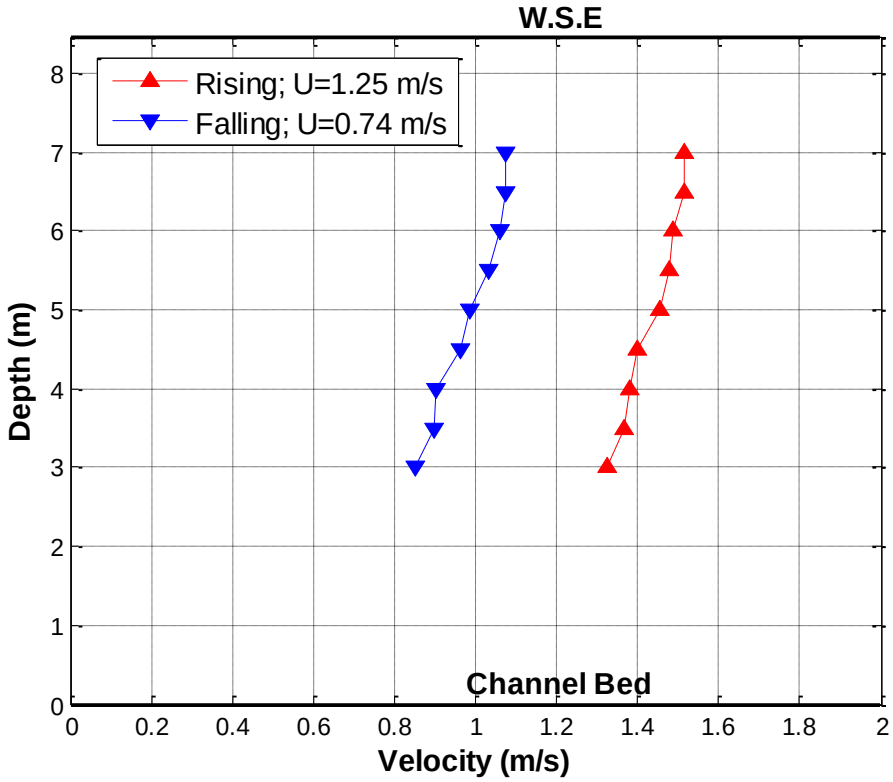


d)

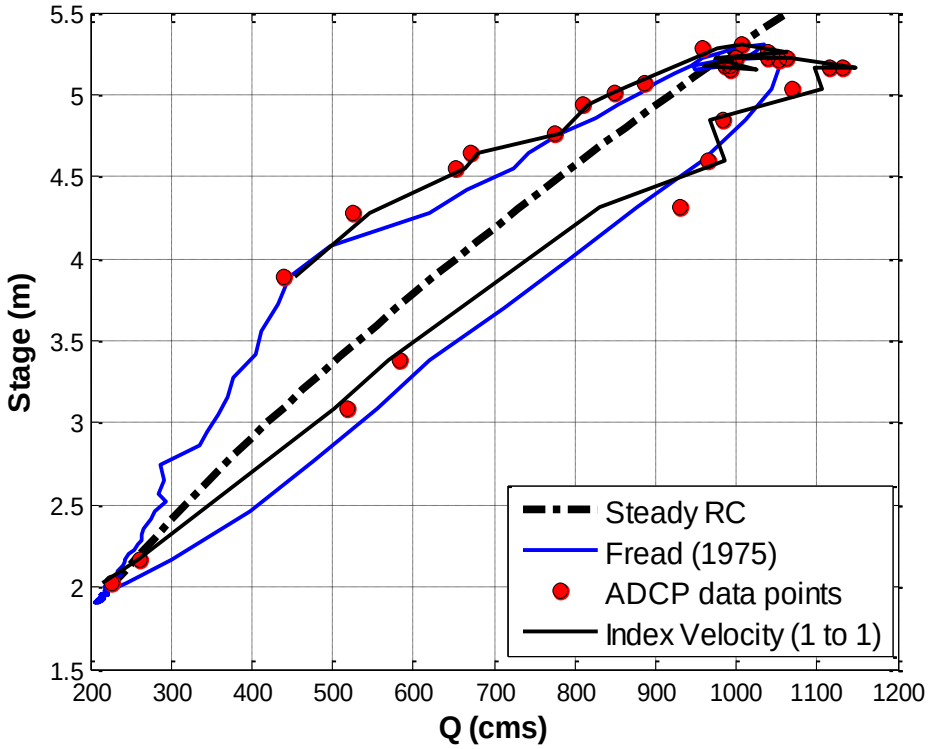


e)

Figure III.21 Analysis results for elements of the VQRC: a) succession of the velocity profiles on the ascending limb of the hydrograph; b) succession of the velocity profiles on the descending limb of the hydrograph; c) the relationship between channel stage and depth average velocity as provided by the ADCP direct measurements; d) the index velocity profiles corresponding to two quasi equal flow depth on the rising and falling limbs of the hydrograph (circles on the plot displayed in c); e) comparison between steady RC, modified Fread method applied to the steady RC, stage-discharge relationship obtained using the VQRC protocol, and direct ADCP measurements

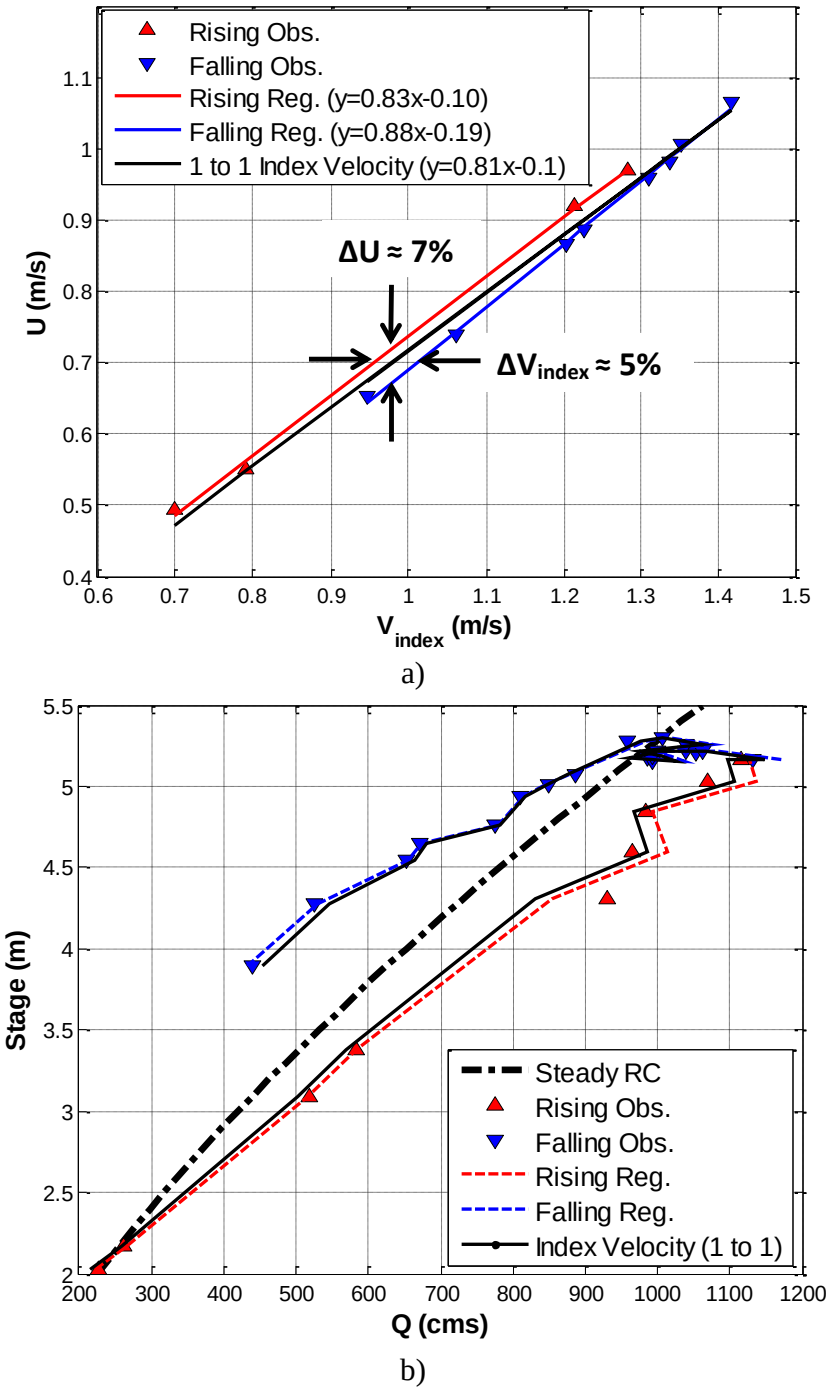


Figure III.22 Implications of the differentiation of the unsteadiness moments during the progression of the flood wave on: a) the VQRC; b) the hQRC using the index-velocity to channel velocity RC

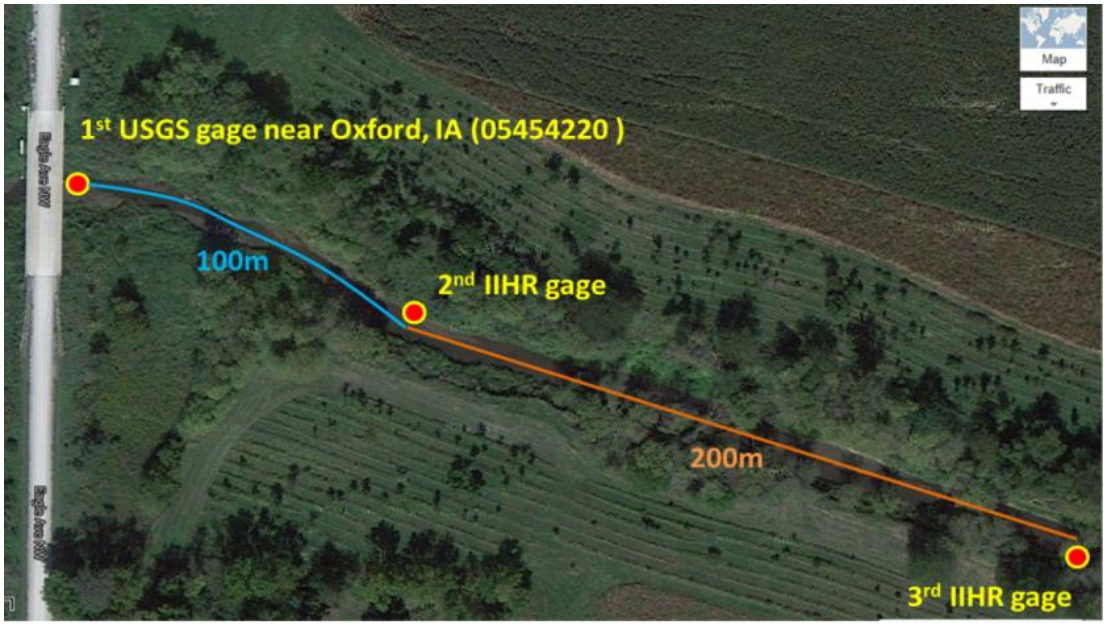


Figure III.23 Google map showing the pressure sensor locations at Clear Creek, Iowa

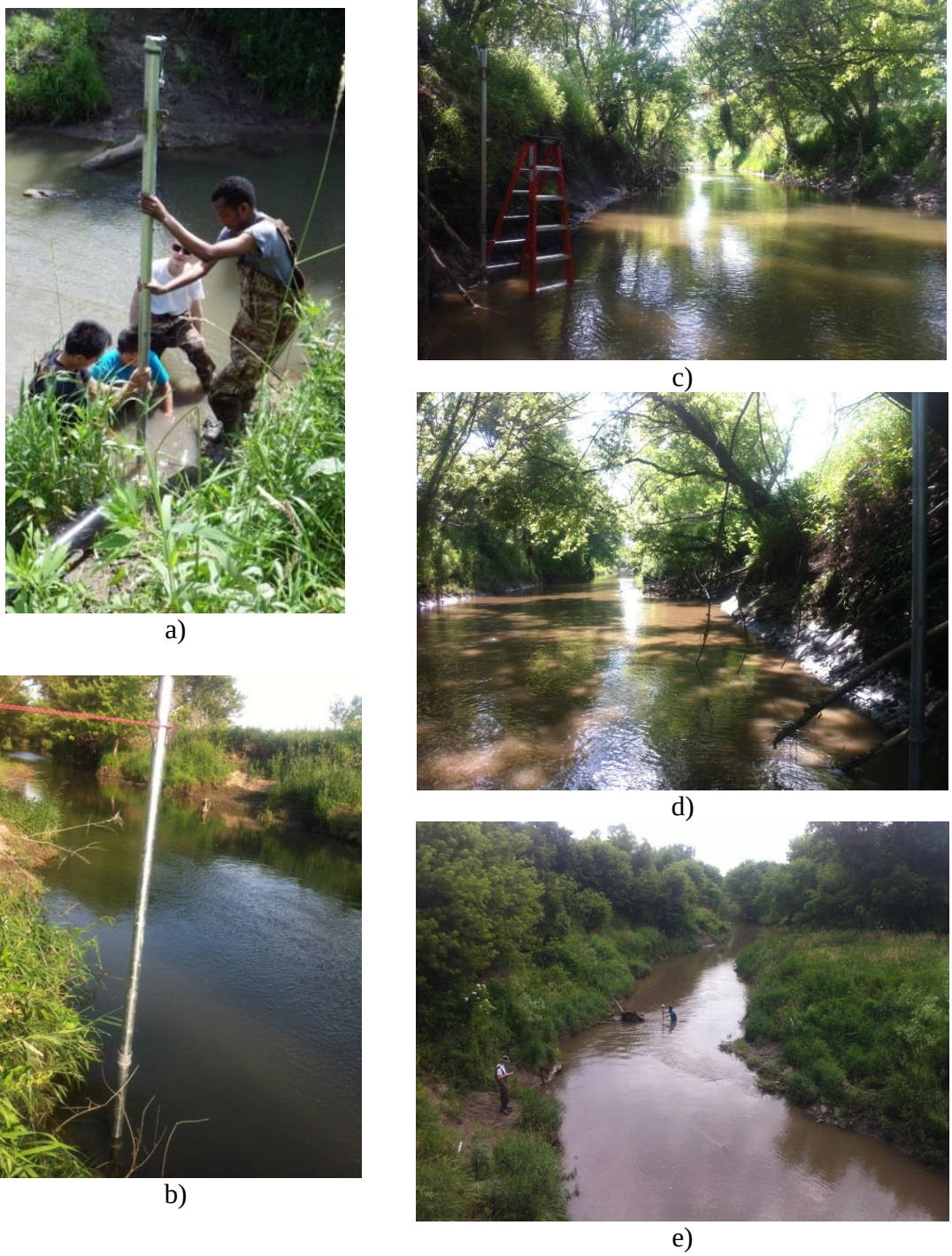

a)

b)

c)

d)

e)

Figure III.24 Field photos taken on June, 2013 when the sensors were deployed: a) and b) upstream sensor; c) and d) downstream sensor; e) stream centerline measurement

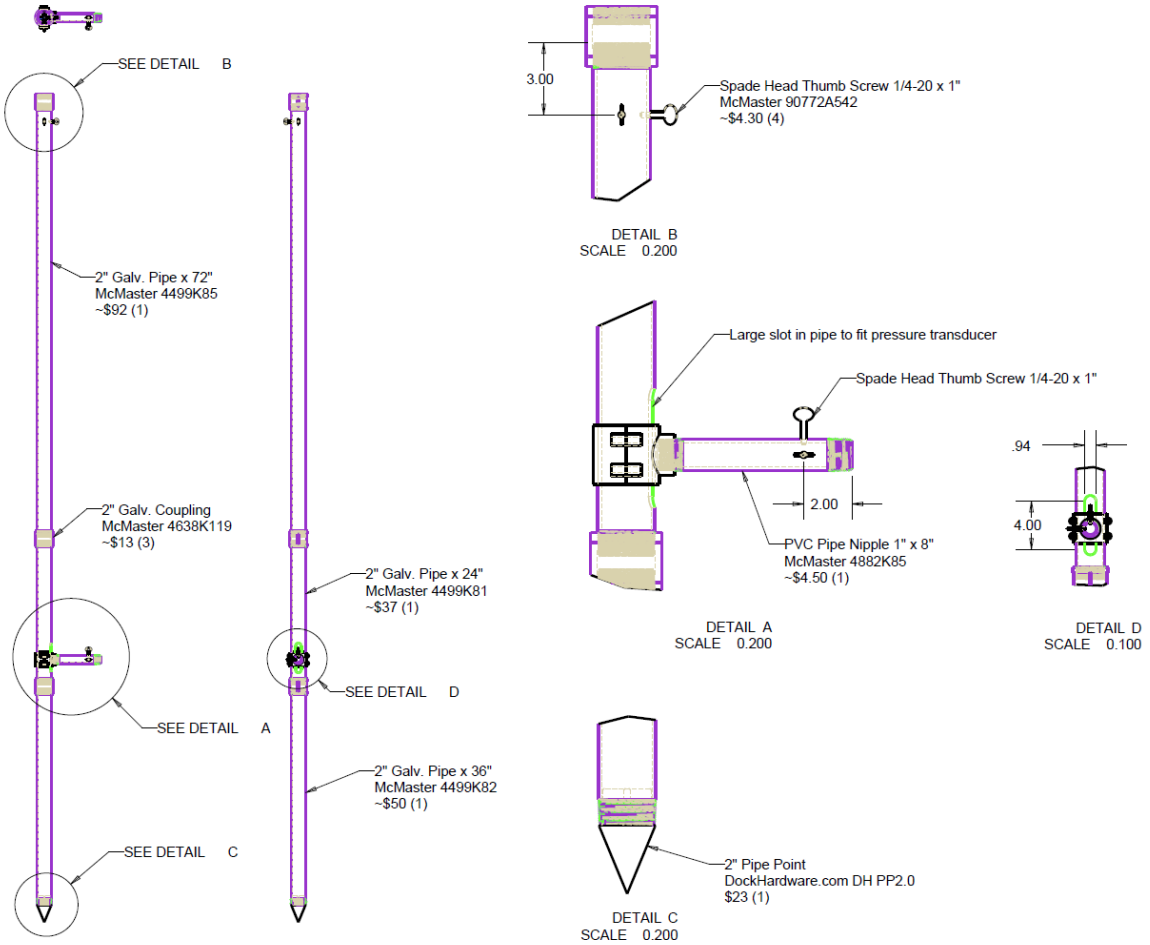


Figure III.25 Pressure transducer casing design

a) Pressure transducer

b) Level sensor

c) COM port in data-logger

d) Lithium battery in data-logger

Figure III.26 Pressure transducers (WL15 level logger)

Source: Global water WL15 manual

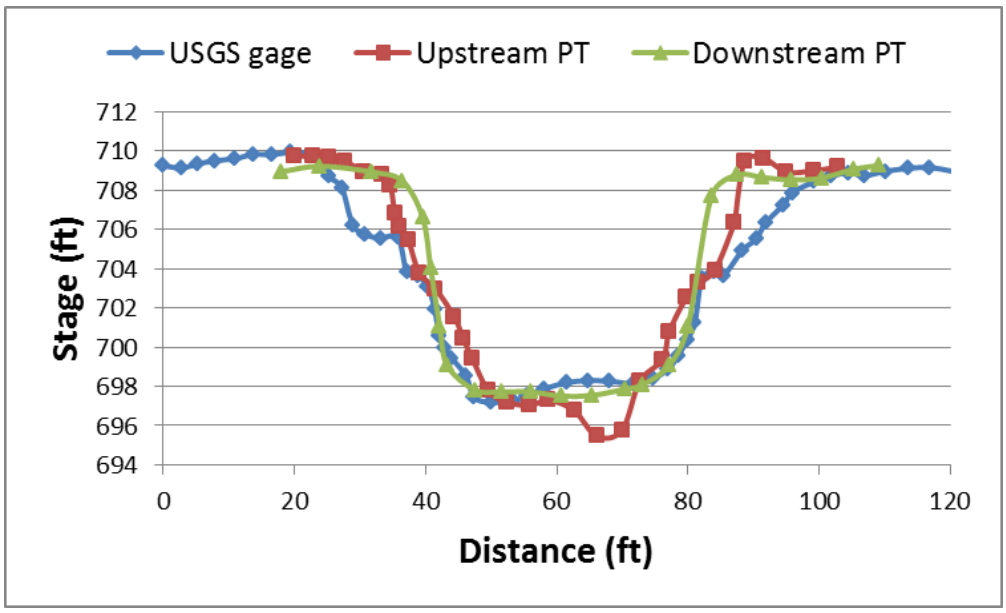


Figure III.27 Surveyed cross-sections

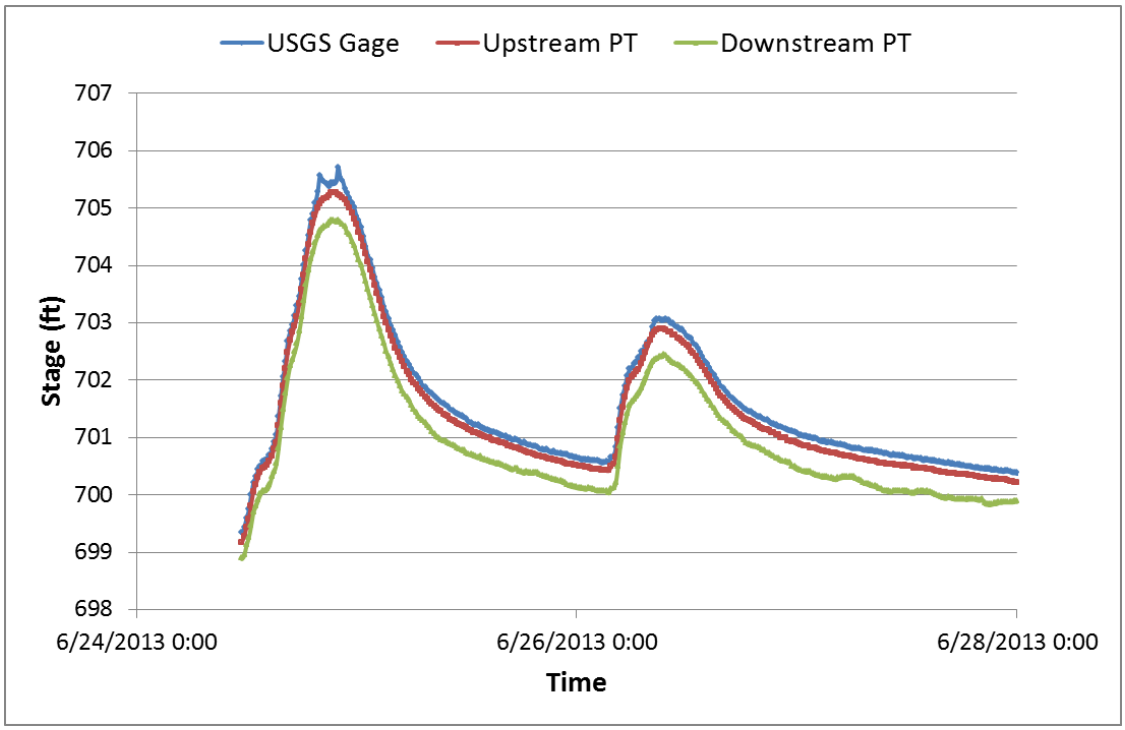


Figure III.28 Event stage hydrographs on June24 (the first) and 26 (the second), 2013

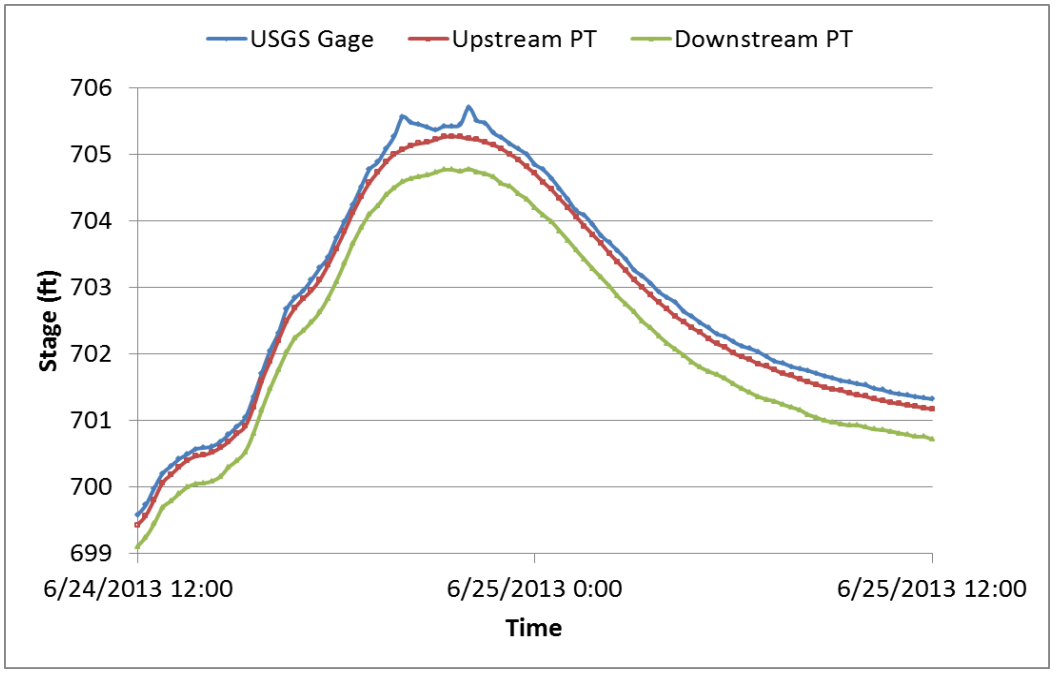


a)

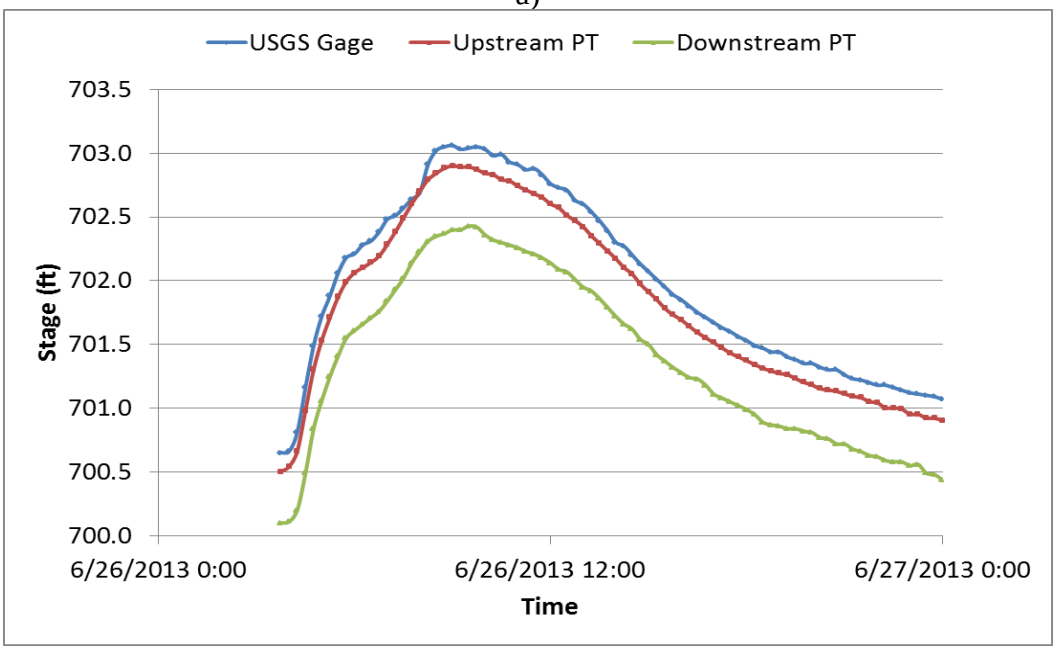


b)

Figure III.29 Stage hydrographs: a) Event on June 24, 2013; b) Event on June 26, 2013

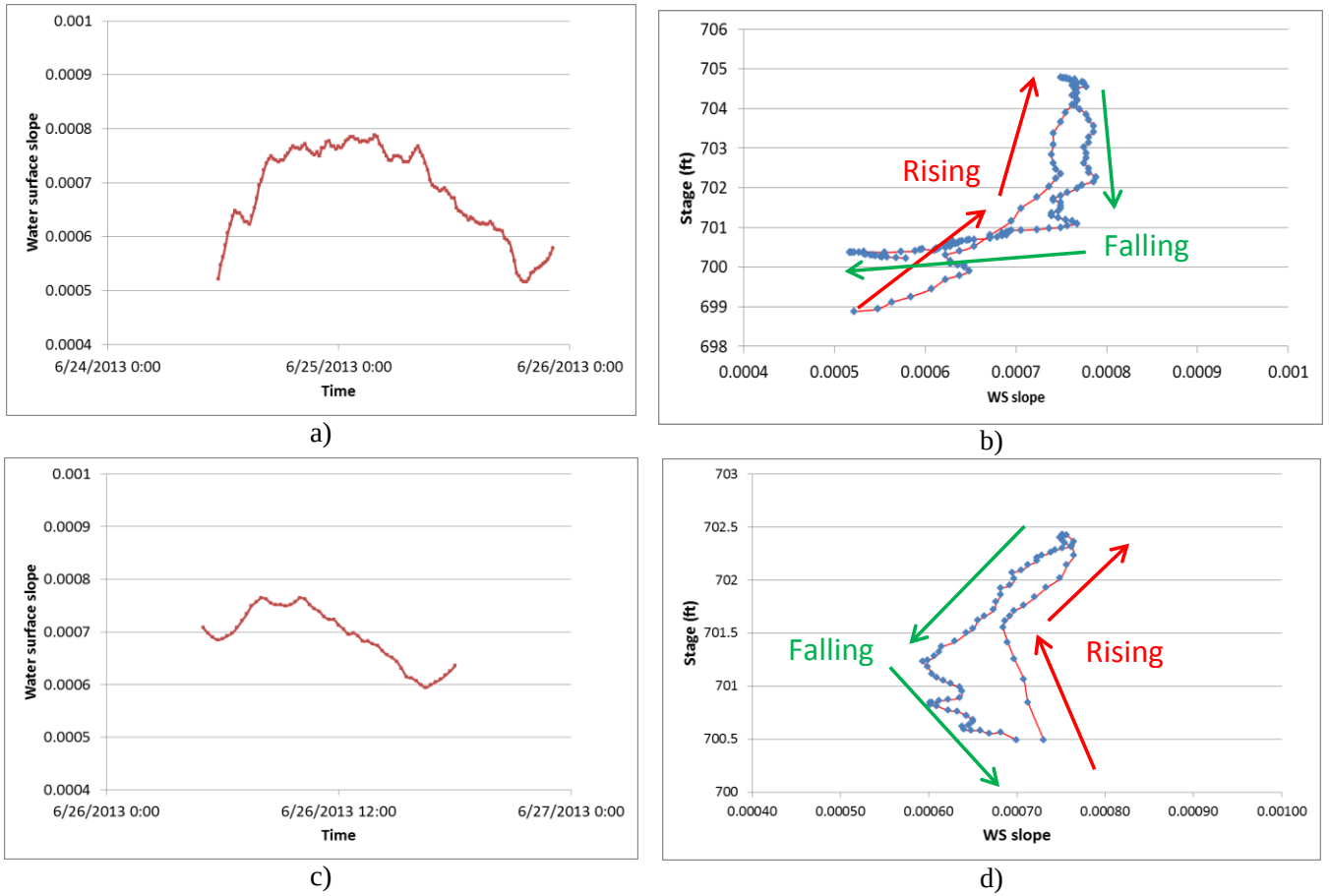


Figure III.30 Dynamic water surface slope and Stage-slope rating: a) and c) Water surface slope between Upstream PT and Downstream PT on June 24, 2013 and June 26, 2013, respectively; b) and d) Stage-slope rating on June 24, 2013 (clockwise) and June 26, 2013 (counter-clockwise), respectively

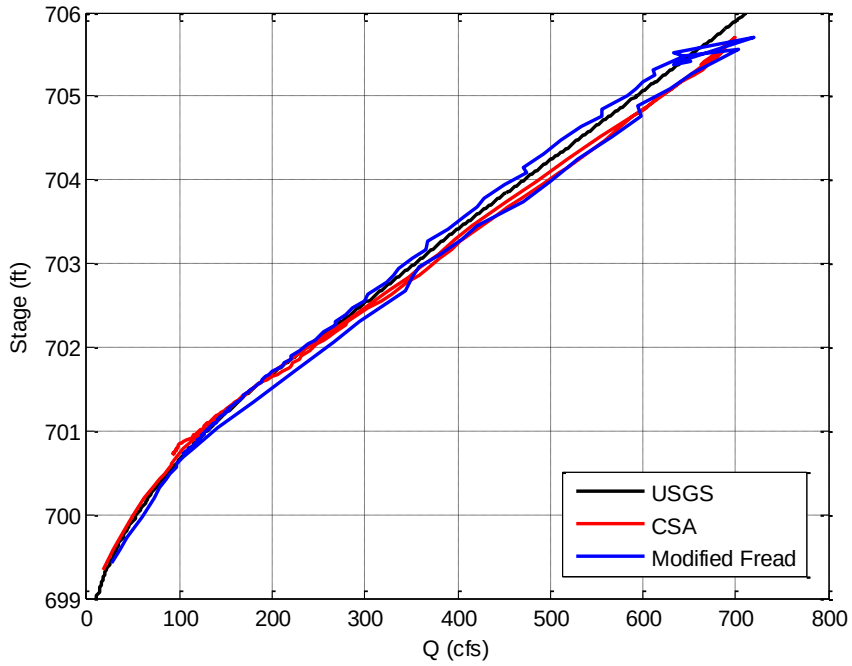


a)

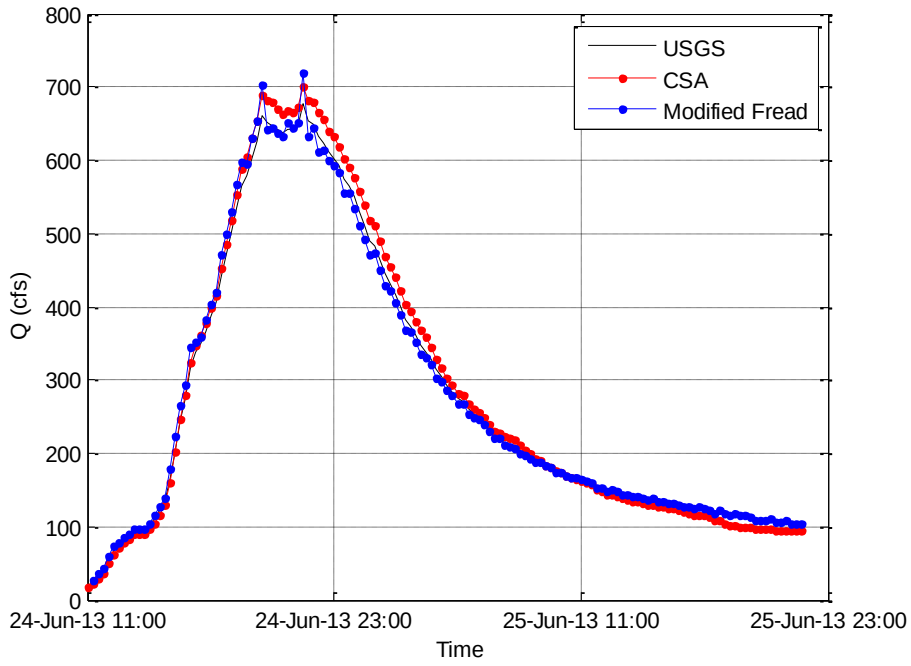


b)

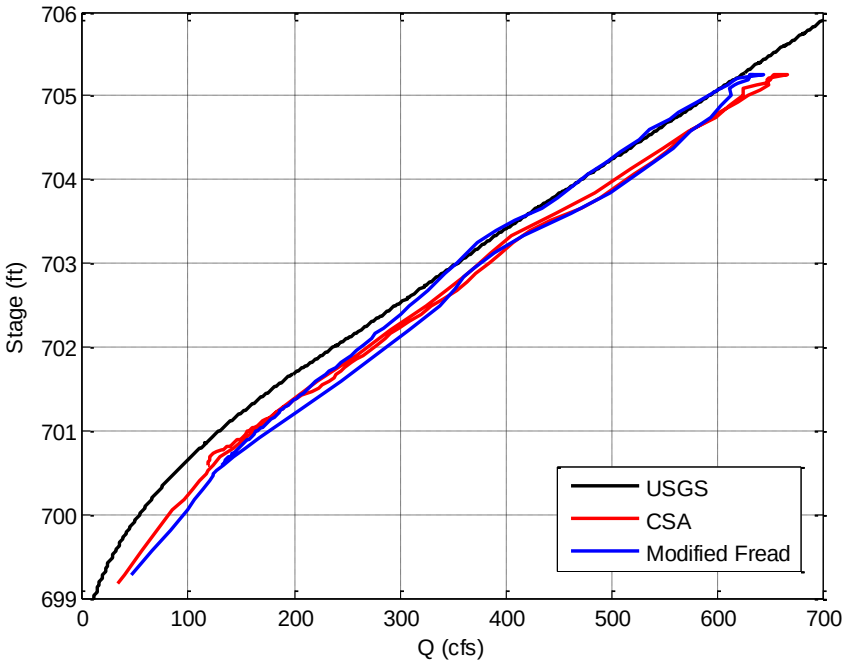


c)

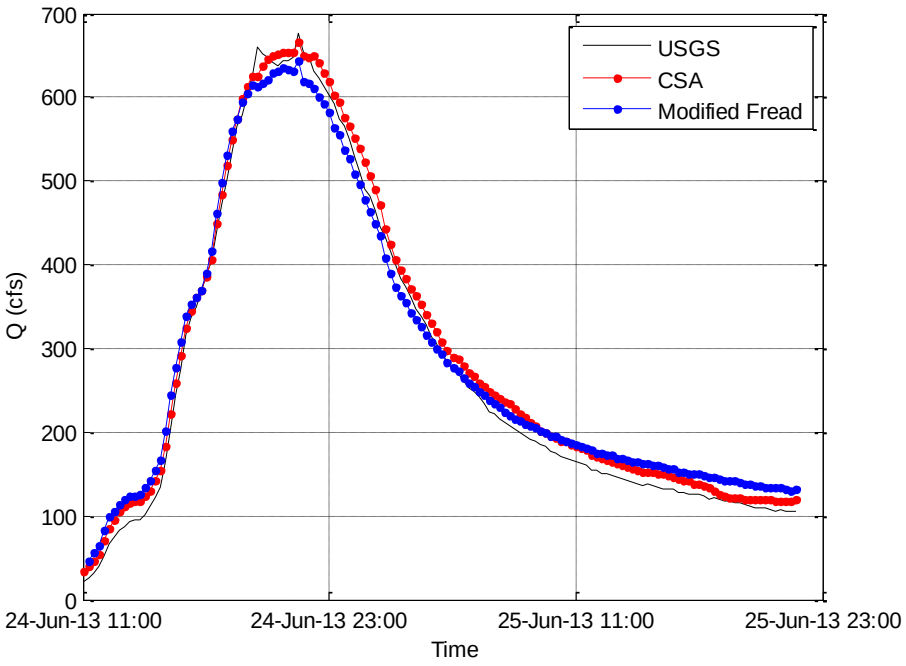


d)

Figure III.31 hQRCs and discharge hydrographs computed using the CSA and the modified Fread method based on the first event on June 24, 2013: a) hQRC at USGS gage; b) discharge hydrograph at USGS gage; c) hQRC at the Upstream PT; d) discharge hydrograph at the Upstream PT

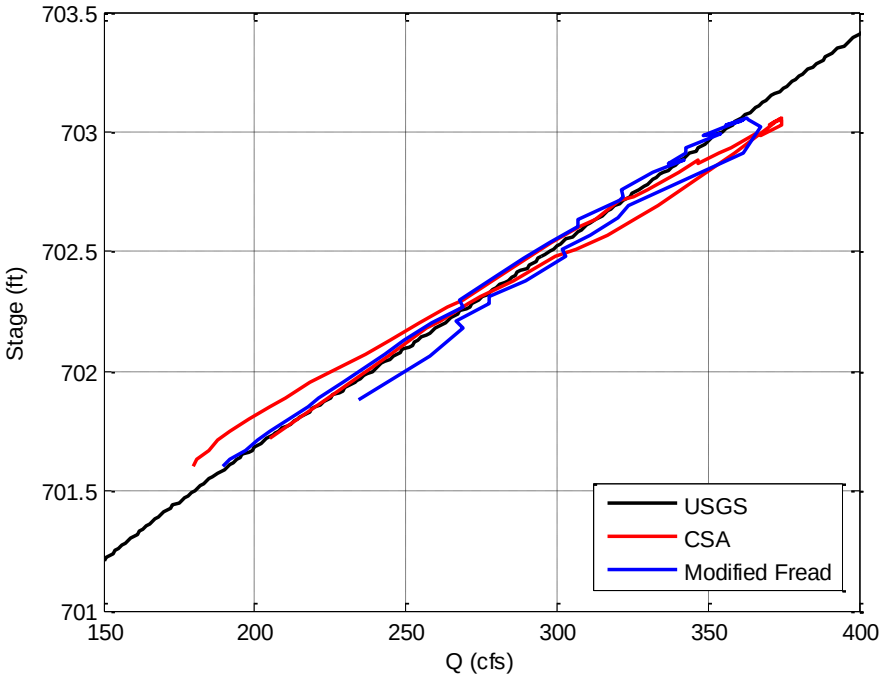


a)

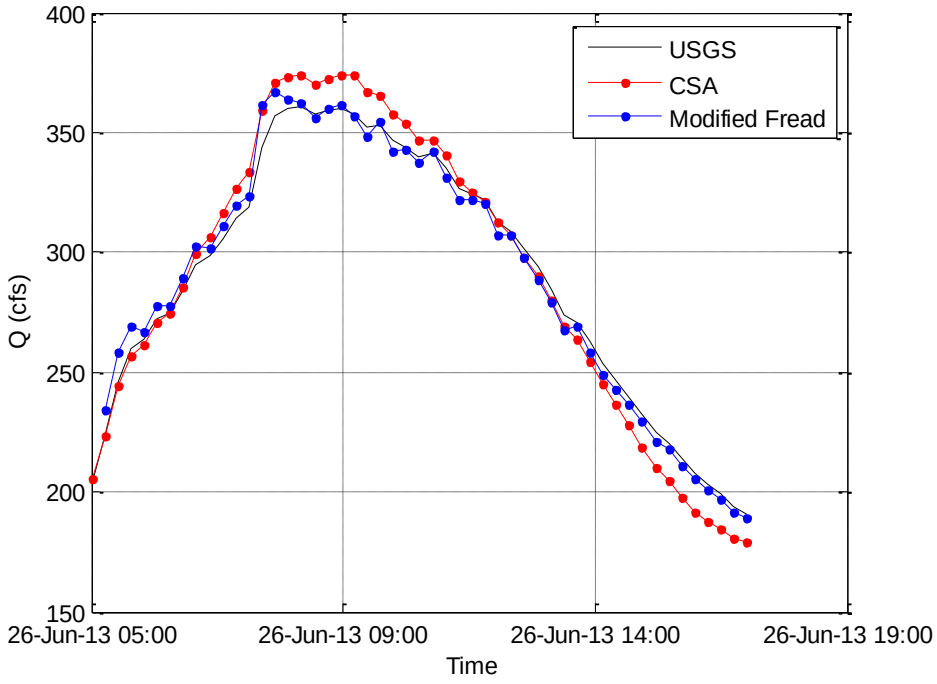


b)

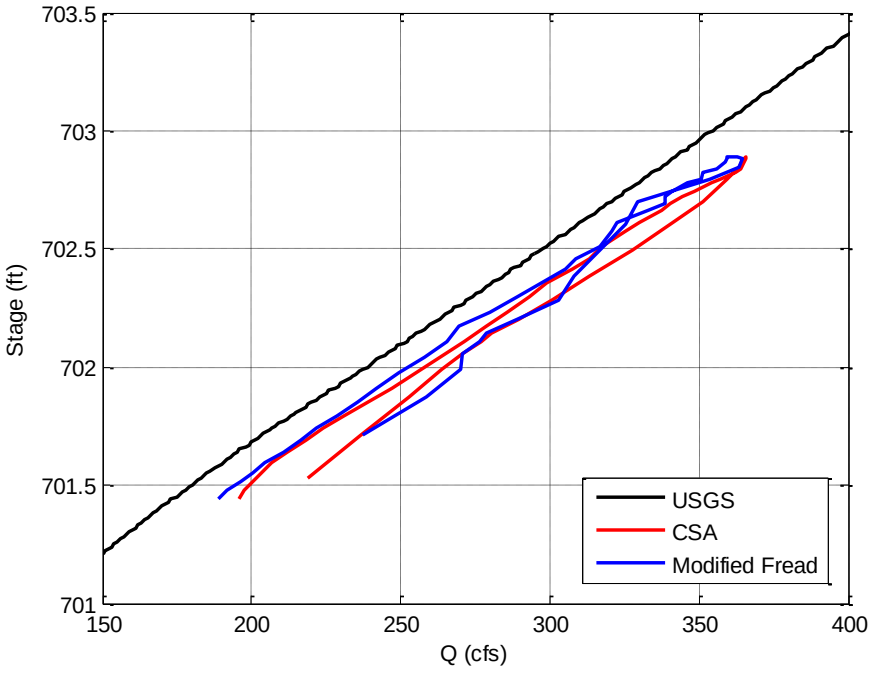


c)

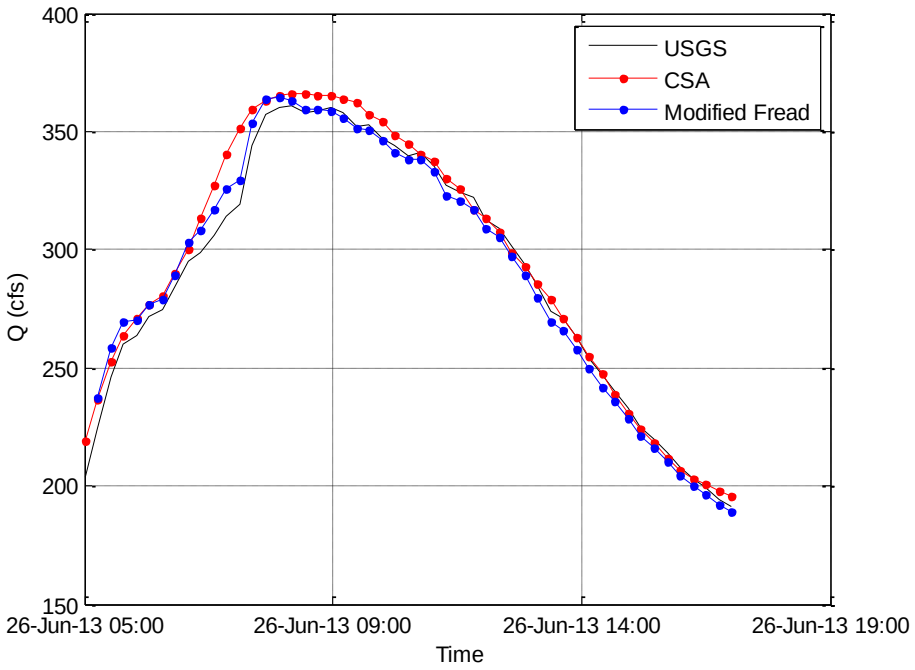


d)

Figure III.32 hQRCs and discharge hydrographs computed using the CSA and the modified Fread method based on the second event on June 26, 2013: a) hQRC at USGS gage; b) discharge hydrograph at USGS gage; c) hQRC at the Upstream PT; d) discharge hydrograph at the Upstream PT

*Reference stream source 1:*

*Irregular channel with meanders and woody debris (logs).*
*Bankfull: n = 0.05 / Overbank: n = 0.10*

a)

*Reference stream source 2:*


Manning's n: 0.047

Manning's n: 0.058

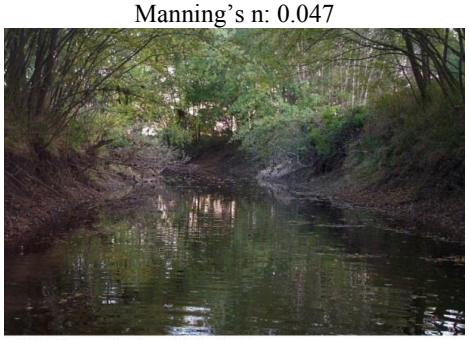


Manning's n: 0.053


Manning's n: 0.050

b)

Figure III.33 Example of reference streams for estimating Manning's roughness coefficient

---

Source 1:
http://www.brisbane.qld.gov.au/documents/building_development/technical_docs/ncd_appendixc_part3.pdf

SOURCE 2:
http://il.water.usgs.gov/proj/nvalues/enter_range.shtml?lowerN=0.045&upperN=0.06

## III.4 Conceptualization of unsteady flow effects on the shape of hQRC

It is known, that the shapes of the loop RCs are significantly changing from site to site and event to event. The shape of the RC is determined by the combined effect of hydro-geological (e.g., soil type and moisture content) and meteorological (e.g. rain intensity and duration) conditions as well as stream hydraulics. The result of this combination is a family of loop RCs reflecting the status of those conditions at various times (see Figure II.7 d)), so it is important to know when and where hysteresis is significant. The following two sub-sections will introduce hysteresis diagnostic methods with an implementation example in Clear Creek, Iowa. Subsequently, the significance of unsteadiness parameters on the shape of RCs will be evaluated using HEC-RAS unsteady model and the modified Fread equation.

### III.4.1 Hysteresis Diagnosis

While unsteady flows develop for each storm conveyed in a river network, their significance in terms of inducing deviations in the steady RCs varies widely. Hysteresis is a function of the site characteristics and the type of storm event, and therefore is not everywhere and anytime of equal concern. It is known that steep sloped stream tends to induce kinematic waves where the hysteresis loop is not so important. Mild sloped stream tends to induce dynamic waves and if the flood hydrograph is violent it might produce a considerable loop. There have been attempts to define thresholds for ranges of parameters associated with site and storm characteristics to diagnose when and where hysteresis is significant. The diagnostic formulas stem in the type of flood routing provided by equation (II.10). A summary of selected criteria for identifications of the storm and site characteristics with significant hysteresis is provided in Table III.2.

Table III.2 Hysteresis diagnostic formulas

| Reference | Criterion description | | | |
|---|---|---|---|---|
| Fread (1973&1975) | a. insignificant when $S_o$>0.001 for 0<*dh/dt*<4ft/hr<br>b. moderately significant when 0.0001< $S_o$ <0.001 for 0.1< *dh/dt* <3 ft/hr<br>c. significant when $S_o$ <0.0001 for *dh/dt* >0.05 ft/hr | | | |
| Mishra and Seth (1996), Mishra and Singh (1999), and Mishra et al. (1996 & 1997) | Wave type | Hysteresis, $\eta$ | Wave number $\hat{\sigma}$ and $\hat{\sigma}F_o$ | Phase difference $\emptyset$ |
| | Kinematic | $\eta < 0.025$ | $\hat{\sigma} \leq 0.03$ | $\emptyset < 0.03$ |
| | Diffusion | $0.025 \leq \eta \leq 0.10$ | $\hat{\sigma}F_o \leq 0.462$ | $0.03 \leq \emptyset \leq 0.13$ |
| | Dynamic | $\eta > 0.10$ | $\hat{\sigma}F_o > 0.462$ | $\emptyset > 0.13$ |
| Ponce et al. (1991) | $\tau = TS_0V/D$<br>$T$ = wave period, commonly taken to be twice the time of rise of the flood wave; $V$ = reference flow mean velocity; and $D$ = reference flow depth;<br>For $\tau$ > 171, the kinematic wave approximation was found to be reasonable (i.e., hysteresis occurs when $\tau$ < 171 - diffusive wave) | | | |
| Takahashi (1969) | $\lambda=V_s/(c*sin\theta)$ *where* $V_s=(h_p+h_b)/T_d$<br>$T_d$ =duration from the base discharge to the peak discharge; $sin\theta$= bed slope;<br>The parameter $\lambda$ implies the ratio of the rising speed of water surface ($V_s$) to the vertical component of celerity $c$ of long waves. | | | |
| Nezu and Nakagawa (1993) | $\alpha= (1/U_c)*V_s$<br>$U_c$ =convection velocity of turbulent eddies and is roughly equal to $(U_b + U_p)/2$; The authors indicated that Takahashi (1969) is not suitable to compare unsteady flows over smooth beds with those over rough beds, because the values of bed slope $S_o = sin\theta$ are quite different between the two, and therefore they proposed a new relationship by replacing $c*sin\theta$ with $U_c$. | | | |
| Graf and Suszka (1985) | $\Gamma=(1/u_{*b})*(\Delta h/\Delta T)$<br>where $u_{*b}$ is the friction velocity of the base flow, $\Delta h$ is the difference of the maximum and base flow depth; $\Delta T$ = $T_{rising}+T_{falling}$ is the time duration of the hydrograph | | | |
| Dottori et al. (2009) | $S_o \geq 5\times10^{-4}$ (steep slope);<br>Good estimation of kinematic or quasi-kinematic conditions | | | |

Note: The subscripts *b* and *p* denote the "base" and "peak" values, respectively.

Excepting the methods proposed by Mishra and Seth (1996), Mishra and Singh (1999), Mishra et al. (1996 & 1997) and Fread (1973 & 1975), the methods listed in Table III.2 simplify Saint Vernant equation by neglecting convective and local accelerations terms which are known to be small relative to the pressure term. Initially, we investigated formulas developed by Mishra and colleagues. The approach accounts for hysteresis by assessing the area of the loop in its non-dimensional form to determine the type of flood routing and the magnitude of unsteadiness, but is limited in terms of determining the thickness of the hysteresis loop. The approach used by Ponce et al. (1991) separates the kinematic from diffusive wave based on a pre-established cut-off value (see Table III.2). The formulas output is providing exact information on how much of hysteresis is going to occur. The same limitation is encountered in the formulas developed by Takahashi (1969), Nezu and Nakagawa (1993), and Graf and Suszka (1985). Dottori et al. (2009) proposed a formula based on the Dyrac (dynamic RC) equation that indicates that hysteresis is not likely to occur when the bed slope is greater than $5\times10^{-4}$.

Based on the above-mentioned considerations, the Fread (1973 & 1975) approach was adopted for hysteresis diagnostic protocol in this study. The reasons for our selection are summarized next. First, the method accounts for *dh/dt* derived from convective acceleration term which was neglected in the other equations. Second, instead of approximating *dh/dt* based on base and peak stages with total durations, it can account for any moment of the stage changes in time. Third, the required physical variables (bed slope, hydraulic depth, *dh/dt*, and Manning's roughness) are in general not very difficult to obtain from direct measurements. Fourth, the output of this method provides the size of the loop in absolute value for stage or discharge which is quite straightforward to understand and readily used (rather than thresholds or non-dimensional values).

The assumptions made in Fread (1973&1975) formula are listed below and the diagnostic equations are described by equations (III.15) through (III.17).

- The hydraulic depth, $D$ is substituted for the hydraulic radius, $R$ in Manning's equation.
- The area of the channel can be represented as $A=BD$ ($B$=Width, $D$=hydraulic depth) assuming rectangular-shaped channels.
- The depth difference, $\Delta h$ between the steady and unsteady RC at the same discharge can be approximated $\Delta D=D_s$ (hydraulic depth based on steady assumption) – $D_u$ (hydraulic depth based on unsteady assumption). Due to this assumption, we did not apply modification to the Fread diagnostic formula (1973 & 1975) to take advantage of the $\Delta h$ term (representing the size of the loop) which is easily determined from stage records.
- The wave celerity coefficient, $K$ is assumed as 1.3 for deriving the equation.
- Gravity force, pressure force, and convective acceleration are all considered in estimating the energy slope and the local and wave subsidence terms are neglected.

$$\Delta h \cong \Delta D = D\left[1-\left(\frac{S_0}{S}\right)^{0.3}\right] \tag{III.15}$$

$$D=\left[\frac{Qn}{1.486B}\right]S^{-0.3} \tag{III.16}$$

$$S \cong S_0+\frac{\partial h}{\partial t}\left[\frac{0.52}{S_0^{1/2}\dfrac{D^{2/3}}{n}}+\frac{0.01S_0^{1/2}D^{2/3}}{Dn}\right]S^{-0.3} \tag{III.17}$$

*where*, $D$ is the hydraulic depth; $S$ is the energy slope; $n$ is Manning's roughness coefficient

This hysteresis diagnostic formula based on Fread equation was implemented in Clear Creek, Iowa for a specific site and event. The site is the USGS gaging station (05454220). And the event is the storm of on April 14, 2012. The bed slope of 0.0007 was established with Trimble R8 GPS RTK (see Figure III.1 (c)). The hydraulic depth

($D$) of 3.05 ft (corresponding to approximately 703.7 ft in NAVD 88 vertical datum) is chosen because the rate of change in depth ($dh/dt$ = 1.6 ft/hr) was the maximum at this hydraulic depth during the course of storm event. The Manning's roughness coefficient ($n$) of 0.055 is assumed using the best available information obtained from USGS steady discharges using the relationship: $n = (1.486AR^{2/3}S_o^{1/2})/Q$.

The diagnostic formula anticipates a $\Delta h$ of approximately 0.4ft (corresponding to 13% difference from the steady curve) and a deviation of $\Delta Q$ of roughly 40cfs (corresponding to 11% difference from the steady curve) as shown in Figure III.34. These differences can be used as estimated uncertainties in the steady RC induced by unsteady flows. The method can be applied on historical records but they also can be used in forecasting mode if the steady RC-based discharges are available (see for example the data-driven forecasting developed by Bhathacharya and Solomantine, 2005)

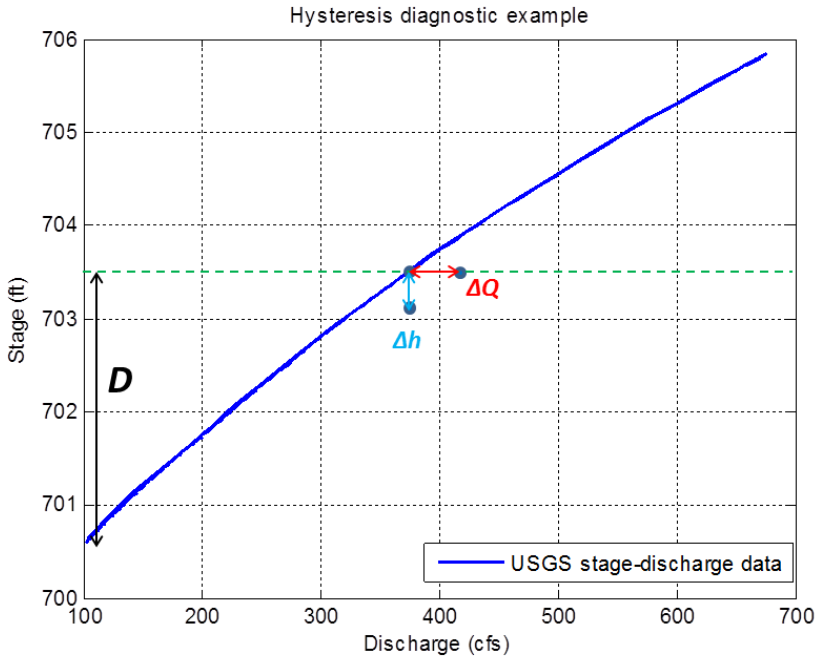


Figure III.34 Example of implementation of the hysteresis diagnostic formula

### III.4.2 Evaluation of the significance of unsteadiness parameters

This section investigates the importance of unsteadiness parameters introduced in the previous section and its sensitivity to storm characteristics and site conditions. The first part of this section analyzes the parameter sensitivity associated with storm characteristics using HEC-RAS unsteady model built for Clear Creek watershed. HEC-RAS model was chosen for this purpose as it is considered suitable for simulating flood wave propagation in natural rivers and streams (e.g. Horritt and Bates, 2002; Castellarin et al. 2009). Moreover, the HEC tools are well developed for conveniently providing flood forecasting and flood inundation maps as well (Knebl et al., 2005). In the second part of the section the sensitivity analysis is conducted for testing parameters related to site conditions such as the channel bed slope and Manning's roughness coefficient. This analysis is based on the modified Fread equation using the storm event on April 14, 2013 as the illustration sample.

*Sensitivity analysis to storm characteristics*

Clear Creek watershed is located in the southeastern corner of the state of Iowa near Iowa City. The watershed is based on 10-digit Hydrologic Unit Code (HUC), HUC 0708020904 Clear Creek – Iowa River, and the size of the watershed is approximately 103 $mi^2$. The watershed consists primarily of farm land with some urban areas that include Oxford, Tiffin, Coralville, and Iowa City. Figure III.35 shows the location of numerical models in the state of Iowa (red polygon), while Figure III.36 presents the HUC-10 Clear Creek watershed boundary (black polygon), as well as HEC-RAS modeled area (red polygon) within that boundary.

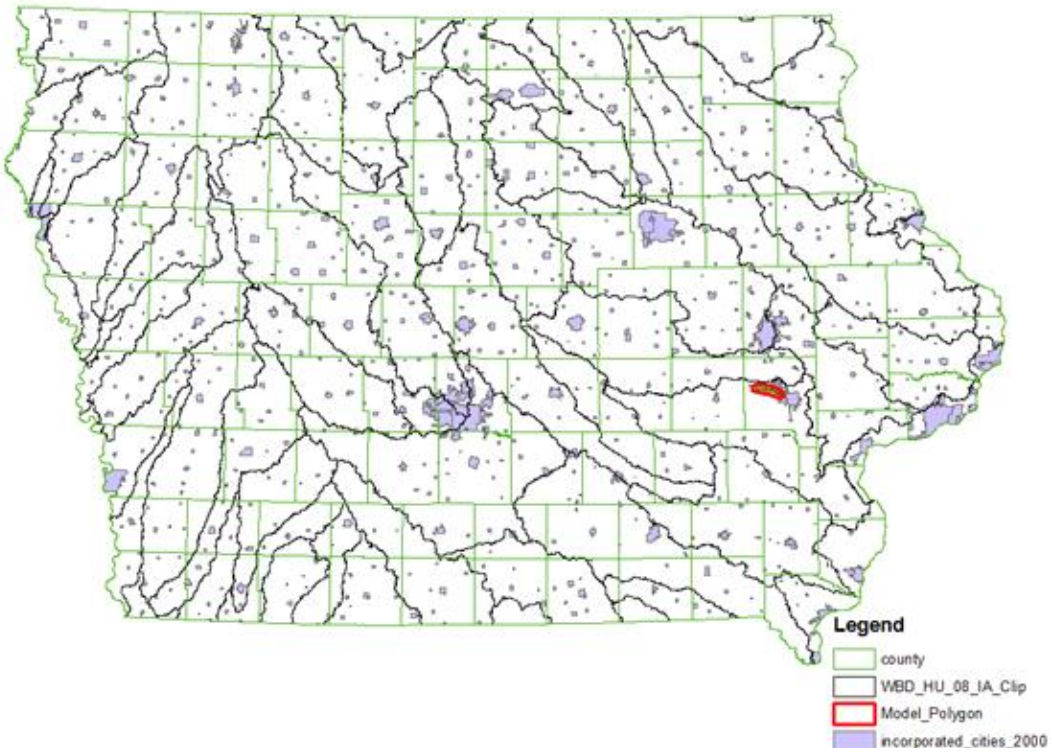


Figure III.35 Location of the study area in the state of Iowa

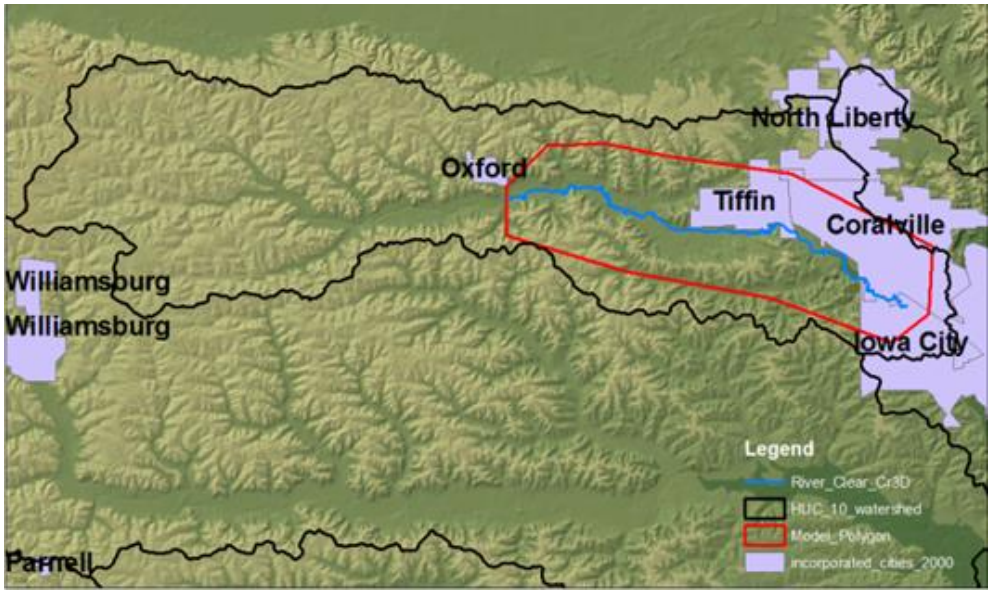


Figure III.36 Locations of Clear Creek watershed and modeling area

The modeled area is described in detail in Figure III.37, along with the location abbreviations (*S1* through *S4*) which will be used conveniently thorough the sections. *S1* is the upstream boundary, *S2* is the location where we are mainly interested in, and *S3* is the downstream location where the second USGS gage (05454300 – Clear Creek near Coralville) exists, and *S4* is the downstream boundary with normal depth assumption. Various types of artificial storm hydrographs are assumed for this investigation.

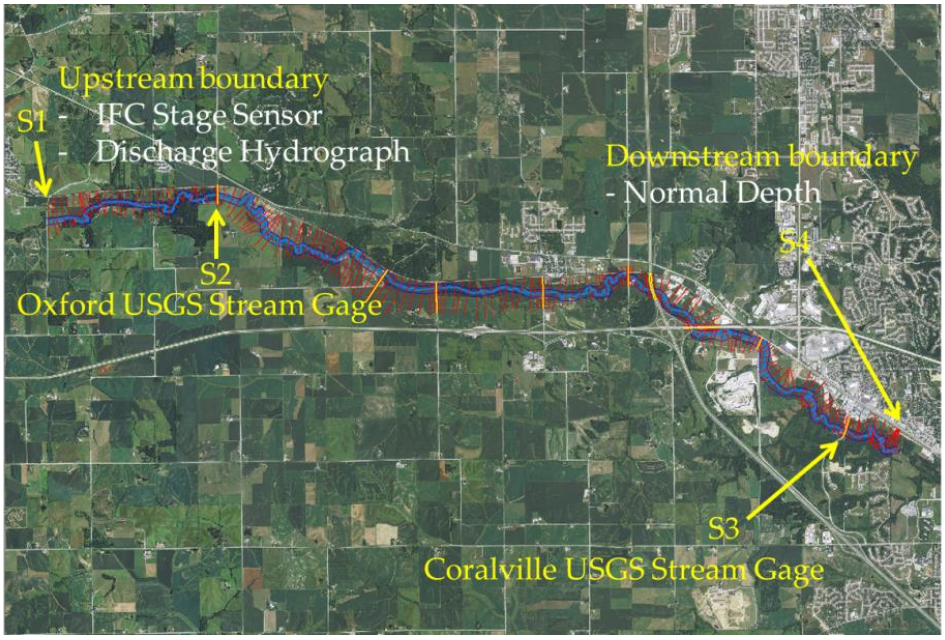


Figure III.37 Modeled area in the first phase HEC-RAS model

The role of the HEC-RAS simulations conducted in this task is two-fold: *a)* to identify the dependencies between the types of incoming hydrographs and corresponding loop RC and *b)* to parameterize the shape of the loop RC as a function of the incoming hydrograph characteristics. The site conditions along with the meteorological conditions are the drivers of the shape of the inflow hydrograph and loop RC.

Figures III.38, III.39, and III.40 describe a based storm hydrographs with changes applied to peak discharge, total duration, and peak discharge timing. The plots in Figure III.38 implies that the larger the event the larger the maximum thickness of loop RCs. The plots in Figure III.39 indicate that a shorter and more intense storm results in a larger the maximum thickness of the loop RC. The plots in Figure III.40 suggest that as the time to peak is longer, the maximum thickness of loop RCs becomes thinner and the curve moves upward.

In summary, it can be concluded that the thickness of the loop (or size of the loop) RC increases when a) the total duration of the storm is short; b) the time to and from the peak to base flow is short; c) the storm intensity is high.

*Sensitivity analysis to site conditions*

While storm characteristics are directly associated with the rate of depth change in time ($dh/dt$) involved in the flood propagation equation, more significant factors in changing the shape of the loop RC are the magnitude of channel bed slope and channel roughness. Using the storm event described in Section III.2.2, the sensitivity to Manning's roughness coefficient and channel bed slope are illustrated in figures III.41 and III.42, respectively. Based on the Manning equation, it is found that 10% variation of those parameters resulted in discharge estimation errors about 20% and 10%, respectively, since discharge are proportional to the square root of slope and inversely proportional to the Manning's roughness coefficient.

Figure III.43 shows results obtained with the modified Fread equation to substantiate the effect of these parameters on the shape of the RCs. Figure III.43 (a) captures the effect of slope: the milder the bed slope the thicker hysteresis loop develops and the loop is evolving in anti-clockwise direction. Figure III.43 (b) illustrates the roughness effect: the higher the Manning's roughness coefficient results in the development of a counter-clockwise loop RC.

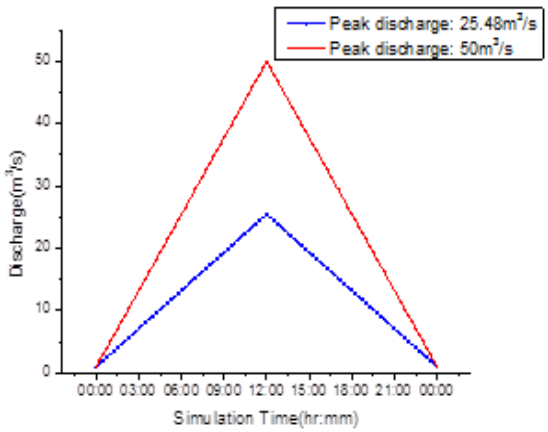


Input hydrograph at S1

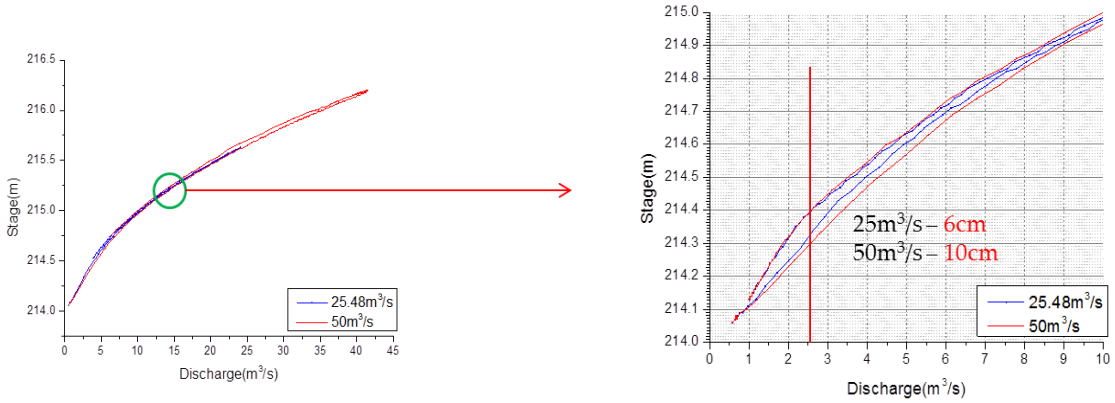


Simulated RCs at S2

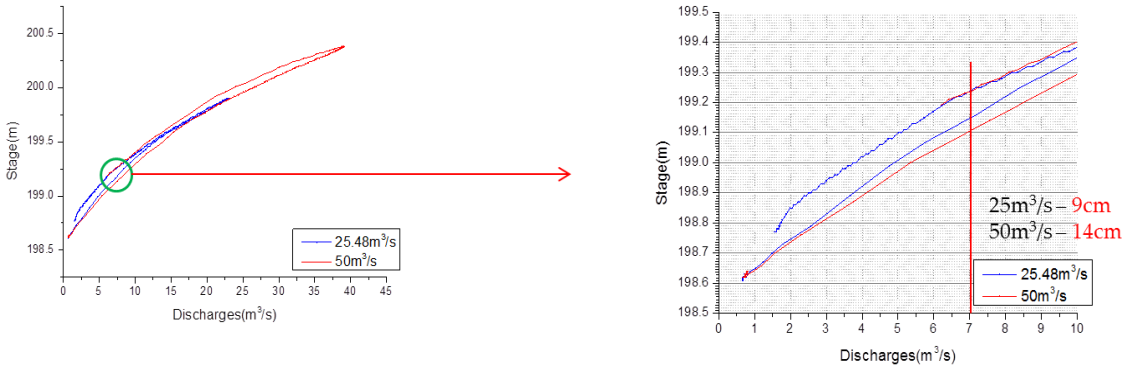


Simulated RCs at S3

Figure III.38 Sensitivity analysis: storm peak discharge

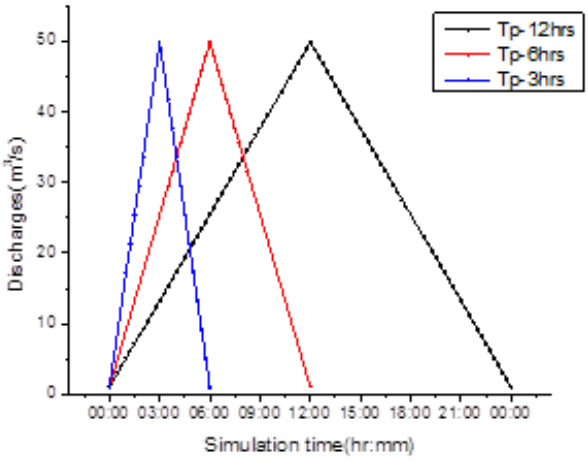


Input hydrograph at S1

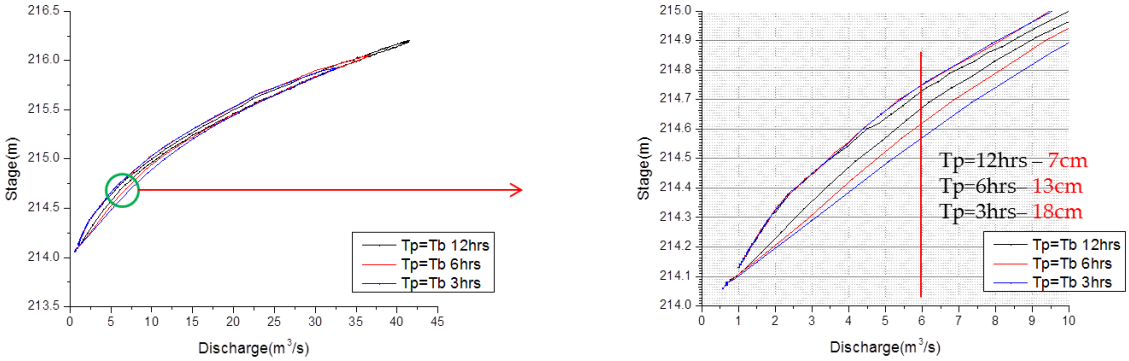


Simulated RCs at S2

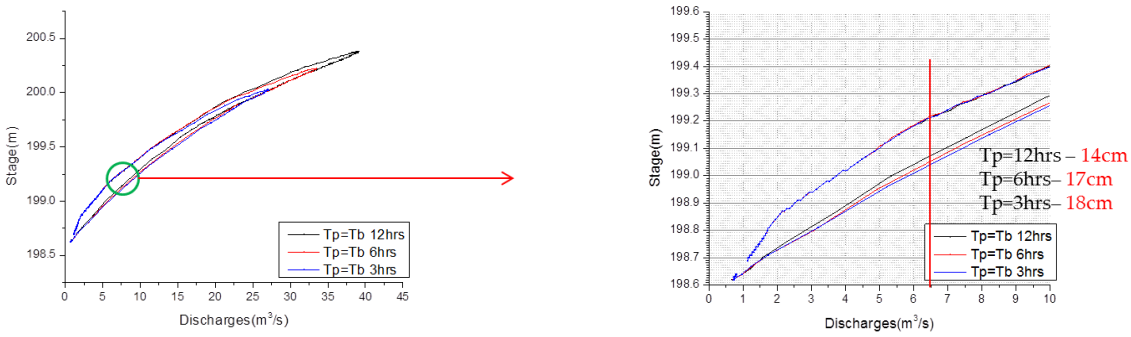


Simulated RCs at S3

Figure III.39 Sensitivity analysis: storm duration

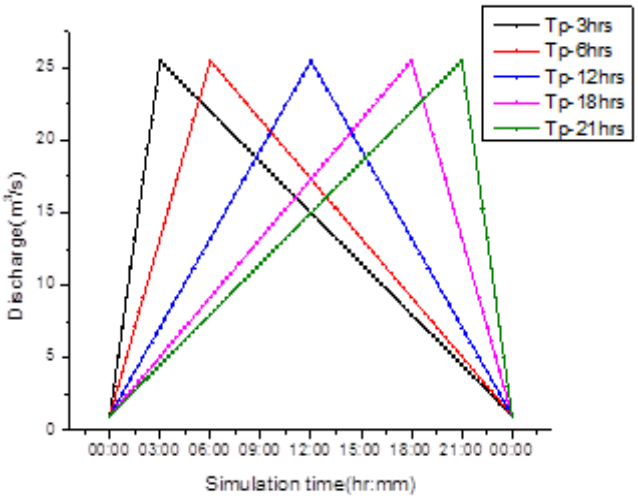


Input hydrograph at S1

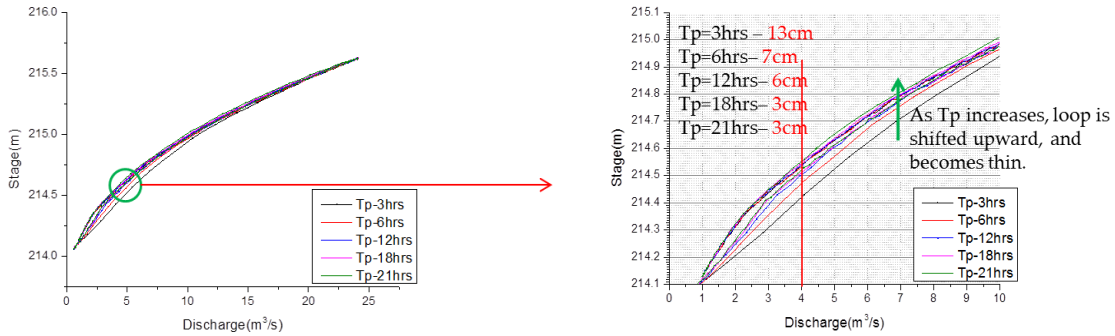


Simulated RCs at S2

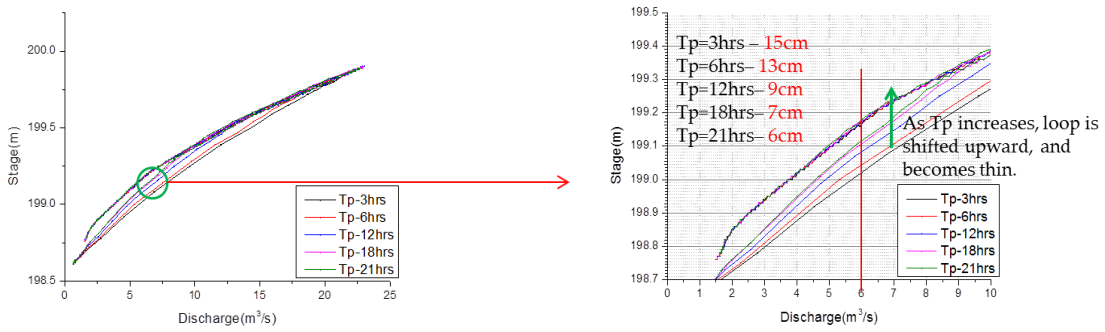


Simulated RCs at S3

Figure III.40 Sensitivity analysis: storm peak discharge timing

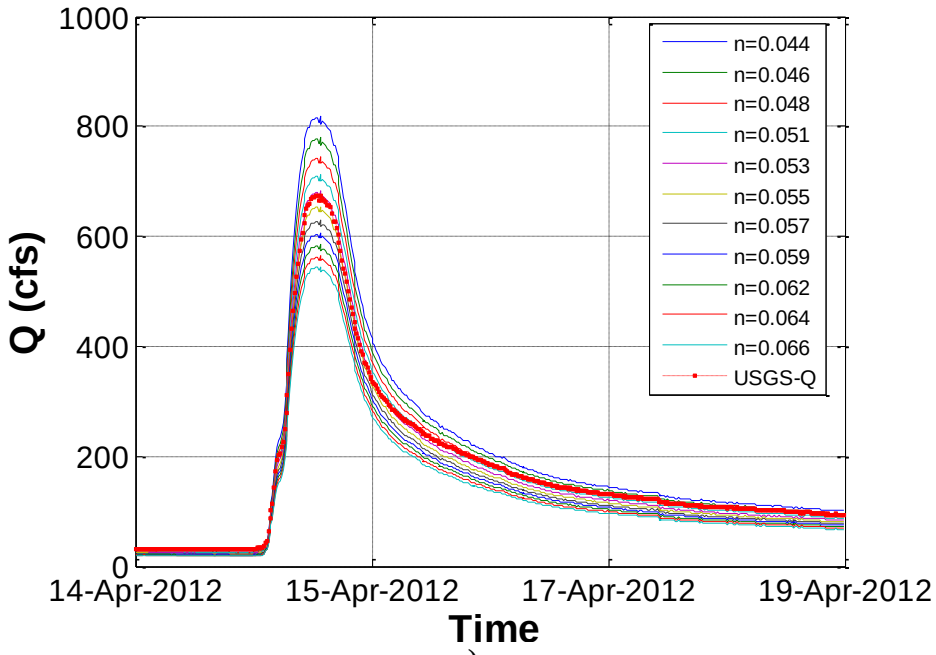


a)

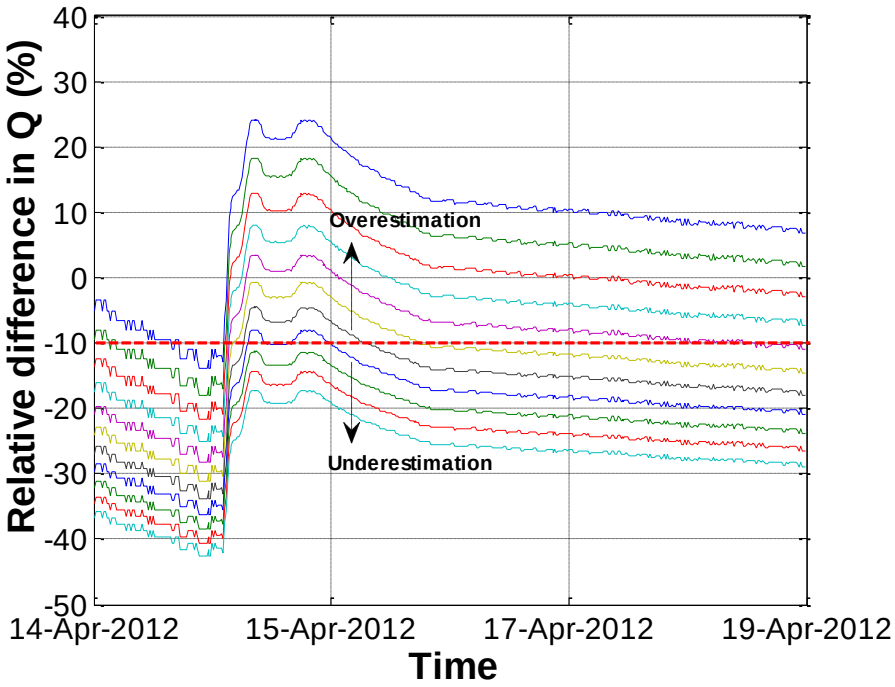


b)

Figure III.41 Effect of Manning's roughness coefficients variation on discharges: a) Discharge hydrographs with variation of Manning's roughness coefficients; b) Relative difference in discharges between USGS and Manning equation due to variation of Manning's roughness coefficients

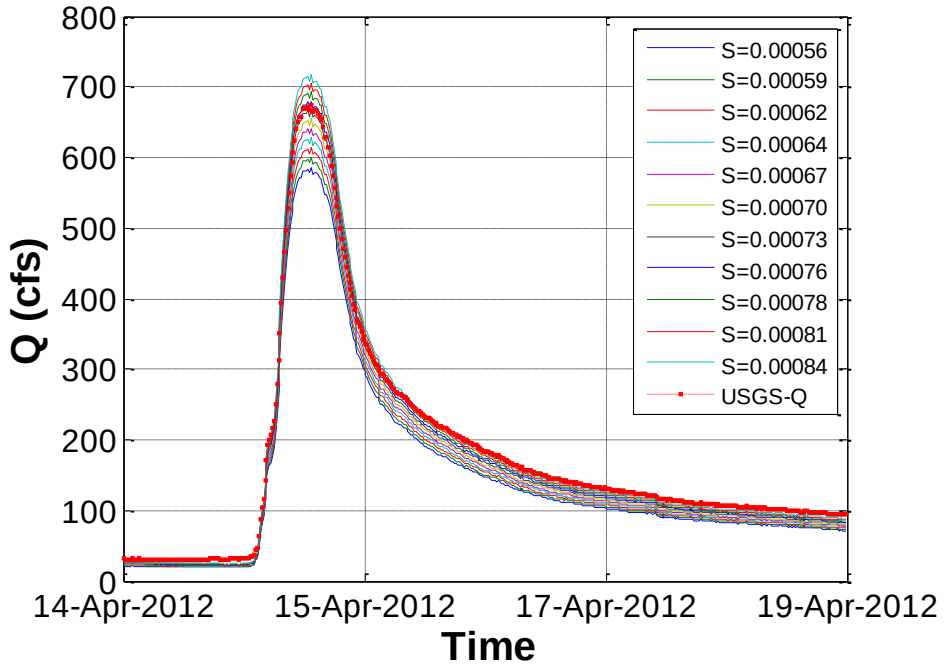


a)

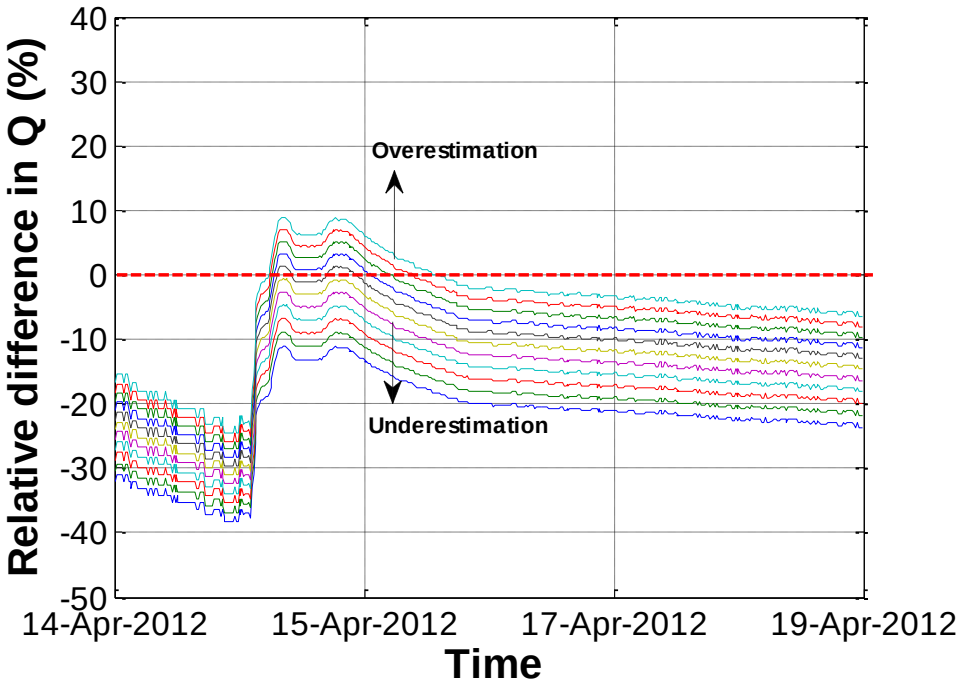


b)

Figure III.42 Effect of channel bed slope variation on discharges: a) Discharge hydrographs with variation of channel bed slope; b) Relative difference in discharges between USGS and Manning equation due to variation of channel bed slope

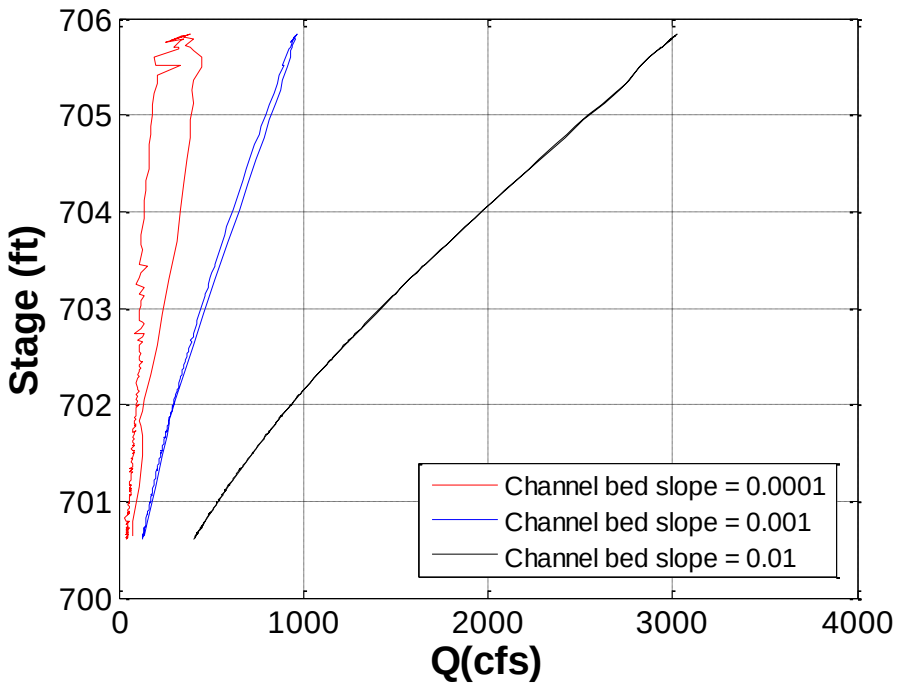


a) *assumed n* = 0.045

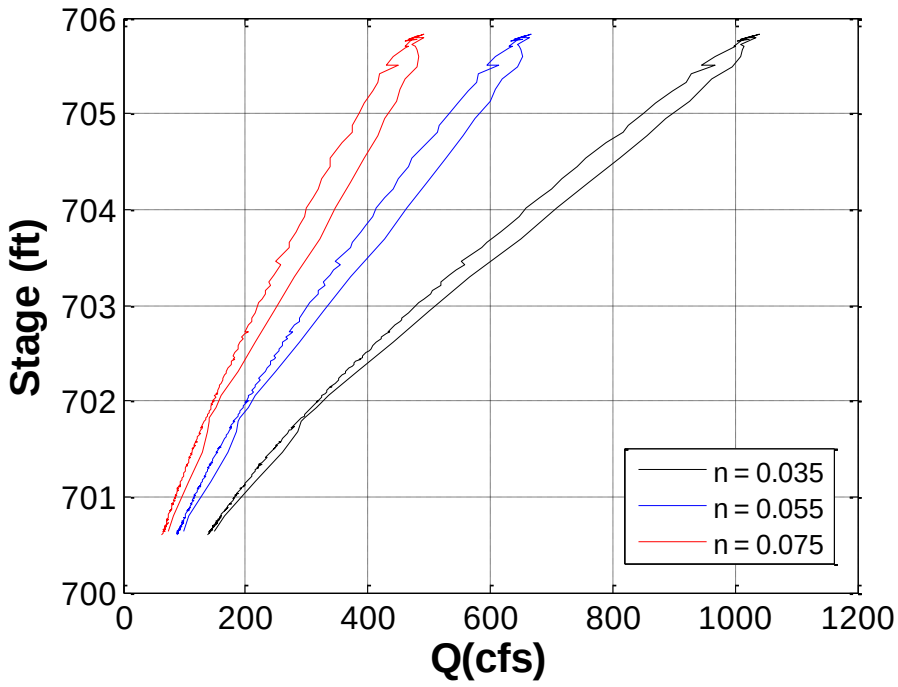


b) *assumed* $S_o$ = 0.0007

Figure III.43 Sensitivity analysis: a) effect of channel bed slope on a shape of RCs; b) effect of Manning's roughness coefficient on a shape of RCs

# CHAPTER IV

# UNCERTAINTY ANALYSIS (UA) IMPLEMENTATION TO HQRC

## IV.1 Uncertainty Analysis Considerations

The study presented in this section is based on Muste et al. (2012).

### IV.1.1 Evaluation of Frameworks

Reporting results of hydrologic and hydraulic studies based on measurements obtained with various instruments or comparing hydrometric measurements among themselves requires a statement of the quality of the measurements involved. Usually the quality of the measurements is expressed quantitatively by the uncertainty of those measurements, and oftentimes the terms "data quality" and "uncertainty" are used interchangeably. Hydrometric measurements are affected by the randomness of the observed physical phenomena and by errors occurring during the various phases of the measurement process. Since the randomness of a physical system and the measurement errors are unavoidable, the true value of a result cannot be obtained. The best way to characterize the "true" value of a measurement is to carefully conduct the measurement process and subsequently provide an estimate of the quality of a measurement through a sound uncertainty analysis (UA). UA is a practical substitute for the variability and errors that cannot themselves be measured, so the UA's estimation should be made in a clear and transparent manner.

UA estimates the interval about a variable or determined result, within which the true value is thought to lie, with a certain degree of confidence (Coleman and Steele, 1995). In addition to providing confidence in the reported measurement, UA provides information on the performance of the measurement systems and indicates where in the process there is need for improvement. UA is utilized in various forms from the initial

planning to the design, debugging, testing, and data analysis. The above-mentioned aspects emphasize the importance of establishing uniform approaches for conducting the UA within specialized professional areas, such as the hydrometric community.

In most situations, an experiment/study involves measurements of a number of individual variables that are subsequently used in a functional relationship, also named the data reduction equation (DRE). A rigorous UA estimates first the elemental sources of uncertainty associated with each of the variables in the DRE (whether they were induced from a direct measurement or not) and subsequently propagates those uncertainties into the final result. While the methods for estimation of the elemental sources of uncertainty are similar among various communities (statistical analysis, previous experience, expert opinion, or manufacturer specifications), the methods used to determine how those sources of uncertainty are accounted for in the final result have differed widely (TCHME, 2003). For several decades, scientists, engineers, and practitioners argued about the appropriate procedure to conduct UA (Abernethy and Ringhiser, 1985). To date, there is still no wide consensus in this regard, but the discourse about the need for unified procedures is making considerable progress.

Early efforts in conceptualizing UA started in the 1950s, when the American Society of Mechanical Engineers (ASME) initiated an effort based on the hallmark paper by Kline and McClintock (1953). After many years of disagreement, ASME's efforts finally achieved consensus in 1986 with the adoption of ASME-PTC 19.1 (ASME 1986). In 1978, world's highest authority in metrology, the Comité International des Poids et Mesures (CIPM) requested the Bureau International des Poids et Mesures (BIPM) to search for an international consensus on the expression of uncertainty in measurements. For this purpose, BIPM and the International Standard Organization (SO) assembled a joint group of international experts to include other five organizations: International Electrotechnical Commission (IEC), International Federation of Clinical Chemistry (IFCC), International Union of Pure and Applied Chemistry (IUPAC), International

Union of Pure and Applied Physics (IUPAP), and International Organization of Legal Metrology (OIML). The result of this multi-agency collaboration is the "Guide to Expression of Uncertainty in Measurement" (GUM 1993). This standard was republished with minor modifications in 1995 to become the first internationally accepted guideline for the conduct of uncertainty analysis. More recently, the Joint Committee for Guides in Metrology (JCGM) has been formed in 1997 to assume responsibility for the maintenance and revision of the GUM.

The GUM framework is based on the most recent advancements and principles in mathematical statistics for the propagation of the elemental sources of errors to the final results. GUM provides general rules for the evaluation and expression of uncertainty in measurement rather than providing detailed and specific instructions tailored to any specific field of study. The guide differs from previous uncertainty assessment methodologies in terms of terminology, classification of errors, and procedures (Herschy, 2002). Studies conducted to compare available UA methodologies (i.e., Steele et al., 1994; Coleman and Steele, 1995) conclude that the GUM framework is more robust and mathematically firmer than alternative methods, such as ASME and American Institute of Aeronautics and Astronautics (AIAA) standards (Taylor and Kuyatt, 1994; NF ENV 13005, 1999). Recently, ASME and AIAA standards have been harmonized with the GUM terminology and procedures through new versions [ASME Standard PTC 19.1 (1998, 2005) and AIAA Standard S-071 (1995, 1999)]. GUM terminology and procedures have been widely adopted by national and regional metrology and related organizations in Europe and the USA (Taylor and Kuyatt, 1994; ANSI, 1997). Several scientific and engineering areas (e.g., NF ENV 13005, 1999; ISO 5168, 2005; UKAS, 2007) have also embraced the guidelines in an attempt to use a uniform method of expressing measurement uncertainty.

The hydrometric community has been continuously seeking to improve procedures for the assessment of the measurement errors, but until recently has not

agreed on one particular framework. Various hydrometric groups have tested methodologies developed by other communities, such as GUM (1993) or AIAA (1995), and concluded that they can be successfully applied for assessment of the measurement uncertainty in laboratory and field hydrologic/hydraulics measurements (Bertrand-Krajewski and Bardin, 2002; Muste and Stern, 2000; Muste et al., 2004; Kim et al., 2005; Kim et al., 2007; Gonzalez-Castro and Muste, 2007; UNESCO, 2007). More such initiatives have been launched recently. The Technical Committee on Hydraulic Measurements and Experimentation (TCHME) of the American Society of Civil Engineers' Environmental & Water Resources Institute formed a Task Committee on Experimental Uncertainty and Measurement Errors in Hydraulic Engineering in 2003 (Wahlin et al., 2005). Similarly, in 2004, the UNESCO's 6th International Hydrology Program initiated an effort to compile guidelines for Integrated Urban Water Management, which also includes sections dedicated to UA (UNESCO, 2007). The World Meteorological Organization's Committee on Hydrology is currently reviewing UA procedures in an effort to recommend uniform approaches for implementation in the national hydrologic services (Pilon et al., 2007). These last initiatives indicate that adopting GUM for conducting UA rather than developing specific standard for hydrometry might be a more practical option.

Selecting and implementing a standard for a professional community is a process that requires long-term commitment and effort. According to Thomas (2002), the following steps are essential in the adoption of a standard: evaluation, prioritization, implementation, planning, accessing standards, getting the standards used, and maintaining the drive. It is obvious that such a process is beyond the scope and means of this thesis, which aims to provide the reader with an overview of judiciously selected standards, while demonstrating that the standards can be successfully applied for assessment of the measurement uncertainty in hydrometry. Specifically, consideration is

given to practical implementation of GUM and the Monte Carlo method recently published as an alternative approach to GUM (JCGM 101, 2008).

### IV.1.2 Implementation procedures for uncertainty analysis

The basic steps in conducting a rigorous uncertainty analysis are:

(1) *Define the measurement process*. The direct or multivariate measurement process through which the physical quantity value is estimated needs to be modelled through a functional relationship between the input and output of the measurement (usually a mathematical expression) and other factors involved in the measurement process. At this stage of the analysis, it is also useful to briefly describe the measurement setup, environmental conditions, and technical information about the instruments to help identify the measurement process errors, including errors not associated with the variable in the modelled measurement.

(2) *Identify the error sources and estimate the corresponding uncertainties*. Once the sources of errors in the measurement process are identified, the uncertainty estimates are developed using measured or assumed probability distributions. The uncertainty of the elemental error sources are described by the square root of the variance of the measurement error distribution.

(3) *Propagate the uncertainties to the final result*. This step is accomplished by using the variance addition rule (a direct method is used in the MCM). For one input variable, the addition to the variance of various sources of uncertainties of that variable is applied. For a multivariate measurement, in addition to considering the variance of the individual input variables, the possible correlations between the measurement process errors need to be considered. For multivariate analysis, it is also important that the input variable uncertainties are weighted by the appropriate sensitivity coefficients. The degrees of freedom for each uncertainty component, as

well as that of the combined uncertainty obtained through the propagation of elemental uncertainties to the final result, are then determined.

(4) *Report the analysis result*. The reports for uncertainty estimates should present an uncertainty budget containing, at minimum, information such as the value of the quantity of interest and its combined total uncertainty probability distribution for each elemental sources of errors, the list of the measurement process uncertainties and associated degrees of freedom for each component and applicable cross-correlated uncertainties, and sensitivity coefficients.

The specific steps for implementing the GUM framework and Monte Carlo Method are provided in Appendix A along with concepts and terminology. The procedures presented in Appendix A will help to facilitate the understanding of calculations used in this Chapter and the practical examples described in Appendix B. The terminology, notations, and procedures used in this research were maintained as they appear in the source references [i.e., GUM, 1933; JCGM 101, 2008] for consistency, rigor, and easy cross-reference.

## IV.2 Uncertainty sources in hQRC

### IV.2.1 Review of the sources of uncertainty in RCs

Uncertainties in RCs stem from a variety of sources. Table IV.1 lists the widely recognized sources of uncertainties using a grouping adapted from Fread (1973). By and large, uncertainties in RCs are widely unknown for specific sites and flow situations, especially for high flows (such as floods) when some of the uncertainties affecting the RCs are considerably increased. Moreover, some of this uncertainties are time depended in a periodic (e.g., vegetation growth) or slowly varying (e.g., change in the stream cross section) manner. The evaluation of these uncertainties is made using experimental (Schmidt, 2002), statistical (Herschy, 1970; Baldassare and Montanari, 2009), and non-statistical (Pappenberg et al., 2006; Shrestha et al, 2007) methods. Given the challenges

and costs associated with these estimations, the current practice for maintaining RC accuracy is repeated based on direct discharge measurements and subsequent adjustments of the RCs to account for the effect of the processes are made over a wide range of flows and stream morphology conditions.

An exhaustive discussion of all the sources of uncertainties listed in Table IV.1 is beyond the scope of the present work. For illustration purposes, Figure IV.1 materializes graphically the implications of having these sources active or neglecting various processes involved (change in cross-section, backwater, hysteresis, etc) on the conventional RC. Special consideration is given herein to sources of uncertainties specific and active during high flows (floods).

### IV.2.2 Uncertainty analysis in RCs for high flows

For high and unsteady flows, many of the sources of uncertainties listed in Table IV.1 might be active depending on the gage locations and storm characteristics. For channel-controlled stream reaches (i.e., channel flow driven by friction), the sources of uncertainties of top importance are those associated with: *a)* the measurement uncertainty, *b)* neglecting the hysteresis effect, *c)* extrapolation of the rating, *d)* change in cross section (overbank flow).

Uncertainty type *c)* is associated with measurement uncertainty as categorized in Table IV.1 due to limited observations or periodic changes of physical conditions in a stream. That is, compared to the number of measurements at small to medium flows, limited observations at high flow conditions lead an uncertainty due to limited information attributed to either incorrect extrapolation of the curves or changes in real physical conditions such as river bed roughness. The extrapolation uncertainty is less documented as the availability of data is scarce for large flows, which are typically infrequent. Simulation results estimated for this uncertainty by Baldassarre et al., 2009 showed 11.5 to 13.8%, and this uncertainty is also known to be increasing with discharge

magnitude (Lang et al., 2010). However, this analysis is considered beyond scope of this study. Moreover, uncertainty type *d)* is active only if not considered in the construction of the RC, a situation not under consideration in the present discussion as well.

For section-controlled stream reaches (local control due to weirs or other channel obstructions), the uncertainty reproduced by the backwater is equally important. The uncertainties produced by unsteady flow, backwater, and change in cross section are typical for flood situations and they have a hysteretic nature that makes their analysis complex due to their superposition.

Therefore, the present research is focused only on two uncertainty sources: measurements and hysteresis. Currently, measurements uncertainties using ADCP were estimated assuming steady-flow condition with customized experiments, so limited to be extensively applied for unsteady flow conditions. However, the uncertainty analysis discussed in Section IV.3.1 is still valuable, since the UA framework itself should be valid for different sites and storm conditions once uncertainty sources for those corresponding conditions become available.

For hysteresis analysis, the assessment of the uncertainty is made for simple flow situations to isolate its components and subsequently consider additional complexities. Specifically, we analyzed the effect of flood flow propagation in channels controlled by friction (channel control) rather than channels with local controls where backwater is inherently involved. Furthermore, the hysteresis-related uncertainty is estimated only for in-bank flow situations as the change in cross section occurring during floodplain flows generate hysteretic uncertainties that are difficult to separate from the mix. Even for this simpler flow situation, the estimation of hysteresis-induced uncertainty is still complex as it is influenced by the speed of travel of the flood wave, wave number, and phase differences and attenuation of the flood wave (Mishra, 1996). Larger or smaller hysteresis loops are created depending of the type of flood waves: dynamic or kinematic.

Physically, a dynamic wave propagates in both upstream and downstream direction, while a kinematic wave propagates only in the downstream direction (Henderson, 1966).

An illustration of the interplay between sources of uncertainties in RC active in high flows is provided in Figure IV.2. Overlooking these uncertainties in the decision-making process for flood situations may result in disastrous consequences, and therefore there is a need to investigate its significance and magnitude taking into accounts both the site and event characteristics as discussed in Chapter III.

A brief review of the available information on the sources of uncertainties acting during high flows follows.

a) Measurement uncertainty for Discharge

Uncertainties associated with measurement process itself such as instrument accuracy, instrument calibration, vertical velocity model, operational conditions, etc. to compute discharges. Estimation of these error sources is conducted assuming steady flow conditions.

This source of uncertainty for the velocity-area method was found to range within 4 -13% (Pelletier, 1988), 4.4% (Carter & Anderson, 1963), 6% (ISO 748, 2007), 7% (Herschy, 1975), and 5-6% (Leonard et al., 2000; Schmidt, 2002) using conventional discharge measurement instrumentation. The similar magnitude of uncertainty using propeller current meter was found 13.5% (Muste et al., 2012; Appendix B). The uncertainty due to ADCP direct discharge measurement was found 4.3% to 5.8% by our customized experiments (Lee et al., 2013, in-press) as subsequently will be described in Section IV.3.1. While these estimates were found for specific flow conditions, Shrestha and Simonovic (2009) demonstrated using fuzzy nonlinear regression that there is considerable increase of this uncertainty with the discharge magnitude.

b) Uncertainties due to Hysteresis

Schmidt (2002) summarized selected literatures up to year of 2002, and indicated that there have been two large streams which have dealt with uncertainty in hQRCs. One

is the methods that lump all uncertainty sources listed in Table IV.1 into single value, and the other is the methods that distinguish the stage-discharge uncertainties due to hysteresis from the other sources. Focused on the latter case, Dickenson (1967) showed 5.7 to 34% of variation of stage-discharge rating uncertainties. Diamond and Christian (1982) presented statistical analysis of errors using least-squares fit of logarithmic curve to estimate the uncertainties associated with hysteresis. Baldassarre and Montanari (2009) presented their numerical analysis showing that the uncertainty induced by the presence of unsteady flow conditions can cause up to 9.8% of error in total discharge estimates. They applied the HEC-RAS model for the Po River reach (Italy) characterized by 200-500m channel width, 10-15m depth, 1000-3000m floodplain width, and an average slope of 0.0002, and compared the discharge error differences based on steady and unsteady RCs. The results showed that the total uncertainty in RC caused by a) interpolation and extrapolation, b) hysteresis, and c) seasonal variation of roughness along the river reach varies from 1.8% to 38.4%. Also, as presented in Chapter III, Faye and Cherry (1980) collected data on 1976 during the storm events in Chattahoochee River, Georgia at four locations, and observed that approximately 2-3ft stage-wise loops which correspond to 20-30% differences relative to the stage changes during the course of storm events. Fread (1975) also observed approximately maximum of 5ft dynamic loop on the Lower Mississippi, Red, and Atchafalaya Rivers in state of Louisiana between year of 1963 and 1967.

Evaluation of the hysteresis-related uncertainties is still in development as the experimental studies are scarce and fragmented (due to the difficulty to acquire the measurements), while the analytical and numerical simulations presented in Section II.3.2 are using various simplifications, and have been few verified on case studies due to the unavailability of data. Currently, the literature does not offer criteria for a comprehensive evaluation of the methods for estimation of the departure of the loop (actual) RC from the steady RC nor for identifying the most appropriate ones for different possible river flow

conditions. Therefore, protocol to account for hysteresis in hQRC based on the methods suggested in Chapter III will be presented in the last section of this chapter.

## IV.3 Uncertainty Analysis for discharge measurements with ADCP: Clear Creek Case Study

The study presented in this section is based on the paper in press (Lee et. al., 2013).

### IV.3.1 Introduction

StreamPro[1] is a 2MHz Acoustic Doppler Current Profiler (ADCP) typically used in medium and small streams with depth up to 6m with an upgrade option. The majority of discharge measurements made by the USGS are in streams with mean depths of less than 1 meter. For larger streams, largely used are ADCPs of various configurations and acoustic pulse characteristics: TRDI Rio Grande[1], TRDI RiverRay[1], Sontek/YSI River Surveyor[1], Sontek/YSI Argonaut-XR[1], etc. The StreamPro is similar to Rio Grande ADCP in many respects (i.e., acoustic geometry, signal processing, data format, operational considerations) with the main distinction being the probe size and that the former are equipped with positioning and rotation recording devices (Global Positioning System -GPS- device and compass) in their standard configurations.

StreamPro can be operated using two deployment methods: moving boat or stationary method (section-by-section). The first method is implemented by slowly traversing the ADCP from a bank to the opposite one using a tagline or walking across a bridge. This method is commonly used as there is no need for personnel to be deployed in the stream and is relatively fast to do a measurement. Several transects are collected and the estimated discharge is obtained as the average of the sample measurements in

[1] The use of product or commercial names does not imply endorsement by the authors or author's institutions or WMO

moving boat method (USGS, 2011). The section-by-section (SxS) method is closer to the conventional discharge measurement protocol, whereby the instrument is positioned successively at several locations over the cross section and a velocity-area method is applied to obtain discharges in consecutive panels (spaces delimited by measured verticals). This method is the method of choice when measuring under ice, when moving bed situations exists, and very low velocity flows.

There is ample literature covering discharge measurements with Streampro using both approaches (Marsden, 2005; Rehmel, 2006; Frizzel and Vermeyen, 2007; Gunawan et al., 2010). These studies indicate that the StreamPro displays a high variability in the measurement of velocities (Frizzell & Vermeyen, 2007; Gunawan, 2010). Notably, the extensive USGS study conducted by Rehmel (2006) using concurrent discharge measurements with Streampro, Price AA, 1200 kHz TRDI RioGrande ADCP, and Sontek/YSI FlowTracker ADV at 20 shallow channel flow sites (different depths, widths, velocities), indicates that:

- on average, the StreamPro has proven capable of measuring discharge within 5% of standard USGS data-collection methods
- for measurements with mean velocities below 0.25 m/s, the discharge in individual transects varies substantially. The variability is high even if eight or more transects are collected (per standard USGS methods). While no persistent bias was detected, this result means that using the StreamPro to make discharge measurements under these low-velocity flow conditions may not be practical because of the time required for obtaining additional and sufficient transects to reduce the uncertainty of the measurements to acceptance levels.

Most of the above mentioned studies assess the quality of the measurements based on repeated measurements and instrument comparisons, not through implementation of rigorous uncertainty analysis using standardized approaches. Few attempts to conduct

uncertainty analysis for acoustic instruments using rigorous procedures are reported in the specialized literature. One recent example is Huang (2012) that, despite some limitations regarding the terminology and level of detail of the analysis, illustrates the use of GUM (1992)-based standards for UA (Muste and Lee, 2013).

Uncertainty analyses, even if rigorous in terms of methodology, can be developed at various levels of detail commensurate with the available resources for conducting the analysis. The full-fledged analysis is based on the mathematical formulation of the measurement process to include the entire data acquisition chain starting from sensor signal to data display (to account for uncertainties in signal conversion, conditioning, post-processing) along with the uncertainties induced by environmental conditions and operational protocols. Attempts to conduct such detailed UA for ADCPs were made by Gonzalez-Castro and Muste (2007) using the AIAA (1999) standardized approach, which is closely related to GUM (1993). The analysis fell short, however, as many of the uncertainty sources involved have no estimates and the customized experiments needed for estimation of elemental sources of uncertainties require extensive efforts which are rarely considered in practical situations. More data are needed to actually implement this analysis.

While there is continuous progress and increased amount of literature addressing the quality of measurements with ADCPs, there is still work to be carried out both in terms of establishing measurement protocols and, more importantly, in assessing the sources of uncertainties involved in the measurement process. While the measurement protocol for Streampro SxS method is well established stemming from the long-term implementation of the discharge measurements with mechanical velocimeters, the protocols for the moving-boat method (for StreamPro and other types of ADCPs) do not have well established and uniform measurement protocols. There are continuous efforts in this regard (RDI, 2008; Mueller & Wagner, 2009; Gunawan, 2010; USGS, 2011: and

Garcia et al., 2012). Gunawan (2010) hypothesizes that it is possible that the measurement protocols might need different specifications for large and small streams.

The following sub-sections will describe the details of UA implementation procedures based on the experiments conducted in lab and field (Clear Creek) between year of 2011 and 2012, and specifically the SxS discharge measurements were conducted on April 4th, 2012 at Clear Creek assuming steady state flow condition. The stage was monitored during the course of measurements, and no visible unsteadiness was identified.

### IV.3.2 Preamble to SxS Streampro ADCP measurements

It is assumed herein that the reader is familiar with the principle and basic operational information about ADCPs. Therefore, no discussions on ADCP technology, configuration, and operational settings are made in this analysis. The discharge measurements reported here were acquired with a standard configuration StreamPro ADCP (no compass or GPS) using SxS method. The StreamPro ADCP, produced by Teledyne RDI Instruments (rdinstruments.com), provides velocity profiles by almost instantaneously sampling velocity in multiple cells (a.k.a. bins) along verticals (i.e., pings or ensembles). Streampro also measures acoustically the depth of the water column. Views of the instrument and floating platform are provided in Figure IV.3.

StreamPro obtains bin velocities by averaging the Doppler phase shift for several pings and then computing the Doppler velocity from the averaged phase data (Mardsen, 2005). StreamPro makes eight sub-pings and then computes the velocity profile. This is done six times each second and the average of the six pings is then output. In all the cases reported in this study, StreamPro was operated in Mode 12, which is Streampro's default water velocity profiling mode. In this mode the StreamPro can output up to 20 cells with sizes of 2-10 cm, giving a total profiling range of 20-200cm, and with the upgraded long range profile mode, 30 cells with sizes of 2-20cm, giving a total profile range of 20-600cm. Using 5 cm probe immersion (submergence), 3 cm blanking distance,

and 5 cm cells, the first cell is centered 10.5 cm below the transducer. In this mode, about 20 cm is the minimum water depth in which two cells of data can be measured. Most of our measurements were obtained in shallow water conditions with a cell size of 3 cm and a max depth of less than 100cm. ADCP cannot measure near the boundaries (free surface and bed), so the area covered by velocity measurements is slightly smaller than the actual cross section as illustrated in Figure IV.4.

Discharge estimation with SxS method uses similar protocols as the conventional mechanical velocimeters. Specifically, vertical velocity profiles are acquired for pre-established time durations at several locations across the stream. The location of the verticals is usually guided by a tag line set across the stream. The distance between the verticals is measured with an alternative instrument and inputted in the Streampro data acquisition software. Similarly, the distance to edges from the first and last measured vertical is measured and inputted in the software.

The unmeasured area at the top and bottom of each vertical is obtained by extrapolating the measured velocity profile in conjunction with velocity models such as logarithmic or exponential distribution laws (RDI, 2009). The ADCP measurement software calculates subsection discharges using the velocity profile and water depth data using the velocity-area method. A model for estimation of the edge discharges is finally used to provide the total discharge through the cross section.

Table IV.1 Uncertainty sources affecting RCs

| Source | Description | Selected References |
|---|---|---|
| Measurement error | Uncertainties in the measurement process of stage, discharge, site and flow characteristics. This source also includes uncertainties associated with regression and extrapolation of the experimental data points. | Pelletier (1988); Carter and Anderson (1963); Herschy (1970, 1975); ISO 748 (2007); Schmidt (2012); Shrestha and Simonovic (2009); Baldassare and Montanari (2009); Muste et al. (2012) |
| Control shift | Uncertainties due to change of the stream cross section or its bed forms, vegetation growth, ice/debris build-up | Simons et al (1973), Linsley et al. (1949), Herschy (1970); Kennedy (1984); Rantz et al (1982); Westerberg et al. (2011) |
| Variable energy slope | Uncertainties due to variable backwater, variable channel storage (overbank flows), unsteady flows | Jones (1916), Boyer (1937), Henderson (1966), Dickenson (1967); Dymond and Christian (1982); Schmidt (2002), Fread (1973) ; Baldassarre and Montanari (2009) |

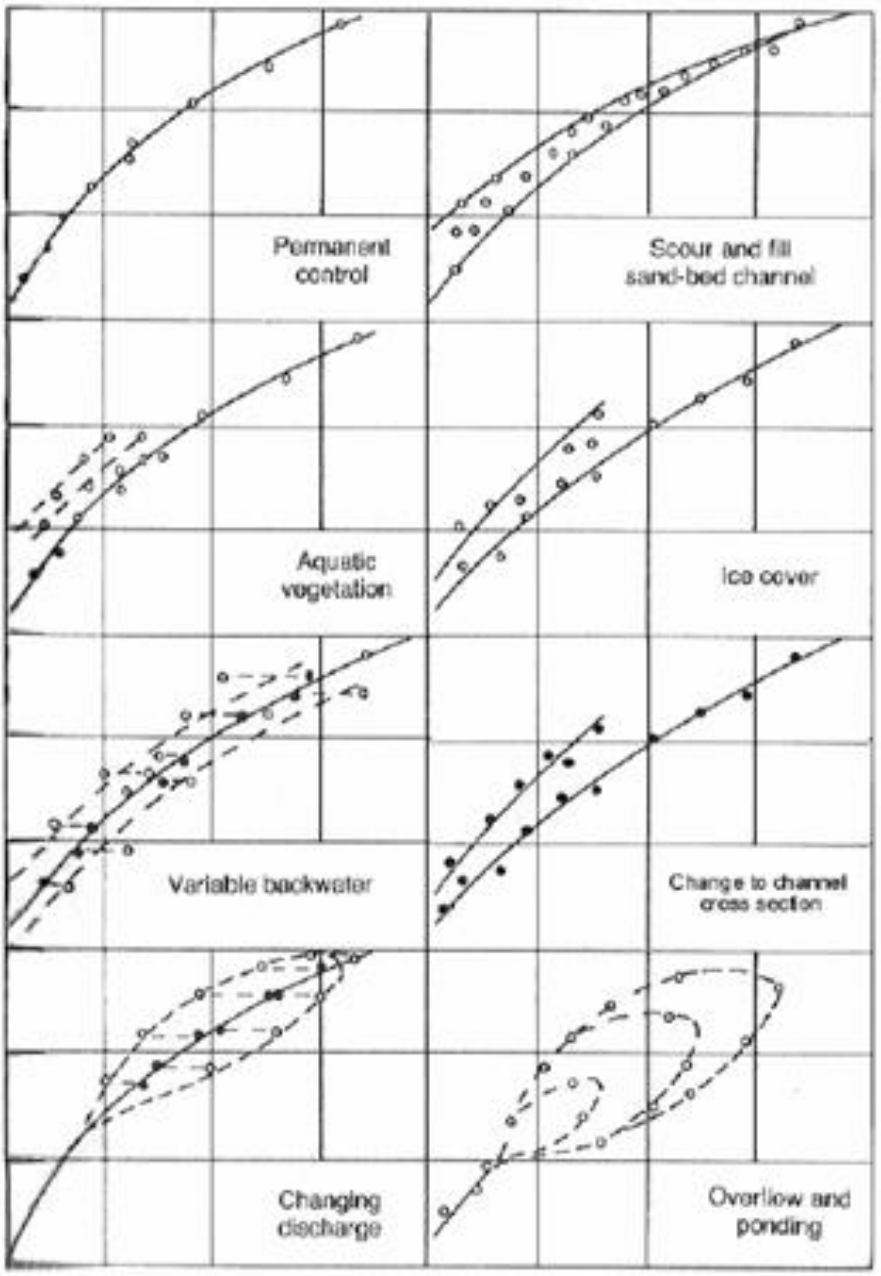


Figure IV.1 Typical effect of different physical processes on ratings

Source: adapted from Herschy (1995)

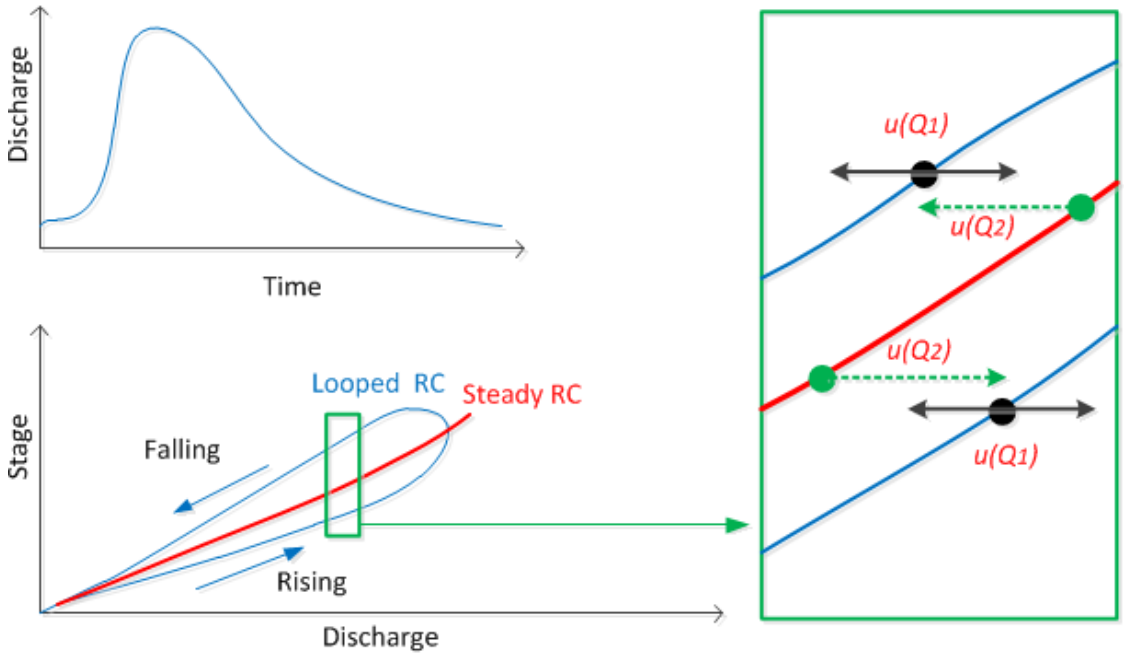


Figure IV.2 Conceptualized uncertainties in hQRC: *u(Q₁) and u(Q₂)* represent the uncertainties itemized in *a)* and *b)* below, respectively.

a)

| Velocity Profiling | |
|---|---|
| # cells | *1–20 standard; 1–30 with upgrade* |
| Min. cell size | *2cm* |
| Max. cell size | *10cm standard; 20cm with upgrade* |
| Max. range | *2m standard; 6m with upgrade* |
| 1st cell start | *7–30cm (from transducer); depends on cell size* |
| Accuracy (cell = 1/2 max.) | *±1.0%±0.2cm/s* |
| Resolution | *0.1cm/sec* |
| Velocity range | *±5m/sec (±2m/sec on standard float)* |
| **Physical Properties** | |
| Weight in air | *5 kg including electronics, transducer, float, and batteries* |
| Dimensions | *Electronics housing: 15 x 20 x 10cm*<br>*Transducer: 3.5cm diam. x 15cm length*<br>*Float: 44 x 70 x 11cm* |
| **Transducer** | |
| Frequency | *2.0MHz* |
| Geometry | *4 beams, 20° beam angle* |
| Beam width | *3°* |
| Material | *Polyurethane* |

b)

Figure IV.3 StreamPro ADCP (http://www.rdinstruments.com/streampro.aspx): a) views of probe and floating platform: b) specifications

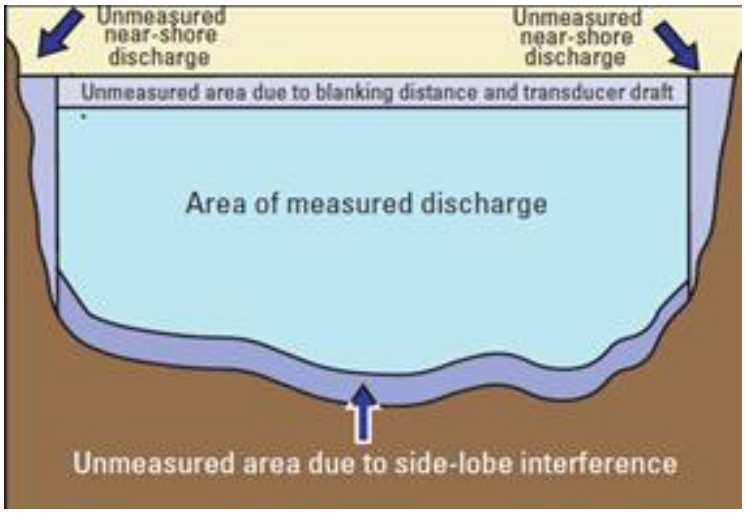


Source: Simpson (2001)

Figure IV.4 Area of the stream cross section measured by ADCPs

### IV.3.3 Measurement process

The measurements for the UA reported below were acquired in a typical Iowa stream: Clear Creek approximately 7.5 m wide located near Oxford in South-East Iowa (USA). Two sets of StreamPro ADCP measurements were acquired during the field test: one set of SxS measurements containing 23 fixed position measurements and 10 moving-boat transects. StreamPro measurements along the cross section were guided by a tag line set on the stream banks. A system of pullies attached to the tag line was used to guide the positioning of the verticals and keep the ADCP platform stable during the data acquisition. The moving boat measurements were acquired along the same tag line. For the SxS method, the first and last verticals were located at 1.2 and 0.7 m from the left and right waterlines, respectively. Following ISO (1088) recommendations, 23 velocity verticals (at 0.25 m interval) were acquired to cover the 5.5 m central area of the channel. Figure IV.5 a) illustrates the probe during measurements. Figure IV.3.b provides the

layout of the measurement in the stream cross section. Figure IV.3 c) depicts a snapshot of the TRDI SxS Pro data acquisition and processing software used to estimate the discharges.

Given the special nature of the present experiment, the StreamPro ADCP operational protocols were strictly followed as recommended in the SxS and moving-boat guidelines (RDI, 2009; Simpson, 2001; Muller and Wagner, 2009). Among the operational considerations strictly checked prior and during the measurements were:

- careful selection of the test section site
- proper mounting of the ADCP on the floating platform
- proper setting of the transducer in the support (45 degrees orientation with respect to the streamwise direction)
- verification of the communication between the probe and the data acquisition computer
- checking for moving bed condition using USGS SMBA software (http://hydroacoustics.usgs.gov/movingboat/SMBA1.shtml), and
- correct input for the variables involved in the data acquisition software (transducer draft setting, sampling time, cell size, number of cells, maximum water depth, etc.).

The location of each vertical was marked on the tag line using a conventional pocket measuring tape with the finest graduation of 0.0009m (0.003ft). Velocities and depths at each vertical were acquired by positioning the StreamPro along the tag line at the pre-established locations for 300s, which is an equivalent of 300 ensembles in the output files. Prior to the measurements, a 900-s long velocity sample was acquired in the deepest location (thalweg) of the cross section to estimate the duration for sampling the flow such as to obtain a reliable mean velocity profile that accounts for the temporal scales of the turbulence. Water depth was directly measured by the StreamPro. A

conventional wading rod with the finest resolution of 0.0009m was used to compare StreamPro measurements at selected verticals. The water depth in the cross section was continuously monitored over the time of measurements to check for potential flow changes, with no change being observed. A Sontek Flowtracker Acoustic Doppler Velocimeter was used to acquire velocities within the edge area that is not measured by the ADCP. The measurement environment at the time of measurements was not affected by adverse conditions (e.g., wind or rain, flow disturbances in the cross section).

The StreamPro moving-boat measurements were acquired for assessing the consistency of the total discharge obtained with the same instrument using different measurement protocols. The moving-boat measurements were post-processed with WinRiver II (RDI, 2007) while the SxS measurements were processed with StreamPro SxS Pro software (RDI, 2010). The discharge estimates obtained using the two alternative measurement protocols were in good agreement as subsequently discussed.

The SxS stream discharge is obtained using the mid-section method (Herschy, 2009). The algorithm assumes that the depth at a number of verticals in a cross section and the distance between the verticals are measured to determine the cross-section area for each panel (or subsection). Depth-averaged stream velocity in each vertical is estimated by the power function regression fit curve based on the sampled velocities in several points along the vertical. Panel discharges are computed as the product of segment area and the depth-averaged velocity. Total discharge is computed as the summation of the panel discharges.

For the measurement situation documented herein and sketched in Figure IV.5 b), the total discharges are estimated based on twenty three sub-discharge panels plus two others at the edges. Given that the ADCPs measures velocities in bins of equal size vertically stacked, the vertical velocity profiles contain a variable number of bin velocities commensurate with the depth magnitude. Using the notations in Figure IV.5 b), the directly measured discharge in the cross-section is defined by equation (IV.1), and the

total discharge including two edge discharges is estimated by equation (IV.2). The left and right edge discharges are estimated using equations (IV.3) and (IV.4), respectively.

$$Q_m = \bar{v}_1 \times d_1 \times (\frac{b_2 - b_1}{2}) + \sum_{n=2}^{22} \left( \bar{v}_n \times d_n \times (\frac{b_{n+1} - b_{n-1}}{2}) \right) + \bar{v}_{23} \times d_{23} \times (\frac{b_{23} - b_{22}}{2}) \quad \text{(IV.1)}$$

$$Q_t = Q_{LE} + Q_m + Q_{RE} \quad \text{(IV.2)}$$

$$Q_{LE} = 0.3535 b_1 d_1 \bar{v}_1 \quad \text{(IV.3)}$$

$$Q_{RE} = 0.3535 (b_{RB} - b_{23}) d_{23} \bar{v}_{23} \quad \text{(IV.4)}$$

*where* $Q_t$ is the total discharge in the cross section, $\bar{v}_n$ is the mean velocity at the $n^{th}$ vertical (and in the associated panel), $d_n$ is the depths measured at the $n^{th}$ vertical, $b_n = (b_{n+1} - b_{n-1})/2$ is the half width between $n$+1$^{th}$ and $n$-1$^{th}$ verticals. Therefore, $b_n$ is associated with the panel width at the $n^{th}$ vertical, and $b_{RB}$ represents the distance measured from the left bank to the right bank.

The analytical formulation provided in equations (IV.1) to (IV.4) was developed having in mind what variables are provided as output by the StreamPro ancillary processing software (e.g., WinRiver II). In this way the analysis can be repeated for other measurement situations using typical measurements.

The direct measurements involved in equation (IV.1) are: depth-averaged velocities and depths (provided by the StreamPro ADCP) and distance between successive verticals (measured with the pocket tape). Equation (IV.1) can be used for calculating $Q_m$, the flow in the area covered by the direct ADCP measurements (corresponding to the gray area in Figure IV.5 b) when only the measured portion of the depth is inputted. Alternatively, the flow through entire cross section excepting the edges can be obtained if the full depth (measured by the ADCP) in conjunction with extrapolation algorithms for the velocity in the vertical are used. Equation (IV.2) in conjunction with equation (IV.1) for the total depth reported by the ADCP provides the

total discharge. The 0.3535 edge coefficient in Equations (IV.3) and (IV.4) is used assuming that the edges are close to triangular shape (Fulford and Sauer, 1986). The RDI's SxS Pro software does not separately report the edge discharges.

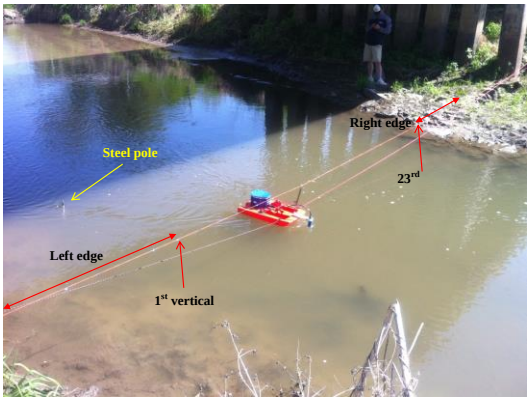


a)

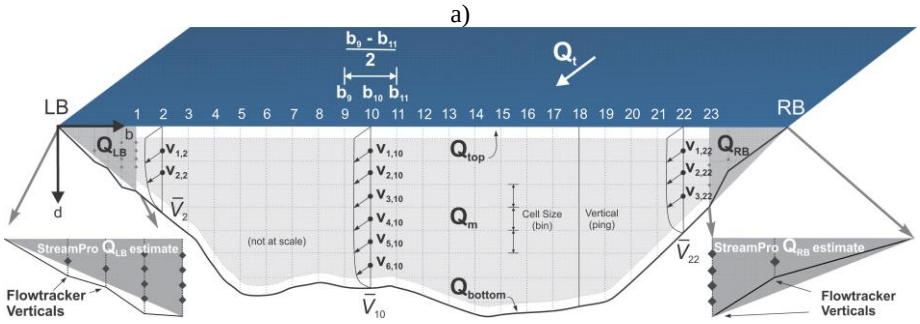


b)

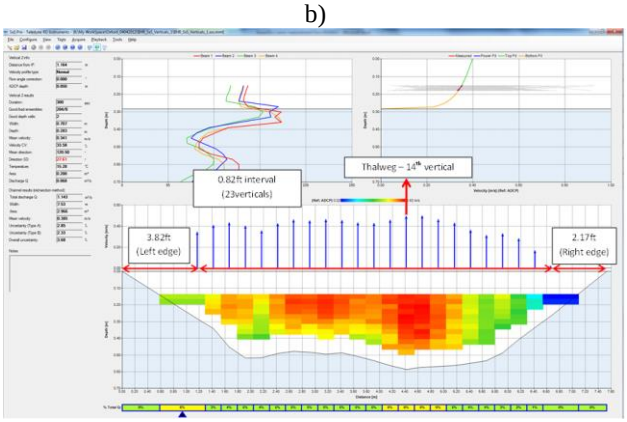


c)

Figure IV.5 StreamPro measurements at the test site: a) location of the cross-section; b) Layout of the StreamPro measurements; c) Screen capture of the Streampro SxS Pro software

## IV.3.4 Assessment of uncertainty sources

### IV.3.4.1 Identification of the sources of uncertainties

The description of the measurement process and the ancillary data reduction equation leading to the final result provide the needed details to define the measurement process from uncertainty analysis perspectives. An inspection of the origin of the sources of uncertainties reveals that they are associated with all the steps of the measurement process. They include: a) Instrument characteristics and operational settings (e.g., instrument accuracy and sampling time); b) methods for estimating the physical quantities (i.e., velocity and discharge); c) measurement approach and protocols (e.g., selection of number of verticals); d) physical conditions of the measurement environment (e.g., flow unsteadiness); e) operational conditions. The structure of these sources grouped around the measured variable for estimating the discharge is provided in Figure IV.6.

### IV.3.4.2 Estimation of standard uncertainties

Research and experience on the assessment the above-listed uncertainty components are at an early stage and their assessment requires significant resources. Most of the available information regarding the quality of ADCPs is based on instrument comparisons (Herschy, 2009). For example, comparison measurements conducted in the US at 12 sites across the country, in rivers ranging in width from 43 to 1100 m were made and with discharges varied in the 21 -1690 $m^3/s$ range. The 31 ADCP measurements differed from measurements with conventional current meter methods by less than 8% and 26 of the measurements were within 5%.

In the original stages of the present research, we searched for available information that specifically targeted the identified sources of uncertainties and presented

a degree of confidence needed for a study on uncertainty analysis. Unfortunately, not much relevant information of this kind is available for ADCPs. Nevertheless, the relevant information obtained by other researchers with conditions being well-defined was used for some of the uncertainty sources. In addition to the above information and manufacturer specifications, we designed a series of tests in laboratory and field to address some of the uncertainty sources. Figure IV.7 illustrates the flow environments for our uncertainty assessment tests. Activities include calibration measurements, customized tests whereby sources of uncertainty were carefully isolated and then evaluated, changes of operational parameters where made to capture the variation of the uncertainty estimates with the change in the magnitude of the variables.

For a portion of the study, we had available two StreamPro probes that were advantageous for our analysis as it enabled us to capture uncertainties across instruments of the same type operated identically. Despite the progress attained, much more work is needed to further the information on various sources of uncertainties involved in the analytical formulations.

Before initiating the assessment of individual sources of uncertainty for the StreamPro, the first concern for the study was to identify the set of instruments to be used for tracing its performance to primary standards (references). The selected reference instruments were used for the calibration measurements both in laboratory and field conditions. The following instruments were used for calibration of the depth and velocity measured with StreamPro:

- Depth – wading rod and measuring tape
- Velocity – Sontek/YSI Flowtracker ADV

The wading rod and conventional tape are reliable instrument and straightforward to operate, and therefore there are no major reservations that they can be used as reference instruments. The Flowtracker was the instrument of choice for referencing velocity as it is suitable for laboratory and field conditions. Prior to the calibration

measurements, the Flowtracker was compared to a Sontek/YSI Micro-ADV in laboratory conditions to verify that it is suitable as a reference to primary velocity standard. Flowtracker and Micro-ADV are acoustics instruments with similar configurations and operating processes. The ADV convergent-beam configuration enables point measurements therefore it provides increased reliability compared with the ADCP divergent-beam configuration that uses additional assumptions for providing velocity measurements in points along a vertical. Micro-ADVs have been verified for their capabilities to characterize mean and turbulence characteristics and were found to provide acceptable results in previous studies (e.g., Voulgaris and Trowbridge, 1998).

The calibration measurements revealed two potential sources of bias in the StreamPro measurements: a) the near-transducer velocity bias (lab and field conditions), and b) the depth measurement (field conditions). While GUM protocol requires to remove biases before to apply UA, we have not applied corrections to the StreamPro measurements from two reasons: a) the lack of resources for the thorough assessment of these uncertainties; and b) the intent to use only the StreamPro data provided by the ancillary software such as to be in a similar situation with a typical users (who does not have the capabilities and resources to estimate these biases).

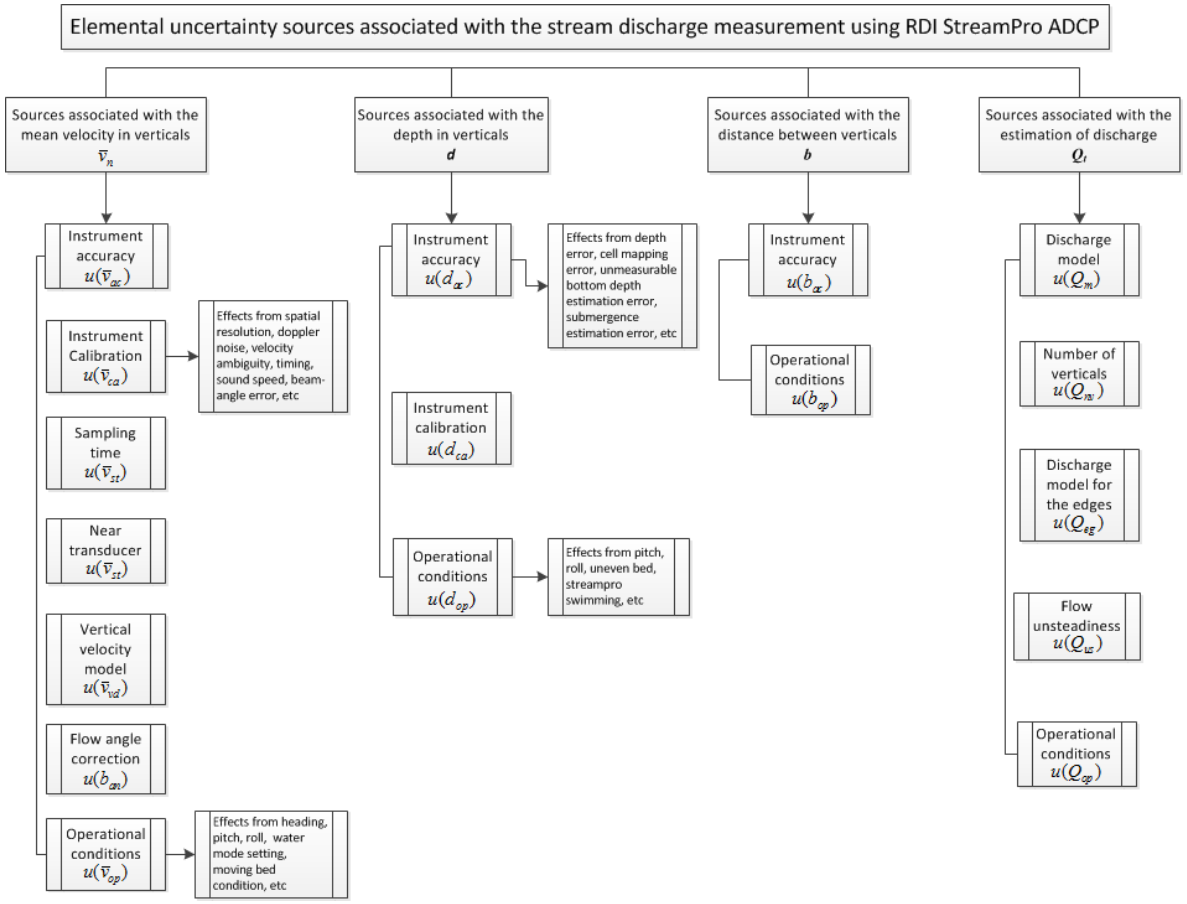


Figure IV.6 Diagram of the sources of uncertainty for SxS ADCP discharge measurements

a) b) c)

Figure IV.7 Photos of the environments for the present tests: a) Laboratory flume with TRDI StreamPro ADCP; b) Field with Sontek/YSI ADV; c) Field with TRDI StreamPro ADCP

Sources associated with the mean velocity in verticals, $\bar{v}_n$

The experiments for this group of uncertainty sources entailed measurements with two StreamPro ADCPs and a FlowTracker ADV. Common setting for the instruments throughout the set of experiments are: blank zone – 0.03 m (~0.1ft); water mode – 12; discharge calculation method – mid-section; and velocity profile model – 1/6 power law. The settings that varied from one experiment to the other are mentioned as the experiments are described.

*Instrument accuracy,* $u(\bar{v}_{ac})$

RDI specification for the instrument accuracy is ±1.0% or $\pm 0.2 \times 10^{-2}$ m/s. Given that in this study we assessed the accuracy of the instrument through end-to-end customized calibration experiments, we disregard the manufacturer specification and use results obtained through calibration experiments (see next section). This procedure will avoid double counting of sources of uncertainties as many sources of errors in this category are active in the calibration experiment. The standard uncertainty for this source

entails, however, the 0.0005 ft/s (0.0016 m/s) value corresponding to half of the last significant digit of the software output for velocity (0.001 ft/s).

*Instrument calibration,* $u(\bar{v}_{ca})$

Two laboratory and two field tests were conducted to assess the uncertainty associated with the StreamPro. The uncertainty was obtained by analyzing the sample statistics of velocity measurements concurrently acquired with the StreamPro ADCP and FlowTracker ADV. For this purpose the FlowTracker was positioned successively in the StreamPro bins using identic operational and environmental conditions in laboratory or field experiments. The bulk flow velocities during the calibration experiments were 0.12 to 0.50 m/s, and therefore the estimated uncertainties apply only for this range. The sampling time of the flow was long enough to attain the stability of the mean velocity. The calibration experiments conducted in laboratory and field conditions do not show systematic differences between the FlowTracker and the two StreamPro velocity measurements, therefore no bias correction was necessary. The calibration uncertainty resulted in 5.24 % and 4.55% of the measured velocity for field and laboratory conditions, respectively. The lower uncertainty for the laboratory condition is attributed to the more uniform flow condition in the experimental flume compared with the stream conditions. The 5.24 % uncertainty was uniformly used for in-bin as well as for the depth-averaged ADCP velocities. The flow conditions and the results of the tests for laboratory experiments are provided in Table IV.2 and Figure IV.8. The same characteristics for the field experiments are provided in Table IV.3 and Figure IV.9.

*Sampling time,* $u(\bar{v}_{st})$

Velocities at any point in the cross-section are continuously and randomly fluctuating in time due to turbulence. The mean velocity used for discharge estimation is determined by sampling the flow over a certain time interval. While the duration of this

measurement is labeled in the literature with various terms [e.g., averaging time (Gunawan, 2010), measuring time (Herschy, 2009; ISO 1088, 2007); exposure time (Garcia et al., 2012)], we use herein the term sampling time. The sampling time uncertainty is site-dependent as the flow temporal scales are defined by the flow regime (Reynolds number), geometry of the channel, and bed roughness. The issue of the appropriate selection of the sampling time to obtain significant average velocity is still under debate (e.g., Garcia et al., 2012; ISO 1088, 2007). In this study, the assessment of this source of uncertainty is similar one of the methods presented in the ISO 1088 (2007). Specifically, long time velocity samples were collected with StreamPro ADCP at fixed location and the acquired velocity time series was then analyzed using the cumulative moving average applied to the velocity time series.

The location for establishing the sampling time was vertical 14 where the flow is the deepest and fastest (see Figure IV.5 b)). The cumulative moving averages of the 900s velocity time series recorded in selected bins covering the vertical are plotted in Figure IV.10. It can be observed that at about 300s the stability of the mean velocity is attained at each measurement point. Based on visual inspection, it can be deemed that a sampling time of 300s is appropriate for this flow situation for all the other verticals in the cross section as vertical 14 is located in the most active turbulence of the cross-section. The relative difference between the average values of the velocity time series for the 300-s long sampling with respect to the 900-s long sampling for all the bins in vertical 14 is plotted in Figure IV.11. Vertical 14 contains 11 bins allowing to qualify this source of uncertainty as Type A uncertainty as samples containing more than 10 realizations are considered statistically significant. Type A uncertainty is the uncertainty evaluated using statistical methods, and Type B is that evaluated by other means (See Appendix A).

The 300s sampling time found necessary for a stable average of the velocity time series agrees well with sampling time found necessary for the stability of the mean velocity in previous studies. In those studies, the rivers were widely varying in width

(from 15 – 11,000 m), depth (from 0.75 to 12 m), and velocity range. Gunawan (2010) synthesize this data as: "Stone and Hotchkiss (2007) reported that velocity profile becomes stable after 250s averaging, after observing the convergence rate of velocity statistics (mean and standard deviation). Szupiany et al. (2007) reported stability velocity profiles at 420 to 600s averaging by observing the convergence rate of mean velocity in various bins. Furthermore, Barua and Rahman (1998) reported that turbulence intensity stabilizes to a nearly constant value of about 300s averaging, or more." Gunawan (2010) found that for a stream similar to the one investigated in the present example (width 8 m, depth 0.75 m, discharges between 0.293 – 4.47 $m^{-3}/s$) the sampling time for attaining the stability of the mean velocity time series at various depth was within 300s.

Distinction should be made between repeated sampling of the flow to estimate the mean velocity (that is further used in the determination of discharge in Equation IV.1) and repeated sampling of the flow for estimation of uncertainty Type A. In some previous studies this two types of repeated measurements were considered interchangeable (e.g., Huang, 2012). Turbulent flows are inherently fluctuating and for reporting the mean values describing mean turbulent flows (e.g., pressure, velocity) the flow needs to be sampled over sufficiently long interval for the mean to be completely independent of the time (Hinze, 1959). Therefore sampling the turbulent flow long enough is a requirement needed to appropriately capture the mean velocity. The sampling time is commensurate with the scales of the turbulent flows and has to be estimated prior to the measurements (Muste et al., 2004.b). The standard deviation of the fluctuations defines the intensity (violence) of the turbulent flows. These fluctuations appear as a random noise in the measurements with instrument with high frequency sampling capabilities such as the StreamPro. Besides the "noise" due to flow turbulence, additional noise can be cumulated in the output signal due to instrument noise (electronic noise, Doppler noise), environmental noise (wave effects, erratic boat operations).

Estimation of the standard uncertainties for uncertainty analysis purposes refers to the standard deviation of the mean velocity. This quantity is obtained through a large number of repeated measurements (fulfilling the requirement of appropriately sampling the turbulent flows) to create the significant statistical sample for assessing the standard uncertainty of the mean velocity. Table IV.4 (raw data) and Figure IV.11 indicate that differences up to 4% are possible in the mean velocity recorded by the StreamPro when 20 seconds are used for sampling the flow. Using the regression line it can be noticed that the standard uncertainty associated with the sampling time for all the measured velocity lowers to 0.23% for 300s sampling time duration. This value was used for the sampling time uncertainty, i.e., $u(\bar{v}_{st})$, for the depth-averaged velocities in the verticals. This approach is conservative leading to an overestimation of the uncertainty due to the sampling time. A more detailed uncertainty assessment can be further obtained if the site characteristics (type of turbulence), the magnitude of the velocities and their position over the depth, along with the settings of the ADCP (especially the cell size, the internal filtering, and averaging procedures) are considered additional parameters in the assessment.

*Near-transducer,* $u(\bar{v}_{tr})$

The concurrent laboratory and field data acquired with FlowTracker and StreamPro showed in some of the tests that in the upper 0.23 m of the depth velocities measured by the StreamPro were low biased, as illustrated in Figure IV.12. This near-transducer error is due to several detrimental effects (i.e., ringing, flow disturbance, multi-beam probe configuration) and has been partially documented in previous studies on Rio Grande ADCPs (e.g., Mueller et al., 2007; Muste et al., 2010).

The full assessment of the near-transducer bias requires customized experiments covering a range of operating conditions (e.g., bin size, flow velocity, sensor geometry and operation) that were beyond the resources available for this study. A decision was

made to not correct for this bias as: a) there are no comprehensive protocols for removing the bias for the StreamPro, and b) the StreamPro software applies proprietary algorithms for conditioning the velocity profile over the entire depth. By and large, these algorithms partially correct this bias as - they are using many directly measured velocities in the lower part of the water column.

*Vertical velocity model,* $u(\bar{v}_{vd})$

This uncertainty source arises because of the limited number of sampling points in a vertical. Computation of the mean velocity in a vertical was made using the dedicated software that ingested the in-bin velocities reported by the StreamPro in conjunction with various algorithms for the vertical velocity distribution. The results were compared with those provided by SxS Pro software that is customarily utilized by instrument operators. The StreamPro associated software entail algorithms for filtering the wrong velocity measurement in bins, averaging of consecutive pings for "reduction of noise" (which is actually not a desirable procedure), and provides several options for fitting a regression line through the measured velocity to fill in the unmeasured portions of the depth and for conditioning the final velocity profile that is subsequently used to obtain the depth-averaged velocity.

ADCPs measure velocities in bins equally spaced over the vertical and leave unmeasured areas near the free surface and bed. Consequently, the location of the velocities sampled over the verticals do not always correspond to the depths for velocity sampling provided in standard protocols (i.e., 0.2, 0.4. 0.6, 0.8 the depth). The difference in the velocity locations between the standard recommendations and ADCP bins might slightly affect the estimated value of the depth-averaged velocities. The difference is not, however, affecting the assessment of the uncertainty component needed for this analysis as the assessment essentially captures the effect of the density of points used in approximating the mean velocity in the vertical. Consequently, the standard uncertainties

related to the vertical velocity models are chosen from ISO 1088 (2007) specifications. These uncertainties were derived from many samples of irregular vertical velocity curves as specified in Table F.1 of ISO 1088 (2007). Uncertainties for each vertical were different in our analysis commensurate with the number of points measured by ADCP in the respective vertical. For verticals where the number of bins exceeded 6, uncertainty associated with 6 points was used in the calculations.

*Flow-angle correction,* $u(\bar{v}_{an})$

Flow-angle errors are induced by two sources. One is the flow-angle error with respect to the tag line and the other one is due to incorrect calibration of compass being used. When the ADCP has a compass, the flow-angle correction can be applied; however, for the ADCP without a compass such as default configuration of the StreamPro, it is advised that correct flow-angle which is normal to the tag line be inputted or at least be estimated if it exists. Huang (2012) found out that 5% and 10% of flow-angle error can cause 0.38% and 1.54% of overestimation in velocity, respectively. It is not because of overestimation of resultant velocity, but because of overestimation of flowing area inducing overestimation in subsection discharge. Moreover, Huang (2012) also indicated that 1% compass error due to incorrect calibration of compass can introduce 0.15% and 0.31% of additional errors at 5% and 10% of flow-angle errors, respectively. It is important to note that this error should be corrected before applying for the uncertainty analysis, because this error type always cause the overestimation of velocity, and therefore they cannot be considered as deviation from the mean. During our measurements care was taken to set properly the instrument to the tag line, therefore this uncertainty was not considered in the analysis.

*Operational conditions,* $u(\bar{v}_{op})$

This uncertainty source captures the effects of the non-uniformity of the suspended scatters in the acoustic beams, flow direction change during the measurements, tag line deflections, disturbance of the water surface by waves, and operator-induced effects. The uncertainty is influenced by the procedures used in the field measurements and natural conditions during the measurements. Velocities were measured in verticals with locations well identified. Specific attention was paid to ensure stability of the float and the ADCP. Ten repeated measurements at the same vertical were acquired in the field experiment to allow a Type A assessment for this uncertainty source (Table IV.5). The StreamPro sampling time was 90 sec with a cell size of 0.03 m for each measurement. Using these results, the standard deviation of the sample was attributed to the operational standard uncertainty. Its value of 0.006 m/s was associated for all depth-averaged velocities measured in verticals.

Additional sources of errors due to operational conditions are the presence of pitch (defined as rotation along the fore/aft axis) and roll (defined as rotation in the direction of the starboard/port axis) rotations during the measurements. They are corrected for if the ADCP is equipped with tilt sensor. Those corrections address both velocity and depth measurements. For small tilting angles these corrections are not significant unless velocity profiles in all three orthogonal coordinates are desired (Simpson 2001). For the StreamPro ADCP measurements conducted in this study the uncertainties associated with pitch-roll-heading were assumed negligible as the measurement protocol was very well controlled. More studies are needed for a thorough assessment of this uncertainty to account for all possible measurement conditions.

Table IV.2 Flow characteristics and instrument settings for the laboratory experiments

| Instrument | Settings | | | Field/Lab | Bulk flow velocity(ft/s) | Depth (ft) | Operation |
|---|---|---|---|---|---|---|---|
| | Cell size(ft) | Number of cells (points) | Sampling time(s) | | | | |
| Lab experiment 1 (StreamPro 1, 2) | | | | | | | |
| StreamPro 1 | 0.1 | 30 | 900 | Lab | 1.1 | 2.9 | Fixed rod |
| StreamPro 2 | 0.1 | 30 | 900 | Lab | 1.1 | 2.92 | Fixed rod |
| Flowtracker | | 5 | 60 | Lab | 1.1 | 2.9 | |
| Wading Rod | | | | | | 2.83-2.9 | |
| Lab experiment 2. (StreamPro 1, 2) | | | | | | | |
| StreamPro 1 | 0.1 | 30 | 900 | Lab | 1.1 | 2.84 | Fixed rod |
| StreamPro 2 | 0.1 | 30 | 900 | Lab | 1.0 | 2.85 | Fixed rod |
| Flowtracker | | 5 | 60 | Lab | 1.1 | 2.83 | |
| Wading Rod | | | | | | 2.83 | |

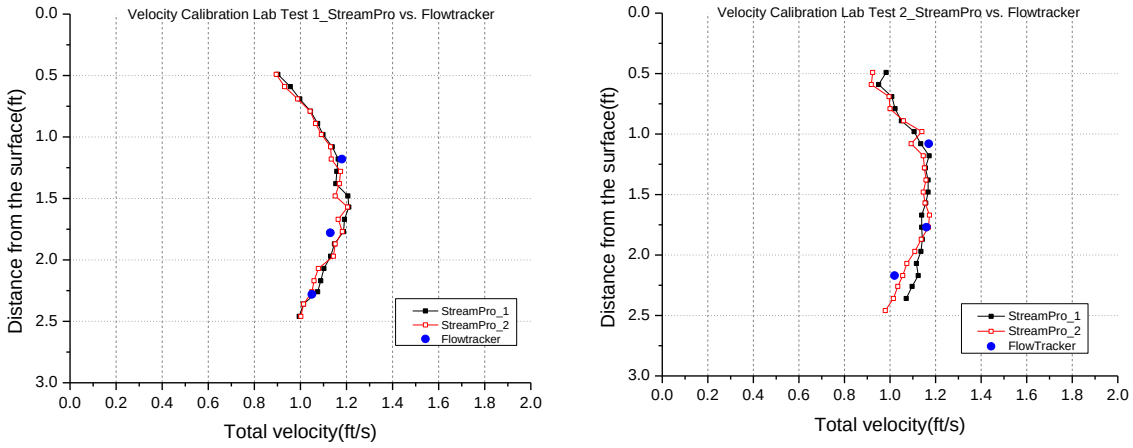


a) b)

Figure IV.8 Comparison between StreamPro and Flowtracker (reference) measurements in laboratory conditions: a) Lab experiment 1; b) Lab experiment 2

Table IV.3 Flow characteristics and instrument settings for the field experiments

| Instrument | Settings | | | Field /Lab | Bulk Flow velocity (ft/s) | Depth (ft) | Operation |
|---|---|---|---|---|---|---|---|
| | Cell size(ft) | Number of cells (points) | Sampling time(s) | | | | |
| Field experiment 1 (StreamPro 1) | | | | | | | |
| StreamPro 1 | 0.2 | 20 | 300 | Field | 0.4 | 1.61 | Hand-held |
| Flowtracker | | 5 | 60 | Field | 0.4 | 1.65 | |
| Field experiment 2 (StreamPro 1, 2) | | | | | | | |
| StreamPro 1 (set1) | 0.1 | 30 | 900 | Lab | 1.6 | 1.54 | Hand-held |
| StreamPro 2 (set1) | 0.1 | 30 | 900 | Lab | 1.6 | 1.57 | Hand-held |
| Flowtracker | | 5 | 60 | Lab | 1.6 | 1.6 | |
| StreamPro 1 (set2) | 0.1 | 30 | 900 | Lab | 1.6 | 1.58 | Hand-held |
| StreamPro 2 (set2) | 0.1 | 30 | 900 | Lab | 1.6 | 1.56 | Hand-held |

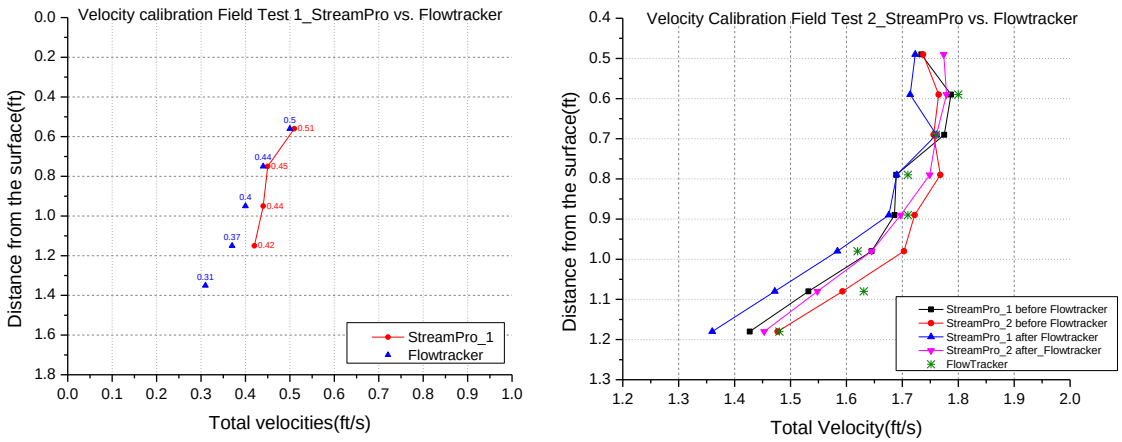


a) b)

Figure IV.9 Comparison between StreamPro and Flowtracker (reference) measurements in field conditions: a) Field experiment 1; b) Field experiment 2

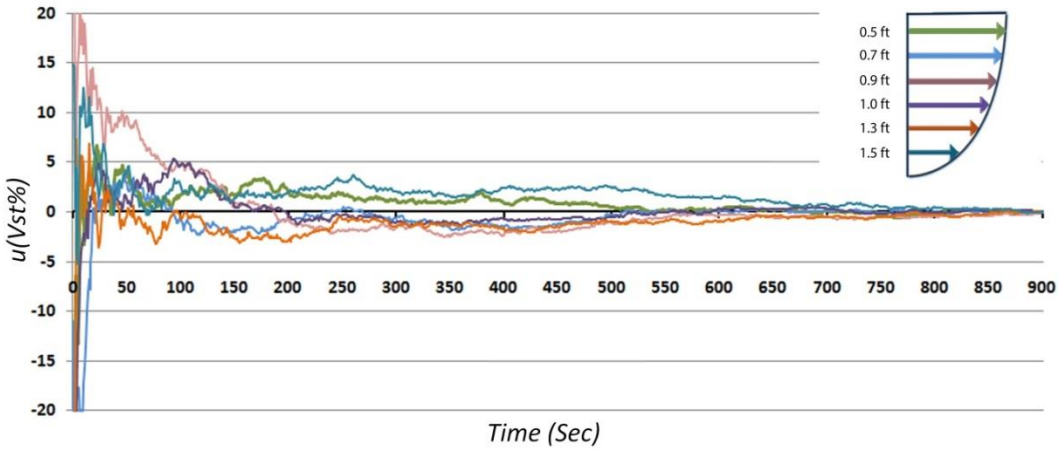


Figure IV.10 Analysis of the sampling time using the velocity time series at vertical 14

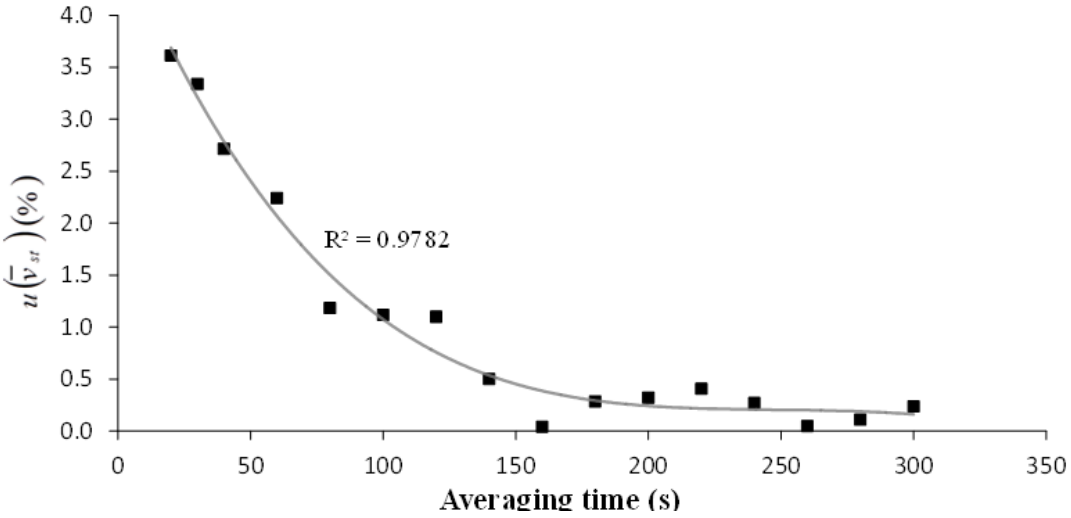


Figure IV.11 Variation of the sampling time standard uncertainty (bulk flow velocity 2 ft/s) – See also Table IV.3

Table IV.4 Average sampling time uncertainty across bins relative to 900s long sampling

| Sampling Time (s) | Bin1 | Bin2 | Bin3 | Bin4 | Bin5 | Bin6 | Bin7 | Bin8 | Bin9 | Bin10 | Bin11 | Relative difference from 900s averaging time |
|---|---|---|---|---|---|---|---|---|---|---|---|---|
| 20 | 4.46 | 3.88 | 0.30 | 6.21 | 14.51 | 2.73 | 2.78 | -3.14 | 3.04 | -1.85 | 6.83 | 3.61 |
| 30 | 2.14 | 4.92 | 0.99 | 7.27 | 6.10 | 0.70 | 3.67 | 1.70 | 2.11 | 0.75 | 6.38 | 3.34 |
| 40 | 3.16 | 2.37 | 2.39 | 5.45 | 8.81 | 2.59 | 2.20 | 1.76 | 0.65 | -0.53 | 1.01 | 2.71 |
| 60 | 2.05 | 2.79 | 2.07 | 4.60 | 9.22 | 0.65 | 2.99 | 0.42 | -1.19 | -0.46 | 1.53 | 2.24 |
| 80 | 0.73 | 4.34 | 1.41 | 2.10 | 5.47 | -1.27 | 3.10 | -0.62 | -2.71 | -0.99 | 1.45 | 1.18 |
| 100 | 1.60 | 2.78 | -0.76 | -0.09 | 4.70 | -1.66 | 4.56 | 1.15 | -0.13 | -3.03 | 3.14 | 1.12 |
| 120 | 2.43 | 2.36 | -1.97 | 0.18 | 4.31 | -0.50 | 3.88 | 1.94 | -0.80 | -0.95 | 1.20 | 1.10 |
| 140 | 2.36 | 3.17 | -1.72 | -1.51 | 2.80 | -1.22 | 1.25 | 1.83 | -2.26 | -1.27 | 2.08 | 0.50 |
| 160 | 2.67 | 3.50 | -1.57 | -1.75 | 0.81 | -2.08 | 0.77 | 0.10 | -2.83 | -0.70 | 1.51 | 0.04 |
| 180 | 3.10 | 3.61 | -1.88 | -2.59 | 0.54 | -3.05 | 0.59 | -0.31 | -2.46 | -2.18 | 1.50 | 0.28 |
| 200 | 2.30 | 4.90 | -0.68 | -1.76 | -0.57 | -3.49 | -0.21 | -1.16 | -3.01 | -1.73 | 1.90 | 0.32 |
| 220 | 1.57 | 4.92 | -0.31 | -1.98 | -1.44 | -3.76 | -0.79 | -1.61 | -2.24 | -1.06 | 2.24 | 0.41 |
| 240 | 1.46 | 4.53 | 0.09 | -2.20 | -2.15 | -4.23 | -0.78 | -0.50 | -1.62 | -0.28 | 2.72 | 0.27 |
| 260 | 1.48 | 4.28 | 0.25 | -1.50 | -1.84 | -3.76 | -0.41 | -0.60 | -0.72 | -0.14 | 3.46 | 0.05 |
| 280 | 1.31 | 3.89 | -0.28 | -0.64 | -1.59 | -4.39 | -0.55 | -0.79 | -0.78 | 0.01 | 2.62 | 0.11 |
| 300 | 1.32 | 3.81 | -0.67 | -0.64 | -1.76 | -3.62 | -1.08 | -0.34 | -1.48 | -0.22 | 2.10 | 0.23 |

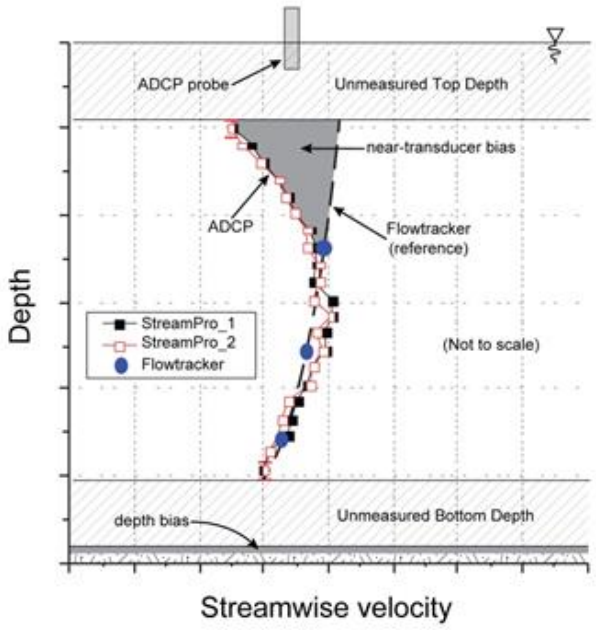


Source: Simpson (2001)

Figure IV.12 Conceptualization of the near transducer velocity and depth measurement bias in StreamPro measurements

Table IV.5 Repeated measurements for assessing the operational condition uncertainty affecting the mean velocities

| Instrument | Settings | | | Field /Lab | Mean velocity (ft/s) | Depth (ft) | Operation |
|---|---|---|---|---|---|---|---|
| | Cell size(ft) | Number of cells (points) | Sampling time(s)* | | | | |
| StreamPro 2 | 0.1 | 30 | 90s | Field | 1.64 | 1.894 | Hand-held |
| | 0.1 | 30 | 90s | Field | 1.665 | 1.89 | Hand-held |
| | 0.1 | 30 | 90s | Field | 1.635 | 1.89 | Hand-held |
| | 0.1 | 30 | 90s | Field | 1.67 | 1.887 | Hand-held |
| | 0.1 | 30 | 90s | Field | 1.658 | 1.877 | Hand-held |
| | 0.1 | 30 | 90s | Field | 1.615 | 1.879 | Hand-held |
| | 0.1 | 30 | 90s | Field | 1.638 | 1.88 | Hand-held |
| | 0.1 | 30 | 90s | Field | 1.687 | 1.888 | Hand-held |
| | 0.1 | 30 | 90s | Field | 1.645 | 1.889 | Hand-held |
| | 0.1 | 30 | 90s | Field | 1.637 | 1.885 | Hand-held |

The reference mean velocity was obtained for 300s time series.

Sources associated with the depth in verticals, *d*

*Instrument accuracy, $u(d_{ac})$*

StreamPro as well as other ADCPs estimate the depth by averaging the return signal of 3 or 4 slightly oblique acoustic beams that reach the stream bed at distinct locations. The ADCP measuring footprint increases with the stream depth. The average of the multi-beam readings is then reported as the depth estimate at the measurement location (defined by the axis of the instrument). A sample file illustrating the four beams reading as reported in the StremPro output file is shown below (values indicated in the rectangle) in Figure IV.13. The resolution of the readings is half of the last significant digit, hence a value of 0.0005 ft (0.0016m) is taken into account for the instrument accuracy.

*Instrument calibration,* $u(d_{ca})$

This uncertainty source includes the combined effects of beam spread on the stream bottom and its penetration into the bed which is further related to the pulse frequency, bed nature and consistency. The uncertainty is site-dependent; therefore, we deem that it is necessary to be evaluated whenever a new site is subjected to ADCP measurements. Reliable assessment of these sources of uncertainty requires specialized experiments with alternative instruments and well-thought experimental procedures as the presence of the bed forms (smooth, ripples, dunes), bed roughness, and the type of sediment transport active during the measurement (i.e., bed load or suspended load) are all factors affecting the uncertainty. It is expected that the StreamPro provides smaller depth readings than the wading rod used for reference, as illustrated by the grey band in Figure IV.12. This error was previously documented for various situations (Pobanz, et al., 2011; Frizzell and Vermeyen, 2007; Gunawan, 2010).

For the present study we proposed an end-to-end approach for the assessment of the uncertainty. The StreamPro depth measurements were compared with the readings on a wading rod of the FlowTracker. Experiments were conducted in laboratory and field conditions in steady flows of constant discharge. The laboratory flume bed was made of plywood roughened to not create acoustic reflections. All field measurements were acquired in the same stream where the bed consistently is soft and predominantly made of silty clay loam soil. The StreamPro was hand-held for all tests and the sampling times were 300 and 900 seconds. No movement of the bed was detected during the measurements. The results show that all the wading rod depth measurements were slightly larger than the StreamPro data (Table IV.6 and IV.7).

The systematic differences between the wading rod and ADCP depth data are obviously biases, and they could have been corrected for all measurements. This correction is not applied in the StreamPro processing software; therefore, we chose to fossilize this average difference as a standard uncertainty associated with the depth

measurement. The decision is based on the fact that there are no protocols for establishing this source of uncertainty with a high level of accuracy. Actually, there is no precise information where near the bed the ADCP measurements are taken over the depth and their relationship with frequency, bed particle type, and sediment concentration at the measurement location. Another aspect that complicates the matter is that depth measurements are averages of the four acoustic beam measurements on different spots on the bed. Consequently, this uncertainty source also depends on the type of bed forms at the measurement site. On the other hand, even the measurements with wading rods are susceptible to interpretation when the stream bed is soft as no precise protocols exists for the amount of pressure to apply on the wading rod to accurately read the "actual flow depth". More uncertainties might arise for wading rod measurements because of the inclined positioning of the rod and the imprecise reading of the free surface water level in the presence of the inherent water surface oscillations.

In summary, while recognizing that the obtained results combine uncertainties of both working and reference instruments, we deem that they are realistic approximation of this important source of uncertainty. The data collected for this type of uncertainty can be considered of Type A category as significantly large sample statistics were acquired for both the laboratory and field measurements for its estimation. Similar to the near-transducer bias error, the assessment of this source of uncertainty is expensive as it depends both on the instrument characteristics, the nature of the bed material in the stream as well as the amount and concentration of the sediment in suspension. Without a standardized or well-defined protocol to reduce the error in a consistent manner, a decision was made to allocate as the depth calibration uncertainty the value of 0.059 ft (0.018m) observed from measurements.

*Operational conditions,* $u(d_{op})$

The non-uniform concentration of the suspended scatters near the bed and the presence of submerged debris and bedforms at the measurement site are all affecting the depth measurements. Also involved are tag line deflections, disturbance of the water surface by waves, slight changes in the ADCP position during the measurements, and other instrument operational considerations. Ten repeated measurements at the same location were used to allow a Type A assessment for this uncertainty source. The measurement results, listed in Table IV.8, provide a standard uncertainty of 0.006 ft (0.0018 m). This value is associated for all the depths measured over the cross section.

As the operating and the flow conditions were not problematic during the field measurement reported here, uncertainties associated with pitch-roll-heading were considered negligible in the present analysis and were not reflected in the overall estimation of uncertainty in discharge. It is considered that the assessment of this uncertainty requires additional measurements that characterize the sediment concentration near the bed, as it is suspected that the depth reading of the ADCPs are dependent of the degree of penetration of the acoustic sound in the high sediment concentration layer near the bed. Similarly to other sources, this is a site-depended uncertainty that requires information from assessments made at sites with similar geomorphological characteristics.

```
     3       3       5      30       6       1      12
12 4 4 15 53 49 2      1       1    0.000    0.000    0.000   17.310
-0.01      0.06     -0.06     -0.01     0.00     0.00     0.00     0.00      1.90      1.94      1.87      1.90
0.00          0.00          0.00          0.00          0.00
30000.0000000 30000.0000000 -32768    -32768          0.0
-0.0           -0.0           -0.0           0.0           14.0           0.0           10.0  0.49   1.48
30 ft BT dB 0.44  0.962
  0.49      2.85    114.30    2.6   -1.2   -0.2   -0.5   79.1   77.4   70.4   78.7  100 2147483647
  0.59      1.41    107.63    1.3   -0.4    0.1   -0.1   78.3   77.4   70.9   77.9  100 2147483647
  0.69      2.03    129.44    1.6   -1.3   -0.2   -0.7   78.8   75.3   69.6   76.6  100 2147483647
  0.79      2.28    133.25    1.7   -1.6   -0.0   -0.6   78.4   74.9   69.2   76.3  100 2147483647
  0.89      1.25    126.45    1.0   -0.7   -0.1    0.4   77.2   74.6   69.7   75.0  100 2147483647
```

Figure IV.13 StreamPro output file

Table IV.6 Summary of the laboratory tests for depth calibration

| Instrument | Settings | | | Field /Lab | Mean Velocity (ft/s) | Depth (ft) | Operation |
|---|---|---|---|---|---|---|---|
| | Cell size(ft) | Number of cells (points) | Sampling time(s) | | | | |
| Set 1 | | | | | | | |
| StreamPro 2 | 0.1 | 30 | 900 | Lab | 1.0 | 2.85 | Hand-held |
| Wading rod | | 5 | 60 | Lab | 1.1 | 2.83 | FIxed |
| Set 2 | | | | | | | |
| StreamPro 2 | 0.2 | 30 | 300 | Lab | 1.2 | 2.94 | Hand-held |
| Wading rod | | 5 | 60 | Lab | 1.4 | 2.88 | Fixed |
| Set 3 | | | | | | | |
| StreamPro 2 | 0.2 | 30 | 300 | Lab | 1.2 | 2.92 | Hand-held |
| StreamPro 2 | 0.2 | 30 | 300 | Lab | 0.6 | 2.92 | Hand-held |
| StreamPro 2 | 0.2 | 30 | 300 | Lab | 1.7 | 2.91 | Hand-held |
| StreamPro 2 | 0.2 | 30 | 300 | Lab | 1.8 | 2.93 | Hand-held |
| Wading rod | | 5 | 60 | Lab | 1.4 | 2.92 | Fixed |

Standard deviation of the StreamPro and wading rod measurements: 0.032ft (0.01 m)

Table IV.7 Summary of the field tests for depth calibration

| Instrument | Settings | | | Field /Lab | Mean velocity (ft/s) | Depth (ft) | Operation |
|---|---|---|---|---|---|---|---|
| | Cell size(ft) | Number of cells (points) | Sampling time(s) | | | | |
| Set 1 | | | | | | | |
| StreamPro | 0.1 | 30 | 900 | Field | 1.6 | 1.54 | Hand-held |
| StreamPro 2 | 0.1 | 30 | 900 | Field | 1.6 | 1.57 | Hand-held |
| Wading rod | | 5 | 60 | Field | 1.6 | 1.6 | Fixed |
| StreamPro 1 | 0.1 | 30 | 900 | Field | 1.6 | 1.58 | Hand-held |
| StreamPro 2 | 0.1 | 30 | 900 | Field | 1.6 | 1.56 | Hand-held |
| Set 2 | | | | | | | |
| StreamPro 1 | 0.2 | 20 | 300 | Field | 0.4 | 1.61 | Hand-held |
| Wading rod | | 5 | 60 | Field | 0.4 | 1.65 | Fixed |
| Set 3 | | | | | | | |
| StreamPro 2 | 0.2 | 30 | 600 | Field | 1.2 | 2.01 | Hand-held |
| StreamPro 2 | 0.2 | 30 | 600 | Field | 1.2 | 1.84 | Hand-held |
| Wading rod | | 5 | 60 | Field | 1.3 | 1.9 | Fixed |
| Set 4 | | | | | | | |
| StreamPro 2 | 0.2 | 30 | 900 | Field | 0.4 | 3.46 | Hand-held |
| StreamPro 2 | 0.2 | 30 | 900 | Field | 0.4 | 3.39 | Hand-held |
| Wading rod | | 5 | 60 | Field | 0.4 | 3.5 | Fixed |

Standard deviation of the StreamPro and wading rod measurements: 0.059ft (0.018m)

Table IV.8 Repeated measurements for assessing the operational condition uncertainty affecting the depth

| Instrument | Settings | | | Field /Lab | Mean velocity (ft/s) | Depth (ft) | Operation |
|---|---|---|---|---|---|---|---|
| | Cell size(ft) | Number of cells (points) | Sampling time(s)* | | | | |
| StreamPro 2 | 0.1 | 30 | 90s | Field | 1.6 | 1.894 | Hand-held |
| | 0.1 | 30 | 90s | Field | 1.7 | 1.89 | Hand-held |
| | 0.1 | 30 | 90s | Field | 1.6 | 1.89 | Hand-held |
| | 0.1 | 30 | 90s | Field | 1.7 | 1.887 | Hand-held |
| | 0.1 | 30 | 90s | Field | 1.7 | 1.877 | Hand-held |
| | 0.1 | 30 | 90s | Field | 1.6 | 1.879 | Hand-held |
| | 0.1 | 30 | 90s | Field | 1.6 | 1.88 | Hand-held |
| | 0.1 | 30 | 90s | Field | 1.7 | 1.888 | Hand-held |
| | 0.1 | 30 | 90s | Field | 1.6 | 1.889 | Hand-held |
| | 0.1 | 30 | 90s | Field | 1.6 | 1.885 | Hand-held |

Standard deviation of the StreamPro and wading rod measurements: 0.006ft (0.0018m)

Sources associated with the distance between verticals, *b*

*Instrument accuracy, $u(b_{ac})$*

The locations of the StreamPro measurements across the stream were established by setting markers on the tag line. The 0.25 m spacing between makers was set using a measuring tape with the finest graduation of 0.0003 ft (0.0009 m). After the tag line was set across the stream, the distances from the edge to first and last marker on the tag line were measured with the same tape. Half the resolution of the finest scale on the measuring tape (i.e., 0.0003 ft) is attributed for this source.

*Operational conditions, $u(b_{op})$*

The improper location of the verticals during section by section measurements unfavorably impacts both velocity and depth measurements. The latter is especially critical as uncertainties associated with the definition of the geometry of the subsection areas has more impact on the total discharge estimation than attributing slightly different velocities by miss-positioning the vertical within the cross section. There are several methods recommended for measuring distances across the cross-section [see ISO 748 (2007) Annex B]. None of them were employed for the present study due to the small size of the stream. ISO 748 (2007) prescribes that this measurement uncertainty should not be greater than 0.5% of the measurement, or better techniques or procedure should be employed. Given the small channel width and the possibility to wade through the stream at all vertical locations, we relied on direct measurements of the distances between verticals as a way of estimating this uncertainty.

The fine resolution of the conventional measuring tape does not, however, ensure the same accuracy for the distance measured between the markers set on the tag line crossing the stream. Issues related to the tag-line anchoring procedure, cable stretching and sagging, and cable deformation due to the repeated relocations of the StreamPro from section to section are also contributing sources to this uncertainty. Some limited quantitative measurements conducted to establish the distance between panels while the StreamPro measurements were taken from vertical to vertical enabled an approximate assessment for this source of uncertainty. Basically, several measurements were taken from the fixed reference pole on the stream bank aligned with the cross-section while the StreamPro was positioned at selected verticals corresponding to the pre-established distances marked on the tag line. The differences recorded were statistically analyzed to provide a value of 0.05ft (0.015 m) for the uncertainty associated with this source of error.

Sources associated with the estimation of total discharge, $Q_t$

*Discharge model, $u(Q_{mo})$*

There are several options for the model used to estimate the discharge in subsections and the total stream discharge. These approaches are reviewed in Section 8 of the ISO 748 (2007). According to this standard, the mid-section method used in the present analysis pertains to the arithmetic methods for discharge estimation. The method is quite widespread in the hydrometric community. There are no studies to document the effect of the discharge estimation model on the total discharge known to these authors. In the absence of systematic studies documenting the effect of the estimation method on the total discharge, we use results from a previous study where this difference was estimated for the same site using different algorithms to determine the total discharge (Muste et al., 2004.a). Based on that study, the standard uncertainty of this source of error is estimated at 0.5%.

*Number of verticals, $u(Q_{nv})$*

This uncertainty source accounts for the approximation of the depths and velocities between verticals. These factors are independent but frequently their variation is correlated. Given the scope of the present work, we chose a number of verticals that strictly followed the ISO 1088 (2007) recommendations: sampling the transect at 0.25 m or 1/50 of the total width (whichever is greater). As the verticals were set apart at 0.25 m (0.82 ft) we attributed 0 to this source of uncertainty.

The availability of a large number of verticals enabled to conduct a sensitivity analysis to determine the influence of the number of verticals on total discharge estimation. Iterative calculations were made whereby all sources of uncertainties were kept the same while gradually decreasing the number of verticals from 23 to 17 and subsequently to 7 (see Figure IV.14). Along with our data, the results of similar analyses

as reported in ISO 1088 (2007) and Boiten (2000) were added for comparison purposes. The polynomial line fit to our data accounts for all of the above-discussed sources of uncertainties (i.e. percentage of the total uncertainties), while the other plots are only capturing uncertainty values associated with the effect of the numbers of verticals used for the discharge estimation (i.e., percentage of relative uncertainties).

*Discharge model for the edges, $u(Q_{eg})$*

As it is described earlier, StreamPro ADCP can be operated using two deployment methods: moving boat or stationary method (section-by-section). While the stationary method based on mid-section discharge model does not distinctively report the edge discharges from the total discharge estimates, moving boat method reports them based on their internal algorithm which is different from the mid-section discharge model. Moreover, even though analytical mid-section discharge model has two separate terms for the edge discharge calculation, these terms are usually disappeared for the practical applications, because the depth and velocity at the two edges are usually zero in most of the situations.

For the equivalent comparisons among the methods, the edge discharge is assumed and defined as the discharges between the banks to the first or last vertical. Figure IV.15 a) and Figure IV.15 b) show the analytical mid-section edge discharge areas (marked yellow) and the estimated discharge between the first or last vertical and the mid-way toward the bank (marked grey). Figure IV.15 c) and Figure IV.15 d) represent the assumed edge discharge areas, and therefore the total discharge excluding two edge discharges can be defined encompassing the discharges between the first and last vertical. A set of velocity measurements with Flowtracker were acquired during our tests for the edges and a graphical comparison was made as shown in Figure IV.16.

The red verticals represent the FlowTracker measurement locations. The vertical at 3.82ft from the left bank is the location where the 1$^{st}$ StreamPro ADCP vertical starts

while the vertical at 2.17ft from the right bank is the location where the 23rd StreamPro ADCP vertical ends. The mean velocities for each of those four vertical are estimated at 0.6*d*. The black verticals represent the midway between the measured verticals, and they divide the flow segments for discharge calculations. We used two options for our analysis. Option 1 provides the edge discharges that a typical user would obtain if using the SxS Pro software (i.e., 0.5). Option 2 uses a widely cited edge coefficient (i.e., 0.3535) provided by Fulford and Sauer (1986). FlowTracker edge discharges are estimated using 0.3535 edge coefficient for both Options 1 and 2. The summary of the results are provided in Table IV.9.

*Flow unsteadiness, $u(Q_{us})$*

The presence of flow unsteadiness during the measurements for discharge estimation requires implementation of special procedures for removing the influence of this effect (see for example Section 6.2. in ISO 1088, 2007). During our study, the stage was continuously checked for verifying the flow condition with respect to unsteadiness. Given that no indications of unsteady flow were found, the uncertainty associated with this source was neglected in the analysis.

*Operational conditions, $u(Q_{op})$*

This uncertainty source captures the effect of changes in instrument operations or in the measurement environment during the collection of the data across the section. If the guidelines for the acquisition of all measured variables (e.g., ISO 748, 2007) are strictly followed, this uncertainty is small. However, even if all the precautions related to measurement of discharge are taken adverse operational conditions add errors. Among these factors are: changes of the material in suspensions from section to section, the presence of temporary secondary currents in the cross section, getting outside the instrument measurement range or the pre-set operational parameter range (e.g., depth,

temperature, salinity), changes in the tag line position, significant disturbance from wind on the flow, floating platform or both, moving bed, change of the operation protocols or other settings of the instruments involuntarily or for undetected reasons, etc. None of the above conditions were noticed during our case study measurements. Given that the operational uncertainties associated with the velocity and depth in the verticals established above are conservative, this uncertainty is assumed negligible.

IV.3.4.3 Summary assessment

A summary of the uncertainty sources as determined in the previous sections is provided in Table IV.10. Besides the values estimated and their provenance, the standard uncertainties are classified as Type A (estimated with statistical methods) or Type B (estimated with other means). The estimates for uncertainties for laboratory and field conditions are provided in order to illustrate the effect of the measurement environment. As expected, uncertainties estimated for laboratory conditions are smaller than those for field conditions.

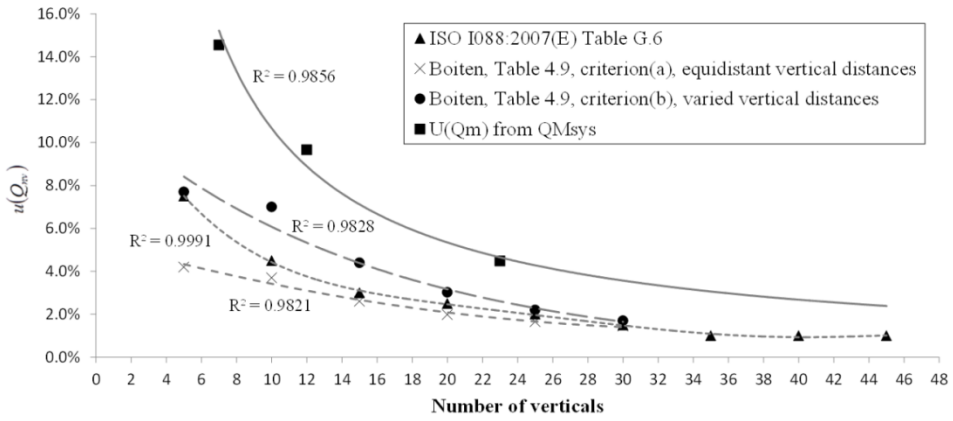


Figure IV.14 Sensitivity analysis of the measured discharge with the change in the number of verticals

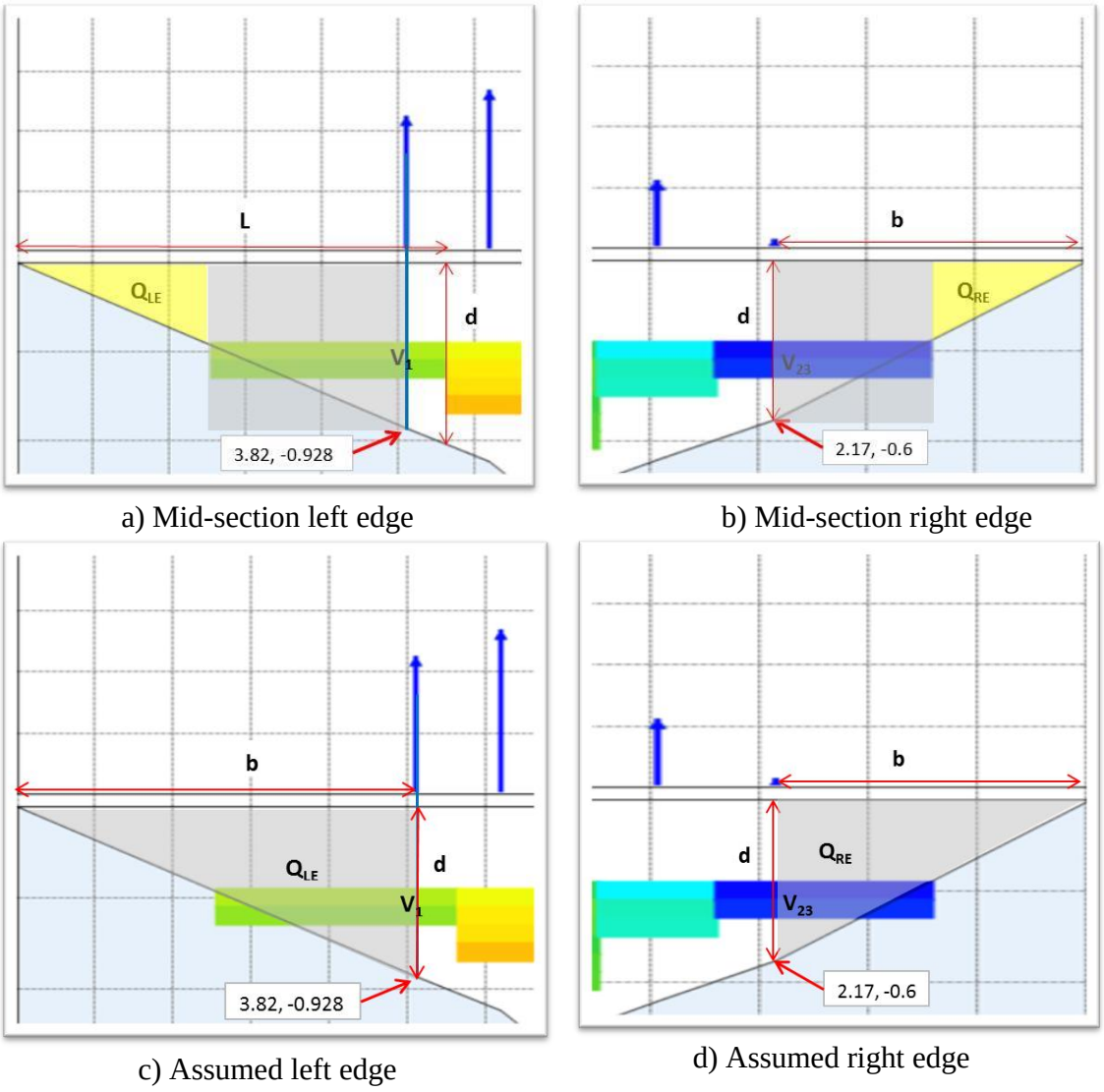


a) Mid-section left edge

b) Mid-section right edge

c) Assumed left edge

d) Assumed right edge

Figure IV.15 Comparison of edge areas based on analytical mid-section model and assumed model

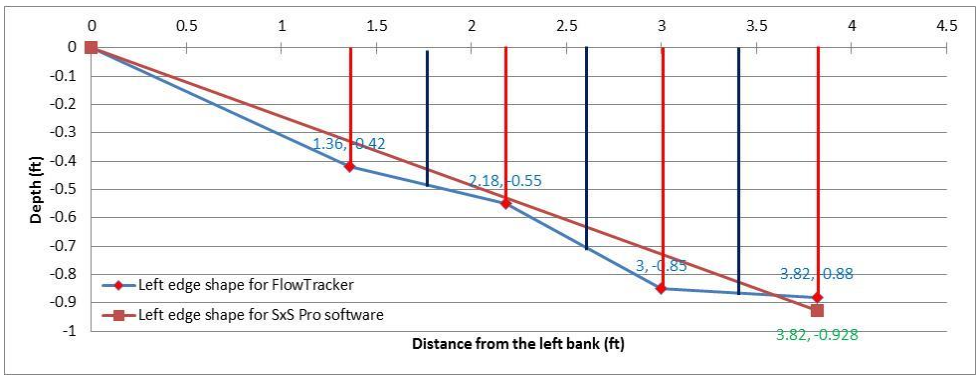


a)

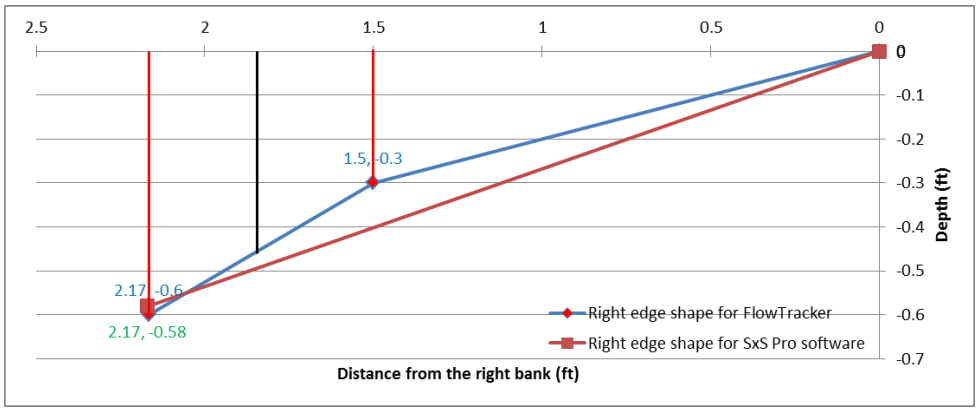


b)

Figure IV.16 Edge discharges using between FlowTracker and SxS Pro software: a) left edge; b) right edge

Table IV.9 Comparison on the estimation edge discharge from FlowTracker and SXS Pro

| | | Flow Tracker (m3/s) | SXS Pro (m3/s) | Difference (m3/s) | Relative difference (%) (vs. $Q_{edge}$) | Relative difference (%) (vs. $Q_t$) |
|---|---|---|---|---|---|---|
| **Option1** | $Q_{LE}$ | 0.3 | 0.6 | 0.3 | 98.77 | 2.44 |
| | $Q_{RE}$ | 0.019 | 0.013 | 0.006 | 32.09 | 0.05 |
| | *Avg.* | | | | **65.43** | **1.24** |
| **Option2** | $Q_{LE}$ | 0.3 | 0.423 | 0.123 | 40.53 | 1.00 |
| | $Q_{RE}$ | 0.019 | 0.009 | 0.01 | 51.99 | 0.08 |
| | *Avg.* | | | | **46.26** | **0.54** |

Table IV.10 Elemental uncertainty sources associated with the stream discharge measurement using StreamPro ADCP

| Source | Notation | Type | Standard uncertainty, $u(x_i)$ | | Estimation source |
|---|---|---|---|---|---|
| Sources associated with the mean velocity in verticals, $\bar{v}_n$ | | | | | |
| Instrument accuracy | $u(\bar{v}_{ac})$ | B | 0.005ft/s (0.0016 m/s) | | RDI |
| Instrument calibration | $u(\bar{v}_{ca})$ | A | Lab (vs. Flowtracker) | Field (vs. Flowtracker) | Field/laboratory tests |
| | | | ± 4.55% | ±5.24% | |
| Sampling time | $u(\bar{v}_{st})$ | B | 0.23% | | Field tests |
| Near transducer | $u(\bar{v}_{tr})$ | | Not evaluated | | - |
| Vertical velocity model | $u(\bar{v}_{vd})$ | B | Variable (see Section IV.1.4.2.1.5) | | ISO 1088(2007) Table F.1 |
| Flow angle correction | $u(\bar{v}_{an})$ | B | Variable (see Section IV.1.4.2.1.6) (Not active) | | Huang (2012) |
| Operational conditions | $u(\bar{v}_{op})$ | A | ± 0.021 ft/s (0.006 m) | | Field tests |
| Sources associated with the depth in verticals, $d$ | | | | | |
| Instrument accuracy | $u(d_{ac})$ | B | 0.005ft (0.0016m) | | RDI |
| Instrument calibration | $u(d_{ca})$ | A | Lab (vs. wading rod) | Field (vs. wading rod) | Field/laboratory tests |
| | | | ± 0.032ft (0.01 m) | ± 0.059ft (0.002m) | |
| Operational conditions | $u(d_{op})$ | A | 0.006ft (0.002m) | | Field tests |
| Sources associated with the distance between verticals, $b$ | | | | | |
| Instrument accuracy | $u(b_{ac})$ | B | 0.003ft (0.0009 m) | | Scale resolution |
| Operational conditions | $u(b_{op})$ | A | 0.05ft (0.015m) | | WMO(2011) |
| Sources associated with the estimation of discharge, $Q_t$ | | | | | |
| Discharge model | $u(Q_{mo})$ | B | 0.50% | | Muste et al. (2004) |
| Number of verticals | $u(Q_{nv})$ | B | 0% | | Field tests |
| Edge discharge model | $u(Q_{eg})$ | B | 2.48% (Option1) and 1.08% (Option2) | | Field tests |
| Flow unsteadiness | $u(Q_{us})$ | B | Not active | | - |
| Operational conditions | $u(Q_{op})$ | B | Not active | | - |

IV.3.5 Combined Standard Uncertainty

The standard and expanded uncertainties for the measured discharges obtained with equation (IV.1) can be written as equation (IV.5) and (IV.6), respectively, and those for the total discharges estimated with equation (IV.2) can be written as equation (IV.7) and (IV.8), respectively. The term for the edge discharge uncertainties in equation (IV.7) is described as one term, because it is reasonable to assume that the uncertainties for each edge are equal weight, and therefore the sum of the edge discharges has either 2.48% or 1.08% of uncertainties with respect to total discharges depending on the edge coefficients used.

$$u_c(Q_m)=\sqrt{\sum_{n=1}^{23}u(\bar{v}_n)^2\left(\frac{\partial Q_t}{\partial \bar{v}_n}\right)^2+\sum_{n=1}^{23}u(d_n)^2\left(\frac{\partial Q_t}{\partial d_n}\right)^2+\sum_{n=1}^{23}u(b_n)^2\left(\frac{\partial Q_t}{\partial b_n}\right)^2}$$
$$\sqrt{+2\sum_{n=1}^{22}\sum_{n+1}^{23}\left(\frac{\partial Q_m}{\partial \bar{v}_n}\right)\left(\frac{\partial Q_m}{\partial \bar{v}_{n+1}}\right)u(\bar{v}_n)u(\bar{v}_{n+1})r(\bar{v}_n,\bar{v}_{n+1})+2\sum_{n=1}^{22}\sum_{n+1}^{23}\left(\frac{\partial Q_m}{\partial d_n}\right)\left(\frac{\partial Q_m}{\partial d_{n+1}}\right)u(d_n)u(d_{n+1})r(d_n,d_{n+1})}$$
$$\sqrt{+2\sum_{n=1}^{22}\sum_{n+1}^{23}\left(\frac{\partial q_n}{\partial b_n}\right)\left(\frac{\partial q_{n+1}}{\partial b_{n+1}}\right)u(b_n)u(b_{n+1})r(b_n,b_{n+1})+u(Q_{mo})^2+u(Q_{nv})^2+u(Q_{us})^2+u(Q_{op})^2}$$

(IV.5)

$$U(Q_m)=ku_c(Q_m) \quad \text{(IV.6)}$$

$$u_c(Q_t)=\sqrt{\sum_{n=1}^{23}u(\bar{v}_n)^2\left(\frac{\partial Q_t}{\partial \bar{v}_n}\right)^2+\sum_{n=1}^{23}u(d_n)^2\left(\frac{\partial Q_t}{\partial d_n}\right)^2+\sum_{n=1}^{23}u(b_n)^2\left(\frac{\partial Q_t}{\partial b_n}\right)^2}$$
$$\sqrt{+2\sum_{n=1}^{22}\sum_{n+1}^{23}\left(\frac{\partial Q_t}{\partial \bar{v}_n}\right)\left(\frac{\partial Q_t}{\partial \bar{v}_{n+1}}\right)u(\bar{v}_n)u(\bar{v}_{n+1})r(\bar{v}_n,\bar{v}_{n+1})+2\sum_{n=1}^{22}\sum_{n+1}^{23}\left(\frac{\partial Q_t}{\partial d_n}\right)\left(\frac{\partial Q_t}{\partial d_{n+1}}\right)u(d_n)u(d_{n+1})r(d_n,d_{n+1})}$$
$$\sqrt{+2\sum_{n=1}^{22}\sum_{n+1}^{23}\left(\frac{\partial q_n}{\partial b_n}\right)\left(\frac{\partial q_{n+1}}{\partial b_{n+1}}\right)u(b_n)u(b_{n+1})r(b_n,b_{n+1})+u(Q_{mo})^2+u(Q_{nv})^2+u(Q_{eg})^2+u(Q_{us})^2+u(Q_{op})^2}$$

(IV.7)

$$U(Q_t)=ku_c(Q_t) \quad \text{(IV.8)}$$

*where* $q_n$ is the subsection discharge. The first three terms in equation (IV.5) and (IV.7) are associated with the uncertainties in depth-averaged velocity $u(\bar{v}_n)$, depth $u(d)$, and distance between verticals $u(b)$, respectively.

Depth, velocities, and widths are directly measured variables and each of them is affected by elemental error sources that were described in Section IV.3.4. Terms 4, 5 and 6 in equations (IV.5) and (IV.7) capture the contribution of the correlated uncertainties. Terms 4 and 5 characterize the correlated uncertainties developed due to the fact that total discharge is the sum of the consecutive panel discharges whereby depths and velocities are measured by the same instrument in consecutive subsections. Term 6 denotes another correlated uncertainty generated as width measurements in equation (IV.1) are not independent because they are measured with the same instrument in individual panels. In general, the three input variables (velocity, depth and width) are affected by correlated uncertainties disregard of the velocity-area method used for estimation of the total discharge (mean- or mid-section) as they are not independent variables in the functional relationship for the total discharge. These terms are difficult to estimate and for the present analysis will be assumed to be zero as there is no available information on their magnitude.

The last four terms in equation (IV.5) are: uncertainties due to discharge model, $u(Q_{mo})$; number of verticals where the velocities over the cross section were acquired, $u(Q_{nv})$, flow unsteadiness during the measurement of the total discharge (uncertainty not related to flow fluctuations due to turbulence), $u(Q_{us})$, and operational conditions, $u(Q_{op})$. Equation (IV.7) has one more term associated with discharge model utilized for the edges $u(Q_{eg})$. Given that they are directly affecting the determination of either the measured or total discharge, their corresponding sensitivity coefficients are unity. It should be noted that the uncertainty due to the number of verticals, $u(Q_{nv})$, should include the effect of the limited number of verticals on both mean velocity field description as well as on the cross section definition. The available literature, however, does not capture the dual effect of

these sources of error. The last uncertainty in equation (IV.5) includes adverse conditions that might affect the accurate measurements over the cross section such operator skills and experience, wind or rain presence, unexpected failure of the depth, width or velocity measurements across the stream. Their effect is captured well if multiple measurements at the site are available under various operating conditions and various users.

Uncertainties associated with the main measured variables (mean velocity in the vertical, depth and width) entail other elemental uncertainty sources that are aggregated through the following relationships:

$$u(\bar{v}_n) = \sqrt{u(\bar{v}_{ac})^2 + u(\bar{v}_{ca})^2 + u(\bar{v}_{st})^2 + u(\bar{v}_{vd})^2 + u(\bar{v}_{an})^2 + u(\bar{v}_{op})^2} \quad \text{(IV.9)}$$

$$u(d_n) = \sqrt{u(d_{ac})^2 + u(d_{ca})^2 + u(d_{op})^2} \quad \text{(IV.10)}$$

$$u(b_n) = \sqrt{u(b_{ac})^2 + u(b_{op})^2} \quad \text{(IV.11)}$$

*where* subscripts *ac*, *ca*, *st*, *vd*, *an* and *op* represents accuracy, calibration, sampling time, velocity model, flow angle correction and operational conditions, respectively. Specifications for all uncertainties in equations (IV.5) through (IV.11) are provided in Table IV.10.

The propagation of the elemental uncertainties to the discharges in the measured and total area of the cross section was conducted using the QMsys Entreprise (Qualisyst Ltd.) software using equations (IV.1) and (IV.2), respectively as definition for the measurement process. The edge estimates were conducted using two options described in Section IV.3.4. The effective degrees of freedom for probability distributions associated with the elemental uncertainties and the final result were determined by the software based on the input information (as shown in Table IV.10). The coverage coefficient *k*, in equations (IV.6) and (IV.8) was considered 2 as the Type A uncertainty used in the analysis is obtained from more than 10 samples and the Type B uncertainties obtained through non-statistical means are derived from large samples.

### IV.3.6 Results reporting and uncertainty budget

Table IV.11 below provides the results for either case of $Q_m$ or $Q_t$. The first row describes the simulated results using QMsys for $Q_m$, and the second row presents the case obtained from WinRiver II moving-boat mode for comparison. The total discharge for the measured area is $Q_m$ = 20.04 $ft^3/s$ that is in good agreement with the 19.4 $ft^3/s$ reported by the WinRiver II software. Differences in $Q_m$ are attributed mostly to the bias in the upper part of the velocity profile (as discussed above) and other filtering algorithms applied in the StreamPro SxS Pro.

The rows from the third to the last present the results for the total discharges based on different methods. The third row is the case based on QMsys SxS, but considering the edge discharges assuming the edge coefficient as 0.5 which is equivalent to the case when using SxS pro software. It has the largest uncertainties, 5.79% among all the cases because the edge discharge uncertainties significantly affected the estimation as presented in Table IV.8 option 1, and therefore SxS pro software user may have to expect this amount of uncertainties by using the software. The fourth row shows the results assuming the edge coefficient as 0.3535, and a significant decrease in expanded uncertainty is observed (3.76%). This means that using the edge coefficient, 0.3535 results in the minimal difference for estimating the edge discharges compared to the one measured with the reference instrument, FlowTracker. The differences in total discharges between the Option 1 (40.33 cfs) and Option 2 (39.74 cfs) were caused by the different edge coefficients. It is also important to note that the fifth row representing the total discharges purely based on SxS pro software is the same as the case in the third row.

Specifically, the total SxS pro discharge in the fifth row was 40.33 cfs and the moving-boat total discharge in the sixth row was 40.23 cfs (0.25% difference). WinRiver II applied to StreamPro moving-boat protocol provides the split of the total discharge in its components (see Figure IV.4). The following values were obtained from the StreamPro moving-boat method: $Q_{measured}$ = 19.41cfs; $Q_{top}$ = 11.85cfs; $Q_{bottom}$ = 6.68cfs;

$Q_{edgeL}$ = 1.67cfs; $Q_{edgRL}$ = 0,61cfs. This split of various discharge components cannot be obtained using the StreamPro SxS Pro software. However, the comparison of edge discharge estimates between SxS and moving boat are not analysed herein, because the author judged that more careful measurements are needed for the current data sets. Since the edge discharge estimates by moving-boat method are very sensitive to the start and end timing when moving the vessel. For example, the software considers approximately the first 10 ensembles as the edge discharges once the record starts, and therefore the early movement or late movement of the vessel introduce the errors for this split. The last row is the result based on USGS stream gage record when the measurements were conducted. There is a significant difference with the ADCP measurements, but the author suspected that the discharge based on USGS RC might had been shifted, but might not be corrected (further investigation needed) at the time of measurements.

The presentation of the results of the measurement situation analysed herein can be then stated as: the measured discharge is $Q_m$ = 20.04 $ft^3/s$ with an interval of uncertainty [19.18 $ft^3/s$, 21.90 $ft^3/s$] estimated at 95 percent confidence level using QMsys SxS. The case represented in the first row is presented only here for example. The uncertainty budget for the different methods is provided in Table IV.12, IV.13, and IV.14 subsequently, and the graphical visualization of the budget is provided in Figure IV.17, IV.18, and IV.19 accordingly.

The total (expanded) uncertainty for the discharge measurement at a 95 percent confidence level varies between 0.86 $ft^3/s$ and 2.33 $ft^3/s$, which correspond to ± 3.76 to ±5.79 percentages of the discharge estimates. The obtained uncertainty estimate compares well with the example provided in the Section 9.3.3 of the ISO 748 (2007) where an estimated of 6% is obtained for a generic example of discharge measurement obtained with current meter sampling 2 velocity points over 20 verticals, bulk flow velocity of about 1 ft/s (3m/s), and sampling time of 3 minutes . The uncertainty budget provided by the QMsys Enterprise software illustrates that uncertainties associated with

the calibration of the StreamPro for depth ($d_{ca}$), edge discharge model ($Q_{eg}$), and the calibration of the StreamPro for velocity ($v_{ca}$) are the most contributing factors to the final uncertainty estimations, but varies with the cases in their magnitude. This budget is a powerful tool for all the actors involved in the measurement process and provides a synoptic view of where the optimization efforts should be allocated.

Table IV.11 Final UA results for StreamPro ADCP measurements

| Discharge | Method | Estimated Q (cfs) | Expanded uncertainty (cfs) | Expanded uncertainty (%) |
|---|---|---|---|---|
| *Qm* | QMsys SxS | 20.036 | 0.862 | 4.30 |
| *Qm* | WinRiver II (traverse) | 19.412 | - | - |
| *Qt* | QMsys based on SxS pro edge algorithm (Option 1) | 40.33 | 2.333 | 5.79 |
| *Qt* | QMsys SxS (Option 2) | 39.738 | 1.494 | 3.76 |
| *Qt* | SxS pro | 40.33 | - | - |
| *Qt* | WinRiver II (traverse) | 40.228 | - | - |
| *Qt* | USGS | 34 | - | - |

Table IV.12 Uncertainty budget for the measured discharge, *Qm*

| Source | Notation | Probability distribution | Divisor* | Contribution to total uncertainty ($ft^3/s$) | Relative contribution to total uncertainty (%) |
|---|---|---|---|---|---|
| Instrument accuracy | $u(\bar{v}_{ac})$ | normal | 2 | 4.74E-04 | 0.255 |
| Instrument calibration | $u(\bar{v}_{ca})$ | rectangular | 1.73 | 5.89E-02 | 31.693 |
| Sampling time | $u(\bar{v}_{st})$ | normal | 2 | 1.13E-04 | 0.061 |
| Vertical velocity model | $u(\bar{v}_{vd})$ | normal | 2 | 1.28E-02 | 6.871 |
| Operational conditions | $u(\bar{v}_{op})$ | *t*-distribution | 1 | 4.80E-03 | 2.584 |
| Instrument accuracy | $u(d_{ac})$ | rectangular | 1.73 | 6.47E-04 | 0.348 |
| Instrument calibration | $u(d_{ca})$ | rectangular | 1.73 | 9.01E-02 | 48.507 |
| Operational conditions | $u(d_{op})$ | normal | 2 | 9.32E-04 | 0.502 |
| Instrument accuracy | $u(b_{ac})$ | rectangular | 1.73 | 8.14E-06 | 0.004 |
| Operational conditions | $u(b_{op})$ | rectangular | 1.73 | 6.57E-03 | 3.533 |
| Discharge model | $u(Q_{mo})$ | normal | 2 | 1.05E-02 | 5.641 |
| Number of verticals | $u(Q_{nv})$ | normal | 2 | 0 | 0 |
| Edge discharge model | $u(Q_{eg})$ | - | - | 0 | 0 |
| Flow unsteadiness | $u(Q_{us})$ | - | - | 0 | 0 |
| Operational conditions | $u(Q_{op})$ | - | - | 0 | 0 |
| Combined Uncertainty | $u(Q_m)$ | normal | | 0.431 | 2.15% |
| Expanded Uncertainty | $U(Q_m)$ | normal($k$=2) | | 0.862 | 4.30% |

*The divisor is the value by which the standard uncertainty is divided to obtain the standard deviation for the probability distribution assumed for the *j-th* source of uncertainty.

Table IV.13 Uncertainty budget for the total discharge, $Q_t$ (Option1)

| Source | Notation | Probability distribution | Divisor* | Contribution to total uncertainty ($ft^3/s$) | Relative contribution to total uncertainty (%) |
|---|---|---|---|---|---|
| Instrument accuracy | $u(\bar{v}_{ac})$ | normal | 2 | 1.69E-03 | 0.124% |
| Instrument calibration | $u(\bar{v}_{ca})$ | rectangular | 1.73 | 2.01E-01 | 14.764% |
| Sampling time | $u(\bar{v}_{st})$ | normal | 2 | 3.87E-04 | 0.028% |
| Vertical velocity model | $u(\bar{v}_{vd})$ | normal | 2 | 4.63E-02 | 3.398% |
| Operational conditions | $u(\bar{v}_{op})$ | *t*-distribution | 1 | 1.71E-02 | 1.253% |
| Instrument accuracy | $u(d_{ac})$ | rectangular | 1.73 | 6.47E-04 | 0.048% |
| Instrument calibration | $u(d_{ca})$ | rectangular | 1.73 | 0.090144 | 6.617% |
| Operational conditions | $u(d_{op})$ | normal | 2 | 9.32E-04 | 0.068% |
| Instrument accuracy | $u(b_{ac})$ | rectangular | 1.73 | 3.13E-05 | 0.002% |
| Operational conditions | $u(b_{op})$ | rectangular | 1.73 | 2.52E-02 | 1.853% |
| Discharge model | $u(Q_{mo})$ | normal | 2 | 1.05E-02 | 0.770% |
| Number of verticals | $u(Q_{nv})$ | normal | 2 | 0 | 0 |
| Edge discharge model | $u(Q_{eg})$ | - | - | 9.68E-01 | 71.075% |
| Flow unsteadiness | $u(Q_{us})$ | - | - | 0 | 0 |
| Operational conditions | $u(Q_{op})$ | - | - | 0 | 0 |
| Combined Uncertainty | $u(Q_m)$ | normal | | 1.167 | 2.89% |
| Expanded Uncertainty | $U(Q_m)$ | normal($k$=2) | | 2.334 | 5.79% |

*The divisor is the value by which the standard uncertainty is divided to obtain the standard deviation for the probability distribution assumed for the *j-th* source of uncertainty.

Table IV.14 Uncertainty budget for the total discharge, $Q_t$ (Option2)

| Source | Notation | Probability distribution | Divisor* | Contribution to total uncertainty ($ft^3/s$) | Relative contribution to total uncertainty (%) |
|---|---|---|---|---|---|
| Instrument accuracy | $u(\bar{v}_{ac})$ | normal | 2 | 1.69E-03 | 0.302% |
| Instrument calibration | $u(\bar{v}_{ca})$ | rectangular | 1.73 | 2.01E-01 | 36.041% |
| Sampling time | $u(\bar{v}_{st})$ | normal | 2 | 3.87E-04 | 0.069% |
| Vertical velocity model | $u(\bar{v}_{vd})$ | normal | 2 | 4.63E-02 | 8.296% |
| Operational conditions | $u(\bar{v}_{op})$ | *t*-distribution | 1 | 1.71E-02 | 3.060% |
| Instrument accuracy | $u(d_{ac})$ | rectangular | 1.73 | 6.47E-04 | 0.116% |
| Instrument calibration | $u(d_{ca})$ | rectangular | 1.73 | 0.090144 | 16.154% |
| Operational conditions | $u(d_{op})$ | normal | 2 | 9.32E-04 | 0.167% |
| Instrument accuracy | $u(b_{ac})$ | rectangular | 1.73 | 3.13E-05 | 0.006% |
| Operational conditions | $u(b_{op})$ | rectangular | 1.73 | 2.52E-02 | 4.523% |
| Discharge model | $u(Q_{mo})$ | normal | 2 | 1.05E-02 | 1.879% |
| Number of verticals | $u(Q_{nv})$ | normal | 2 | 0 | 0 |
| Edge discharge model | $u(Q_{eg})$ | - | - | 1.64E-01 | 29.387% |
| Flow unsteadiness | $u(Q_{us})$ | - | - | 0 | 0 |
| Operational conditions | $u(Q_{op})$ | - | - | 0 | 0 |
| Combined Uncertainty | $u(Q_m)$ | normal | | 0.747 | 1.88% |
| Expanded Uncertainty | $U(Q_m)$ | normal($k$=2) | | 1.494 | 3.76% |

*The divisor is the value by which the standard uncertainty is divided to obtain the standard deviation for the probability distribution assumed for the *j-th* source of uncertainty.

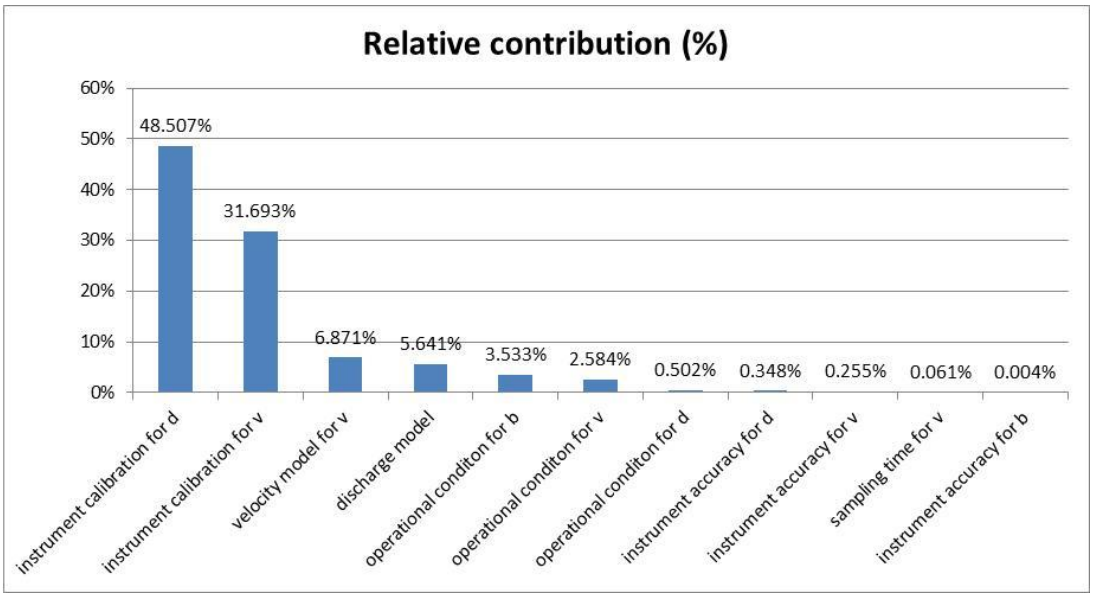


Figure IV.17 Graphical illustration of the relative contribution of the combined uncertainty for $Q_m$

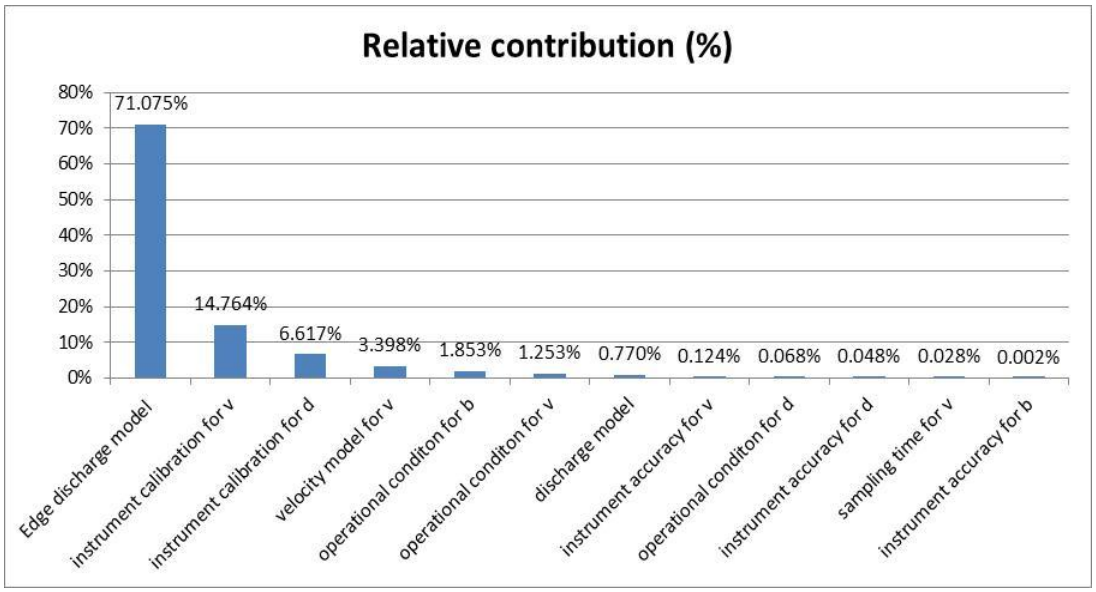


Figure IV.18 Graphical illustration of the relative contribution of the combined uncertainty for $Q_t$ (Option1)

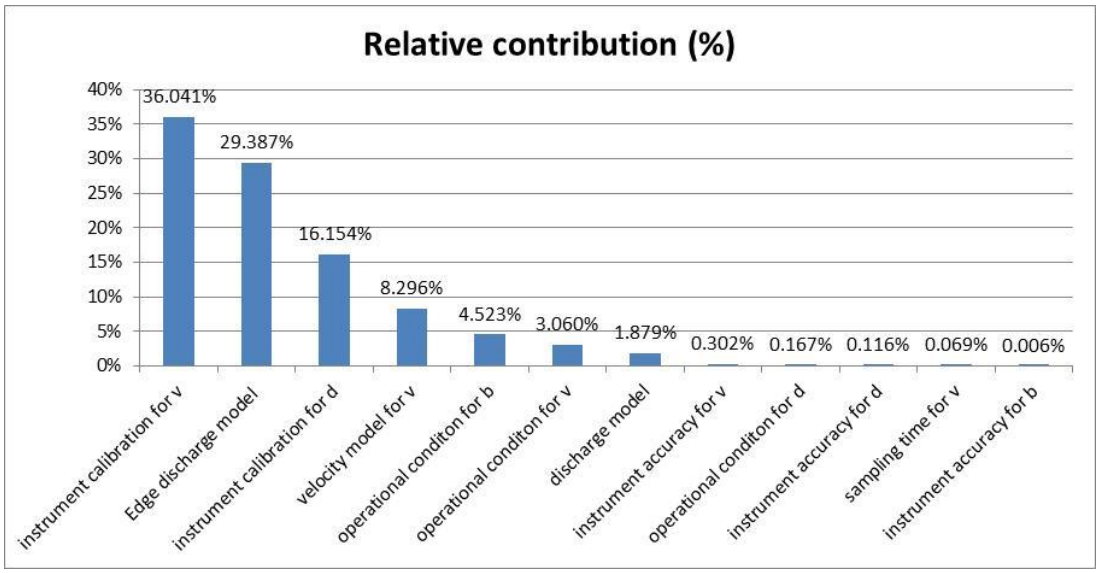


Figure IV.19 Graphical illustration of the relative contribution of the combined uncertainty, $Q_t$ (Option2)

## IV.3.7 Summary of the assessment

The present analysis was conducted using a step-by-step implementation of the GUM (1993). The provided example illustrates that GUM framework can be successfully applied for practical measurements pertaining to hydrometry. The evaluation methods for the uncertainty components entailed information from prior observations and other non-statistical means (Type B) and repeated observations acquired during the actual measurements of various input variables (Type A). The latter uncertainties were assessed through customized experiments whereby individual or combined sources of uncertainties were isolated and estimated. The full-fledged uncertainty analysis presented herein is generic and can be applicable beyond this experiment.

The uncertainty estimates are, however, specific and they incorporate only the uncertainty sources active during the conduct of the measurement process. In other

words, as each measurement is a unique realization its uncertainty analysis inherently captures the specificity of the measurement environment and operational environment. The estimated measurement uncertainties in fact may vary with the flow conditions such as velocities, depths, widths of the channel, amount of inflow discharges, etc. It is deemed that the uncertainties estimated in this section are conservative for most of the small rivers even for the strong unsteady flow conditions. As additional uncertainty assessment data is collected, some common features of the analysis might be detected and used as prior knowledge for new analyses. For this purpose the creation of an uncertainty analysis database grouped around measurement types, instruments, and river types would be beneficial if incrementally developed.

The final result for the stream discharge and the propagation of the components of uncertainties in individual measured variables and other sources were propagated into the final result with the help of QMSys software. The software is based on the GUM (1993) framework. The software aids the user in many steps of the data reduction process as well as in visualizing calculated results and reporting summaries. The software requires the editing of the data reduction equation (equations IV.1 to IV.4) and of the uncertainty propagation equations (equations IV.5 to IV.11) through a dedicated graphical user interface (GUI). During the editing, the actual values of the measured quantities as well as their uncertainties are introduced for further processing. The partial derivatives (i.e., sensitivity coefficients) are calculated inside the software. Table IV.15 and IV.16 provide the QMsys equation editors used for the estimation of either measured or total discharges, respectively.

Table IV.15 Screen capture of the QMsys equation editor for $Q_m$

| <Data Reduction Equation> | |
|---|---|
| Qm=D_1*Vavg_1*((B_2-B_1)/2)+D_2*Vavg_2*((B_3-B_1)/2)+D_3*Vavg_3*((B_4-B_2)/2)+D_4*Vavg_4*((B_5-B_3)/2)+D_5*Vavg_5*((B_6-B_4)/2)+D_6*Vavg_6*((B_7-B_5)/2)+D_7*Vavg_7*((B_8-B_6)/2)+D_8*Vavg_8*((B_9-B_7)/2)+D_9*Vavg_9*((B_10-B_8)/2)+D_10*Vavg_10*((B_11-B_9)/2)+D_11*Vavg_11*((B_12-B_10)/2)+D_12*Vavg_12*((B_13-B_11)/2)+D_13*Vavg_13*((B_14-B_12)/2)+D_14*Vavg_14*((B_15-B_13)/2)+D_15*Vavg_15*((B_16-B_14)/2)+D_16*Vavg_16*((B_17-B_15)/2)+D_17*Vavg_17*((B_18-B_16)/2)+D_18*Vavg_18*((B_19-B_17)/2)+D_19*Vavg_19*((B_20-B_18)/2)+D_20*Vavg_20*((B_21-B_19)/2)+D_21*Vavg_21*((B_22-B_20)/2)+D_22*Vavg_22*((B_23-B_21)/2)+D_23*Vavg_23*((B_23-B_22)/2)+Qmo+Qnv | |
| <Depth> | <Width> |
| D_1=D1ac+D1ca+D1op | B_1=B1ac+B1op |
| D_2=D2ac+D2ca+D2op | B_2=B2ac+B2op |
| D_3=D3ac+D3ca+D3op | B_3=B3ac+B3op |
| D_4=D4ac+D4ca+D4op | B_4=B4ac+B4op |
| D_5=D5ac+D5ca+D5op | B_5=B5ac+B5op |
| D_6=D6ac+D6ca+D6op | B_6=B6ac+B6op |
| D_7=D7ac+D7ca+D7op | B_7=B7ac+B7op |
| D_8=D8ac+D8ca+D8op | B_8=B8ac+B8op |
| D_9=D9ac+D9ca+D9op | B_9=B9ac+B9op |
| D_10=D10ac+D10ca+D10op | B_10=B10ac+B10op |
| D_11=D11ac+D11ca+D11op | B_11=B11ac+B11op |
| D_12=D12ac+D12ca+D12op | B_12=B12ac+B12op |
| D_13=D13ac+D13ca+D13op | B_13=B13ac+B13op |
| D_14=D14ac+D14ca+D14op | B_14=B14ac+B14op |
| D_15=D15ac+D15ca+D15op | B_15=B15ac+B15op |
| D_16=D16ac+D16ca+D16op | B_16=B16ac+B16op |
| D_17=D17ac+D17ca+D17op | B_17=B17ac+B17op |
| D_18=D18ac+D18ca+D18op | B_18=B18ac+B18op |
| D_19=D19ac+D19ca+D19op | B_19=B19ac+B19op |
| D_20=D20ac+D20ca+D20op | B_20=B20ac+B20op |
| D_21=D21ac+D21ca+D21op | B_21=B21ac+B21op |
| D_22=D22ac+D22ca+D22op | B_22=B22ac+B22op |
| D_23=D23ac+D23ca+D23op | B_23=B23ac+B23op |

<Velocity>

Vavg_1=V1ac+V1ca+V1st+V1vd+V1op
Vavg_2=V2ac+V2ca+V2st+V2vd+V2op
Vavg_3=V3ac+V3ca+V3st+V3vd+V3op
Vavg_4=V4ac+V4ca+V4st+V4vd+V4op
Vavg_5=V5ac+V5ca+V5st+V5vd+V5op
Vavg_6=V6ac+V6ca+V6st+V6vd+V6op
Vavg_7=V7ac+V7ca+V7st+V7vd+V7op
Vavg_8=V8ac+V8ca+V8st+V8vd+V8op
Vavg_9=V9ac+V9ca+V9st+V9vd+V9op
Vavg_10=V10ac+V10ca+V10st+V10vd+V10op
Vavg_11=V11ac+V11ca+V11st+V11vd+V11op
Vavg_12=V12ac+V12ca+V12st+V12vd+V12op
Vavg_13=V13ac+V13ca+V13st+V13vd+V13op
Vavg_14=V14ac+V14ca+V14st+V14vd+V14op
Vavg_15=V15ac+V15ca+V15st+V15vd+V15op
Vavg_16=V16ac+V16ca+V16st+V16vd+V16op
Vavg_17=V17ac+V17ca+V17st+V17vd+V17op
Vavg_18=V18ac+V18ca+V18st+V18vd+V18op
Vavg_19=V19ac+V19ca+V19st+V19vd+V19op
Vavg_20=V20ac+V20ca+V20st+V20vd+V20op
Vavg_21=V21ac+V21ca+V21st+V21vd+V21op
Vavg_22=V22ac+V22ca+V22st+V22vd+V22op
Vavg_23=V23ac+V23ca+V23st+V23vd+V23op

Table IV. 16 Screen capture of the QMsys equation editor for $Q_t$

<Data Reduction Equation>

Qm=Qle+D_1*Vavg_1*((B_2-B_1)/2)+D_2*Vavg_2*((B_3-B_1)/2)+D_3*Vavg_3*((B_4-B_2)/2)+D_4*Vavg_4*((B_5-B_3)/2)+D_5*Vavg_5*((B_6-B_4)/2)+D_6*Vavg_6*((B_7-B_5)/2)+D_7*Vavg_7*((B_8-B_6)/2)+D_8*Vavg_8*((B_9-B_7)/2)+D_9*Vavg_9*((B_10-B_8)/2)+D_10*Vavg_10*((B_11-B_9)/2)+D_11*Vavg_11*((B_12-B_10)/2)+D_12*Vavg_12*((B_13-B_11)/2)+D_13*Vavg_13*((B_14-B_12)/2)+D_14*Vavg_14*((B_15-B_13)/2)+D_15*Vavg_15*((B_16-B_14)/2)+D_16*Vavg_16*((B_17-B_15)/2)+D_17*Vavg_17*((B_18-B_16)/2)+D_18*Vavg_18*((B_19-B_17)/2)+D_19*Vavg_19*((B_20-B_18)/2)+D_20*Vavg_20*((B_21-B_19)/2)+D_21*Vavg_21*((B_22-B_20)/2)+D_22*Vavg_22*((B_23-B_21)/2)+D_23*Vavg_23*((B_23-B_22)/2)+Qre+Qmo+Qnv

| <Depth> | <Width> |
|---|---|
| D_1=D1ac+D1ca+D1op | B_1=B1ac+B1op |
| D_2=D2ac+D2ca+D2op | B_2=B2ac+B2op |
| D_3=D3ac+D3ca+D3op | B_3=B3ac+B3op |
| D_4=D4ac+D4ca+D4op | B_4=B4ac+B4op |
| D_5=D5ac+D5ca+D5op | B_5=B5ac+B5op |
| D_6=D6ac+D6ca+D6op | B_6=B6ac+B6op |
| D_7=D7ac+D7ca+D7op | B_7=B7ac+B7op |
| D_8=D8ac+D8ca+D8op | B_8=B8ac+B8op |
| D_9=D9ac+D9ca+D9op | B_9=B9ac+B9op |
| D_10=D10ac+D10ca+D10op | B_10=B10ac+B10op |
| D_11=D11ac+D11ca+D11op | B_11=B11ac+B11op |
| D_12=D12ac+D12ca+D12op | B_12=B12ac+B12op |
| D_13=D13ac+D13ca+D13op | B_13=B13ac+B13op |
| D_14=D14ac+D14ca+D14op | B_14=B14ac+B14op |
| D_15=D15ac+D15ca+D15op | B_15=B15ac+B15op |
| D_16=D16ac+D16ca+D16op | B_16=B16ac+B16op |
| D_17=D17ac+D17ca+D17op | B_17=B17ac+B17op |
| D_18=D18ac+D18ca+D18op | B_18=B18ac+B18op |
| D_19=D19ac+D19ca+D19op | B_19=B19ac+B19op |
| D_20=D20ac+D20ca+D20op | B_20=B20ac+B20op |
| D_21=D21ac+D21ca+D21op | B_21=B21ac+B21op |
| D_22=D22ac+D22ca+D22op | B_22=B22ac+B22op |
| D_23=D23ac+D23ca+D23op | B_23=B23ac+B23op |

<Velocity>

Vavg_1=V1ac+V1ca+V1st+V1vd+V1op
Vavg_2=V2ac+V2ca+V2st+V2vd+V2op
Vavg_3=V3ac+V3ca+V3st+V3vd+V3op
Vavg_4=V4ac+V4ca+V4st+V4vd+V4op
Vavg_5=V5ac+V5ca+V5st+V5vd+V5op
Vavg_6=V6ac+V6ca+V6st+V6vd+V6op
Vavg_7=V7ac+V7ca+V7st+V7vd+V7op
Vavg_8=V8ac+V8ca+V8st+V8vd+V8op
Vavg_9=V9ac+V9ca+V9st+V9vd+V9op
Vavg_10=V10ac+V10ca+V10st+V10vd+V10op
Vavg_11=V11ac+V11ca+V11st+V11vd+V11op
Vavg_12=V12ac+V12ca+V12st+V12vd+V12op
Vavg_13=V13ac+V13ca+V13st+V13vd+V13op
Vavg_14=V14ac+V14ca+V14st+V14vd+V14op
Vavg_15=V15ac+V15ca+V15st+V15vd+V15op
Vavg_16=V16ac+V16ca+V16st+V16vd+V16op
Vavg_17=V17ac+V17ca+V17st+V17vd+V17op
Vavg_18=V18ac+V18ca+V18st+V18vd+V18op
Vavg_19=V19ac+V19ca+V19st+V19vd+V19op
Vavg_20=V20ac+V20ca+V20st+V20vd+V20op
Vavg_21=V21ac+V21ca+V21st+V21vd+V21op
Vavg_22=V22ac+V22ca+V22st+V22vd+V22op
Vavg_23=V23ac+V23ca+V23st+V23vd+V23op

## IV.4 Protocol to account for unsteady flow effect in hQRC

As described so far, hysteresis is associated with the flow unsteadiness produced by the propagation of the storm (flood) waves following rain events or other flow releases in the channel. Evaluation of the hysteresis-related uncertainties is still in development as the experimental studies are scarce and fragmented due to the difficulty to acquire measurements throughout the propagation of the storm-driven wave. Most of the analytical and numerical simulations presented in Section II.3.2 are using various simplifications and they have been not verified against real data from the reasons mentioned above. Currently, the literature does not offer criteria for a comprehensive evaluation of the methods for estimation of the departure of the loop (actual) RC from the steady RC nor for identifying the most appropriate ones for different possible river flow conditions. Using the experimental evidence, knowledge and tools developed in the study this section assembles a practical framework for taking into account the effect of hysteresis at gaging sites for practically any storm situation and site.

For streamgages equipped with real-time direct discharge measurement instruments (e.g., H-ADCP, LSPIV, or similar), the loop RCs can be built on the fly as the flood events unfold. These stations are currently scarce and still under scrutiny in terms of optimum protocols. While this approach is technologically achievable with the new generation of instruments, the current protocols for estimating discharges need to be revised to make sure that they work well for unsteady flows. In particular, sampling frequency of the direct measurements needs to be adjusted to the dynamics of the flood wave propagation through the station. Based on the experimental evidence of this study (still a limited set of experimental data), it can be concluded that the VQRC method and continuous slope- area method are good candidates for replicating the actual flows during unsteady events. Further research is suggested to critically evaluate the validity of the present assumption for a variety of sites and storm situations.

For gaging stations based on steady hQRCs (they represent the vast majority in the US), a combination of data-mining inferences and analytical tools are proposed herein to correct or account for the hysteresis-induced uncertainties. The flow diagram for the proposed protocol is provided in Figure IV.20. The protocol assumes the current procedures for building the hQRCs remain the same. The end result of the proposed protocol is that the provisional (for the gaging stations transmitting estimates in near-real time) or final discharges are assigned with uncertainty accounting for the hysteresis effect using the best available knowledge and data.

The first step of the protocol is to estimate if the gaging site is prone to hysteresis based on a diagnostic formula (Equations III.15 through III.17) that uses parameters associated with the gaging site: bed slope, Manning's roughness coefficients, the maximum rate of change of depth in time, and hydraulic depth at flood peak. Use of this formula for previous storm hydrographs (archived in the station database) will indicate if the site has potential for developing significant hysteresis when storms of specific characteristics occur. Hysteresis is considered as significant in the present context if the maximum difference between the rising and falling limb for the same stage is larger than 5% of the discharge estimated from the steady RC. The sites that will be found least prone to hysteresis by the above formulas will continue to use steady RCs.

If the sites are found to have significant hysteresis, one of the following paths can be approached: a) direct application of the modified Fread formula or b) data-mining of archived data records. Path a), the direct application of the modified Fread formula, is straightforward to be implemented using a script applied to the incoming records but it is computationally expensive so it will delay the publication of the data. Path b) is essentially based on prior analysis whereby the historical records are analyzed to investigate the type of storm hydrographs experienced at the gaging site. We proposed two subsequent options, labeled Option 1 or Option 2 in Figure IV.20. In Option 1, the historical storm events are clustered and classified according to their characteristics, i.e.,

such as flood frequency (i.e., magnitude of peak discharges covering small to extreme flood events in x-axis) and temporal gradients (*dh/dt* in y-axis). Using these pieces of information look-up diagram is created to be used in conjunction with the developing storm as presented in Figure IV.21. As a further refinement, a series of such diagrams can be created to reflect the seasonality of the changes in channel roughness. It is important to note that look-up diagram should be updated once significant geomorphological changes are observed (e.g., rating curve shifting).

Option 2 illustrates the method by applying the modified Fread equation to the whole historical gage records to get the maximum possible uncertainty ranges which are likely to occur at the specified site. This method is made with the intent to simplify the implementation of the protocol as it is known that each individual storm creates its own loop RC, which would make the implementation much more complex. Caution should be made not to cross-select the events with different rating curves.

Option 2 has been applied is applied to the historical records of our focus site, the USGS 05454220 streamgaging site on Clear Creek, Oxford, IA, and the results presented in Figure IV.22. For illustration purposes only the storm events between May 22, 2011 and June 16, 2011 were selected for the analysis. They correspond to small to moderate scale storms (300-800cfs) as shown in Figure IV.22 (a). No shift of the RC was applied to the steady hQRC within this period (USGS RC no.5), and therefore the thickness of the loop RC is assumed to be solely related to the effect of hysteresis without contributions from possible shifts in RC applied by USGS when there are changes at the gage location.

Figure IV. 22(b) contains the results of the analysis. The modified Fread formula applied for these events are showed as a cloud (red dots) in Figure IV.22 (b) regardless of an order of those events. Since RC shape is determined by the combined effect of hydro-geological (e.g., soil type and moisture content) and meteorological (e.g. rain intensity and duration) conditions as well as stream hydraulics, each of the red dots represents the actual discharge-stage pair reflecting the status of the river at the specific time. The green

circles in Figure IV.22 represent the direct discharge measurements obtained between 2001 and 2011. It can be observed that broadly speaking the spread of the direct discharge measurements agree with the thickness of the cloud. Since direct discharge measurements data is not available for the specified events period (usually scarce for event based scale), this comparison is assumed valid even though the site conditions might had been changed for 10 years since 2001. Therefore, one can generalize that the maximum possible uncertainty due to hysteresis is up to 20% around the steady hQRC. This observation leads to a preliminary inference that states the uncertainty of the RC might be mostly related to the time when the measurements are made rather than on the experimental uncertainty. In other words, the thickness of the cloud is the area of possibilities for the flow if it would be accurately captured rather than associated with the uncertainty in discharge measurement. The former departure from the steady hQRC can be related to the physics of the flow and has a unique distribution while the second source of uncertainty is presumably constant for the entire flow range.

It is expected that the proposed protocol herein would correctly be used to address the hysteresis uncertainties on the fly as flood event unfolds. The continuous records of data (as provided for example by the USGS) is well posed to be tested by data mining protocol, and may enable forecasting streamflows at the station using techniques as described in Bhathacharya and Solomantine (2005) or Sudheer and Jain (2003).

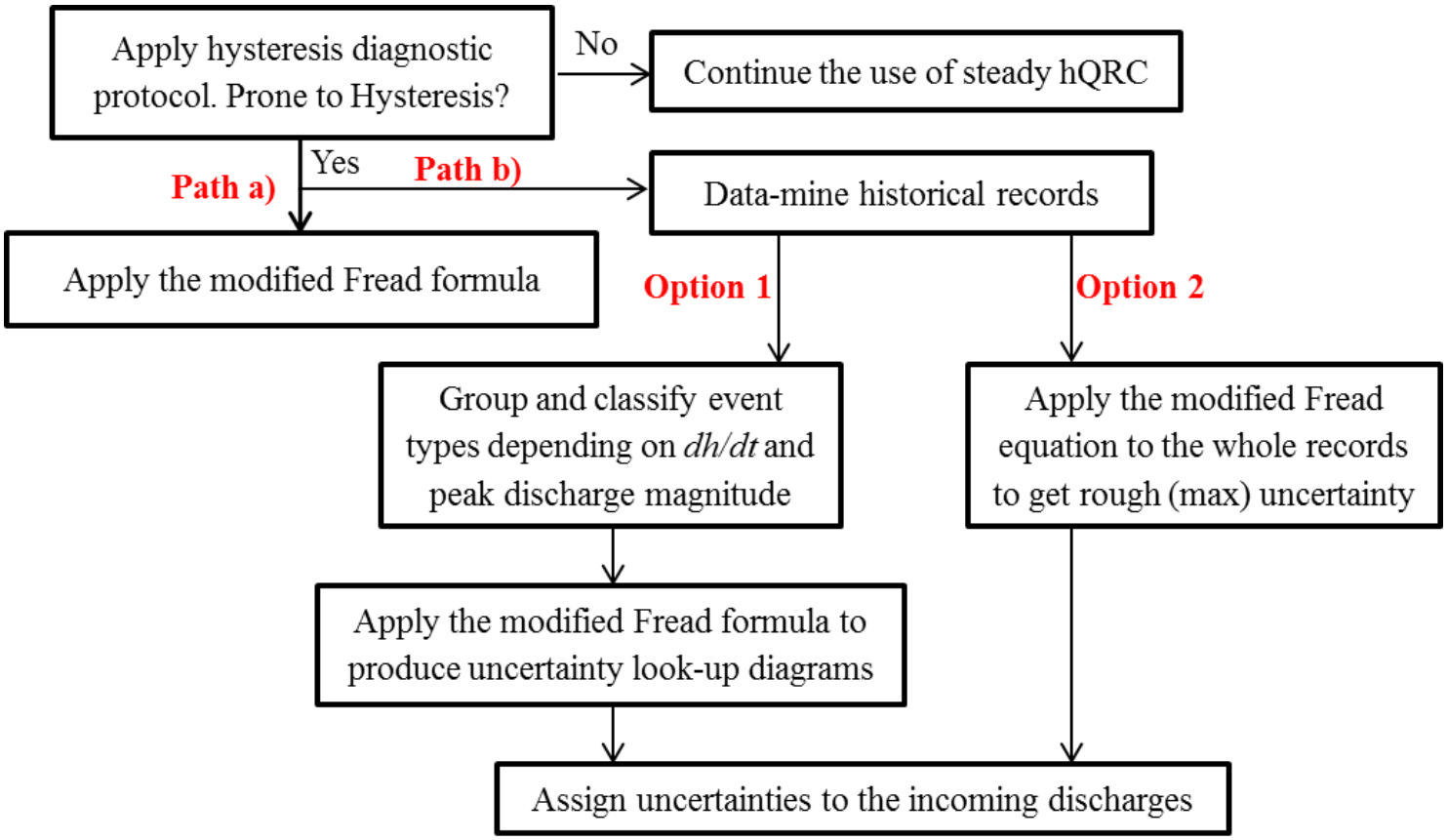


Figure IV.20 Protocol flowchart accounting for unsteady flow effect in hQRC

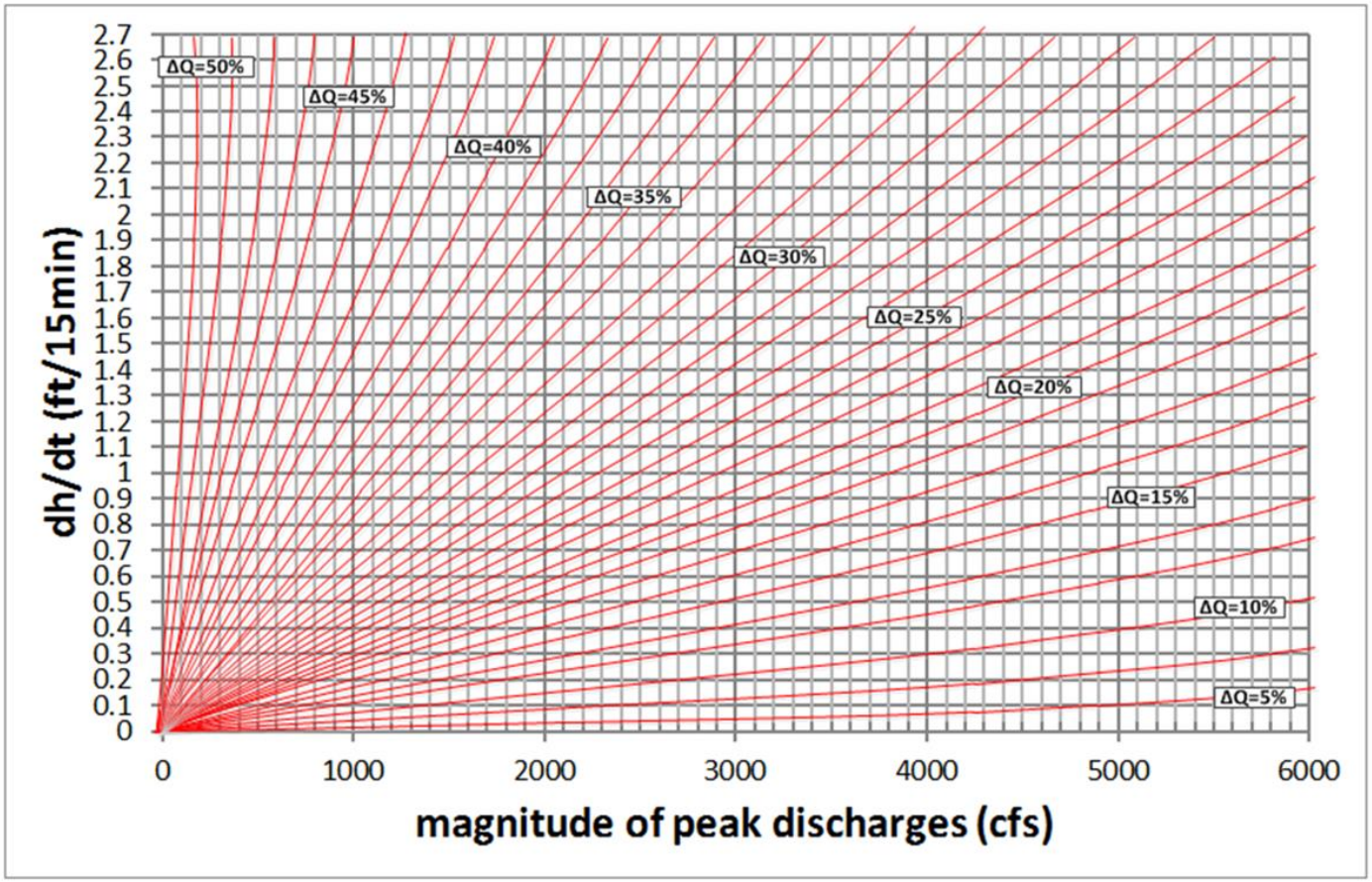


Figure IV.21 Example of hysteresis diagram at a gating site

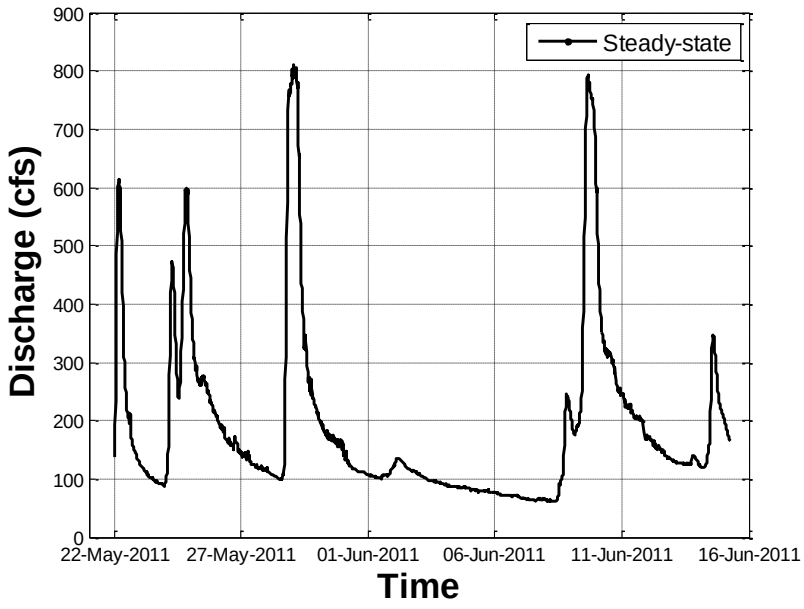


a)

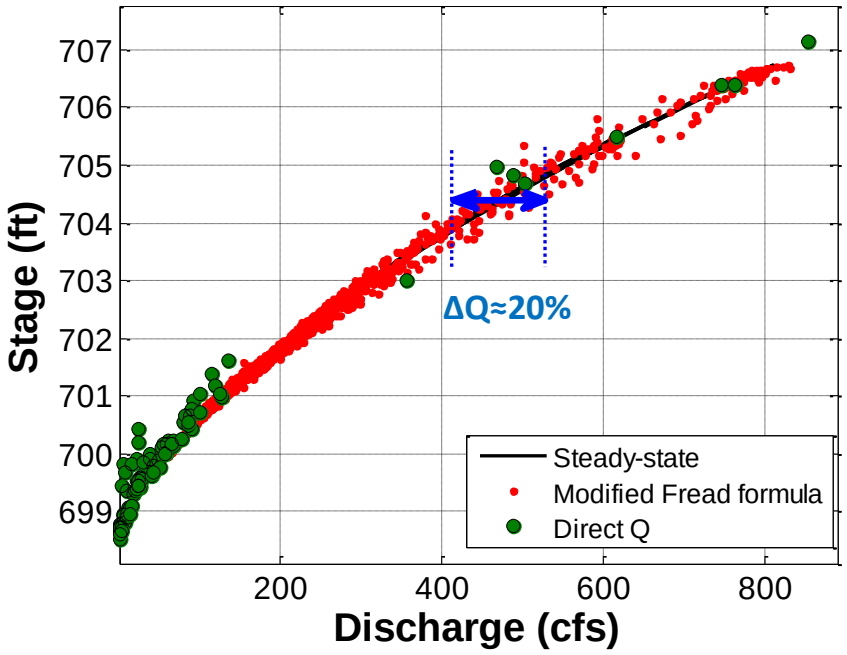


b)

Figure IV.22 Assessment of the uncertainty associated hysteresis for the steady hQRC at USGS station 05454220 in Clear Creek: a) Event hydrographs between May 22, 2011 and June 16, 2011; b) Comparison between directly measured discharges (2001-2011) and the computed discharges for those events in a)

# CHAPTER V

# SUMMARY, IMPLICATIONS AND RECOMMENDATION

## V.1 Summary

The overarching goal of this study is to explore the uncertainty of the conventional approach for constructing hQRCs and to evaluate methodologies for accurate and continuous monitoring of discharge in steady and unsteady open channel flows. While the study also includes the estimation of direct discharge measurement uncertainty, the central goal of the study is to assess the uncertainty generated in the discharges estimated via RCs in situations of unsteady flows. Currently, most of the inland river hQRCs are built under the steady flow assumption and used as such for steady and unsteady flows.

The available literature does not offer uniform criteria for a comprehensive evaluation of the accuracy of the methods for development of RCs, nor for identifying the most appropriate ones for different river flow conditions. The RCs' uncertainty, regardless of the way they were developed (empirical and/or analytical formulations), is largely unknown, especially for unsteady conditions at high flows (such as floods) when the deviations of the steady RCs discharge estimates from the actual flows (a.k.a. hysteresis) are considerably increased. More importantly, there is no systematic effort to evaluate the impact of hysteresis in medium and smaller streams where floods are increasingly present in the last decade (e.g., Iowa and Cedar Rivers in the U.S.).

The main contribution of this research is the development of a uniform end-to-end methodology for assessing the uncertainty in RCs generated by hysteresis along with means to conveniently examine the uncertainty magnitude due to unsteady flows as a function of the site and storm event characteristics. The measurement techniques and analysis methodologies proposed herein are applicable to any river size and allow to

dynamically track the flood wave propagation and to evaluate the uncertainty associated with the use of conventional RCs in unsteady flows.

The specific findings and contributions of this study are listed below:

a. Modification of Fread approach (1975) solving 1-D shallow flow equation to be applicable for rivers irrespective of their size.
b. Substantiation of the hysteretic behavior of the hQRC using direct discharge measurements acquired during unsteady flows in several widely-varied river sizes (case studies documented for Clear Creek in Oxford, IA, Chattahoochee River in USA, and Ebro River in Spain).
c. Evaluation of the sensitivity to hysteresis for alternative RC protocols (VQRC and CSA method).
d. Identification hysteresis diagnostic formula suitable for rapid and efficient assessment of the hysteresis-prone gaging sites. The characterization and evaluation of the significance of unsteadiness parameters was established using 1D HEC-RAS unsteady model and the 1D modified Fread equation.
e. Assessment of the uncertainty in direct discharge measurements acquired with TRDI StreamPro ADCP using standardized uncertainty analysis framework (GUM, 1993).
f. Establishment of comprehensive protocols to account for hysteresis at a gaging site.

Short descriptions of the specific findings and contributions are subsequently summarized to provide a glimpse in their technical aspects.

a) The modification to Fread approach (1975) solving 1-D shallow flow equation is presented in Chapter III. The modification was triggered by the fact that Fread's (1975) formula was originally developed assuming that the hydraulic radius is equivalent to hydraulic depth. Moreover, the cross-sectional area is considered to be proportional to the depth as it is the case for the rectangular channel geometry.

The assumption holds for large rivers at flood-prone large sites (e.g., Mississippi) as proven by comparison with direct measurements during unsteady flows (most of the direct measurements are taken at such sites). For small streams the assumption is not always valid therefore a modification to Fread formula was necessary to account for the exact channel geometry parameters such as hydraulic radius ($R$), wave celerity coefficient ($K$), and average flood wave slope ($r$). The new formulation also improves the accuracy of the conveyance factor and energy slope irrespective of the river size.

The modified Fread equation was tested for both small stream (Clear Creek) and medium rivers (Chattahoochee River in Georgia USA and Ebro River in Spain). In Clear Creek case, it was found that there are significant differences (up to 7.5%) in the prediction of the discharges using the original and modified formulas for a specific event. Most of this difference is associated with the use of a simplified assumption (i.e., the hydraulic depth in the conveyance factor) in Manning equation rather that in the estimation of the energy slope. The contribution of the energy slope was limited to about 1%, and therefore substantiating the superior accuracy of the modified Fread equation. Similarly, the use of the modified Fread formula enables to use the actual value for the wave celerity coefficient ($K$) using surveyed channel geometry rather than the recommended constant value ($K$=1.3 is often considered to be reasonable approximation for many natural channels). The estimated uncertainty associated with hysteresis using the steady-based discharge values as reference ranged from -4% to +11% using the modified Fread equation.

The modified Fread equation was also tested for unsteady events in Chattahoochee River (Georgia) and Ebro River (Spain) against direct discharge measurements taken with appropriate measurement protocols to capture the flood wave propagation dynamics. The analytical results agree well with the direct

measurements indicating the usefulness of the modified Fread equation. For the last two cases, the sizes of the rivers were similar each other (approximately 300ft width). Specifically, the range of relative differences for the discharges at the same depth and for the depths at the same discharge which correspond to the points on the rising and falling limbs of the hydrographs are about 40% and 30% for Ebro River event and about 24% and 30% for the Chattahooche River event at Georgia Highway 141 (the best fit of the modified Fread results to the direct discharges).

b) The substantiation of the hysteretic behavior of the hQRC is demonstrated through a combination of methods, including direct measurements, analytical derivations, and creation of virtual instruments simulating the measurement protocols used for acquiring direct discharge measurements for the VQRC (see Chapter III.3.1). A set of data collected during a simulated storm event by the local monitoring agency in Ebro River (Spain) was obtained and analyzed to illustrate the hysteretic behavior of the hQRC accounting for hysteresis. The same set of data was utilized to create a virtual instrument that was subsequently used to replicate the VQRC (see Chapter III.3.2). Direct field measurements were acquired by the author and used in conjunction with the CSA method. The directly measured discharges were used for reference and to infer the hysteretic behavior of the hQRC and VQRC as well as for testing the validity of the modified Fread equation in all analyzed cases.

c) The data assembled as described in item b) was used to investigate the sensitivity to hysteresis of the alternative RC protocols, i.e., (VQRC method and CSA method (see Chapter III.3.2 and III.3.3, respectively). The VQRC method reveals a good agreement between the stage-discharge relationships obtained via VQRC and modified Fread method applied to steady hQRC. This indicates the fact that the actual index velocity captured as the unsteady flow progresses will lead to two

different discharges for the same depth on the rising and falling limbs of the hydrograph even if the VQRC is unique. Some degree of improvement in capturing aspects of unsteady flow by the VQRC method found to be made by "segmentation approach" which intends to separately account for the phases of the flow (rising and falling limbs). That is, the relationship between index velocity and the channel mean velocity can be either a single regression or a double segmented regression curve. As expected, the one-to-one VQRC (single regression) displays slightly smaller difference than the segmented VQRC (double regression) for points of the same depth on the rising and falling limbs. The difference is a reflection of the different acceleration rates occurring on the two phases of the unsteady event, and can be concluded that segmented RC better captures the unsteady dynamics.

The CSA method was examined with respect to both its utility for continuously monitoring discharges using steady flow assumptions and the capability to capture the hysteretic behavior of the hQRC during unsteady flow. It was found that CSA method using surveyed geometry, estimated Manning's roughness coefficient, and free-surface slope can be used as a surrogate for continuous estimation of the discharges. The results showed that the CSA and the modified Fread methods give predictions that are close to the USGS discharges even though the magnitude of the hysteresis is not sufficiently large in computed cases, hence it is difficult to make inferences. However, Figures III.30 b) and III.30 d) clearly describe the hysteretic behavior as the slope has distinct trajectories on the rising and falling limbs of the hydrograph. The CSA method supplied with real-time measurement of the free surface slope applied to unsteady flow events confirms that it is capable to capture well the dynamics of the flow, with the rising and falling limb of hydrographs distinct when represented in stage-discharge coordinates.

d) It is expected that the hysteresis magnitude is not essential for normal/typical storm events propagating in small channels. Its importance increases with the intensity and magnitude of the storm events, especially if the channel reaches are set on very low slopes. Given that the additional resources required to dynamically capture the flow characteristics during unsteady events are considerable (either in terms of measurements or analytical predication), engineering judgment should be used to establish where and when is needed to invest additional efforts. For this purpose a diagnostic method based on the Fread (1975) formula was tested for its capability to assess the potential for hysteresis development (see Chapter III.4.1). The method is relatively simple being based on four input quantities (bed slope, hydraulic depth, *dh/dt*, and Manning's roughness coefficient).The proposed diagnostic formula was successfully tested using available stage and discharge records at a gaging station on a small stream (Clear Creek, Iowa).

The significance of unsteadiness parameters are conceptualized using a HEC-RAS numerical model and the modified Fread equation The numerical modeling runs were also aimed at providing insights into the impact of various variables on the hysteresis magnitude (with thickness being the most important parameter). For this purpose, a HEC-RAS unsteady model was developed for Clear Creek encompassing a USGS gaging station. The sensitivity analysis applied to an actual stream reach with real boundary and initial conditions showed that the thickness of the loop (or size of the loop) is increased when

i. the total duration is short
ii. the time to and from the peak to base flow is short
iii. the flood intensity is high

Other notable dependencies were observed related to channel slope, Manning's roughness coefficient, and rotation direction for the loop (hysteretic) curve using the modified Fread equation as described in Chapter III.4.2.

e) Chapter IV reports a full-fledged uncertainty analysis using a standardized framework for conducting the analysis. The analysis was applied to a set of direct discharge measurements acquired with a StreamPro ADC in Clear Creek during steady-flow conditions. The provided ADCP measurement example illustrates that standardized framework can be successfully applied for practical measurements pertaining to hydrometry. The uncertainty estimates are; however, specific and they incorporate only the uncertainty sources active during the conduct of the measurement process. It is deemed that the uncertainties estimated in this section are conservative for most of the small rivers even for the strong unsteady flow conditions. As additional uncertainty assessment data is collected, some common features of the analysis might be detected and used as prior knowledge for new analyses.

f) A protocol for corrective adjustments to the hQRC estimates that account for unsteady flows effects was proposed in the last section of the Chapter IV. For gaging stations where the steady hQRC is used (they represent the vast majority in the US), a combination of data-mining inferences and analytical tools are proposed herein to correct or account for the hysteresis-induced uncertainties in steady hQRCs. The flow diagram for the proposed protocol is provided in Figure IV.20. If the sites are found to have significant hysteresis, one of the following paths can be approached: a) direct application of the modified Fread formula or b) data-mining of archived data records. Path a), the direct application of the modified Fread formula, is straightforward to be implemented using a script applied to the incoming records but it is computationally expensive so it will delay the publication of the data. Path b) is essentially based on prior analysis

whereby the historical records are analyzed to investigate the type of storm hydrographs experienced at the gaging site. We proposed two subsequent options, labeled Option 1 or Option 2 in Figure IV.20. In Option 1, the historical storm events are clustered and classified according to their characteristics, i.e., such as flood frequency (i.e., magnitude of peak discharges covering small to extreme flood events in x-axis) and temporal gradients (dh/dt in y-axis). Using these pieces of information look-up diagram is created to be used in conjunction with the developing storm as presented in Figure IV.21. As a further refinement, a series of such diagrams can be created to reflect the seasonality of the changes in channel roughness. It is important to note that look-up diagram should be updated once significant geomorphological changes are observed (e.g., rating curve shifting). Option 2 illustrates the method by applying the modified Fread equation to the whole historical gage records to get the maximum possible uncertainty ranges which are likely to occur at the specified site. Option 2 is applied to Clear Creek, Oxford, Iowa, and it was observed that broadly speaking the spread of the direct discharge measurements agree well with the thickness of the computed maximum uncertainty as exemplified in Figure IV.22. It is expected that the proposed protocol herein would correctly be used to address the hysteresis uncertainties on the fly as flood event unfolds.

## V.2 Implications

Critical to managing flood risk is a good understanding of the processes, proper encapsulation of essential features in the forecast models and evaluation of the uncertainties for the numerous variables involved (e.g., precipitation, streamflow, topographic representation, modeling parameters and techniques). In most cases, simple models and limited observations are used to produce static inundation maps. There are few locations (currently about 57) where static inundation maps are produced by National

Weather Service (NWS) models tied to U.S. Geological Survey (USGS) real-time streamgage data (http://water.weather.gov/ahps2). Most often the USGS streamgage records are used for calibrating and defining boundary conditions for the models.

Some of the relevant limitations for the present context are: a) there is no quantitative indication on how far away from forecast points the maps are valid when using static inundation maps (usually 1-2 miles upstream/downstream); b) streamflow estimates are based on limited number of peak flow records bringing into question the accuracy of predicting 100- or 500- year floods (probability of occurrence of a specified flow in any year); c) flood streamflow forecasting relies on extrapolation of relationships that are not valid in unsteady flows. The limited accuracy of the current practice has triggered mapping science initiatives at agencies charged with flood mitigation and forecasting (Anschwaden et al., 2009). For example, pilot projects targeting real-time dynamic flood mapping have been recently initiated by USGS (White River, IN) and NWS (Tar River, NC). These initiatives are envisioned to become long-term undertakings with consideration of improved science and technologies.

Fig V.1 illustrates an end-to-end process for determining inundation maps. The processes related to producing dynamic inundation map are marked in red. While the static floodplain mapping can predict map extent relatively well, it lacks the capabilities to specify the timing and location of the flood wave propagating through the stream and adjacent floodplain. More realistic information is provided by dynamic inundation maps. Flood researchers and practitioners link the upland rainfall-runoff processes with stream hydraulics through RCs. Therefore, the current analytical techniques for constructing RCs are limited in scope as they do not capture the dynamics of the flood wave propagation through the streams. The significance of neglecting hysteresis on producing the inundation maps needs further investigations and development of new measurements protocols. With the advent of the acoustic instrumentation we are in a good position to

advance our capabilities to create dynamic flood mapping if proper protocols to track dynamically the stream flows are developed.

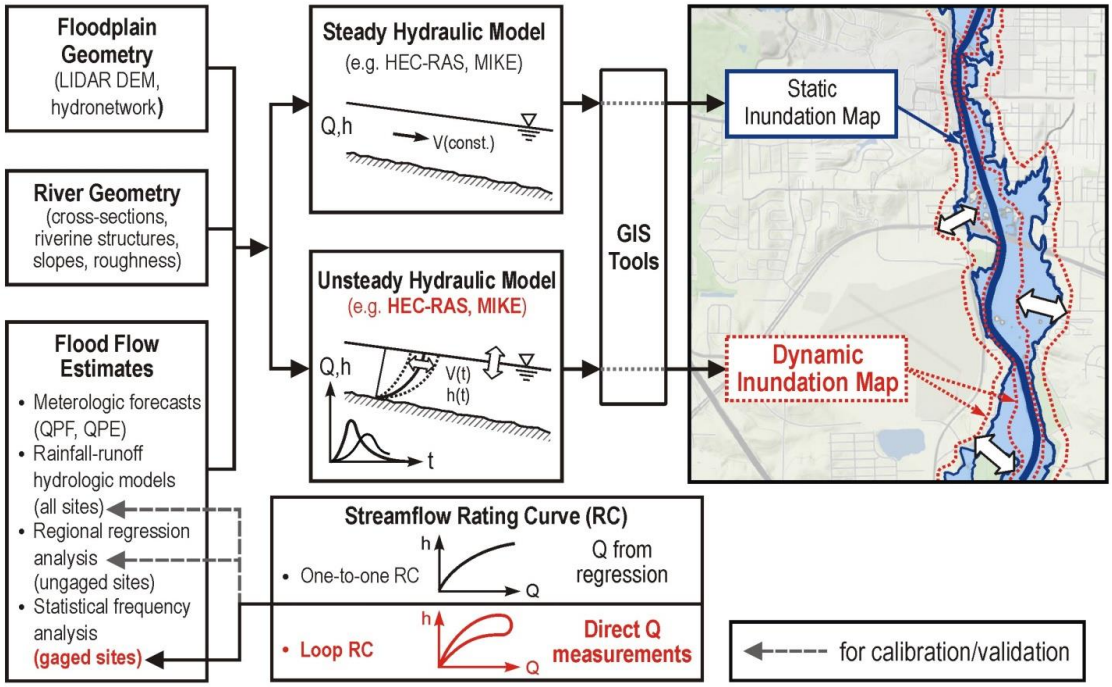


Figure V.1 Flowchart for the end-to-end inundation mapping process

Besides flood mapping, the dynamic tracking of stream flows has important implications on all river transport processes. There are several studies that have already observed various aspects of the effect of the unsteady flows (i.e., storm event propagation) on sediment processes (Ho, 2010; Bombar et. al., 2011, Qu, 2003, Graf and Suszka, 1985, Singh and Tayfur, 2008, Singh et. al., 2004, Song and Graf, 1997, Yen and Lee, 1995, etc.). It is found, for example, that the sediment transport rates for the same discharges are known to be different in rising and falling phases, and the peak sediment transport rates occurs before the peak flow discharges in general (clockwise hysteresis).

Also, the sediment transport rates are known to be larger at the rising limb of hydrograph than that of falling limb (Ho, 2010; Loperfido, 2007; Ahanger et. al., 2013). Yen and Lee (1995) described that the bed deformation and sediment size varies well with the unsteadiness of the flow hydrograph. Graf and Suszka (1985) explained that the percentage increase in total volume of sediments due to unsteady flows is associated with dimensionless unsteadiness parameter, and the total volume of sediment is always larger in unsteady flow than that in steady flow.

Similar observations were made in conjunction with the geo-chemical aspects of river dynamics. For example, Carroll et al. (2007) demonstrated that hysteresis in unsteady flows is correlated with the concentration levels of dissolved solutes, as the phase of the hydrograph is associated with the major source of water bodies such as surface water, soil water, and groundwater which have different solutes. The above examples suggest that the implications of changing the current ad-hoc sampling protocols to an event-based approach are far reaching and with great potential to provide new insights into the mechanics of river transport processes. The new protocols are better suited to follow the mechanics of the processes as they are actually occur in field conditions

## V.3 Future work

The essential message of the present study is that the current protocols to monitor the rivers (initiated a century ago) require a thorough review and adjustments to make good use of the capabilities of the new instrumentation technology currently available on a wide scale. From this perspective, the study reveals many opportunities for further developments. Some of them are listed below:

1. Further validation of the modified Fread equation with various protocols for estimation of the discharge through RCs (especially hQRC) at a variety of gaging sites and flow conditions.

2. Development of an algorithms and ancillary software to correct the discharge estimated with the conventional hQRCs for unsteady effects at the sites prone to considerable hysteresis. It is anticipated that these algorithms can be more detailed in the current protocols to provide uncertainties of the real-time discharge estimates "on the fly" as the flood event unfolds in a convenient and accurate way.
3. Further research on the potential of the CSA method to capture the dynamics of the stream flow by measuring in real-time the channel energy slope. The stage measurement techniques are mature and reliable and can be packaged in stand-alone observing systems with remote communication at a fraction of the cost of the current RC based protocols for discharge estimation.
4. The data acquired and assembled for this study have been purposely limited to stream reaches under channel controls in order to substantiate the isolated effect of hysteresis Extension of the same analysis for sites that are also exposed to backwater effects is suggested as during unsteady flow events the two effects (temporal and spatial variation of the flow conditions) are combined in a complex interrelationship.
5. Testing and evaluating the implications of using loop RCs in the modeling of inundation maps for a variety of flow events and landscapes (with emphasis on urban flooding). Testing should include the evaluation of the impact of using loop RCs as initial conditions for unsteady flow models as well as (more importantly) the timing and spatial development of the inundated area as floods rise and recede.
6. Testing the feasibility of replacing the modified Fread equation in this study with data-driven modeling applied to discharge time series. Previous studies on forecasting river discharges using this type of modeling showed promise in

predicting flow estimates as provided by steady hQRCs (Damle & Yalcin, 2007, Van den Boogard et al., 1998, Ayewah, 2003; Islam & Sivakumar, 2002).

7. The creation of the uncertainty analysis database to include observations and results on a) direct discharge measurements (grouped around measurement types, instruments, and river types) and b) on the effect of hysteretic behavior would be beneficial if incrementally developed.
8. Following more insights from the above studies can lead to a series of investigations of the effect of the actual flow dynamics and the processes that are intimately coupled with the flow transport (sediment, pollutants) and ecological-related aspects (interaction with in-stream vegetation and aquatic life).

# APPENDIX A

# EVALUATION OF UA FRAMEWORK

The subsequent sections of the chapter will provide a critical review of UA framework (GUM, 1993) in terms of concepts, terminology, and implementation steps. The implementation steps for Monte Carlo method will also be introduced. A critical review presented herein is based on Muste et al. (2012).

## A.1 Concepts and Terminology

This section introduces basic principles and concepts pertinent to uncertainty analysis. It is assumed herein that the reader has basic knowledge of statistics concepts used in engineering standards, such as standard deviation, mean, and probability distribution function. In this study, we replicate the terminology and definitions from the original sources using a verbatim approach for rigor and consistency. The terminology associated with GUM and MCM general frameworks is based on JCGM 200 (2007), while the engineering standard considered in the discussion AIAA (1995) and ASME (1998) maintains some specific terms. Table A.1 provides the terminology of GUM frameworks and the AIAA and ASME engineering standard, respectively. A useful resource to complement the discussion in this section of the paper is JCGM 104 (2009). Most of the text will use the JCGM 200 (2007) terminology, if not otherwise specified.

*Measurement and Uncertainty Analysis*. The objective of a measurement is to determine the value of a measurand that is the value of the particular quantity to be measured. The term measurand in the GUM terminology is equivalent to the term true value used by the engineering standards. Measurements can be regarded as direct (such as the weighing) or, as is most often the case, a combination of several measured values of different quantities used in an analytical relationship to obtain the value of a measurand (e.g., discharge measurement).

Table A.1 Differences in terminology between GUM framework and engineering standards

| ISO (1993) | AIAA-S-071-1995 | ASME PTC 19.1-1998 |
|---|---|---|
| Uncertainty of a direct measurement | | |
| • input quantity<br>• type A standard uncertainty<br>• type B standard uncertainty<br>• combined standard uncertainty | • individual variable, $X_i$<br>• bias limit, $B_i$<br>• precision limit, $P_i$<br>(differently estimated for single and multiple test measurements)<br>• total uncertainty | • independent parameter<br>• systematic uncertainty<br>• random uncertainty<br>(differently estimated for single and multiple test measurements)<br>• measurement uncertainty |
| Uncertainty of a result using more than one input quantity | | |
| • functional relationship | • data reduction equation | • derived result |
| | • bias limit (accounts for correlated errors) | • systematic uncertainty (accounts for correlated errors) |
| | • precision limit (differently estimated for: single test with single readings, single test with averaged readings, multiple tests; accounts for correlated precision errors) | • random standard deviation (differently estimated for: single and multiple tests) |
| | | • sensitivity coefficients |
| • sensitivity coefficients | • sensitivity coefficients | • uncertainty of the result (at a specified confidence level) |
| • combined standard uncertainty (accounts for correlated input quantities) | • combined standard uncertainty | |
| • expanded uncertainty (accounts for the level of confidence) | • uncertainty at specified confidence level | |
| • coverage factor ( degrees of freedom and *t*-distribution) | (coverage factor)<br>• coverage factor (degrees of freedom and *t*-distribution) | • coverage factor (degrees of freedom and *t*-distribution) |

A measurement has imperfections such that even if the quantities were to be measured several times, in the same way and circumstances, a different indication value would be in general obtained (this is usually referred to as the repeatability uncertainty). Such indication values are regarded as instances of an indication quantity. The dispersion of the indication values would relate to how well the measurement is made. The

dispersion and the number of indication values would provide information relating to the average value as an estimate or approximation of the true (but unknown) value of the measurand. Consequently, this estimate is complete only when accompanied by a statement of its uncertainty. In practice, the required specification or definition of the measurand is dictated by the required accuracy of measurement. The accuracy of a measurement indicates the closeness of agreement between the result of a measurement and the true value of the measurand.

Uncertainty analysis (UA) is a rigorous methodology for determining uncertainties in measurement results using statistical and engineering concepts. The measurement process for a specified measurand does not entail only the instrument(s) used to produce the final, but also the measurement methods and procedures, as well as the effect of the influence quantities (environmental factors). Collectively, these components form the measurement system. A measurement model that is associated with the measurement system is defined. In GUM, the model is referred to as the functional relationship. The items required by a model to define a measurand are labelled as input quantities. The output quantity in a measurement model is the measurand. The input and output quantities are treated mathematically as random variables and are characterized by mean values, standard deviations, and probability distributions. The probability distributions are determined from measurements or by using the best available knowledge. Correction terms should be included in the model when the conditions of the measurements are not exactly as stipulated. There will be an uncertainty associated with the estimate of a correction term, even if the estimate is zero, as is often the case. Data about the quantities representing physical constants involved in the functional relationship should also be considered in the model.

It is particularly important to note that in hydrometric applications, flow measurements vary widely in space and time when compared with other areas. Most notably, the time variation can span a wide range of scales. For example, the flow in a

river is subjected to turbulent fluctuations (of the order of seconds or minutes), while during a flood event the discharge varies continuously during flood wave propagation (over hours or even days).

*Errors and Uncertainties*. The measurement error is defined as the result of a measurement minus the true value of the measurand. Neither the true value of the measurand nor the result of the measurement can ever be known exactly because of the uncertainty arising from various effects. Distinction should be made between error and uncertainty: uncertainty is the estimate of the error. The uncertainty of the result of a measurement reflects the lack of exact knowledge of the value of the measurand. The uncertainty arises from both random effects and from imperfect correction of the results for systematic effects. Using the JCGM 200 (2007) definition, the uncertainty is the non-negative parameter characterizing the dispersion of the quantity values being attributed to a measurand. In practice, there are many possible sources of uncertainty in a measurement, including incomplete definition of the measurand, imperfect realization of the definition of the measurand, non-representative sampling, inadequate knowledge of the effects of environmental conditions, imperfections in reading analog instruments, finite instrument resolution or discrimination threshold, inexact values of measurement standards and reference materials, inexact values of constants and other parameters obtained from external sources and used in the functional relationship, approximations and assumptions incorporated in the measurement method and procedure, and variations in repeated observations of the measurand under apparently identical conditions.

Traditionally, errors were classified as random and systematic. Random errors presumably arise from unpredictable or stochastic temporal and spatial variation of factors that influence the results of the measurement. These errors give rise to variations in repeated observations of the measurand. Although it is not possible to compensate for the random errors of a measurement result, they can usually be reduced by increasing the number of observations. Frequently in engineering practice, a number of measurements

are used to establish a conventional true value (see Figure A.1 (left)). The systematic error (also termed bias), unlike the random error, cannot be eliminated, but it can be estimated and then corrected through carefully designed experiments (calibrations). If a systematic error arises from a recognized effect of an influence quantity and its effect can be quantified, then a correction can be estimated and applied to the measurement to compensate for the effect. It is assumed that after such a correction has been applied, the expected value of the error arising from the particular effect is zero. The effect of systematic and random errors on repeated measurements is shown in Figure A.1 (right). Detecting, identifying, estimating, and correcting systematic errors may be extremely difficult in practice. Comparison with standards, certified reference material, calibration and verification of instruments, and comparison with alternative measurement methods are some of the means to track systematic errors.

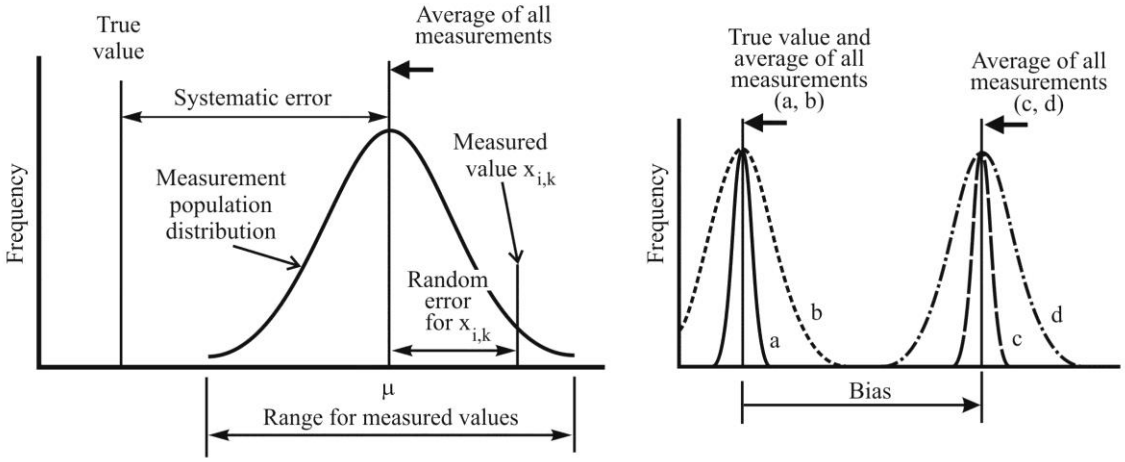


Figure A.1 Errors and their effects: (left) errors in the measurement of an input quantity ( $\mu$ is the mean of the measurement population) (adapted from Coleman and Steele 1995); and (right) illustration of the measurement error effect: a: unbiased, precise, accurate (ideal situation); b: unbiased, imprecise, inaccurate; c: biased, precise, inaccurate; and d: biased, imprecise, inaccurate.

In contrast to the traditional approach of classifying errors and uncertainties in a measurement, the GUM provides a different perspective. In particular, GUM classifies errors based on the approach used to evaluate them, rather than their effect on the results expressed by the traditional engineering systematic (bias) and precision (random) errors. By defining uncertainties as the dispersion of the values that could reasonably be attributed to the measurand, the underlying concept of GUM is that there is no inherent difference between the uncertainty components arising from random and systematic effects. Both effects are assumed to exist as dispersions around the measured value. Consequently, uncertainties are always estimated using probability density functions or frequency distributions; hence their classification should be based on the method used to estimate their numerical values, i.e., Type A evaluated by statistical methods, Type B by other means. Uncertainties in category A are evaluated by statistical analysis of repeated observations to obtain statistical estimates. Uncertainties in category B are evaluated by other means, i.e., assumed probability distributions based on scientific judgment and consideration of a pool of comparatively reliable information that may include previous measurements, calibrations, and experience or general knowledge of the behaviour and properties of relevant instruments and measurement procedures.

Another way of interpreting the GUM classification is that it distinguishes between information that comes from sources local to the measurement process (Type A) and information from other sources (Type B). For the final uncertainty, it makes no difference how the components are classified, because GUM treats Type A and Type B evaluations in the same manner. Typically, Type A uncertainty captures the randomness of the measurement process generated by various sources when repeated measurements (more than once) are available, while Type B is necessary when one (single) measurement or no measurements are available. Consequently, previous knowledge or engineering judgment is required. As an example of Type A evaluation of a systematic uncertainty, consider the situation of a measuring instrument calibrated against a

standard. The calibration process normally involves taking a number of readings. The elements of the uncertainty associated with the calibration that result from random effects will then be evaluated statistically (Type A). When the calibrated measuring instrument is used in a measurement process, the evaluation of the uncertainty has to include the uncertainty in the calibration. However, the errors obtained through the calibration will contribute to the new measurements in a systematic manner. The effect of random errors in the calibration process will have become "fossilized" into an effect that is systematic, and they become Type B uncertainty. As another example of the use of Type B evaluation for a random uncertainty, consider a measurement made with an instrument that displays the reading to just three digits, and is performed just once (M3003, 2007). This will introduce an error defined by the limited resolution of the reading, which is random in nature. The true value of the measurand can lie anywhere in the range of ±0.5 *x* (value of the least significant digit) with equal probability.

*Propagation of uncertainties*. The determination of the uncertainty of the output variable using the functional relationship connecting input and output variables is known as the law of propagation of uncertainties in the GUM approach (when applying the MCM approach, the probability distribution of the output variable is obtained by the propagation of the probability distributions of the input variables in the functional relationship). The standard uncertainty of the output quantity is obtained using the functional relationship of the measurement along with the standard uncertainties of the input quantities in a quadrature that includes the so-called sensitivity coefficients. The sensitivity coefficient for an input quantity is obtained as the partial derivative of the functional relationship with respect to that specific quantity. This equation is an approximate for the measurement model and is derived using the Taylor series expansion, neglecting terms higher than first order (AIAA, 1995; GUM, 1993). The sensitivity coefficients associated with each of the input quantities describe how the estimate of the output quantity will be influenced by small changes in the estimates of the input

quantities. When the input quantities or their respective standard uncertainties contain dependencies, the above uncertainty propagation equation contains covariances (JCGM 200, 2007) that may decrease or increase the combined total uncertainty of the output variable. Usually, the result of a measurement is expressed as the best estimate for the measurand and a confidence interval with a specified probability (level of confidence). This interval is expected to contain a large fraction of the distribution of values that can be reasonably attributed to the measurand. Such an interval is defined using a coverage factor that multiplies the combined standard uncertainty of the output quantity. The value of the coverage factor is chosen on the basis of the level of confidence required for the measurement to fall in a given (confidence) interval.

The standards make references to several alternatives for assessing uncertainties in final results and special measurement situations. For example, the AIAA (1995) standard discusses an "end-to-end" calibration alternative that is accepted in situations when the set of input quantities cannot be replicated directly within the same set of environmental conditions in a short period of time. The end-to-end calibration is dubbed the 'top-down approach' in NIST (2003). That approach is simpler and more convenient compared to the effort needed to estimate uncertainty and sensitivity coefficients at the level of individual inputs and make use of the uncertainty propagation equation. While debate continues on whether or not the two approaches are equivalent, the propagation of uncertainty equation is assumed to be more rigorous. If all the variables involved in a quantity can be replicated simultaneously under fixed conditions (e.g., in the same lab at a fixed time), the uncertainty of the final results should be based on each measured quantity by using a propagation of error formula approach. The engineering standards also distinguish between single and multiple measurements (readings) depending on the number of sets of measurements available. If all the measurements associated with a test are performed only once (one set of test, a single test), even if one or more variables in the data reduction equation have more than one measurement (e.g., an instrument

sampling with high frequency during that measurement), the test is considered single test. If the multivariable test is conducted several times and all the measurements are recorded, the test is qualified as a multiple test.

An alternative approach to the widespread UA based on Taylor series expansion for propagation of the elemental errors to the final results (e.g., GUM, 1993) is through the use of Monte Carlo Method (MCM). In this approach, the best estimate of each variable in the functional relationship is first input. Then the estimated uncertainty for each variable is set. A uniform random number generator is used to produce distributions (e.g., Gaussian, triangular, log-normal, etc.) of scaled uncertainties for individual running tests. Using the input values for all the variables, the calculation of the final result is made. This process is repeated *M* times (10,000 to 250,000 iterations, or even more, are needed). In the end, the mean, the standard deviation, and the coverage interval for a given level of confidence of the distribution of the output values are calculated. MCM implementation is recommended in situations where linearization of the measurement model (the functional relationship) provides an inadequate representation. For linear or linearized models and input quantities for which the probability distribution functions (PDFs) are Gaussian, a MCM is known to yield results consistent with the GUM uncertainty framework (JCGM 101, 2008).

## A.2 GUM framework

The GUM implementation, graphically depicted in Figure A.3, entails the following steps (GUM 1993):

*(1) Define the measurement process*. A mathematical relationship of the measurement relates the measurand and input quantities. The measurement process has to provide an estimate (measurement) of each input quantity and the influence quantities involved in the measurement process.

(2) *Evaluate the standard uncertainty of each input estimate,* $u(x_i)$. Standard uncertainties can be evaluated using statistical methods (Type A) or other methods (Type B).

(2.a) *Type A evaluation*. The standard uncertainty $u(x_i)$ of an input quantity $X_i$ determined from $n$ independent repeated observations is $u(x_i) = s(\overline{X}_i)$, calculated as follows:

$$s^2(\overline{X}_i) = \frac{s^2(x_{ik})}{n} \text{ where } s^2(x_{ik}) = \frac{1}{n-1}\sum_{k=1}^{n}(x_{ik} - \overline{x_i})^2 \; ; \; \overline{x_i} = \frac{1}{n}\sum_{k=1}^{n} x_{ik} \qquad \text{(A.1)}$$

The variable $X_i$ is a random variable subjected to $n$ independent observations (large number, i.e., more than 30), $x_{ik}$ obtained under the same measurement conditions. Based on the available data, several situations can be distinguished [small measurement sample and knowledge from one set of previous observations, small measurement sample and knowledge from several sets of previous observations, and large measurement sample of current measurements (recommended)]. In Type A evaluations of measurement uncertainties, the assumption is often made that the distribution best describing the quantity is Gaussian. When uncertainties are determined from a small number of values, the corresponding distribution can be taken as a *t*-distribution.

(2.b) *Type B evaluation.* Type B evaluations are those carried out by means other than the statistical analysis of a series of observations. This evaluation type is necessary when no current measurements or one (single) measurement are available. Consequently, previous knowledge is required. As Type B assessments have to ensure similar confidence levels as those obtained for Type A evaluations, they require a knowledge of the probability distribution associated with the uncertainty and the associated degree of freedom.

Type B of standard uncertainty is based on the expected dispersion of measurements and the assumed probability distribution. The dispersion, $a_i$, is the

estimated semi-range of a component of uncertainty associated with an input estimate, $x_i$, as defined in Figure A.2. The probability distribution can take a variety of forms, but is generally acceptable to assign well-defined symmetric geometric shapes (i.e., rectangular, Gaussian, triangular) for which the standard uncertainty can be obtained from a single calculation (see Figure A.2). Typical examples of rectangular probability distributions include (ISO 2005): maximum instrument drift between calibrations; error due to limited resolution of an instrument's display or digitizer; and manufacturers' tolerance limits. A normal probability distribution can also be used in association with calibration certificates quoting a confidence level (or coverage factor) with the expanded uncertainty. The uniform (rectangular) probability distribution is used when the only information available about a quantity is the maximum bounds within which all values of the quantity are assumed to lie. For intermediate situations between normal and rectangular distributions, triangular distributions can be used.

In some measurement situations, the upper and lower bounds for an input quantity are not symmetrical with respect to the best estimate due to, for example, a drift in the instrument. For such situations, the asymmetric distribution would be appropriate for estimating the standard uncertainty. The asymmetric distribution can be only applied using MCM.

(3) *Add uncertainty components for each input variable.* The various sources of uncertainties for a variable, irrespective of their provenance and type (A or B), are compounded using the root-sum-square (RSS) combination using:

$$u(x_i)^2 = \sum_{j=1}^{K} u(x_i)_j^2 \qquad \text{(A.2)}$$

*where* $u(x_i)_j$ is the $j$-th elemental error associated with the variable $x_i$.

(4) *Determine the estimated results.* Use the functional relationship to calculate the measurand $y$ in conjunction with the determined input quantities $x_i$.

(5) *etermine the combined standard uncertainty, $u_c(y)$.* The combined standard uncertainty is obtained using the following equation:

$$u_c^2(y) = \sum_{i=1}^{N} \left( \frac{\partial f}{\partial x_i} \right)^2 u^2(x_i) + 2 \sum_{i=1}^{N-1} \sum_{j=i+1}^{N} \frac{\partial f}{\partial x_i} \frac{\partial f}{\partial x_j} u(x_i, x_j) \tag{A.3}$$

*where* $f$ is the functional relationship and each $u(x_i)$ is estimated using either the Type A or B evaluation, or both. $x_i$ and $x_j$ are estimates of $X_i$ and $X_j$, and $u(x_i, x_j) = u(x_j, x_i)$ is the estimated covariance associated with $x_i$ and $x_j$. $N$ is the number of input variables. The partial derivatives, called sensitivity coefficients, are evaluated at $X_i = x_i$ using

$$c_i = \partial f / \partial X_i \tag{A.4}$$

(6) *Determine the expanded uncertainty*, using

$$U = k u_c(y) \tag{A.5}$$

*where k* is the coverage factor. Ideally, uncertainty estimates are based upon reliable Type B and Type A evaluations with a sufficient number of observations such that using a coverage factor of $k = 2$ will ensure a confidence level close to 95 percent. If any of these assumptions are not valid, *the effective degrees of freedom* needs to be estimated using the Welch-Satterthwhaite formula:

$$v_{eff} = \frac{u_c^4(y)}{\sum_{i=1}^{N} \frac{u_i^4(y)}{v_i}} \tag{A.6}$$

*where* $u_c^2(y) = \sum_{i=1}^{N} u_i^2(y) = \sum_{i=1}^{N} \left( c_i u(x_i) \right)^2$ and $c_i$ is the sensitivity coefficient.

(7) *Report the results together with the combined and expanded uncertainty.* The result of a measurement is expressed as $Y = y \pm U = y \pm k u_c(y)$, which is interpreted as the best estimate of the value attributable to the measurand $Y$, and that $y - U$ to $y + U$ is an interval that may be expected to encompass a large fraction of the distribution of values that could reasonably be attributed to $Y$. The reports for uncertainty estimates should present an uncertainty budget containing, at minimum, information such as

probability distribution type, standard uncertainty, sensitivity coefficient, degrees of freedom, etc.

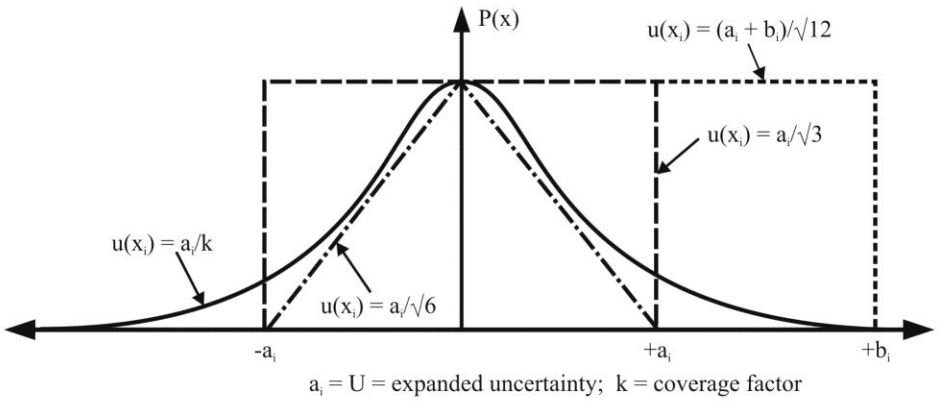


Figure A.2 Probability distributions used to estimate Type B uncertainties

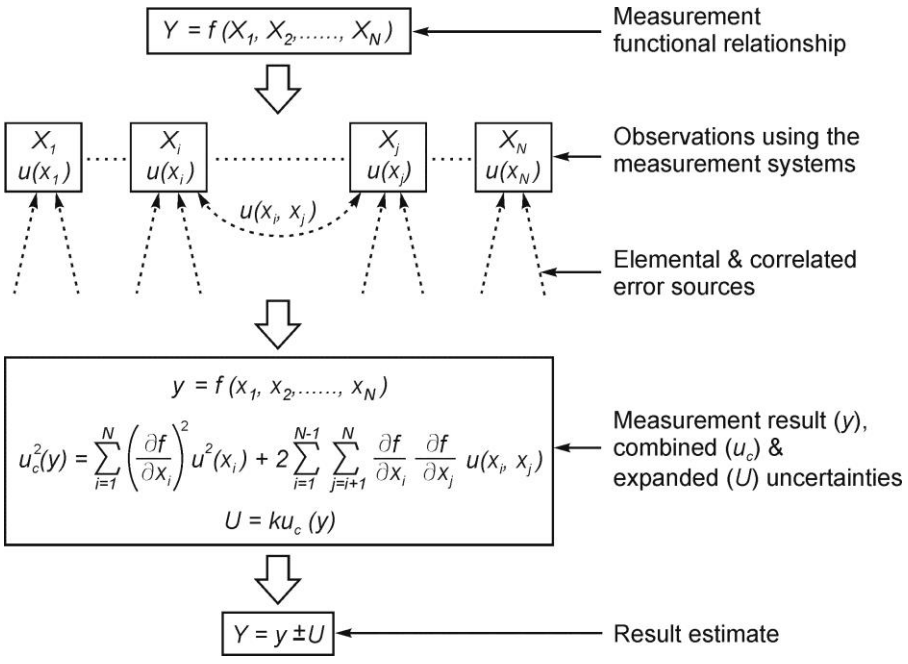


Figure A.3 Flowchart illustrating the GUM implementation steps

## A.3 Monte Carlo Method

The GUM uncertainty framework can be expected to work well in many circumstances. However, if there are assumptions that do not hold, the analysis might not give valid and meaningful results. The Monte Carlo Method (MCM) is more frequently used, as the degree of difficulty is less than GUM. As a rule of thumb, if GUM usage is proven to be favourable, it should be used as the uncertainty framework. If not, MCM can be considered instead. Provided below are the steps for implementing MCM, most often conducted with software. The presentation closely follows JCGM 101 (2008).

The implementation steps are:

(1) *Select the number of trials M* to be made (a value of $M = 10^6$ can often be expected to deliver approximately 95 percent coverage interval for the output quantity, such that this length is correct to one or two significant decimal digits). As there is no guarantee that $M = 10^6$ or any specific pre-assigned number will suffice, an adaptive MCM (which selects *M* adaptively as the trials progress until various results of interest have stabilized in a statistical sense) can be used.

*(2) Sampling from probability distributions and evaluation of the model*

*M* vectors $x_r$, $r = 1, \ldots, M$, are drawn from the PDFs $gx_i(\xi_i)$ for the *N* input quantities $X_i$. The model is evaluated for each of the *M* draws from the PDFs for the *N* input quantities. Draws are as $x_1, \ldots, x_M$, where the *r*-th draw $x_r$ contains $x_{1,r}, \ldots, x_{N,r}$, and $x_{i,r}$ being a draw from the PDF for $X_i$. The model values ($y_r$) are

$$y_r = f(x_r),\ r = 1, \ldots, M \qquad (A.7)$$

Figures A.4 a) and b) graphically depict MCM and GUM for $N = 3$ independent input quantities. In Figure A.4 a), the $gx_i(\xi_i)$ $i = 1, 2, 3$, are Gaussian, triangular, and Gaussian, respectively, and the output PDFs $g_Y(\eta)$ is asymmetric. The asymmetric distribution can be associated with non-linear models or asymmetric $gx_i(\xi_i)$.

(3) *Sort model values* into strictly increasing order, using the sorted model values to provide *G* [a discrete representation of the distribution function $G_Y(\eta)$ for the output quantity *Y*].

(4) *Estimate the mean of the output quantity, y* of *Y* and the associated standard uncertainty, *u*(*y*) using statistical means.

(5) *Estimate an appropriate coverage interval* for *Y*, for a stipulated coverage probability *p* [apply the adaptive Monte Carlo procedure if necessary to provide (approximations to) the standard uncertainty *u*(*y*) and the endpoints $y_{low}$ and $y_{high}$ of the required (probabilistically symmetric or shortest) 100*p* % coverage interval for the output quantity]. A numerical result is deemed to be stabilized if twice the standard deviation associated with it is less than the targeted numerical tolerance, $\delta$ associated with the standard uncertainty *u*(*y*) as described.

The conditions for MCM application are [JCGM 101 (2008), Chapter 5.10.1]:

- $f$ is continuous with respect to $X_i$ –*s* in the neighbourhood of the best estimates $x_i$ of the $X_i$.
- The distribution function for *Y* is continuous and strictly increasing
- The PDF for *Y* is:

  (i) Continuous over the interval for which this PDF is strictly positive,

  (ii) Unimodal (single-peaked), and

  (iii) Strictly increasing (or zero) to the left of the mode and strictly decreasing (or zero) to the right of the mode.
- A sufficiently large value for *M* is used.

*Additional steps for the validation of MCM in GUM context*

(6) *Estimate numerical tolerance* $\delta$ *associated with a numerical value z*: the coverage intervals obtained by the GUM uncertainty framework should be compared to those obtained with MCM to determine whether the required number of decimal digits has

been obtained. Let $n_{dig}$ denote the number of significant decimal digits regarded as meaningful in a numerical value $z$. The numerical tolerance $\delta$ associated with $z$ is obtained by:

- expressing $z$ in the form $c \times 10^{\ell}$, where $c$ is an $n_{dig}$ decimal digit integer and $\ell$ an integer
- taking $\delta = \frac{1}{2}10^{\ell}$

Example: Assume that the estimate of the mean for the output quantity is $y$ = 100.02147 g. The standard uncertainty is $u(y) = 35 \times 10^{-5}$ g, and both significant digits are being regarded as meaningful. For $n_{dig} = 2$, $c = 35$, and $\ell = -5$ the resultant tolerance value is $\delta = 1/2 \times 10^{-5}\text{g} = 5 \times 10^{-6}\text{g}$.

(7) *Estimate the absolute differences of the respective endpoints ($d_{low}$ and $d_{high}$) of the two coverage intervals*. Specifically, determine

$$d_{low} = |y - U - y_{low}| \text{ and } d_{high} = |y + U - y_{high}| \quad \text{(A.8)}$$

*where U* is an expanded uncertainty as defined in GUM (for a given confidence level), and therefore $y - U$ and $y + U$ represent the upper and lower uncertainty intervals, while $y_{low}$ and $y_{high}$ are the endpoints obtained from MCM.

(8) *Compare $d_{low}$ and $d_{high}$ with* $\delta$ to determine whether the GUM uncertainty framework is valid. If both $d_{low}$ and $d_{high}$ are less than $\delta$, the comparison is favourable, and the GUM uncertainty framework has been validated for this case.

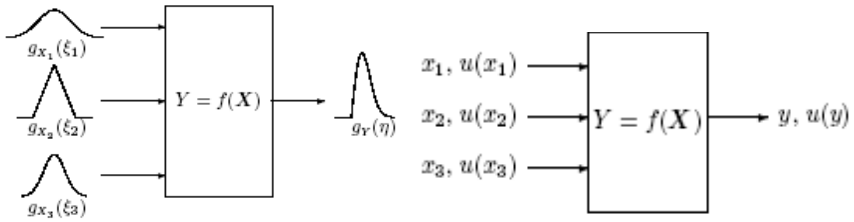


a) b)

Source: JCGM 101 (2008)

Figure A.4 Simplified schematic diagram: (a) Propagation of distributions (MCM); (b) The law of propagation of uncertainties (GUM)

# APPENDIX B

# UA IMPLEMENTATION EXAMPLE

Appendix B will provide a critical review of implementation example for discharge measurements acquired with a mechanical current meter (Muste et al., 2012).

## B.1 Introduction

Mechanical velocimeters pertain to the conventional current measurement instrument family and they have been for a long time the most used instruments for discharge estimation. Current meters are precision instruments calibrated to measure the velocity of flowing water. Several types of current meters are available for use, including rotating-element mechanical meters, electromagnetic meters, acoustic meters and optical meters. They contain a rotating element that is changing its angular velocity proportional with the velocity of the current. By placing the current meter in the stream and counting the number of revolutions of the rotor over a given period of time, the velocity at that point can be determined from a rating developed for the meter.

The instrument is extensively covered with respect to all its aspects (types, configurations, operation guidelines) in the hydrometric literature (Herschy, 2009; ISO 2537, 2007; WMO, 2010) and will be not further discussed here. Most often velocity measurements are acquired at fixed locations in the stream (also called verticals). The meter records velocities at several points in the vertical to approximate the vertical velocity distribution. Repeating this procedure at several verticals along with simultaneous measurements of depths and of the distance between verticals, allows to the calculation of the discharge in the so defined subdivisions (panels). The discharge is calculated with one of the available velocity-area methods (see for example, ISO 1088, 2007). The total discharge for the cross section is obtained by summation of the adjacent discharge panels.

## B.2 Measurement process

At the time of this writing, the authors do not have a set of measurements to support the illustration of uncertainty analysis implementation to this typical hydrometric application. As a surrogate, we will use information available in relevant literature (Boiten, 2000; Herschy, 2009; WMO, 2010; WMO 2011). Use of previous information is not an uncommon situation for conducting uncertainty analyses, as the full-fledged UA requires specially designed experiments with appropriate replication levels (AIAA 1999) that are rarely covered in the budget of a conventional measurement. In such instances, one has to make use of the "best available information". The data for the example provided below follows the measurement situation described in Boiten (2000, page 85).

The discharge measurements used as background for our analysis were conducted using a Price AA current-propeller meter positioned successively at three depths in several verticals across the channel (WMO, 2010). While not many specifics are provided in the reference on the data acquisition, we will assume here a standard measurement scenario that allows us to associate uncertainty estimates for each of the elemental error sources using information available in the specialized literature. The positioning of the current meter at the desired location was made with an A-Pack reel connected to a depth indicator with the finest graduation of tenths of a metre (WMO 2010). Velocity measurements were acquired from a bridge spanning the channel at seven verticals across the stream cross section. The locations of the verticals were marked on the bridge, and the distances between markers were subsequently measured with a conventional pocket measuring tape. The water depth in each vertical was measured with a sounding reel fitted with a counter (WMO, 2010). In this example, it is assumed that conventional protocols for the measurements with different instruments were closely followed (Buchanan and Somers, 1969) and that the measurement environment at the time of each measurement had not been adversely affected (e.g., by wind or rain, or flow unsteadiness). The layout of measurements is illustrated in Figure B.1.

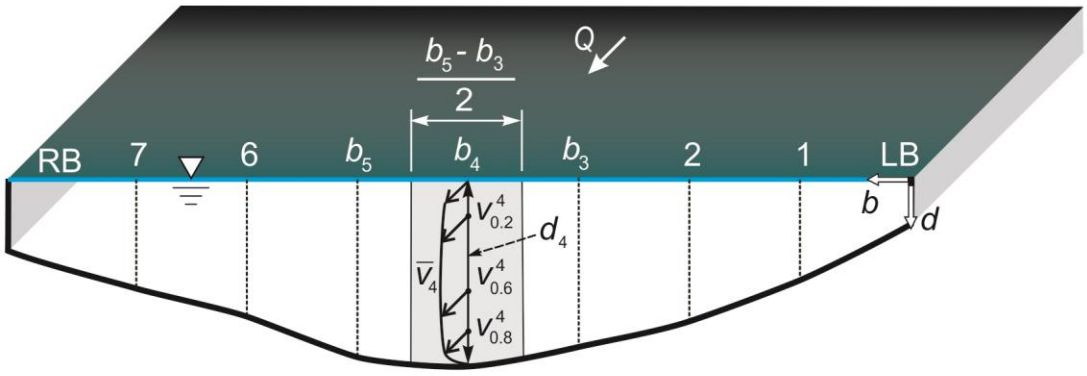


Figure B.1 Schematic of the layout of the velocity measurement locations

The propeller current-meter estimates velocities by measuring the number of revolutions per second, *n*, for a given measuring time, *t* (Boiten, 2000, p.86). The velocity at a point in the vertical is obtained by determining the rate of the revolutions (Equation (B.1)) and calibration equations (Equations (B.2)).

$$n = n_1 / t \tag{B.1}$$

where *n* is the number of revolutions per second, $n_1$ is the total number of revolutions during a measuring time, *t* is the measuring time

$$\begin{aligned} n < 0.63 \qquad & v = 0.246n + 0.017(m/s) \\ n > 0.63 \qquad & v = 0.260n + 0.008(m/s) \end{aligned} \tag{B.2}$$

Velocities acquired in three points located at 0.2 *d*, 0.6 *d*, and 0.8 *d* (where *d* is the depth of flow as measured from the water surface) are used to obtain the depth-averaged velocity, $\bar{v}$ , at each vertical (WMO, 2010). The three-point method is typically recommended when the flow is uniform and two-dimensional whereby the vertical distribution of the streamwise velocity can be assumed to be logarithmic. At least 0.75m flow depth is required to use this method. The mean velocity in a vertical is given by

$$\bar{v} = 0.25v_{0.2} + 0.5v_{0.6} + 0.25v_{0.8} \quad \text{(B.3)}$$

In order to exemplify the estimation of Type A uncertainties, we consider a hypothetical scenario whereby the point measurements in vertical 4 were replicated ten times at each depth location (i.e., 0.2 *d*, 0.6 *d*, and 0.8 *d*) for a total duration of 50 seconds at each location. The acquisition of these velocities was made by changing the position of the current-meter reel after each measurement, so as to capture the error associated with the positioning of the probe. The results provide a minimum, but relevant, statistical sample that captures errors characterizing the measurement environment (flow conditions and operator-related effects).

Finally, the discharge of the stream is obtained using the mid-section method (Herschy, 2009). In this method it is assumed that the velocity sampled at each vertical represents the mean velocity in a segment or panel of the cross section. The $m = 7$ verticals create seven segments plus two others at the beginning and end of the cross section (as illustrated in Figure B.1). The mean velocity in each vertical is obtained as described above using $n = 3$ point measurements at specified location on the vertical, as illustrated in Figure B.1. The summary of the direct and calculated velocities used in the discharge estimation is provided in Table B.1. Using the notations in Figure B.1, the DRE for the discharge measurement process is provided by Equation (B.4)

$$Q_t = \left(\bar{v}_{LB} \times d_{LB} \times \left(\frac{b_1 - b_{LB}}{2}\right)\right) + \sum_{n=1}^{7}\left(\bar{v}_n \times d_n \times \left(\frac{b_{n+1} - b_{n-1}}{2}\right)\right) + \left(\bar{v}_{RB} \times d_{RB} \times \left(\frac{b_{RB} - b_7}{2}\right)\right) \quad \text{(B.4)}$$

*where* $Q_t$ is the total discharge in the cross section, $\bar{v}_n$ is the mean velocity at the $n^{th}$ vertical (and in the associated panel), $d_n$ is the depths measured at the $n^{th}$ vertical, $b_n = \frac{b_{n+1} - b_{n-1}}{2}$ is the half width between $n$+1$^{th}$ and $n$-1$^{th}$ verticals. In Figure B.1, $b_n$ is associated with the panel width at the $n^{th}$ vertical (i.e., 4), and $b_0$ and $b_8$ represent $b_{LB}$ and $b_{RB}$, respectively. The two discharge components at the edges of the water are obtained assuming a parabolic velocity distribution in the verticals toward the banks (Boiten, 2000).

Table B.1 Measured depths, widths, velocities, and calculated discharges

| Section | Distance from the left bank (b (m)) | Depth d (m) | velocity (at 0.2d) $v$ (m/s) | velocity (at 0.6d) $v$ (m/s) | velocity (at 0.8d) $v$ (m/s) | Mean velocity $\bar{v}$ (m/s) | Discharge Q (m3/s) |
|---|---|---|---|---|---|---|---|
| LB | 0 | 1 | 0 | 0 | 0 | 0 | 0 |
| 1 | 10 | 2.24 | 0.544 | 0.523 | 0.450 | 0.51 | 11.424 |
| 2 | 20 | 3.16 | 0.741 | 0.705 | 0.606 | 0.69 | 21.804 |
| 3 | 30 | 3.72 | 0.804 | 0.783 | 0.679 | 0.76 | 28.272 |
| 4 | 40 | 4.16 | 0.850 | 0.830 | 0.705 | 0.8* | 33.28 |
| 5 | 50 | 4 | 0.840 | 0.809 | 0.694 | 0.79 | 31.6 |
| 6 | 60 | 3.08 | 0.726 | 0.694 | 0.601 | 0.68 | 20.944 |
| 7 | 70 | 2.44 | 0.502 | 0.460 | 0.382 | 0.45 | 10.98 |
| RB | 80 | 1.62 | 0 | 0 | 0 | 0 | 0 |
| | | | | | | Total Discharge | 158.30 |

Source: Boiten (2000)

Note: measuring time was 50 sec.

Note *: mean and standard uncertainty for operational conditions ($u(\bar{v}_{op})$) in vertical 4 was based on 10 repeated measurements (Type A uncertainty).

## B.3 Estimation of the standard uncertainties

Provided below are the estimates of the standard uncertainties in $\bar{v}_n$, $d$, and $b$, respectively $u(\bar{v}_n)$, $u(d)$, and $u(b)$, using available information. In addition to the directly measured variables, other sources of errors are considered that are related to methods of calculating of the discharge and operational conditions (measurement environment and instruments' operations). Table B.2 provides the summary of uncertainty components assessment based on prior information (Type B) as documented by previous experimental or expert knowledge relevant to our case study. The literature lists different values for the

same elemental sources of errors, so a critical selection was applied for use in this example.

Table B.2 Elemental uncertainty sources associated with the stream discharge measurement

| Source | Notation | Type * | Standard uncertainty*** u(xi) | Estimation source |
|---|---|---|---|---|
| Sources associated with the mean velocity in verticals, $\bar{v}_n$ | | | | |
| Instrument accuracy | $u(\bar{v}_{ac})$ | B | 1.5% | Thibodeaux (2007) for v > 0.2 m/s |
| Sampling time | $u(\bar{v}_{st})$ | B | 3% | ISO 748 (2007), Table E.3 |
| Vertical velocity model | $u(\bar{v}_{vd})$ | B | 4.8% | ISO 1088 (2007), Table F.1 |
| Operational conditions** | $u(\bar{v}_{op})$ | A | 0.0066 m/s | 10 repeated measurement in vertical 4 |
| Sources associated with the depth in verticals, d | | | | |
| Instrument accuracy | $u(d_{ac})$ | B | 0.009 m | Instrument resolution** |
| Operational conditions | $u(d_{op})$ | B | 0.02 m | ISO 748 (2007), Table E.2 |
| Sources associated with the distance between verticals, b | | | | |
| Instrument accuracy | $u(b_{ac})$ | B | 0.0009 m | Instrument resolution** |
| Operational conditions | $u(b_{op})$ | B | 0.1524 m | WMO (2011) |
| Sources associated with the estimation of discharge, Qt | | | | |
| Discharge model | $u(Q_m)$ | B | 0.5% | Muste et al. (2004) |
| Number of verticals | $u(Q_{nv})$ | B | 5.7%**** | ISO 1088 (2007), Table G.6 |
| Discharge model for the edges | $u(Q_{eg})$ | B | Not available | |
| Flow unsteadiness | $u(Q_{us})$ | B | 0 | |
| Operational conditions | $u(Q_{op})$ | B | 2.7% | WMO (2011) |

*classification compliant with GUM (1993)

**estimated as half of the instrument resolution assumed as a rectangular distribution

*** relative estimates are converted to absolute (dimensional) values in our calculations

****percentage of the mean velocity in the vertical – not discharge in the subarea

## B.4 Combined Standard Uncertainty

Equation (B.4) defines the discharge measurement process. In essence, the discharge measurement depends on the point velocity and depth measurements at verticals, the measurement of the distances between verticals, the models assumed for the vertical velocity profile and the estimation of the discharge in the cross section. Each of this variables and methods will produce uncertainties that require individual assessments for consideration of their impact on the total reported discharge uncertainty.

The standard and expanded uncertainties for the measurement process can be written as:

$$u_c(Q_t) = \sqrt{\sum_{n=0}^{8} u(\bar{v}_n)^2 \left(\frac{\partial Q_t}{\partial \bar{v}_n}\right)^2 + \sum_{n=0}^{8} u(d_n)^2 \left(\frac{\partial Q_t}{\partial d_n}\right)^2 + \sum_{n=0}^{8} u(b_n)^2 \left(\frac{\partial Q_t}{\partial b_n}\right)^2}$$
$$\sqrt{+2\sum_{n=0}^{7}\sum_{n+1}^{8}\left(\frac{\partial Q_t}{\partial \bar{v}_n}\right)\left(\frac{\partial Q_t}{\partial \bar{v}_{n+1}}\right)u(\bar{v}_n)u(\bar{v}_{n+1})r(\bar{v}_n,\bar{v}_{n+1}) + 2\sum_{n=0}^{7}\sum_{n+1}^{8}\left(\frac{\partial Q_t}{\partial d_n}\right)\left(\frac{\partial Q_t}{\partial d_{n+1}}\right)u(d_n)u(d_{n+1})r(d_n,d_{n+1})}$$
$$\sqrt{+2\sum_{n=0}^{7}\sum_{n+1}^{8}\left(\frac{\partial Q_t}{\partial b_n}\right)\left(\frac{\partial Q_t}{\partial b_{n+1}}\right)u(b_n)u(b_{n+1})r(b_n,b_{n+1}) + u(Q_m)^2 + u(Q_{nv})^2 + u(Q_{eg})^2 + u(Q_{us})^2 + u(Q_{op})^2} \quad \text{(B.5)}$$

$$U(Q_t) = k u_c(Q_t) \quad \text{(B.6)}$$

The first three terms in Equation (B.5) are associated with the uncertainties in mean vertical velocity, depth and distance between verticals, $u(\bar{v}_n)$, $u(d)$, and $u(b)$, respectively. Each of these uncertainties entails other elemental uncertainty sources that are aggregated through the following relationships:

$$u(\bar{v}_n) = \sqrt{u(\bar{v}_{ac})^2 + u(\bar{v}_{st})^2 + u(\bar{v}_{vd})^2 + u(\bar{v}_{op})^2} \quad \text{(B.7.a)}$$

$$u(d_n) = \sqrt{u(d_{ac})^2 + u(d_{op})^2} \quad \text{(B.7.b)}$$

$$u(b_n) = \sqrt{u(b_{ac})^2 + u(b_{op})^2} \quad \text{(B.7.c)}$$

The next three terms in Equation (B.5) represent correlated uncertainties for velocity, depth and distances, with $r(x_i, x_i)$ representing the correlation coefficient between the related variables. These additional terms are needed as the total discharge is based on a summation of subareas of the cross sections measured successively with the same instruments. The last five terms are directly related to the estimation of the total discharge, so their corresponding sensitivity coefficients are 1. It should be noted that the uncertainty due to the number of verticals, $u(Q_{nv})$, should include the effect on limited number of verticals on both mean velocity field description as well as of the resolution of the cross sectional area estimation. The available literature, however, does not capture the double effect of these sources of error. Specifications for the uncertainties in Equations (B.5) to (B.7) are provided in Table B.2.

The propagation of the elemental uncertainties to the total discharge was conducted using the QMsys Entreprise (Qualisyst Ltd.) using Equation (B.4) as defined for the measurement process. A snapshot of the QMsysy editor for the present example is illustrated in Figure B.2. The correlated terms were not accounted for as there is no information available for their estimation. Excepting uncertainty $u(\bar{v}_{op})$, the elemental uncertainties were assumed to have infinite degrees of freedom therefore the effective degrees of freedom for the measurand was also infinite, since the degrees of freedom induced by velocity variables does not affect the effective degrees of freedom for estimating the measurand. For assembling uncertainties estimated with various degrees of freedom, the software used the Welch-Satterthwhaite formula:

$$v_{eff} = \frac{u_c^4(y)}{\sum_{i=1}^{N} \frac{u_i^4(y)}{v_i}} \tag{B.8}$$

*where* $u_c^2(y) = \sum_{i=1}^{N} u_i^2(y) = \sum_{i=1}^{N} \left(c_i u(x_i)\right)^2$ and $c_i$ is the sensitivity coefficient, i.e., the partial derivative of the results with respect to the input variable.

| <Data Reduction Equation> | |
|---|---|
| Q=D_LB*Vavg_LB*((B_1-B_LB)/2)+D_1*Vavg_1*((B_2-B_LB)/2)+D_2*Vavg_2*((B_3-B_1)/2)+D_3*Vavg_3*((B_4-B_2)/2)+D_4*Vavg_4*((B_5-B_3)/2)+D_5*Vavg_5*((B_6-B_4)/2)+D_6*Vavg_6*((B_7-B_5)/2)+D_7*Vavg_7*((B_RB-B_6)/2)+D_RB*Vavg_RB*((B_RB-B_7)/2)+Qm+Qnv+Qop | |
| **<Depth>** | **<Width>** |
| D_LB=DLBac+DLBop<br>D_1=D1ac+D1op<br>D_2=D2ac+D2op<br>D_3=D3ac+D3op<br>D_4=D4ac+D4op<br>D_5=D5ac+D5op<br>D_6=D6ac+D6op<br>D_7=D7ac+D7op<br>D_RB=DRBac+DRBop | B_LB=BLBac+BLBop<br>B_1=B1ac+B1op<br>B_2=B2ac+B2op<br>B_3=B3ac+B3op<br>B_4=B4ac+B4op<br>B_5=B5ac+B5op<br>B_6=B6ac+B6op<br>B_7=B7ac+B7op<br>B_RB=BRBac+BRBop |
| **<Velocity>** | |
| Vavg_LB=0.25*VLB_0.2+0.5*VLB_0.6+0.25*VLB_0.8+VLBac+VLBst+VLBvd<br>Vavg_1=0.25*V1_0.2+0.5*V1_0.6+0.25*V1_0.8+V1ac+V1st+V1vd<br>Vavg_2=0.25*V2_0.2+0.5*V2_0.6+0.25*V2_0.8+V2ac+V2st+V2vd<br>Vavg_3=0.25*V3_0.2+0.5*V3_0.6+0.25*V3_0.8+V3ac+V3st+V3vd<br>Vavg_4=0.25*V4_0.2+0.5*V4_0.6+0.25*V4_0.8+V4ac+V4st+V4vd<br>Vavg_5=0.25*V5_0.2+0.5*V5_0.6+0.25*V5_0.8+V5ac+V5st+V5vd<br>Vavg_6=0.25*V6_0.2+0.5*V6_0.6+0.25*V6_0.8+V6ac+V6st+V6vd<br>Vavg_7=0.25*V7_0.2+0.5*V7_0.6+0.25*V7_0.8+V7ac+V7st+V7vd<br>Vavg_RB=0.25*VRB_0.2+0.5*VRB_0.6+0.25*VRB_0.8+VRBac+VRBst+VRBvd | |

Figure B.2 Snapshot of the QMsys equation editor

## B.5 Result Reporting and Uncertainty Budget

The uncertainty budget for the discharge measurement is provided in Table B.3 and also plotted in Figure B.3. The total (expanded) uncertainty for the discharge measurement at a 95 percent confidence level is $U(Q_t) = \pm 21.44$ m$^3$/s, which corresponds to ± 13.53 percent of the total estimated discharge. The uncertainty budget provided by the QMsys Enterprise software illustrates that uncertainties associated with the number of verticals and operational conditions for discharge estimation make the largest contribution to the total uncertainty, followed by those associated with the vertical velocity model. The result of the measurement situation analysed herein can be then

stated as: total discharge is $Q_t$ =158.44 $m^3/s$ with an interval of uncertainty [137.00 $m^3/s$, 179.87 $m^3/s$] estimated at 95 percent confidence level.

The MCM uncertainty estimation was conducted using the same software, i.e., QMsys Enterprise. From the variety of options for the random number generator (RNG), we chose for this example the recently developed CMWC4096 generator (Qualisyst Ltd.). This choice provided a long period ($2^{131086}$) for the cycle, enough to ensure that RNG does not cycle when it generates pseudo-random numbers. We assigned normal or rectangular distributions for Type B uncertainty components and *t*-distribution for the Type A uncertainty component (velocities measured at 0.2 *d*, 0.6 *d*, and 0.8 *d* in vertical 4).

The numerical simulation results are summarized in Table B.4, along with the results obtained from the analytical first-order second-moment GUM framework. The data in the table illustrates that the expanded standard uncertainties estimated by the three alternative approaches (analytic GUM and two types of MCM) are in good agreement. The MCM validation with respect to the GUM Uncertainty Framework (GUF) was also verified by calculating the tolerance interval (see Table B.4). In this validation, it was assumed that one significant decimal digit is meaningful. Given that the absolute difference between the endpoints of the two coverage intervals ($d_{low}$ and $d_{high}$) was less than the numerical tolerance ($\delta$), we can conclude that GUF was validated for this case study.

Table B.3 Uncertainty budget for the discharge estimation

| Source | Notation | Probability distribution | Divisor* | Contribution to total uncertainty ($m^3/s$) | Relative Contribution to total uncertainty (%) |
|---|---|---|---|---|---|
| Instrument accuracy | $u(\bar{v}_{ac})$ | normal | 2 | 0.95 | 4.46 |
| Sampling time | $u(\bar{v}_{st})$ | normal | 2 | 1.91 | 7.90 |
| Vertical velocity model | $u(\bar{v}_{vd})$ | normal | 2 | 2.06 | 14.32 |
| Operational conditions | $u(\bar{v}_{op})$ | *t*-distribution | 1 | 0.17 | 0.80 |
| Instrument accuracy | $u(d_{ac})$ | rectangular | 1.73 | 0.55 | 2.61 |
| Operational conditions | $u(d_{op})$ | normal | 2 | 0.36 | 1.65 |
| Instrument accuracy | $u(b_{ac})$ | rectangular | 1.73 | 0.07 | 0.33 |
| Operational conditions | $u(b_{op})$ | rectangular | 1.73 | 0.35 | 1.61 |
| Discharge model | $u(Q_m)$ | normal | 2 | 0.78 | 3.69 |
| Number of verticals | $u(Q_{nv})$ | normal | 2 | 10.22 | 42.71 |
| Edge discharge model | $u(Q_{eg})$ | | | - | |
| Flow unsteadiness | $u(Q_{us})$ | | | - | |
| Operational conditions | $u(Q_{op})$ | normal | 2 | 4.27 | 19.92 |
| Combined Uncertainty | $u(Q_t)$ | normal | | 11.22 | 6.76 |
| Expanded Uncertainty | $U(Q_t)$ | normal ($k$=2) | | 21.44 | 13.53 |

*The divisor is the value by which the standard uncertainty is divided to obtain the standard deviation for the probability distribution assumed for the *j-th* source of uncertainty.

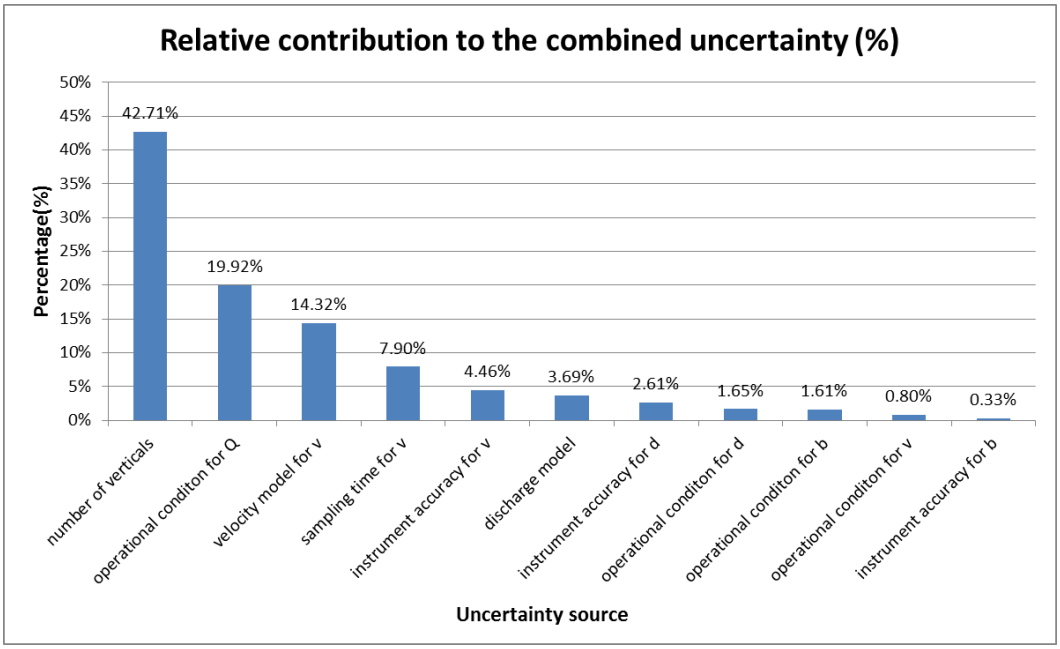


Figure B.3 Graphical illustration of the relative contribution of the combined uncertainty

Table B.4 Comparison between GUM framework and MCM uncertainty estimates

| Assessment Method | Number of trials (M) | Estimated mean ($y$) | Combined Standard Uncertainty ($u_c(y)$) | Expanded standard uncertainty (at 95 % confidence interval) | | $d_{low}$ | $d_{high}$ | Numerical tolerance $\delta$ | GUF** Validated? |
|---|---|---|---|---|---|---|---|---|---|
| GUM | n/a | 158.44 $m^3/s$ | ± 10.72 $m^3/s$ | ± 21.44 $m^3/s$ | ± 13.53 % | n/a | n/a | n/a | n/a |
| MCM | $10^6$ | 158.43 $m^3/s$ | ± 10.72 $m^3/s$ | ± 21.42 $m^3/s$ | ± 13.52 % | 0.001 | 0.021 | 0.05 | Yes |
| Adaptive MCM | $0.22\times10^6$ | 158.40 $m^3/s$ | ± 10.73 $m^3/s$ | ± 21.47 $m^3/s$ | ± 13.55 % | 0.022 | 0.017 | 0.05 | Yes |

**GUF stands for GUM Uncertainty Framework

# REFERENCES

Abernethy., Robert B., and Barbara Ringhiser., 1985. The history and statistical development of the new ASME-SAE-AIAA-ISO measurement uncertainty methodology. In Proc. AIAA/SAE/ASME/ASME 21st Joint Propulsion Conf, 8-10.

Ahanger, M.A., Asawa, G.L. and Lone, M.A., 2013. Hysteresis effect on sediment rating curves. J. Acad. Indus. Res. Vol. 1(8), 481-484.

AIAA., 1995. Assessment of wind tunnel data uncertainty. AIAA S-071-1995, Washington, DC.

AIAA., 1999. Assessment of experimental uncertainty with application to wind tunnel testing. AIAA S-017A, Washington DC 6: 1-15.

ANSI., 1997. American National Standard for Expressing Uncertainty-U.S. Guide to the Expression of Uncertainty in Measurement, ANSI/NCSL Z540-2-1997, American National Standards Institute, NCSL International, Boulder, CO.

Aschwanden, C., Reed, S. and Cepero, K., 2009. Inundation Mapping Using Hydraulic Models and GIS: Case Studies of Steady and Unsteady Models on the Tar River, NC. Proceedings of the World Environmental and Water Resources Congress, Kansas City, MO.

ASME., 1986. Measurement Uncertainty, ASME PTC 19.1, ASME New York, NY.

ASME., 1998. Test Uncertainty. PTC 19.1.1, American Society of Mechanical Engineering, New York, NY (revision of ANSI/ASME (1986).

ASME., 2005. Test Uncertainty. PTC 19.1, American Society of Mechanical Engineering, New York, NY (revision of ASME PTC 19.1-1998).

Ayewah, N., 2003. Prediction of spatial temporal events using a hidden Markov model. Department of Computer Science and Engineering, Southern Methodist University, Dallas, TX.

Barkau, R.L., 1982. Simulation of the July 1981 Flood Along the Salt River. Report for CE695BV, Special Problems in Hydraulics, Department of Civil Engineering, Colorado State University, Ft. Collins, CO.

Barua, D.K. and Rahman, K.H., 1998. Some aspects of turbulent flow structure in large alluvial rivers. J. Hydraul. Res. 36(2), 235–252.

Benson, M.A. and Dalrymple, Tate., 1967. General field and office procedures for indirect discharge measurements: U.S. Geological Survey Techniques of Water-Resources investigations book lin3, chap. Al, 30.

Bertrand-Krajewski, J.L. and Bardin, J.P., 2002. Uncertainties and Representativity of Measurements in Stormwater Storage Tanks. Proceedings 9th International Conference on Urban Drainage, Portland, OR.

Bertrand-Krajewski, J.L., Laplace, D., Joannis, C. and Chebbo, G., 2000. Mesures en hydrologie urbaine et assainissement [Measurements in urban drainage and sewer systems]. Paris (France): Éditions Tec&Doc, ISBN 2-7430-0380-4, 808 (in French).

Bertrand-Krajewski, J.L. and Muste, M., 2008. Understanding and managing uncertainty. in: Fletcher, T.D., Deletic´. A. (Eds.), Data Requirements for Integrated Urban Water Management, 333.

Bhattacharya, B. and Solomatine, D.P., 2005. Neural Networks and M5 Model Trees in Modelling Water Level–Discharge Relationship. Neurocomputing, 63, 381–396.

Birgand, F., Benoist, J.C., Novince, E., Gilliet, N., Saint-Cast, P. and LeSaos., 2005. Mesure des debits a l'aide de debitmetres ultrasonique Doppler- Cas ded petits cours d'eau ruraux. Ingineries, 41, 23-38.

Blanchard, M., 1932. A Discharge Diagram for Uniform Flow in Open Channels. Transactions, American Society of Civil Engineers, 96(Paper No. 1807), 865-870.

Boiten, W., 2000. Hydrometry. A.A. Balkema, Rotterdam, The Netherlands.

Bombar, G., Elçi, Ş., Tayfur, G., Güney, M. Ş. and Bor, A., 2011. Experimental and numerical investigation of bed-load transport under unsteady flows. Journal of Hydraulic Engineering, 137(10), 1276-1282.

Boyer, M.C., 1937. Analysis of Methods of Adjusting Stage and Discharge for Measurements During Changing Stage. Water Resources Bulletin, unpublished manuscript of the Water-Resources Branch of the U.S. Geological Survey, 192-200.

Boyer, M.C., 1939. Determining Discharge at Gaging Stations Affected by Variable Slope. Civil Engineering, 9(9), 556-558.

Buchanan, T.J. and Sommers, W.P., 1969. Discharge Measurements at Gaging stations. Techniques of Water Resources Investigations of the U.S. Geological Suyrvey, Book 3, Chapter A8, U.S. Government Printing Office, Washington, D.C.

Carroll, K.P., Rose., Seth. and Peters, N. E., 2007. Concentration/Discharge Hysteresis Analysis of Storm Events at the Panola Mountain Research Watershed, Georgia, USA. Proceedings of the 2007 Georgia Water Resources Conference, March 27-29, 2007, Athens, Georgia.

Castellarin, A., Di Baldassarre, G., Bates, P.D. and Brath, A., 2009. Optimal cross-sectional spacing in Preissmann scheme 1D hydrodynamic models. Journal of Hydraulic Engineering, 135(2), 96-105.

Charskar (undated). http://www.hydrology-project.gov.in/%5Cdownload%5Cmanuals%5CSurfaceWater%5CSoftware%5CEstimationofdischargebyArea-SlopeMethod.pdf.

Chatley, H., 1919. River Discharge. Engineering, 108, 322.

Chow, V.T., 1959. Open Channel Hydraulics. McGraw-Hill, New York, NY, 680.

Coleman, H.W. and Steele, W.G., 1995. Engineering Application of Experimental Uncertainty Analysis. AIAA Journal, 33(10), 1888-1896.

Damle, C. and Yalcin, A., 2007. Flood Prediction Using Time Series Data Mining. J. of Hydrology, 333, 305– 316.

Davenport, R.W., 1943. Discussion of Early Contributions to Mississippi River Hydrology, by C.S. Jarvis. Transactions, American Society of Civil Engineers, 108(Paper No. 2190), 629-663.

Di Baldassarre, G. and Montanari, A., 2009. Uncertainty in river discharge observations: a quantitative analysis. Hydrology and Earth System Sciences Discussions, 6, 39-61.

Di Silvio, G., 1969. Flood wave modifications along prismatic channels. J. HydrAULI. Div. ASCE, 95, 1589-1614.

Dottori, F., Martina, L.V. and Todini, E., 2009. A Dynamic Rating Curve Approach to Indirect Discharge Measurements. Hydrol. Earth Syst. Sci, 13, 847-863.

Eisenlohr, W.S., 1964. Discharge ratings for streams at submerged section controls. in: Contributions to the Hydrology of the United States, 1963 (Water-supply Paper 1779-L), U.S. Geological Survey, 32.

Faye, R.E. and Cherry, R.N., 1980. Channel and dynamic flow characteristics of the Chattahoochee River, Buford Dam to Georgia Highway 141. Geological Survey Water-supply Paper 2063, U.S. Government Printing Office, Washington, DC.

FEMA., 1992. Floodplain Management in the United States: An Assessment Report—Vol. 2: Full report. Report to Federal Interagency Floodplain Management Task Force, Report prepared by L. R. Johnston Associates for Federal Emergency Management Agency, Washington, D.C.

Fenton, J.D., 1999. Calculating hydrographs from stage records. Proc. 28th IAHR Congress, Graz, Austria.

Fenton, J.D. and Keller, R.J., 2001. The Calculation of Streamflow from Measurement of Stage. Technical Report, Cooperative Research Centre for Catchment Hydrology and Centre for Environmental Applied Hydrology, Department of Civil and Environmental Engineering, The University of Melbourne, Australia

Ferrer, C., Moreno, M.L. and Sanchez, R., 2013. The Influence of hysteresis in the development of stage-discharge relationships. Congress SHF Hydrometrie 2013, Paris, France.

Fread, D.L., 1973. Technique for implicit dynamic routing in rivers with tributaries. Water Resources Research, 9(4), 918-926.

Fread, D.L., 1975. Computation of Stage-Discharge Relationships Affected by Unsteady Flow. Water Resources Bulleting, 11(2), 213-228.

Fread, D.L., 1976. Flood routing in meandering rivers with flood plains. Rivers 76, 3rd Annual Symp. on Inland Waterways for Navigation, Flood Control and Water Diversions, Colorado State Univ., 1, 16–35.

Fread, D.L., 1982. A Dynamic Model of Stage-Discharge Relations Affected by Changing Discharge. NOAA Technical Memorandum NWS HYDRO-16, National Weather Service, Silver Spring, MD, 54.

Fread, D.L., 1985. Channel routing. M.G. Anderson, T.P. Burt (Eds.), Hydrological Forecasting, Wiley, New York.

Frizell, K.W. and Vermeyen, T.B., 2007. Comparing Apples and Oranges: Teledyne/RDI StreamPro ADCP and the OTT QLiner River Discharge Measurement System. Proceedings of Hydraulic Measurements and Experimental Methods (HMEM) conference, Lake Placid, New York, USA

Fulford, J.M., 1992. Characteristics of U.S. Geological Survey Discharge Measurements for Water Year 1990. U.S. Geological Survey Open-File Report 92-493, Reston, VA.

Fulford, J.M. and Sauer, V.B., 1986. Comparison of velocity interpolation methods for computing open-channel discharge. In Subitsky. S.Y. (ed.) Selected papers in the hydrologic sciences, U.S. Geological Survey Water-Supply Paper, 2290, 139-144.

Galloway, G.E., 2008.a. Our National Flood of Unheeded Warnings. L.A. Times and Washington Post.

Galloway, G.E., 2008.b. Flood Risk Management in the United States and the Impact of Hurricane Katrina. Int. Journal of River Basin Management, 6(4), 301-306.

Garcia, C.M., Tarrab, L., Oberg, K., Szupianny R. and Cantero, M.I., 2012. Variance of Discharge Estimates Sampled Using ADCPs from Moving Platforms. J. Hydraul. Eng. 138 (8), 684-694.

Gilcrest, B.R., 1950. Flood Routing. in: Engineering Hydraulics (Proceedings of the Fourth Hydraulics Conference, Iowa Institute of Hydraulic Research, June 12-15, 1949), edited by H. Rouse, John Wiley and Sons, Inc., New York, 635-710.

Gonzalez-Castro, J. A. and Muste, M., 2007. Framework for estimating uncertainty of ADCP measurements from a moving boat by standardized uncertainty analysis. J. Hydraul. Eng. 133(12), 1390–1410.

Graf, W.H. and Suszka, L., 1985. Unsteady flow and its effect on sediment transport. Proceedings of the 21st Congress, IAHR, Melbourne, Australia, 1–5.

Graf, W.H. and Qu, Z., 2004. Flood Hydrographs in Open Channels. Proceedings of the Institute of Civil Engineers Water Management,157, 45-52.

Gunawan, B., 2010. A Study of Flow Structures in a Two-stage Channel Using Field Data, A Physical Model and Numerical Modelling. PhD Thesis Dissertation, The University of Birmingham, UK.

Gunawan, B., Sterling, M. and Knight, D.W., 2010. Using an acoustic Doppler current profiler in a small river. Water and Environment Journal, 24, 147-158.

GUM., 1993. Guide to the Expression of Uncertainty in Measurement. ISBN 92-67-10188-9. BIPM, IEC, IFCC, ISO, IUPAC, IUPAP, OIML, International Organization for Standardization, Geneva, Switzerland.

Hall, M.R., Hall, W.E. and Pierce, C.H., 1915. A Method of Determining the Daily Discharge of Rivers of Variable Slope. in: Contributions to the Hydrology of the United States, 1914, (U.S. Geological Survey Water-Supply Paper 345), by N.C. Grover, 53-65.

HEC., 2000. Hydraulic Engineering Centre (HEC): Hydraulic Reference Manual.U.S. Army Corps of Engineers, Davis, California, USA.

HEC., 2008. Hydraulic Engineering Centre (HEC): Hydraulic Reference Manual.U.S. Army Corps of Engineers, Davis, California, USA.

Henderson, F.M., 1963. Flood Waves in Prismatic Channels. Journal of the Hydraulics Division, American Society of Civil Engineers, 89(HY4), 39-67.

Henderson, F.M., 1966. Open Channel Flow. Macmillan Company, INC, New-York.

Herschy, R.W., 2002. The Uncertainty in a Current Meter Measurement. Flow Measurement and Instrumentation,13, 281-284.

Herschy, R.W., 2009. Streamflow Measurements. 3rd edition, Taylor & Francis, New York, NY.

Hinze, J.O., 1959. Turbulence: An Introduction to its Mechanisms and Theory. McGraw-Hill Book Company, Inc., New York, NY.

Ho, Hao-Che., 2010. Investigation of unsteady and non-uniform flow and sediment transport characteristics at culvert sites. PhD diss., University of Iowa, http://ir.uiowa.edu/etd/814.

Horritt, M.S. and Bates, P.D., 2002. Evaluation of 1-D and 2-D numerical models for predicting river flood inundation. Journal of Hydrology, 268 (1–4), 87–99.

Huang, H., 2012. Uncertainty Model for In Situ Quality Control of Stationary ADCP Open-Channel Discharge Measurement. J. Hydraul. Eng., 138(1), 4-12.

Islam, M.N. and Sivakumar, B., 2002. Characterization and prediction of runoff dynamics: a nonlinear dynamical view. Advances in water resources, 25(2), 179-190.

ISO 1070., 1992. Slope–Area Method. International Organization for Standardization, Geneva, Switzerland.

ISO 5168., 2005. Measurement of Fluid Flow – Procedures for the Evaluation of Uncertainties. International Organization for Standardization, Geneva, Switzerland.

ISO 748., 2007. Hydrometry- Measurement of Liquid Flow in Open Channels Using Current-meters and Floats. International Organization for Standardization, Geneva, Switzerland.

ISO 1088., 2007. Hydrometry-Velocity-area Methods Using Current-meters-Collection and Procesing of Data for Determination of Uncertainties in Flow Measurement. International Organization for Standardization, Geneva. Switzerland.

ISO 2537., 2007. Hydrometry. Liquid flow measurement in open channels. Rotating element current-meters. International Organization for Standardization, Geneva, Switzerland.

Jain, S. and Lall, U., 2000. Magnitude and Timing of Annual Maximum Floods: Trends and Large-Scale Climatic Associations for the Blacksmith Fork River, Utah. Water Resources Research, 36(12), 3641-3651.

JCGM 200., 2007. International vocabulary of Metrology-Basic and general concepts and associated terms (VIM). ISO/IEC Guide 99: 2007, Geneva, Switzerland.

JCGM 101., 2008. Supplement 1 to the GUM (Guide to the expression of uncertainty in measurement, - propagation of distributions using a Monte Carlo method. BIPM, available on line at: http://www.bipm.org/en/publications/guides/gum.

JCGM 104., 2009. Uncertainty of Measurement- Part 1: Introduction to Expression of Uncertainty in Measurement. ISO/IEC Guide 98-1: 2009, Geneva. Switzerland.

Joannis, C. and Bertrand-Krajewski J.L., 2009. Incertitudes sur un mesurande défini comme une valeur intégrée d'un signal continu discrétisé en fonction du temps - Application aux mesures hydrologiques enregistrées in situ [Uncertainty in a measurand defined as the integrated value of a continuous signal discretised in time], La Houille Blanche, 3, 82-91 (in French).

Jones, B.E., 1916. A Method of Correcting River Discharge for a Changing Stage. Water Supply Paper 375, U.S. Geological Survey, 117-130.

Jones, C.S. and Schilling, K.E., 2011. From agricultural intensification to conservation: Sediment transport in the Raccoon River, Iowa, 1916–2009. J. Environ. Qual. 40, 1911–1923.

Kennedy, E.J., 1984. Discharge ratings at gaging stations. Techniques of Water-Resources Investigations Book 3, Chapter A 10, U.S. Geological Survey, 58.

Kim, D., Muste M. and Weber L., 2005. Development of new ADCP post-processing and visualization capabilities. Proceedings XXXI IAHR Congress, Seoul, Korea.

Kim, D., Muste, M., Gonzalez-Castro, J. A. and Ansar, M., 2005. Graphical User Interface for ADCP Uncertainty Analysis. Proceeding ASCE World Water & Environmental Resources Congress, Anchorage, AK.

Kim, Y., Muste, M., Hauet, A., Bradley, A. and Weber, L., 2007. Uncertainty Analysis for LSPIV In-situ Velocity Measurements. Proceedings 32nd IAHR Congress, Venice, Italy.

Kline, S.J. and McClintock, F.A., 1953. Describing Uncertainties in Single-Sample Experiments. Mechanical Engineering, 75, 3-8.

Knebl, M.R., Yang, Z.L., Hutchison, K. and Maidment, D.R., 2005. Regional scale flood modeling using NEXRAD rainfall, GIS, and HEC-HMS/RAS: a case study for the San Antonio River Basin Summer 2002 storm event. Journal of Environmental Management, 75(4), 325-336.

Knight, D.W., 2006. River flood hydraulics: calibration issues in one-dimensional flood routing models. In: Knight DW, Shamseldin AY (eds) Chapter 18 in river basin modelling for flood risk mitigation, Taylor & Francis, Chichester, 335–385.

Lamberti, P. and Pilati, S., 1990. Quasi-kinematic flood wave propagation. Meccanica, 25, 107–114.

Lang, M., Pobanz, K., Renard, B., Renouf, E. and Sauquet, E., 2010. Extrapolation of rating curves by hydraulic modelling with application to flood frequency analysis. Hydrological Sciences Journal–Journal des Sciences Hydrologiques, 55(6), 883-898.

Le Coz, J., Pierrefeu, G. and Paquier, A., 2008. Evaluation of river discharges monitored by a fixed side-looking Doppler profiler. Water Resour. Res., 44, 1–13, doi:10.1029/2008WR006967.

Lee, K. and Muste, M., 2011. Comparison of Standardized Approaches for Conduct of Uncertainty Analysis. Proceedings ASCE Annual Civil engineering Conference, Memphis, TN.

Lee, K., Ho, H-C., Muste, M. and Wu, C-H., 2013, Uncertainty in Open Channel Discharge Measurements Acquired with StreamPro ADCP. Journal of Hydrology, Available online 27 November 2013, ISSN 0022-1694, http://dx.doi.org/10.1016/j.jhydrol.2013.11.031.

Levesque, V.A. and Oberg, K.A., 2012. Computing discharge using the index velocity method. U.S. Geological Survey, Techniques and Methods 3–A23, 148.

Lewis, D.D., 1939. Practical Methods of Determining Discharge for Gaging Stations on Streams Where the Slope is Affected by Variable Discharge. Water Resources Bulletin, unpublished manuscript of the Water-Resources Branch of the U.S. Geological Survey, 487-489.

Liggett, J.A. and Jean, A.C., 1975. Numerical methods of solution of the unsteady flow equations. Unsteady flow in open channels, 1, 89-178.

Linsley, R.K., Kohler, M.A. and Paulhus, J.L.H., 1949. Applied Hydrology. First Edition, McGraw-Hill Book Company, Inc., New York, 689.

Loperfido, J.V., 2007. High-frequency sensing of Clear Creek water quality: mechanisms of dissolved oxygen and turbidity dynamics and nutrient transport. PhD. Thesis, Univ. of Iowa, Iowa City.

M3003., 2007. The Expression of Uncertainty and Confidence in Measurement. United Kingdom Accreditation Service, Feltham, United Kingdom.

Mahmood, K. and Yevjevich, V., 1975. Simulation of unsteady overland flow. Unsteady Flow in Open Channels. II, 485–508.

Malone, T. and Shallcross, W., 2007. Development of a flood forecasting database for the Lower Mekong River. Mission Report, Mekong River Commission.

Marchi, E., 1976. La Propagazione delle onde di piena, Atti Accademia Nazionale Lincei, 64, 594–602 (in Italian).

Marsden, R., 2005. StreamPro ADCP Performance Characteristics. Proceedings of the IEEE/OES Eighth Working Conference on Current Measurement Technology.

Matott, L.S., Babendreier, J.E. and Purucker, S.T., 2009. Evaluating uncertainty in integrated environmental models: A review of concepts and tools, Water Resources Research 45, W06421, doi: 10.1029/2008WR007301.

Mishra, S.K. and Seth, S.M., 1996. Use of hysteresis for defining the nature of flood wave propagation in natural channels. Hydrological Sciences-Journal-des Sciences Hydrologiques 41(2), 153–170.

Mishra, S.K. and Singh, V.P., 1999. Hysteresis-based flood wave analysis. Journal of Hydrologic Engineering, American Society of Civil Engineers 4(4), 358–365.

Mishra, S.K., Sah, S., Sharma, N. and Seth, S.M., 1996. Defining flood wave propagation characteristics using hysteresis of rating curves. HYDRO96, 11–13, December, IIT (Indian Institute of Technology), Kanpur.

Mishra, S.K., Jain, M.K. and Seth, M.K., 1997. Characterization of flood waves by rating curves. Journal of Nordic Hydrology, 28(1), 51–64.

Mishra, S.K., 2009. Uncertainty and sensitivity analysis techniques for hydrologic modeling. Journal of Hydroinformatics, 11(3-4), 282–296, doi:10.2166/hydro.2009.048.

Mitchell, W.D., 1954. Stage-Fall-Discharge Relations for Steady Flow in Prismatic Channels. Water-Supply Paper 1164, U.S. Geological Survey, 162.

Morlock, S.E., Nguyen, H.T. and Ross, J., 2002. Feasibility of acoustics Doppler velocity meters for the production of discharge records from U.S. Geological Survey stream-flow-gaging stations. U.S Geological Survey, Water-resources Investigations Report, Indianapolis, IN.

Mueller, D.S., Abad, J.D., García, C.M., Gartner, J.W., García, M.H. and Oberg, K.A., 2007. Errors in Acoustic Doppler Profiler Velocity Measurements Caused by Flow Disturbance. J. Hydraul. Eng., 133(12), 1411-1420.

Mueller, D.S. and Wagner, C., 2009. Measuring Discharge with ADCPs from a Moving Boat. US Geological Survey Techniques and Methods 3A-22, USGS, Reston, VA.

Mujumdar, P.P., 2001. Flood wave propagation – The Saint Venant Equations. Resonance, 66-73.

Muste, M. and Stern, F., 2000. Proposed Uncertainty Assessment Methodology for Hydraulic and Water Resources Engineering. Proceedings of ASCE 2000 Joint Conference on Water Resources Engineering and Water Resources Planning & Management, Minneapolis, MN (CD-ROM).

Muste, M., Yu, K., Gonzalez-Castro, J. and Starzmann, E., 2004. Methodology for Estimating ADCP Measurement Uncertainty in Open-Channel Flows. Proceedings World Water & Environmental Resources Congress 2004 (EWRI), Salt Lake City. USA

Muste, M., Yu, K., Pratt, T. and Abraham, D., 2004.b. Practical Aspects of ADCP Data Use for Quantification of Mean River Flow Characteristics: Part II: Fixed-Vessel Measurements. Flow Meas. Instrum, 15(1), 17-28.

Muste, M., Kim, D. and Gonzalez-Castro, J.A., 2010. Near-Transducer Errors in ADCP Measurements: Experimental Findings. J. Hydraul. Eng., 136(5), 275-289.

Muste, M. and Lee, K., 2011. Development of the Decision-aid Tool for Uncertainty Analysis. Report for "Assessment of the Performance of Flow Measurement Instruments and Techniques" Study, World Meteorological Organization, Geneva, Switzerland.

Muste, M., Lee, K. and Bertrand-Krajewski, J.L., 2012. Standardized uncertainty analysis for hydrometry: a review of relevant approaches and implementation examples. Hydrological Sciences Journal, 57 (4), 643–667.

Muste, M. and Lee, K., 2013. Quantification of Hysteretic Behavior in Stream Flow Rating Curves. Proceeding of 2013 IAHR World Congress, Chengdu, China.

Muste, M. and Lee, K., 2013, Discussion of "Uncertainty Model for In Situ Quality Control of Stationary ADCP Open-Channel Discharge Measurement" by Hening Huang. Journal of Hydraulic Engineering 139:1, 102-104.

Nezu, I. and Nakagawa, H., 1993. Basic structure of turbulence in unsteady open-channel flows. Proc. 9th Symp. on Turbulent Shear Flows, Kyoto, Japan, 7.1.1-7.1.6.

Nezu, I. and Nakagawa H., 1995. Turbulence measurements in unsteady free-surface flows. Flow Measurement and Instrumentation, 6(1), 49-59.

Nezu, I., Kadota, A. and Nakagawa, H., 1997. Turbulent structure in unsteady depth-varying open-channel flows. Journal of Hydraulic Engineering, 123(9), 752–763.

NF ENV 13005 (Norme Francaise – Europaische VorNorm)., 1999. Guide pour L'Expression de L'incertitude de Mesure, AFNOR, Paris, France (in French).

Nihei Y. and Sakai T., 2006. Study of river-discharge measurements with a bottom-mounted ADCP. Proceedings River Flow International Conference on Fluvial Hydraulics, Lisbon, Portugal, 6-8 September 2006, Eds. Alves E.C.T.L., Cardoso A.H., Leal J.G.A.B. and Ferreira R.M.L., Taylor and Francis.

NIST., 1994. Guidelines for Evaluating and Expressing Uncertainty of NIST Measurement Results. 2nd Edition (prepared by B.N. Taylor & C. E. Kuyatt), National Institute of Standards and Technology, Gaithersburg, MD.

NIST., 2003. E-Handbook of Statistical Methods. NIST/SEMATECH, available on line at: http://www.itl.nist.gov/div898/handbook/.

Pappenberg, F., Matgen, P., Beven, K.J., Henry, J.B., Pfister, L. and de Fraipont, P., 2006. Influence of uncertain boundary conditions and model structure on flood inundation prediction. Advances in Water Resources, 29, 1430-1449.

Perry, L., 1932. Discussion of a Discharge Diagram for Uniform Flow in Open Channels, by M. Blanchard. Transactions, American Society of Civil Engineers, 96(Paper No. 1807), 871- 873.

Perumal, M., Shrestha, K.B. and Chaube, U.C., 2004. Reproduction of Hysteresis in Rating Curves. Journal of Hydraulic Engineering, 130(9), 870-878.

Pilon, P.J., Fulford, J.M., Kopaliani, Z., McCurry, P.J., Ozbey, N. and Caponi, C., 2007. Proposal for the Assessment of Flow Measurement Instruments and Techniques. Proceedings XXXII IAHR Congress, Venice, Italy.

Pobanz, K., Le Coz, J. and Pierrefeu, G., 2011. Intercomparison of ADCPs on the Rhone downstream of Genissiat Dam. Groupe Doppler France, Intercomparison ADCP 2, IRSTEA, Lyon, France.

Ponce, V.M., 1989. Engineering Hydrology Principles and Practices. Prentice Hall, Englewood Cliffs, NJ.

Ponce, V.M., 1991. The kinematic wave controversy. J. Hydr. Engrg., ASCE, 117(4), 511–525.

Ponce, V.M. and Simon, D.B., 1977. Shallow water propagation in open channel flow. J.Hydr. Div. , 103, 1461–1476.

Posey, C.J., 1943. Flood Wave Characteristics as Related to Flood Routing. Proceedings Second Hydraulics Conference, University of Iowa Studies in Engineering, Bulletin 27, 224-233.

Petersen-Øverleir, A., 2006. Modelling stage-discharge relationships affected by hysteresis using the Jones formula and nonlinear regression. Hydrol. Sci. J., 51, 365–388.

Qu, Z., 2003. Unsteady open-channel flow over a mobile bed. PhD Thesis, Ecole Polytechnique Federale de Lausanne, Lausanne, Switzerland.

Rantz, S.E. and others., 1982. Measurement and Computation of Streamflow. United States Geological Survey Water Supply Paper 2175, Vol 1, 2.

RDI., 2010. Section-by-Section (SxS) Pro Data Acquisition and Processing Software Package. Teledyne RD Instruments, Poway, CA.

RDI., 2012.a. StreamPro & Section by Section Software Operation Manual. Teledyne RD Instruments, Poway, CA.

RDI., 2012.b. StreamPro ADCP Guide. Teledyne RD Instruments, Poway, CA.

RDI., 2012.c. WinRiver II Software User's Guide. Teledyne RD Instruments. Poway, CA.

Rehmel, M.S., 2006. Field Evaluation of Shallow-Water Acoustic Doppler Current Profiler Discharge Measurements. Proceedings of ASCE-EWRI Congress, May 21-25, Omaha, NE.

Ruhl, C.A. and Simpson, M.R., 2005. Computation of discharge using the index-velocity method in tidally affected areas. U.S. Geological Survey, Scientific Investigations Report 2005-5004, Reston, VA.

Rutter, E.J., Graves, Q.B. and Snyder, F.F., 1938. Flood Routing. Proceedings, American Society of Civil Engineers, 64(Part I), 291-310.

Sassi, M.G., Hoitink, A.J.F., Vermeulen, B. and Hydayat., 2011. Discharge estimation from H-ADCP measurements in a tidal river subject to sidewall effects and a mobile bed. Water Resources Research, 47, 14.

Schmidt, A.R., 2002. Analysis of Stage-discharge Relations for Open Channel Flows and their Associated Uncertainties. Ph.D. thesis, Univ. of Illinois at Urbana-Champaign, Champaign, IL.

Shrestha, R.R., Bárdossy, A. and Nestmann, F., 2007. Analysis and propagation of uncertainties due to the stage–discharge relationship: a fuzzy set approach. Hydrological Sciences Journal, 52(4), 595-610.

Shrestha, R.R. and Simonovic, S.P., 2009. Fuzzy Nonlinear Regression Approach to Stage-Discharge Analyses: Case Study. Journal of Hydrologic Engineering, 15(1), 49-56.

Simpson, M.R., 2001. Discharge Measurements Using a Broadband Acoustic Doppler Current Profiler. US Geological Survey Open File Report, Reston, VA.

Smith, C.F., Cordova, J.T. and Wiele, S.M., 2010. The Continuous Slope-Area Method for Computing Event Hydrographs. USGS Science Investigation, Report 2010–5241.

Singh, A.K., Kothyari, U.C. and Raju, K.G.R., 2004. Rapidly varying transient flows in alluvial rivers. J. Hydraul. Res., 42(5), 473–486.

Singh, V.P. and Tayfur, G., 2008. Kinematic wave theory for transient bed sediment waves in alluvial rivers. J. Hydrol. Eng., 13(5), 297–304.

Song, T. and Graf, W.H., 1996. Velocity and turbulence distribution in unsteady open-channel flows. Journal of Hydraulic Engineering, 122(3), 141-154.

Song, T., and Graf, W.H., 1997. Experimental study of bed-load transport in unsteady open-channel flow. Int. J. Sediment Res., 12, 63–71.

Steele, W.G., Ferguson, R.A., Taylor, R.P. and Coleman, H.W., 1994. Comparison of ANSI/ASME and ISO Models for Calculation of Uncertainty. ISA Transactions, 33, 339-352.

Stern, F., Muste, M., Beninati, M. L. and Eichinger, W.E., 1999. Summary of Experimental Uncertainty assessment Methodology with Example. Iowa Institute of Hydraulic Research, The University of Iowa, Iowa City, IA, IIHR Technical Report, 406.

Stewart, A.M., Callegary, J.B., Smith, C.F., Gupta, H.V., Leenhouts, J.M. and Fritzinger, R.A., 2012. Use of the continuous slope-area method to estimate runoff in a network of ephemeral channels, southeast Arizona, USA. Journal of Hydrology, Volumes 472–473, 23 November 2012, 148-158, ISSN 0022-1694, http://dx.doi.org/10.1016/j.jhydrol.2012.09.022.

Stone, M.C. and Hotchkiss, R.H., 2007. Evaluating velocity measurement techniques in shallow streams. J. Hydraul. Res., 45(6), 752-762.

Sudheer, K.P. and Jain, S.K., 2003. Radial Basis Function Neural Network for Modeling Rating Curves. Journal of Hydrologic Engineering, 8(3), ISSN 1084-0699/2003/3, 161–164.

Szupiany, R.N., Amsler, M.L., Best, J.L. and Parsons, D.R., 2007. Comparison of fixed- and moving-vesselflow measurements with an aDP in a large river. J. Hydraul. Eng., 133, 1299-1309.

Takahashi, H., 1969. Theory of one-dimensional unsteady flows in a prismatic open channel. Annu. of Dis. Prevo Res., Inst., Kyoto Univ., Kyoto, Japan, Vol. 12B, 515-527 (in Japanese).

Tawfik, M., Ibrahim, A. and Fahmy, H., 1997. Hysteresis Sensitive Neural Network for Modeling Rating Curves. Journal of Computing in Civil Engineering, II(3), ISSN 0887-3801/97/0003, 206-211.

Taylor, B.N. and Kuyatt, C.E., 1994. Guidelines for Evaluating and Expressing the Uncertainty of NIST Measurement Results. NIST Technical Note, 1297.

TCHME., 2003. Annotated Bibliography on Uncertainty Analysis. Task Committee on Experimental Uncertainty and Measurement Errors in Hydraulic Engineering, EWRI, ASCE. Available on line at: http://www.dri.edu/People/Mark.Stone/Tchme/task.html.

Thibodeaux, K.G., 2007. Testing and evaluation of inexpensive horizontal-axis mechanical current meters. USCID Fourth International Conference, 1295-1308.

Thomas, H.A., 1937. The Hydraulics of Flood Movements in Rivers. Carnegie Institute of Technology, Engineering Bulletin, 70.

Thomas, F., 2002. Open Channel Flow Measurement Using International Standards: Introducing a Standards Programme and Selecting a Standard. Flow Measurement and Instrumentation, 13, 303-307.

Tu,H. and Graf, W.H., 1992. Velocity distribution in unsteady open-channel flow over gravel beds. J. Hydrosci. and Hydr. Engrg., 10 (1), 11–25.

UNESCO., 2007. Data Requirements for Integrated Urban Water Management. Eds. Fletcher, T.D. and Deletic, A., Taylor and Francis, Oxfordshire, UK.

UKAS., 2007. The Expression of Uncertainty and Confidence in Mesurement. United Kingdom Accreditation Service, Middleesex, UK.

USGS., 2011. Exposure time for ADCP Moving-boat discharge Measurements Made During Steady Flow Conditions, USGS Office of Surface Water Technical Memorandum, 2011.08.

Van den Boogard, H.F.P., Gautam, D.K. and Mynett, A.E., 1998. Autoregressive neural networks for the modeling of time series. edited by Babovic E.V. and Larsen C.L., Hydroinformatics 98, Balkema, Rotterdam, The Netherlands, 41-748.

Wahlin, B., Wahl, T., Gonzalez-Castro, J. A., Fulford, J. and Robeson, M., 2005. Task Committee on Experimental Uncertainty and Measurement Errors in Hydraulic Engineering: An Update. Impacts of Global Climate Change. Proceedings of World Water and Environmental Resources Congress, Anchorage, Alaska.

Wiggins, W.C., 1925. Correcting Discharge Measurements for Changing Stage. Water Resources Branch, Circular No. 479, unpublished manuscript of the Water-Resources Branch of the U.S. Geological Survey, 10, 285.

WMO., 2010. Manual on Stream Gauging. Volume I: Fieldwork. World Meteorological Organization, Geneva, Switzerland.

WMO., 2011. Assessment of the Performance of Flow Measurement Instruments and Techniques. World Meteorological Organization Project, Personal communication, Commission for Hydrology, Geneva, Switzerland.

Yen, B.C. and Tang, W.H., 1977. Reliability of Flood Warning. in: Stochastic Processes in Water Resources Engineering (Proceedings of the 2nd International Symposium on Stochastic Hydraulics, Lund, Sweeden, 1976), Water Resources Publications, Littleton, CO, 333-347.

Yen, C.L. and Lee, K.T., 1995. Bed topography and sediment sorting in channel bend with unsteady flow. J. Hydraul. Eng., 121(8), 591–599.